

**Water Quality Assessment using Landsat 8 and Sentinel-2: A  
case study of the Umdloti Estuary, KwaZulu-Natal, South  
Africa**

By

**Matthew Ellero**

**Submitted in fulfilment of the academic requirements for the Degree of Master of Science  
in the School of Agricultural, Earth and Environmental Sciences, University of KwaZulu-  
Natal.**

**July 2018**

As the candidate's supervisor I have/have not approved this thesis for submission.

Signed: 

Name: Prof Michael Gebreslasie

Date: 20/07/2018

## Abstract

Estuaries are amongst the most productive and important ecosystems on the planet but are vulnerable to physico-chemical alterations within their waters. Water quality and health monitoring therefore requires the timely retrieval of physico-chemical concentrations. Whilst accurate, water quality retrieval performed through field sampling is often expensive, time consuming and unsuitable across larger spatial scales. remote sensing offers a possible solution to these problems. This study therefore assessed the ability of Landsat 8 and Sentinel-2 remotely sensed imagery in estimating physico-chemical health within the Umdloti Estuary, South Africa. Sampling of the Umdloti Estuary was conducted over winter and spring where the in situ conditions of temperature, turbidity, secchi disk depth (SDD), salinity, electrical conductivity (EC), total dissolved solids (TDS), chlorophyll-a (chl-a), dissolved oxygen (DO) and pH were retrieved through field and lab testing. Remote sensing algorithms were thereafter used to estimate the values of these parameters. Results from the comparison of the two approaches showed that temperature and turbidity were able to be accurately retrieved with best respective coefficients of determination ( $R^2$ ) of 0.96 and 0.97 and root mean squared error (RMSE) of 2.648 °C and 2.944 NTU. Chl-a, TDS and EC had respective inaccurate  $R^2$  values of 0.031, 0.576 and 0.037 but accurate RMSE of 0.902 µg/l, 638.159 mg/l and 1.801 µS/cm. These parameters were poorly modelled but accurate absolute concentrations could be estimated. Salinity, DO, pH and SDD estimation was poor. These parameters had a respective  $R^2$  values of 0.45, 0.53, 0.23 and 0.0007 as well as RMSE of 5.84, 1.91 ppm, 2.15 and 1.43 m. The optical inactivity of these physico-chemical parameters and unique complexity of estuarine waters were likely culprits in failed estimation. Positively, algorithms modified by this study showed greatly increased accuracy and future promise in the estimation of every parameter except secchi disk depth and pH. The estuary was determined to be in poor health due to a lack of improvements in physico-chemical conditions since it was last classified as poor. In future, studies should continue to refine algorithms for use in Umdloti Estuary and its health should be safeguarded.

## **Preface**

The experimental work described and presented in this dissertation was carried out in the School of Agricultural, Earth and Environmental Sciences, University of KwaZulu-Natal, Durban, from July 2017 to July 2018 under the supervision of Prof. Michael Gebreslasie.

This study represents the original work by the author, Matthew Ellero, and has not been submitted in any form for any degree, diploma or award at this or any other tertiary institution. Except for those acknowledged as such, all figures, sketches and maps were drawn by the author. The use of information sources and work of others has been duly acknowledged as such in the text.

## Declaration - Plagiarism

I, Matthew Ellero, declare that:

1. The research reported in this thesis, except where otherwise indicated, is my original research.
2. This thesis has not been submitted for any degree or examination at any other university.
3. This thesis does not contain other persons' data, pictures, graphs or other information, unless specifically acknowledged as being sourced from other persons.
4. This thesis does not contain other persons' writing, unless specifically acknowledged as being sourced from other researchers. Where other written sources have been quoted, then:
  - a. Their words have been re-written but the general information attributed to them has been referenced
  - b. Where their exact words have been used, then their writing has been placed in italics and inside quotation marks, and referenced.
5. This thesis does not contain text, graphics or tables copied and pasted from the Internet, unless specifically acknowledged, and the source being detailed in the thesis and in the References sections.

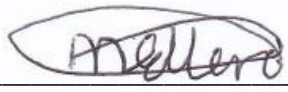
Signed: 

Date: 20/07/2018

Matthew Ellero

## Declaration - Publications

The author of this dissertation will be working towards the production of individual research papers from this dissertation, as well as the submission of these papers to the relevant journals for publication.

Signed: \_\_\_\_\_

Date: 20/07/2018

Matthew Ellero

## Acknowledgements

I would like to thank:

- My supervisor, Prof. Michael Gebreslasie, for introducing me to the wonderful world of remote sensing, for always having an open door to any problems I had encountered over the course of the project, for helping to organise equipment and testing and for all the words of encouragement and general advice. Thanks a million Mike. You are an amazing lecturer and supervisor.
- Mr E. Powys for his invaluable help in organising equipment and the general help offered throughout the course of the study.
- Ms N. Rambaran for going the extra mile to ensure I was able to complete my chl-a testing.

## Table of contents

### Contents

CHAPTER ONE: INTRODUCTION .....	1
1.1) Background.....	1
1.2) Problem contextualisation and justification.....	2
1.3) Aims and objectives.....	4
1.4) Chapter sequence and summation.....	4
CHAPTER TWO: LITERATURE REVIEW .....	6
2.1) Introduction.....	6
2.2) Estuaries.....	6
2.2.1 General characteristics .....	6
2.2.2 Classifications of various estuary types .....	7
2.2.3 Importance of estuaries .....	10
2.2.4 Threats to estuaries.....	12
2.2.5. South African estuaries .....	17
2.3) The physico-chemical components of estuarine health .....	22
2.3.1 Role of Temperature in estuaries.....	22
2.3.2 Role of Turbidity and secchi disk depth (SDD) in estuaries .....	23
2.3.3 Role of Salinity, Total dissolved solids (TDS) and Electrical conductivity (EC) in estuaries.....	24
2.3.4 Role of Chlorophyll-a (Chl-a) in estuaries .....	25
2.3.5 Role of Dissolved oxygen (DO) in estuaries.....	26
2.3.6 Role of pH in estuaries .....	26
2.4) Estimation of the physico-chemical components of estuarine health .....	27
2.4.1 Traditional and Remote sensing based methods of physico-chemical parameter estimation .....	27
2.4.2 Traditional and remote sensing based temperature retrieval.....	28
2.4.3 Traditional and remote sensing based Turbidity and secchi disk depth (SDD) retrieval .....	29
2.4.4 Traditional and remote sensing based salinity, total dissolved solids (TDS) and electrical conductivity (EC) retrieval .....	31
2.4.5 Traditional and remote sensing based Chlorophyll-a (Chl-a) retrieval .....	33
2.4.6 Traditional and remote sensing based Dissolved oxygen (DO) retrieval.....	34
2.4.7 Traditional and remote sensing based pH retrieval .....	35

CHAPTER THREE: STUDY AREA .....	37
3.1) Introduction.....	38
3.2) Description of the study area .....	38
CHAPTER FOUR: METHODOLOGY .....	44
4.1) Introduction.....	44
4.2) Methodology .....	44
4.2.1 Data collection.....	44
4.2.2 Physico-chemical parameter estimation from remote sensing images.....	52
4.2.3 Accuracy assessment.....	65
4.2.4 Modified algorithms and distribution maps .....	67
CHAPTER FIVE: RESULTS .....	69
5.1) Introduction.....	69
5.2) Descriptive statistics .....	69
5.3) Statistical analyses .....	71
5.3.1 Temperature estimation.....	71
5.3.2 Turbidity estimation .....	75
5.3.3 SDD estimation .....	80
5.3.4 Salinity estimation.....	86
5.3.5 TDS estimation.....	92
5.3.6 EC estimation .....	96
5.3.7 Chl-a estimation .....	101
5.3.8 DO estimation .....	110
5.3.9 pH estimation .....	114
CHAPTER SIX: DISCUSSION AND CONCLUSION .....	120
6.1) Introduction.....	120
6.2) Discussion.....	120
6.2.1 Temperature estimation using remote sensing .....	120
6.2.2 Turbidity estimation using remote sensing .....	121
6.2.3 SDD estimation using remote sensing.....	122
6.2.4 Salinity, TDS and EC estimation using remote sensing.....	123
6.2.5 Chl-a estimation using remote sensing.....	124
6.2.6 DO estimation using remote sensing.....	125
6.2.7 pH estimation using remote sensing.....	125
6.2.8 Reasons for the success and failure of remote sensing estimation.....	125



6.2.9 Comparison of performance between Landsat 8 and Sentinel-2.....	128
6.2.10 Assessment of estuarine health.....	129
6.2.11 Limitations and Recommendations .....	134
6.3) Conclusion .....	137
REFERENCES.....	138

## List of figures

Figure 2.1: Generalised morphology for estuaries classified through various geomorphological methods (Trujillo and Thurman, 2011). .....	8
Figure 2.2: Generalised morphology for estuaries classified through various water circulatory methods (Trujillo and Thurman, 2011). .....	9
Figure 2.3: Overview of the relationship between the overall eutrophication process, the symptoms and influence factors such as nutrient loads (adapted from Bricker <i>et al.</i> , 2008). .....	25
<i>Umdloti Estuary during winter sampling</i> .....	37
Figure 3.1: The location of Umdloti with respect to (A) South Africa, (B) the province of Kwazulu-Natal, (C) and the eThekweni municipality. A Sentinel-2 image of the Umdloti Estuary (29° 39' 07" S; 31° 07' 43" E) is also included (D). .....	43
Figure 4.1: Flow diagram displaying basic outline of steps taken to obtain results over course of the study. ....	45
Figure 4.2: Google Earth image showing the sampling points (1 – 15) at which water samples were collected and used for physico-chemical parameter estimation (Source: “Umdloti Estuary” 29° 39' 07" S; 31° 07' 43" E. Google Earth. 16 December 2017. 2 February 2018). .....	48
Figure 4.3: Comparison of Landsat 7 ETM+, Landsat 8 and Sentinel-2 band numbers and the wavelengths they cover against a backdrop of atmospheric transmission (NASA, 2015). .....	51
Figure 5.1: Temperature distribution across the Umdloti Estuary for winter (A) and spring (B) .....	73
Figure 5.2: Scatterplots of observed vs. calculated values for all temperature estimation algorithms .....	74
Figure 5.3: Scatterplots of observed vs. calculated values for turbidity estimation algorithms 11 to 13. ....	77
Figure 5.4: Scatterplots of observed vs. calculated values for turbidity estimation algorithms 14 to 16. ....	78
Figure 5.5: Scatterplots of observed vs. calculated values for turbidity estimation algorithms 17, 18 and 70. ....	79
Figure 5.6: Turbidity distribution across the Umdloti Estuary for winter (A) and spring (B) ....	80
Figure 5.7: Scatterplots of observed vs. calculated values for SDD estimation algorithms 19 to 21. ....	83
Figure 5.8: Scatterplots of observed vs. calculated values for SDD estimation algorithms 22 to 24. ....	84
Figure 5.9: Scatterplots of observed vs. calculated values for SDD estimation algorithms 25, 26 and 71. ....	85

Figure 5.10: SDD distribution across the Umdloti Estuary for winter (A) and spring (B). .....	86
Figure 5.11: Scatterplots of observed vs. calculated values for salinity estimation algorithms 27 to 29.....	89
Figure 5.12: Scatterplots of observed vs. calculated values for salinity estimation algorithms 29 to 31.....	90
Figure 5.13: Scatterplot of observed vs. calculated values for salinity estimation algorithm 72.91	
Figure 5.14: Salinity distribution across the Umdloti Estuary for winter (A) and spring (B).....	91
.....	94
Figure 5.15: Scatterplots of observed vs. calculated values for TDS estimation algorithms 33, 34 and 35.....	95
Figure 5.16: Scatterplots of observed vs. calculated values for TDS estimation algorithms 36 and 73.....	95
Figure 5.17: TDS distribution across the Umdloti Estuary for winter (A) and spring (B).....	96
Figure 5.18: Scatterplots of observed vs. calculated values for EC estimation algorithms 37. ..	98
Figure 5.19: Scatterplots of observed vs. calculated values for EC estimation algorithms 38 to 41.....	99
Figure 5.20: Scatterplots of observed vs. calculated values for turbidity estimation algorithms 41 and 74.....	100
Figure 5.21: EC distribution across the Umdloti Estuary for winter (A) and spring (B). .....	100
Figure 5.22: Scatterplots of observed vs. calculated values for chl-a estimation algorithms 42 to 44.....	104
Figure 5.23: Scatterplots of observed vs. calculated values for chl-a estimation algorithms 45 to 47.....	105
Figure 5.24: Scatterplots of observed vs. calculated values for chl-a estimation algorithms 48 to 50.....	106
Figure 5.25: Scatterplots of observed vs. calculated values for chl-a estimation algorithms 51 to 53.....	107
Figure 5.26: Scatterplots of observed vs. calculated values for chl-a estimation algorithms 54 to 56.....	108
Figure 5.27: Scatterplots of observed vs. calculated values for chl-a estimation algorithms 57 and 75.....	109
Figure 5.28: Chl-a distribution across the Umdloti Estuary for winter (A) and spring (B). ....	110
Figure 5.29: Scatterplots of observed vs. calculated values for DO estimation algorithms 58 and 59.....	112

Figure 5.30: Scatterplots of observed vs. calculated values for DO estimation algorithms 60 and 76.....	113
Figure 5.31: DO distribution across the Umdloti Estuary for winter (A) and spring (B). .....	114
Figure 5.32: Scatterplots of observed vs. calculated values for pH estimation algorithms 61..	116
Figure 5.33: Scatterplots of observed vs. calculated values for pH estimation algorithms 62 to 64.....	117
Figure 5.34: Scatterplots of observed vs. calculated values for pH estimation algorithms 65, 66 and 77 .....	118
Figure 5.35: pH distribution across the Umdloti Estuary for winter (A) and spring (B). .....	119
Figure 6.1: Image taken during winter sampling showing large amounts of plastic pollution present. ....	134

## List of tables

Table 4.1: Differences in specifications between Landsat 8 and Sentinel-2 remote sensors (adapted from Roy <i>et al.</i> , 2014 and Drusch <i>et al.</i> , 2012). .....	50
Table 4.2: Surface emissivities calculated from NDVI adapted from Zhang <i>et al.</i> , (2006). .....	55
Table 4.3: Temperature estimation equations adapted for Landsat 8 and Sentinel-2. ....	56
Table 4.4: Turbidity estimation equations adapted for Landsat 8 and Sentinel-2. ....	57
Table 4.5: SDD estimation equations adapted for Landsat 8 and Sentinel-2. ....	58
Table 4.6: Salinity estimation equations adapted for Landsat 8 and Sentinel-2. ....	60
Table 4.7: TDS estimation equations adapted for Landsat 8 and Sentinel-2. ....	60
Table 4.8: EC estimation equations adapted for Landsat 8 and Sentinel-2. ....	61
Table 4.9: Chl-a estimation equations adapted for Landsat 8 and Sentinel-2. ....	63
Table 4.10: DO estimation equations adapted for Landsat 8 and Sentinel-2. ....	64
Table 4.11: pH estimation equations adapted for Landsat 8 and Sentinel-2. ....	65
Table 4.12: Newly generated physico-chemical estimation algorithms. ....	68
Table 5.1: Descriptive statistics from parameters retrieved from in situ sampling. ....	70
Table 5.2: Accuracy of the estimated temperature (°C) using Landsat 8 for Umdloti Estuary. ..	71
Table 5.3: Accuracy of the estimated temperature (°C) using Sentinel-2 for Umdloti Estuary. ..	72
Table 5.4: Accuracy of the estimated temperature (°C) using newly generated estimation algorithms for Umdloti Estuary. ....	72
Table 5.5: Accuracy of the estimated turbidity (NTU) using Landsat 8 for Umdloti Estuary. ....	75
Table 5.6: Accuracy of the estimated turbidity (NTU) using Sentinel-2 for Umdloti Estuary. ..	76
Table 5.7: Accuracy of the estimated turbidity (NTU) using newly generated estimation algorithms for Umdloti Estuary. ....	76
Table 5.8: Accuracy of the estimated SDD (m) using Landsat 8 for Umdloti Estuary. ....	81
Table 5.9: Accuracy of the estimated SDD (m) using Sentinel-2 for Umdloti Estuary. ....	81
Table 5.10: Accuracy of the estimated SDD (m) using newly generated estimation algorithms for Umdloti Estuary. ....	82
Table 5.11: Accuracy of the estimated salinity using Landsat 8 for Umdloti Estuary. ....	87
Table 5.12: Accuracy of the estimated salinity using Sentinel-2 for Umdloti Estuary. ....	87
Table 5.13: Accuracy of the estimated salinity using newly generated estimation algorithms for Umdloti Estuary. ....	88
Table 5.14: Accuracy of the estimated TDS (mg/l) using Landsat 8 for Umdloti Estuary. ....	92
Table 5.15: Accuracy of the estimated TDS (mg/l) using Sentinel-2 for Umdloti Estuary. ....	93

Table 5.16: Accuracy of the estimated TDS (mg/l) using newly generated estimation algorithms for Umdloti Estuary.....	93
Table 5.17: Accuracy of the estimated EC ( $\mu\text{S}/\text{cm}$ ) using Landsat-8 algorithms for Umdloti Estuary.....	96
Table 5.18: Accuracy of the estimated EC ( $\mu\text{S}/\text{cm}$ ) using Sentinel-2 algorithms for Umdloti Estuary.....	97
Table 5.19: Accuracy of the estimated EC ( $\mu\text{S}/\text{cm}$ ) using newly generated estimation algorithms for Umdloti Estuary.....	98
Table 5.20: Accuracy of the estimated chl-a ( $\mu\text{g}/\text{l}$ ) using Landsat 8 for Umdloti Estuary.....	101
Table 5.21: Accuracy of the estimated chl-a ( $\mu\text{g}/\text{l}$ ) using Sentinel-2 for Umdloti Estuary.....	102
Table 5.22: Accuracy of the estimated chl-a ( $\mu\text{g}/\text{l}$ ) using newly generated estimation algorithms for Umdloti Estuary.....	103
Table 5.23: Accuracy of the estimated DO (ppm) using Landsat 8 for Umdloti Estuary.....	110
Table 5.24: Accuracy of the estimated DO (ppm) using Sentinel-2 for Umdloti Estuary.....	111
Table 5.25: Accuracy of the estimated DO (ppm) using newly generated estimation algorithms for Umdloti Estuary.....	111
Table 5.26: Accuracy of the estimated pH using Landsat 8 for Umdloti Estuary.....	114
Table 5.27: Accuracy of the estimated pH using Sentinel-2 for Umdloti Estuary.....	115
Table 5.28: Accuracy of the estimated pH using newly generated estimation algorithms for Umdloti Estuary.....	116

## List of abbreviations

Abbreviation	Meaning
ASTER	Advanced Spaceborne Thermal Emission and Reflection Radiometer
BOD	Biological oxygen demand
CDOM	Coloured dissolved organic matter
Chl-a	Chlorophyll-a
cm	Centimetres
CO <sup>2</sup>	Carbon Dioxide
CWT	Clean Water Team
DN	Digital numbers
DO	Dissolved oxygen
EC	Electrical conductivity
EPA	Environmental protection Agency
ESA	European Space Agency
ETM+	Enhanced Thematic Mapper Plus
ExG	Excess green
GIS	Geographical Information System
GPS	Global Positioning System
ha	Hectares
HPLC	High performance liquid chromatography
IWRM	Integrated Water Resources Management
IWRMPJVN	Integrated Water Resources Management Plan Joint Venture Namibia
JTU	Jackson turbidity units
l	Litres
LDCM	Landsat data continuity mission
LST	Land surface temperature
m	Metre

$\text{m}^3.\text{S}^{-1}$	Metres per second
mg	Milligrams
ml	Millilitres
mm	Millimeters
NASA	National Aeronautics and Space Administration
NBA	National Biodiversity Assessment
NDVI	Normalized difference vegetation index
NGO	Non-governmental organization
NOAA	National Oceanic and Atmospheric Administration
NRAVI	Normalized ratio aquatic vegetation index
NTU	Nephelometric Turbidity Unit
OLI	Operational land imager
Oxfam	Oxford Committee for Famine Relief
pH	Potential of hydrogen
POEs	Permanently open estuaries
ppm	Parts per million
ppt	Parts per thousand
PSU	Practical salinity units
R	South African Rand
$R$	TOA reflectance
$R^2$	Coefficient of Determination
RAVI	ratio aquatic vegetation index
RHP	River Health Programme
RMSE	Root Mean Squared Error
$R_{rs}/R_{rs}$	Remote sensing reflectance
SDD	Secchi disk depth
SEE	Standard Error of Estimate
SST	Sea surface temperature



SWIR	Shortwave infrared
TDS	Total dissolved solids
TIRS	Thermal infrared sensor
TM	Thematic mapper
TOA	Top of atmosphere
TOCEs	Temporary open-closed estuaries
TSM	Total suspended matters
UNESCO	United Nations Educational, Scientific and Cultural Organization
UNICEF	United Nations Children's Fund
USEPA	United States Environmental Protection Agency
USGS	United State Geological Survey
WHO	World Health Organisation
µg	Micrograms
µS	Micro-Siemens
°C	Degrees Celsius

## CHAPTER ONE: INTRODUCTION

### 1.1) Background

Water is the Earth's most precious resource. Comprising around 70% of the planet, life without water would not be possible as it is so today. It is therefore natural that water-based environments comprise some of the most ecologically important features on Earth. Wetlands are a broad and significantly important sub-grouping of these water-based environments. Wetlands are defined by Ramsar as: "areas of marsh, fen, peatland or water, whether natural or artificial, permanent or temporary, with water that is static or flowing, fresh, brackish or salt, including areas of marine water the depth of which at low tide does not exceed six metres" (Medwet, 2017). These wetlands form some of the most ecologically important and productive landscapes on the planet (McLusky and Elliot, 2004). The importance of these areas is so great that though they occupy less than 3% of the globe, they provide around 40% of all renewable ecosystem services (Zedler and Kercher, 2005). Some of the globally significant services provided include biodiversity support, water quality improvement, flood abatement and carbon management (Zedler and Kercher, 2005).

Estuaries fall within the wetland grouping and form on the transition zones between river and seawater. Estuaries differ from other wetlands in that they often display larger variations in environmental variables. These variables, such as salinity, temperature and water levels, vary throughout the day or seasonally and are influenced by factors such as the state of the estuarine mouth, waves, tides and riverine input. The variation of these factors largely control the functioning of the estuary and the quality of ecosystem services the estuary may provide. Essential estuarine services include the provision of nursing grounds and highly productive habitats for a variety of fish, plants and birds amongst other types of wildlife (Klemas, 2011); the acting as a buffer against destructive coastal threats such as tsunamis and storm waves (Morris *et al.*, 2002) and direct use values in the form of aquaculture, recreational, cultural and water storage purposes (Clarkson *et al.*, 2013). Estuaries therefore form an essential ecosystem to a great many organisms. The importance of estuaries to humans is no different. In South Africa alone the revenue generated through fishing in and around estuaries was estimated to be around R1.2 billion in 2011 (Van Niekerk and Turpie, 2012). It is therefore of paramount importance to maintain the healthy functioning of estuaries.

## 1.2) Problem contextualisation and justification

Despite this need to maintain the health of estuaries, they are highly vulnerable environments. This vulnerability has led to estuaries and their surrounding wetlands being considered amongst the most threatened ecosystems on the planet (Butchart *et al.*, 2005). In South Africa this story is no different. Discounting the large St Lucia Estuary, only around 10 - 14% of the area comprising South African estuaries are sufficiently protected (Driver *et al.*, 2012). Within the eThekweni municipality itself, the River Health Programme (RHP) found that only two estuaries could be considered as experiencing normal natural conditions while around seventeen were considered to be in poor condition (Forbes and Demetriades, 2008). Marshes and other wetlands types that often form around estuaries are faring no better. Large amounts of these areas have already been devastated in the past as they were often associated with being rich farming and grazing lands. This led to their subsequent draining and over utilisation, resulting in over 50% disappearing (Driver *et al.*, 2012).

The factors leading to the disappearance of estuaries are called stressors. These stressors are mostly anthropogenic in origin and come from three main sources: 1) introduced by activities that take place in and around the estuary 2) through changes in the riverine flow to the estuary and 3) through land use changes in the catchment areas that feed the estuary disappearing (Driver *et al.*, 2012). These may take on forms such as local dredging, pollution, overexploitation and agricultural or residential land use change. This all ultimately results in fragmentation and habitat destruction (Klemas, 2011; Driver *et al.*, 2012). In future, these dangers to estuarine health are only likely to increase. Massive changes associated with continued climate change such as alterations in temperature, precipitation and rising sea levels may eventually lead to catastrophic habitat destruction (Titus *et al.*, 2009).

Due to these dangers faced by estuaries, there is now a great drive towards the protection of these areas within South Africa. Historically, South Africa has often been regarded as one of the forefront nations concerned with water reform and management as shown by its Integrated Water Resources Management (IWRM) program (Movik *et al.*, 2016). Proper water quality assessments and monitoring form some of the most important methods in the management of water resources and water-based ecosystems (Fichot *et al.*, 2015). Monitoring allows for protection plans to be put in place to safeguard these important environments (Klemas, 2011). This monitoring of estuaries has traditionally been done through on the ground measurements and the collection of water samples. However, these methods are often time consuming and

study areas may be far or otherwise difficult to access. Costs are also usually very high and this especially has limited the ability of monitoring systems across Africa and many other nations (IWRMPJVN, 2010). Finally, monitoring projects are severely limited in scale as costs often increase exponentially as area increases, often leading to a lack of testing being done to suitably check water quality.

One way to overcome these monitoring disadvantages is through the use of remote sensing imagery. Important water quality indicators such as chlorophyll-a (chl-a), turbidity, temperature and nutrients all directly change the optical properties of water bodies (Fichot *et al.*, 2015). This apparent change allows for the development of remote sensing techniques to aid in the estimation of these various physico-chemical parameters. Using remote sensing methods is both faster and allows the estimation of these parameters over a continuous area unlimited in size on a repetitive basis (Hellweger *et al.*, 2004; Somvanshi *et al.*, 2012). It may also end up being much cheaper as it eliminates expensive testing and transport costs. Despite the great potential for remote sensing methods to form the perfect monitoring systems, they are not without their own issues. The fact that accuracy of water quality estimation through remote sensing is often not sufficiently precise and needs to be used together with in situ sampling is one of these issues (Gholizadeh *et al.*, 2016).

With South Africa already having many estuaries in poor condition and at risk of getting worse, it is important to determine the ability of free and easily accessible remote sensors in obtaining data relating to the health of these systems. Kwazulu-Natal is home to 76 different well studied and researched estuaries. These include the St. Lucia (the largest in southern Africa), Durban Bay and Mpenjati estuaries amongst others (Mann *et al.*, 2002). Many are threatened. The Umdloti Estuary is one such threatened estuary. Here, the mouth of the Mdloti River forms an estuarine environment near the town of La Mercy, with patches of wetland supported directly up river. The estuary has had a poor history with regard to ecosystem health and has often been classified as being in a poor-fair condition (Van Niekerk and Turpie, 2012). The Mdloti river itself also passes several residential areas along the way and in the past has been particularly vulnerable to pollution from plastics and industrial effluents which all flow into the Umdloti Estuary (Naidoo *et al.*, 2015).

The vulnerable Umdloti Estuary in South Africa therefore presented the perfect opportunity in assessing the ability of remote sensing methods for the estimation of water quality and health. This study aimed to compare the reliability of remote sensing imageries and algorithms in their

ability to accurately estimate physico-chemical parameters within the Umdloti Estuary. Algorithms were also modified in this study to try and improve on this estimation. This allowed for a determination as to whether the convenience and accuracy provided by remote sensing imagery could be considered superior and as a suitable replacement for in situ methods. Through determination of these parameters, the water quality and health of the estuary was inferred and possible solutions as to what actions may be necessary to ensure its continued health given.

### **1.3) Aims and objectives**

**Aim:** To determine the accuracy of using Landsat 8 and Sentinel-2 remote sensors in determining water quality over winter and spring in the Umdloti Estuary.

**Objectives:**

1. To determine in situ the physico-chemical parameters in the Umdloti Estuary during winter and spring seasons
2. To assess physico-chemical parameters using Landsat 8 and Sentinel-2 in the Umdloti Estuary during the spring and winter seasons.
3. To determine the overall water quality health of the estuary based on the retrieved physico-chemical parameters.

### **1.4) Chapter sequence and summation**

**Chapter 1** - The first chapter provides a basic introduction relating to estuaries as well as the major threats that are faced by them. The potential of remote sensing and its applications for the monitoring the health of estuaries is also provided. Finally, the overall aims and objectives to be accomplished and investigated by this study are given.

**Chapter 2** - Chapter 2 provides a literature review that focuses on various aspects associated with the study. This includes an in-depth analysis on what estuaries are and some of their characteristics, how they are classified, their importance to both nature and humanity and finally threats to their survival. Also explored are the various physico-chemical parameters and how they are collected both traditionally and using remote sensing, along with what effects they have on water quality.

Chapter 3 - Chapter 3 covers detailed descriptions of the study area. This includes a general overview of the climatic, biological, geological, hydrological and other general aspects relating to the Umdloti Estuary. A map of the study area was also provided.

Chapter 4 - Chapter 4 covers the various methodologies used for both the Landsat 8 and Sentinel-2 estimation of physico-chemical parameters. This includes detailed descriptions of the in situ, laboratory and remote sensing methods and processes used in physico-chemical retrieval and estimation. Finally, the steps taken during accuracy assessment are also given.

Chapter 5 - Chapter 5 consists of the displaying and describing of the results that were obtained from the following of methodology. This chapter includes tables on the physico-chemical data that were retrieved in situ and those estimated through remote sensing algorithms. This chapter also includes accuracy assessments as well as distributional maps for each parameter.

Chapter 6 - The final chapter involves a discussion of the findings that had been obtained over the course of the study. This discussion is supported by relevant literature. This chapter also identified constraints experienced by this current study and provided recommendations on actions to be taken. Finally, this chapter also provides a suitable conclusion for the study.

## CHAPTER TWO: LITERATURE REVIEW

### 2.1) Introduction

This chapter provided a concise theoretical review and background of the concepts that were related to the core focus of this study. This began with a review on the general information, classification, importance and threats relating to estuaries both globally and in South Africa. Thereafter, the review focused on the various physico-chemical parameters and how these parameters affected the water quality health as well as how they had been extracted both traditionally and through remote sensing methods.

### 2.2) Estuaries

#### 2.2.1 *General characteristics*

Estuaries were defined in a South African context by Day (1980), as: “a coastal body of water in intermittent contact with the open sea and within which sea water is measurably diluted with fresh water from land drainage”. Estuaries are found worldwide at places where both rivers and seas meet. As a result they share a mixture of characteristics with both of these adjoining water bodies (Savenije, 2006). These include mixtures of flow direction (both towards and away from the ocean), water storage (estuaries both transport and store water) and salinity (usually a mixture of salty and fresh water called brackish water). This mixing of two usually completely segregated environments, along with their direct connections with the sea, land and rivers, result in estuaries forming highly dynamic and ecologically unique ecosystems. In fact, estuaries form some of the most ecologically important features on the planet (NOAA, 2017). These environments present homes to a variety of unique floral and faunal communities, all specially adapted to thriving in the highly dynamic brackish habitat (NOAA, 2017). They also provide an array of essential ecosystem services such as nurseries or breeding grounds.

Estuarine dynamics are highly influenced by their neighbouring water bodies. Influences include riverine influences, the influx of salt water and oceanic tides and waves (Savenije, 2006). Freshwater is obtained through land drainage which flows into rivers and eventually into estuarine systems. This dilutes salinity whilst also providing nutrients and sediments. All oceanic influences are heavily regulated by the state of the estuarine mouth, which helps determines whether estuarine water will be more riverine, brackish or salty (van Niekerk, 2007).

The presence of the estuarine mouth is a unique characteristic of estuaries. The mouths of estuaries with large adjoining rivers usually form the site of important commercial ports such as those found in New York, Tokyo, San Francisco, London and Buenos Aires (Trujillo and Thurman, 2011).

Due to all these influences, estuaries often display a larger variation with regard to physico-chemical parameter concentrations than most other environments. The variations within these physico-chemical parameters act as strong selective pressures as to what organisms are able to survive and thrive within estuarine systems, therefore dictating estuarine “health”. One such variation characteristic of almost any estuary are the large variations that may be found in their salinity (Trujillo and Thurman, 2011). Salinity may range from 0 practical salinity units (PSU) at the point where the river runs into the estuary to well over 35 PSU at the estuarine mouth where the boundary of the ocean and estuarine waters are found (NOAA, 2017). However, salinity may massively decrease or increase depending on whether the mouth is open and on the flow of fresh water into the estuary. Maintaining these dynamic physico-chemical parameter ranges is therefore paramount to maintaining estuarine health.

### *2.2.2 Classifications of various estuary types*

Estuaries are classified in several ways. One method of classifying estuaries is through their geomorphological origin (NOAA, 2008). The majority of estuaries that are present today were formed around 18 000 ago due to the massive 120 m sea level rise that accompanied the end of the last ice age (Trujillo and Thurman, 2011). The most common type of estuary are those that form as a result of the drowning of river valleys (Trujillo and Thurman, 2011). Here, the sea level has risen much higher when relative to the lands rise. Fjord-type estuaries form when glaciers that were present during Pleistocene times created deep and wide U-shaped valleys (Savenije, 2006). In present times these glaciers have all already been melted and the resulting low valleys allow for the flow of the sea into it. This allows for the salt water to be able to move into river valleys, resulting in an estuary. These types of estuaries are also sometime called coastal plain estuaries (Trujillo and Thurman, 2011). Bar-built estuaries on the other hand are estuaries that form as a result of where the deposition of sediment has separated shallow estuaries from the sea (NOAA, 2008). These sand bars are deposited through wave action and occur parallel to shore. They are also called lagoon-type estuaries. Finally, tectonically produced estuaries are those which are formed by the subsistence of land due to faulting,



landslides and volcanoes (NOAA, 2017). These are only found in areas with tectonic activity. Various examples of geomorphological estuaries are displayed in Figure 2.1.

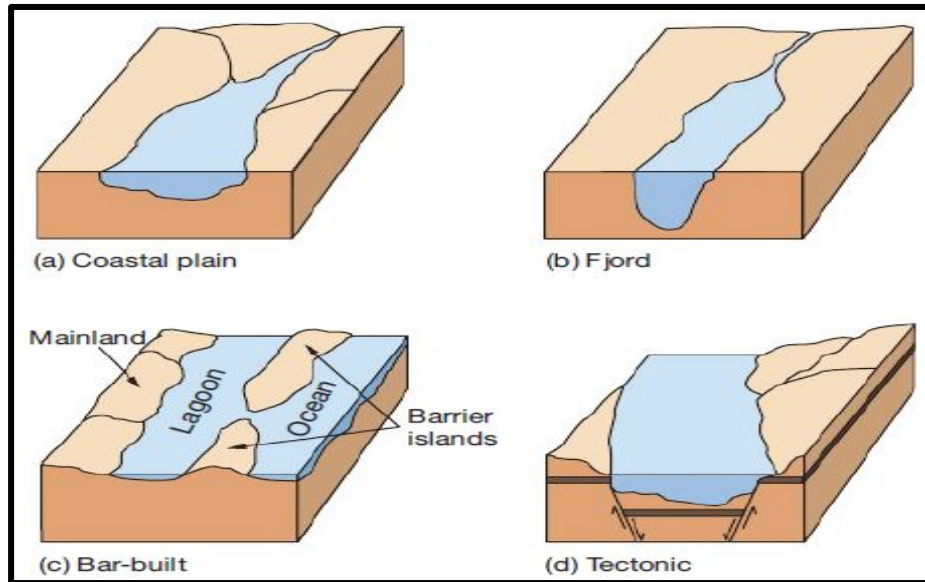


Figure 2.1: Generalised morphology for estuaries classified through various geomorphological methods (Trujillo and Thurman, 2011).

It is also possible to classify estuaries based not only on their origin but also through how water circulates through them. The method of mixing of both the fresh and salt estuarine water can result in greater variation of physico-chemical parameters across the estuary (Trujillo and Thurman, 2011). This is because salinity plays a major role in controlling the density of water and therefore the functioning of the estuary (Ohrel and Register, 2006). Major or minor differences in density between two groups of water may result in the development of a cline or allow for the free mixing of water respectively, greatly affecting the distribution of substances dissolved within water such as oxygen or nutrients. Trujillo and Thurman (2011), notes that there are four types of estuaries that can be classified based on water circulation. These include vertically mixed estuaries, slightly stratified estuaries, highly stratified estuaries and salt wedge estuaries. A vertically mixed estuary is an estuary that is shallow, low-volume estuary and where water flows directly from the river head to estuarine mouth (Trujillo and Thurman, 2011). In this type of estuary, salinity increases as one travels from the river head to estuarine mouth (due to the influx of salty sea water). Salt water and fresh water mix evenly and this results in salinity being the same as top water through all depths. A slightly stratified estuary is a generally deeper estuary where salinity increases as one travels from the head toward the mouth

(NOAA, 2008; Trujillo and Thurman, 2011). The difference here is that the water separates into two layers, with one is the less-salty and dense (forming upper water and originating from the river), whilst the other layer is the both salty and dense (forms lower water and originates from the ocean). This results in a net surface flow of low salinity water towards the mouth and a net surface flow of higher salinity water towards the head. A highly stratified estuary consists of deep estuary where the water salinity of the upper layers increases until about the same as sea water from head to mouth (NOAA, 2008; Trujillo and Thurman, 2011). The deep water layer on the other hand remains at roughly uniform salinity through the estuarine area. This results in the formation of a halocline and prevents much mixing of denser bottom waters and less dense top water. Finally, a salt wedge occurs when salt water from the ocean penetrates deep into the estuary towards the river mouth (forming a wedge) (NOAA, 2008; Trujillo and Thurman, 2011). This type of estuary is characteristic of deep and high volume rivers. Top water is the same salinity as river water from head to mouth. However, a strong halocline develops in the lower waters, with it being more developed nearest to the mouth of the estuary.

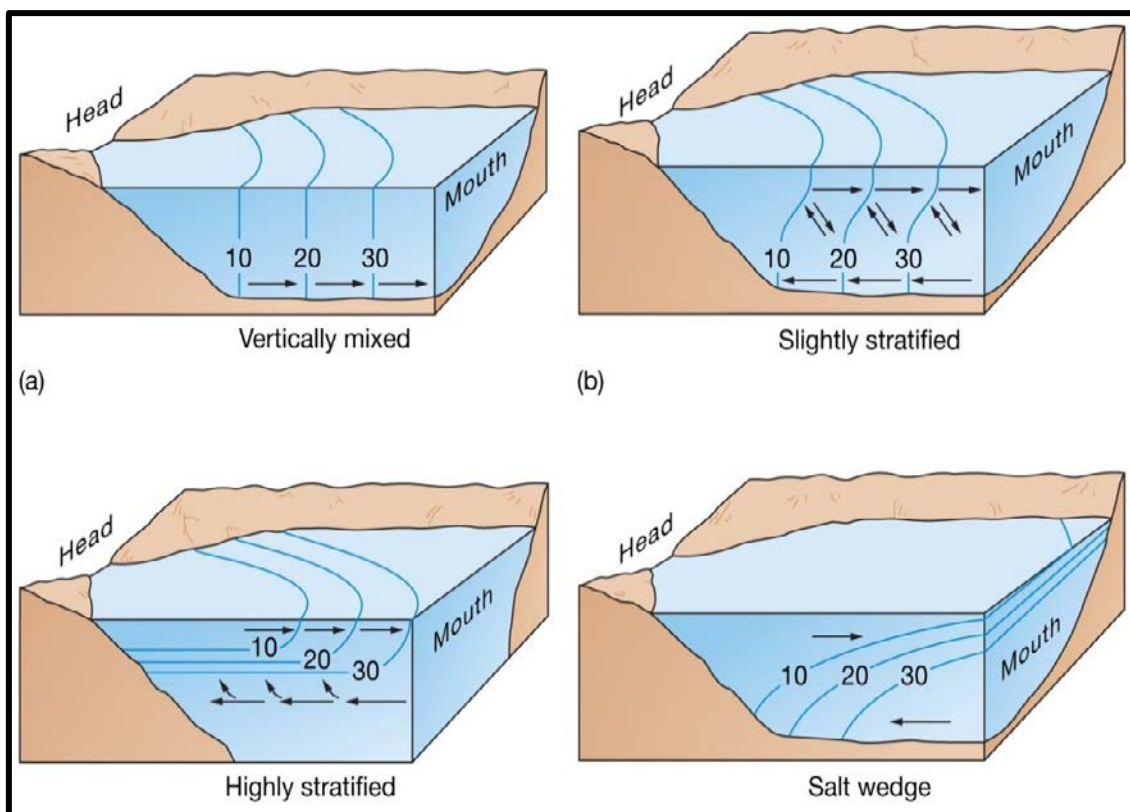


Figure 2.2: Generalised morphology for estuaries classified through various water circulatory methods (Trujillo and Thurman, 2011).

### 2.2.3 Importance of estuaries

Estuaries are amongst the most productive features on the planet and provide a variety of ecosystem services that benefit the world culturally, economically and ecologically (NOAA, 2008; Pinto *et al.*, 2016). The productivity of these environments is mostly due to the way in which the oceanic and riverine environments interact. This interaction comprised of the inflow of oceanic salt water and riverine fresh water contribute an abundance of productivity boosting sediments and nutrients (McLusky and Elliott, 2004; Savenije, 2006). Outputs of this productivity are expressed in the form of ecosystem services. Fisher and Turner (2008), described ecosystem services as the elements within an ecosystem which are used either actively or passively and are considered beneficial to humans or other organisms. Ecologically, many life forms such as fish, birds and marine mammals greatly rely on the estuarine environment for the provision of these services such as habitat, nutrition, breeding, nurseries and for migratory stop overs (Savenije, 2006; NOAA, 2017). This in turn also aids in their ability to support a high level of biodiversity (Trujillo and Thurman, 2011). Costanza *et al.* (1998), estimated that the value of services estuaries provided worldwide amounted to over 4.1 trillion dollars.

One of the most significant services estuaries provide is in the form of important breeding grounds and nurseries. Estuaries are therefore essential to the well-being of both fisheries and to the greater surrounding coastal areas (Trujillo and Thurman, 2011). The popularity of estuaries as nurseries is thought to be due to the sheltered protection of marine young from large predators or due to the provision of more abundant, varied sources of food and general good conditions that are required for growth (Beck *et al.*, 2001; Sheridan and Hays, 2003; Cabral *et al.*, 2007; Muller, 2017). Moore *et al.* (2016), noted the importance of estuaries in providing a nursery, nutrition and as a migration stopover point within the juvenile Pacific salmon life cycle. In the study, the Skeena River Estuary provided an important stop over as the juvenile salmon make their way out to the ocean from upriver. Some species spent as long as thirty days feeding within the estuary and grew between 0.2 - 0.5 mm a day (Moore *et al.*, 2016). This was a considerable size increase before venturing on into the ocean. The reliance of flatfish on estuaries as nursery sites has already being well established in literature (Riou *et al.*, 2001; Able *et al.*, 2005; Cabral *et al.*, 2007). Here, estuaries provided the usual benefits to juveniles whilst also offering beneficial biotic and abiotic factors such as reduced predation and suitable temperature and salinity levels (Cabral *et al.*, 2007). Juveniles of species that use the estuary as

a nursery such as the Pacific salmon are often later of great economic value as they recruit into adults on whom fisheries are based (Baran and Hambrey, 1999).

Estuaries play a vital role in maintaining fisheries around the world due to their unique habitat (Jordan and Peterson, 2012). Within the United States alone, over 50% of commercial fisheries landings were estuarine-dependent species, resulting in the creation of two million jobs and over \$117 billion contribution to the United States economy (U.S Commission on Ocean Policy, 2004). Jordan and Peterson (2012), determined that popular types of fish caught include salmon, perch, sturgeons, herrings, seatrout and eels. In addition Jordan and Peterson (2012), also identified that most of the world commercial crustaceans such as crabs, shrimp and oysters spend most, if not all of their life based within an estuary.

Wetland features such as salt marshes and mangroves are also closely linked to the presence of estuaries. These act to purify the water through the removal of sediments, nutrients and pollutants such as pesticides and herbicides before their entrance into estuaries (Mitsch and Gosselink, 2007). This is due to the fact that as water passes through these wetlands, the friction from upright vegetation aid to slow down the flow of water, allowing for settlement of sediments (Morgan *et al.*, 2009). This positively impacts on both human health and the health of surrounding ecosystems. Breaux *et al.* (1995), determined that the savings generated through the filtering of wastewater by the American southern Louisiana marsh swamps was estimated to be around \$1962 ha<sup>-1</sup> to \$37500 ha<sup>-1</sup>. These wetlands also form some of the most biodiversity rich ecosystems on the planet (USEPA, 1997; Trujillo and Thurman, 2011).

Estuaries may even play a substantial role in ecoengineering and recreating environments that have been damaged and degraded through human activities. Elliott *et al.* (2016), examined several cases where ecoengineering was taking place. Whilst some environments were not able to be created at all or at least sustainably, it was noted that sustainable successes were possible and would play important future roles in both wetland and estuarine management.

In addition they help combat global warming through their carbon sequestration. Accelerated rates of global warming through the emission of greenhouse gases may also be partially mitigated through the safekeeping of estuaries. Calculations performed by Campbell (2010), show that on average, estuaries sequester around 180 000 tonnes of atmospheric carbon per year. In addition, estuaries and their associated wetlands do not substantially release the greenhouse gas methane as is often the case with other types of wetlands (Campbell, 2010).

Estuaries provide important areas for recreation and tourism (Barbier *et al.*, 2011). This is often due to the natural beauty displayed by estuarine environments and activities available (de Sousa *et al.*, 2014). Fishing, swimming, bird watching, diving and water skiing are just some of the popular activities that may take place (Harris *et al.*, 2016; Pinto *et al.*, 2016). Activities such as dolphin watching and feeding within estuaries also provide an important source of income to local communities (Garrod and Wilson, 2004). This is evidenced in the Cananéia estuary in Brazil with estuarine tourism displaying an increasing trend in popularity (Filla and Monteiro-Filho, 2009). Higher pollution levels within estuaries often discourage its recreational usage. Pinto *et al.* (2016), found the Mondego Estuary in Portugal was swum in more often by non-locals who generally had little knowledge of pollution levels within the estuary. The study also found that as knowledge of the true extent of pollution within the estuary increased, less people considered visiting the estuary for recreational purposes.

Barbier (2014), also mentions the value attached to estuarine areas in the mitigation of storm damage. When there are instances of flooding, estuaries act to absorb and store a large amount of excess water (USEPA, 1997). In the wake of the devastation from the 2004 Indian Ocean tsunami and the 2005 Hurricane Katrina, the loss of estuarine buffers protecting vulnerable coasts against destructive storms was first highlighted (Arkema *et al.*, 2013). There has since being a considerable collection of evidence supporting the ability of coastal estuaries, mangroves and marshes amongst others in attenuating waves and buffering winds (Barbier *et al.*, 2008, 2011; Gedan *et al.*, 2011; Shepard *et al.*, 2012). This is due to their ability to attenuate or reduce the height of waves and storm surges as they approach shore (Barbier, 2014). This can be put down mainly due to their reticulated structures that act as barriers or through the presence of vegetation that provides friction against waves and winds (Gedan *et al.*, 2011; Shepard *et al.*, 2012). Although difficult to put a precise value on the protection offered, hurricane simulations run by Barbier (2014), on the United States Gulf Coast gave an estimated \$23 ha<sup>-1</sup> to \$463,730 ha<sup>-1</sup> of savings in damage through the presence of estuaries and other natural protective coastal features during storms.

#### 2.2.4 Threats to estuaries

Since the dawn of the earliest civilisations, humanity has shared a special relationship with coasts. In 1998, it was estimated that around 61% of the world's population lived within coastal zones or near estuaries (Alongi, 1998). More recently Bianchi (2007), speculated that by 2025, this figure could be expected to rise to around 75%, with the vast remainder of people living

around major rivers. Estuaries in particular are popular sites for human settlement. Of the world's 32 largest cities, 22 are located on estuaries (Ross, 1995). It is therefore unsurprising that human activities greatly impact on estuarine health, leaving them one of the most threatened ecosystems on the planet (NOAA, 2017). With the world's population expected to exceed over nine billion by 2050, this will only likely lead to increases in the already significant pressures experienced by estuaries due to subsequent increases in economic activities, pollution and demand for water (WHO/UNICEF, 2010).

In order to determine what constitutes an unhealthy estuary, there needs to be a definition of a healthy one. Attempting to define what constitutes a healthy estuary is difficult but can be visualised through what characteristics an estuary should ideally possess. Harris *et al.* (2016), provides an overview of what many of these characteristics should be. A healthy estuary should be one that maintains water quality that is beneficial to both people and other organisms that live within an estuary. It should also provide a natural buffer against storms and floods whilst maintaining high levels of biodiversity through the provision of unique habitats. Finally, any animal species that require the use of estuaries as breeding or nursery grounds should have access and be able to prosper within the estuary. Estuaries exposed to conditions that negatively alter its ability to meet these criteria can be considered to be experiencing a health decline.

The most significant threats facing estuaries are those that are anthropogenic in origin. Anthropogenic activities within estuaries lead to major decreases in water quality, the loss of habitat or its alteration and the diminishment of natural resources (Kennish, 2002). Activities that cause issues include tourism related activities, urban land development and reclamation, waste disposal and pollution, agriculture and aquaculture, shipping, invasive aliens and both recreational and commercial fishing (USEPA, 1997; Kennish, 2002).

One of the biggest threats remains inappropriate land usages such as the conversion of estuaries and surrounding wetlands into agricultural lands. This results in immediate habitat destruction and fragmentation and leads to its unsuitability for supporting plant and animal life. Further, the damage done through these actions is often irreparable. Good *et al.* (1998), found that in the United States, around 38% of estuaries were lost to these activities alone. In some areas, the habitat loss due to these activities was as high as 60% (NOAA, 2017). Besides the habitat loss, these activities may lead to increases in sediment, nutrient and pollution levels resulting in possible eutrophication, hypoxia and anoxia (Robb, 2014). This in turn alters estuarine productivity and trophic structure (Crossland *et al.*, 2005).

The construction of dams often do not consider the downstream economic and environmental consequences of this construction (Harris *et al.*, 2016). Once built, these dams often lead great reductions in the nutrient loads carried by rivers (Ochiewo *et al.*, 2002). This could clearly be seen from the reduced landings by commercial fisheries based in the Sofala Bank fishery off of Mozambique. The alteration of freshwater flow here resulted in an estimated loss of between 10 to 20 million dollars in fish catches (Harris *et al.*, 2016). The construction water or waste carrying pipes may also lead to significant removals of vegetation and the degradation of riparian areas.

The large scale use of river water for farming or forestry plantations may lead to significant reductions in the volume of water received by the estuary. This decreased flow may result in the alteration of mouth functioning (resulting in a commonly closed state). This in turn can lead to decreased salinities, increased sedimentation and back-flooding (Driver *et al.*, 2012).

Commercial and recreational fishing has also been shown to alter the composition of species living within the estuary due to the preferential removal of targeted species (Kennish, 2002; Robb, 2014). This is especially harmful when the estuaries serve as important breeding or nursery grounds. The collection of usually resilient “bait organisms” (used by fisherman to lure fish into biting their hooks) is also harmful as through the use of tools such as spades, the introduction of sediment into the suspended water and habitat destruction may become a problem (Wooldridge, 2007). The removal of popular bait species such as the sand and mud prawns in South African estuaries may also impact on the higher trophic levels. This was shown in the Swartkops estuary where consumption by predators such as local bird life exceeded levels removed through bait collectors (Hanekom, 1992).

Pollution is another worldwide major threat to estuaries, with it being especially damaging to their water quality. Traditionally, humanity has viewed estuaries and waterways as dumping sites for wastes. Despite increasing public awareness and legislations, this pollution continues to pose a large and growing problem (Driver *et al.*, 2012). Pollution sources include agricultural products that enter streams through runoff or irrigation (such as pesticides, herbicides and fertilisers), waste water treatment works (WWTW) that end up discharging effluents directly into the river, factories and industries that discharge industrial effluent such as oils and heavy metals and storm water runoff which often carries contaminants such as litter, toxins and untreated sewage (Robb, 2014). Pollution may also negatively alter the nutrient loadings, allow for the introduction of chemical contaminants and facilitate the spread of pathogens within the

estuary (Kennish, 2002). The Umdloti Estuary has itself being a victim of pollution with many plastic contaminants plaguing the water body (Naidoo *et al.*, 2015).

Sea level rise and climate change are major long term threats to estuaries (Harris *et al.*, 2016). Scavia *et al.* (2002), points out some of the ways in which climate change and accelerated levels of global warming are impacting on estuarine health. Already one of the greatest threats to estuaries, increased levels of eutrophication are likely to occur due to an increase in nitrates from an altered nitrogen cycle and increased temperatures. Just before the turn of the millennium, Bricker *et al.* (1999), found that around half of all estuaries in the United States showed signs of excessive eutrophication levels. Increases in temperature will lead to the increased acidification of oceans and estuarine waters, inhibiting the growth of shelled organisms and increasing the susceptibility of organisms to pollution via trace metals (Feely *et al.*, 2010; Okey *et al.*, 2012).

Due to sea level rises associated with the global warming phenomenon, large portions comprising coastal zones will in future end up flooded. This will result in increased salt water intrusion into estuaries and rivers and the forced retreat of these coastal environments (Donnelley and Bertness, 2001). Even estuaries with surrounding salt marshes (which allow for the accumulation of sediment resulting in an elevation buffer against sea level rise) are likely to be thrown out of equilibrium as sea level rise accelerates (Morris *et al.*, 2002). Li *et al.* (2014), found this to already be presenting a problem to one of Shanghai's most important water storage estuaries, predicting future problems with obtaining freshwater as the system becomes more saline. Rises in both temperatures and salinity are likely to affect the productivity of estuarine ecosystems as a result of changes in the distribution of sensitive suspension feeders such as oysters, mussels and clams (Scavia *et al.*, 2002). The increase or decrease of these important organisms will results in massive changes to phytoplankton abundance as well as the water clarity (Scavia *et al.*, 2002). A change in precipitation patterns and associated reduced freshwater inflow may also lead to a decrease in the areas covered by estuaries or the increased influx of salinity into the system (Moore *et al.*, 1997).

The introduction of aquaculture and mariculture to both estuarine and riverine areas present their own unique threats. Runoff and effluents carrying both the excrement and nutrients used to raise aquacultural species often end up in rivers and estuaries. These often lead to negative impacts. Glibert and Terlizzi (1999), found that elevated urea levels due to the presence of aquaculturally grown striped bass led to increases in the blooms of dinoflagellates within east



coast American estuaries. These present a potential danger in the forms of eutrophication and red tides. Estuarine habitat structures are also impacted upon through the introduction of aquaculture. Sea grasses, salt marshes and other local structures have been on a worldwide decline with aquaculture thought to play a role (Waycott *et al.*, 2009; Dumbauld *et al.*, 2015). Oyster based aquaculture has been shown to induce steep declines of over 50% in Willapa Bay seagrass density and size, impacting heavily on these structures (Wagner *et al.*, 2012). Aquaculture may not always necessarily lead to a decrease in local fish species. Dumbauld *et al.* (2015), found little difference within Willapa Bay in juvenile salmon distribution in modified and natural estuarine areas.

Finally, the threats posed by alien invasive species are itself significant. Species that are farmed and able to escape may lead to the competitive extinction of many local species as well as the introduction of new diseases and genetic combination, leading again to population reductions or species local extinction. The Kowie Estuary faced such an alien invasion from Largemouth bass in South Africa (Murray *et al.*, 2015). Due to its popularity as a sports fish, largemouth bass are common alien invasive to waters around the world, prompting much scientific study (Taylor *et al.*, 2015). Murray *et al.* (2015), found that the invasion of bass into the estuary and river put significant predatory pressures on the juveniles of marine fish species, leading to impairments in fish recruitment and possible future local extinction. Alien species may also be introduced through the release of ships ballast water, through their attachment on ships hull's and the illegal release of invasive species directly by humans (Zibrowius, 1991). Brackish water (such as that found in estuaries) has been shown to offer the highest probability of survival for aquatic invasive aliens (Paavola *et al.*, 2005). Gruszka (1999), found that estuaries are not only susceptible to alien invasions but may also provide stepping stones to the expansion of alien invasive along coastlines. Gruszka (1999), further added that the eradication of marine invasive aliens is often near impossible and comes at a high cost, further adding to the long term problems that will be faced by the estuaries. It is not only fish species that may invade estuaries. Tong *et al.* (2012), found that *Spartina alterniflora*, an alien invasive seagrass from North America was widespread amongst many Chinese estuaries and contributed to significantly increased levels of methane found within the estuaries. Methane is a greenhouse gas that may lead to increasing rates of global warming if entering the atmosphere.

### 2.2.5. South African estuaries

South Africa has 291 estuaries spread across the country's coastline, totalling a combined area of 171 046 ha (Nel *et al.*, 2011; Driver *et al.*, 2012; van Niekerk and Turpie, 2012). This area constitutes all that is needed for an estuary to maintain its functionality, including areas of open water, floodplains and salt marshes (Cilliers and Adams, 2016). These 291 estuaries were classified into 46 different types of estuarine ecosystems as determined by the National Biodiversity Assessment (NBA) (van Niekerk and Turpie, 2012). South African estuaries all fall within one of three biogeographical regions: cool temperate (16%), warm temperate (24%) and subtropical (60%) (Whitfield and Baliwe, 2013; Cilliers and Adams, 2016). Biogeographical regions differ greatly in both amounts and variability of rainfall received (van Niekerk and Turpie, 2012). Further secondary influences of the biogeographical regions include differences in river inflow, catchment sizes and shape (van Niekerk and Turpie, 2012). Of all the estuaries in South Africa, St Lucia Estuary is the largest and accounts for more than half of all the estuarine land (Driver *et al.*, 2012). This area was declared South Africa's first world heritage site and is home to a wide array of floral and faunal species. Similar to the ecological importance of St Lucia, other estuaries also positively contribute to South Africa. These estuaries play a major role in providing areas for fishing, recreation, animal breeding and nursery grounds as well as in the delivery of sediments used to build up beaches and nutrients important to food webs. However, anthropogenic pressures have for the past four decades had significant impacts on their health and functioning (Cilliers and Adams, 2016). Despite their importance and following a trend common globally, estuaries constitute one of the most vulnerable and threatened ecosystems within South Africa (Turpie *et al.*, 2002; Cilliers and Adams, 2016).

South African estuaries differ from one another due to several factors. These factors that contribute towards estuarine variability within South Africa include catchment sizes, gradients, riverine and marine sediments, different types of climates and the fluvial discharge from rivers (Cooper, 2001). Forbes and Demetriades (2008), placed South African estuaries in one of five types. Estuarine lakes are estuaries that exceed a water area of 1200 ha and usually form from drowned river valleys. These are usually separated from the sea by vegetated dunes. These areas may eventually become completely cut off from the ocean and lose all estuarine characteristics (such as in Lake Sibaya). However, they may also have temporary access to the ocean. St Lucia is one such example of an estuarine lake. Estuarine bays also exceed a water area of 1200 ha and are permanently linked to the oceans. These are characterised by the dominance of marine

species, high salinity and the presence of wetlands such as mangroves forming around the estuary. Durban bay is one such example. River mouths are estuaries that are dominated by riverine influences. These estuaries are characterised by low salinities, are usually permanently opened but have a small tidal prism and are dominated by riverine organisms. An example of this type of estuary is the uMkhomazi river mouth.

However, within South Africa there are two broad types of estuaries that dominate the country's coasts: Temporary open-closed estuaries (TOCEs) and Permanently open estuaries (POEs) (van Niekerk, 2007; Forbes and Demetriades, 2008). POEs generally require large catchment areas as well as a relatively high runoff that occurs throughout the year (van Niekerk, 2007). The volume of water within the estuary is also usually large enough for tidal influxes to maintain the open mouth conditions (van Niekerk, 2007). TOCEs on the other hand are identified through the isolation of estuarine and sea water through the formation of a sandy berm across the estuary mouth during certain periods of no or insufficient river inflow (van Niekerk, 2007). These estuaries stay closed off, until the period where their basins have been filled with sufficient water to breach through the berm. This breaching results in a flushing out of the water and sediments that have been collecting since mouth closure. Eventually an equilibrium between river inflow and tidal influxes is achieved. The major forces required to that maintain the conditions that are required for an open mouth can be reduced to river and tidal flow, whilst major closing forces can be considered to be due to sediment inflow as well as oceanic waves (van Niekerk, 2007). During periods of high intensity precipitation or storms, estuaries are usually opened whilst in other conditions they remain closed. Around 70% of South African estuaries have temporarily open-closed access between the river and sea systems (Whitfield, 1992).

Estuaries are recognised as being amongst the most productive ecosystems within South Africa (van Niekerk and Turpie, 2012). South African estuaries play a major role to both the economy and ecosystem through the provision of various ecosystem services and goods (Cooper *et al.*, 2003; Lamberth and Turpie, 2003; Turpie and Clark, 2007). Estuaries are considered places of beauty and are desirable locations for homes or visits. Areas surrounding estuaries often benefit financially from substantially higher rates and property values along estuarine shores (Breen and McKenzie, 2001). Economic activities related to estuary-based tourism may as well provide a considerable source of income to local communities (Breen and McKenzie, 2001).

One of the most significant functions South African estuaries perform is that of a nursery. It was estimated by Lamberth and Turpie (2003), that about 80 of the 160 fish that are found within estuaries are used by fisheries. Further, at least 60% of these fish are either entirely or partially dependent on the nursery functions provided by estuaries. Although significantly larger catches were made in the inshore waters when compared to estuarine catches (28 000 vs. 2 480 tons per annum), up to 83% of those catches are heavily dependent on estuaries (Van Niekerk and Turpie, 2012). The revenue generated through fishing these species provided a significant income estimated at R1.2 billion in 2011 (Van Niekerk and Turpie, 2012). Examples of popular estuarine dependent species include *Argyrosomus japonicus* (dusky kob), *Lithognathus lithognathus* (white steenbras) and *Carcharhinus leucas* (Zambezi/Bull sharks).

These estuaries also support the formation of around 90 000 ha of adjacent wetland habitat such as salt marshes and mangroves (Lamberth and Turpie, 2003). Areas such as these provide a wealth of raw materials to local peoples with it being estimated that vegetation harvesting from the St Lucia system alone generates over R4.7 million annually (Turpie *et al.*, 2005). These wetlands further serve as important areas for carbon sequestration. Within estuaries and wetlands, carbon is sequestered into the biomass making up these areas and into its soils (Crooks *et al.*, 2011). Wetlands surrounding estuaries have the added advantage of emitting negligible methane into the atmosphere (Van Niekerk and Turpie, 2012). This means estuaries and associated wetlands are important entities in mitigating the higher levels of greenhouse gases contributing towards global warming. South Africa possesses over 27 300 ha of salt marshes, mangroves, swamp forest, submerged macrophytes and sand and mud banks (Van Niekerk and Turpie, 2012). These all contribute towards carbon sequestration and produce comparatively negligible to low levels of methane in the process.

Estuaries may also serve as important buffers against both flooding and storm damage. South African estuaries provide around 61 000 ha of open water storage which function to collect water during flood events (Van Niekerk and Turpie, 2012). These perform significantly better at containing of floodwaters than ordinary river mouths. Evidence of these protective effects could be seen during the 2011 August floods near Slang Estuary, Oesterbaai (Van Niekerk and Turpie, 2012). Here, anthropogenic alterations to the estuary removed base flows and allowed erosion of surrounding sand dunes and reduction in water storage capacity of estuary. During the subsequent rainfalls, adjacent low-lying developments were flooded. Sandy berms that develop in front of over 75% of South African estuaries also protect coastlines from storm damage (Van Niekerk and Turpie, 2012). If any storm water has sufficient enough force to pass these

protective berms, they usually enter into the estuary and cause negligible damage to coastal developments.

The livelihoods of local communities may also be highly influenced through estuaries as explored by Van Niekerk and Turpie (2012). *Sarcocornia* and *Salicornia* are halophytes found within estuaries that may be utilised as either a food or fuel source. In South Africa, they are still underutilised but are fast becoming more popular. *Juncus kraussii* and *Phragmites australis* are local reeds that are used by local communities in the creation of baskets and mats. Mangroves that form around estuaries are also intensively harvested for either firewood or construction purposes, although this is done mostly illegally.

Despite the many significant benefits that estuaries provide in South Africa, they face a great number of threats. Flow modification is one of these threats and refers to either the increase or decrease in freshwater flow to estuaries. South African examples of decreased inflows include from direct abstractions (such as in Keurbooms Estuary), construction of dams (such as in the Orange and Palmiet Estuaries) and through the cumulative effects of small dams found within farms and local communities (such as in the Bushmans Estuary) (Van Niekerk and Turpie, 2012). Increases in the volume of inflow may be due to transfers between basins (such as in the Sundays estuary), through the addition of water from WWTW (such as in Mhlanga Estuary) and finally through the hardening of a catchment (such as that found within the Kuils Estuary) (Van Niekerk and Turpie, 2012). Reductions or increases in baseflows by as much as 50% may have significant impacts on the functioning of estuaries.

Another major threat is that of pollution and its impacts within South African estuaries. Municipal and industrial waste waters as well as storm and agricultural runoff's are through to be the largest land based contributors to estuarine pollution. These introduce excessive amounts of nutrients and toxins into the estuarine system, leading to negative impacts on estuarine life. Driver *et al.* (2012), identifies in particular the threat of future desalinisation plants as a particular problem in South Africa due to the brine effluents produced.

The overutilisation and exploitation of estuarine resources is another major threat. The overexploitation of fish species in particular may lead to changes in population size, biomass, sex ratios and the eventual recruitment collapse of a species from which there is little chance of recovery (Van Niekerk and Turpie, 2012). Around 18% of estuaries in South Africa currently face significant threats from extreme to moderate overfishing (Van Niekerk and Turpie, 2012).

Only around 14% of estuaries have no fishing pressures being placed on them (Van Niekerk and Turpie, 2012). In addition the collection of bait organisms within estuaries for the purpose of fishing may further add to its overexploitation. Over 84% of estuaries have bait collection pressure placed on them (Van Niekerk and Turpie, 2012). This is currently not a problem as bait populations have proven themselves to be resilient in the face of these pressures so far (Van Niekerk and Turpie, 2012).

Inappropriate land use developments have had a detrimental impact on many an estuary. In South Africa, there have been a substantial number of issues created through the building of bridges across estuaries. This may lead to stabilisation of the usually dynamic estuarine channels. During times of heavy flooding, this may lead to the concentrated erosion of sediments under the bridge, leading to changes in flow, habitat and biota. This was evident in the Uilkraals Estuary where the local bloodworm *Arenicola loveni* has disappeared from the upper reaches of the estuary after the construction of a bridge (Heydorn and Bickerton, 1982). Sand mining activities are also a particular problem, leading to high suspended loads and habitat destruction (Van Niekerk and Turpie, 2012). In Kwazulu-Natal, Van Niekerk and Turpie (2012), found that 18 estuaries supported sand mining operations and were vulnerable to these impacts. In total, only less than 10% of all estuaries found within South Africa appear to have no developmental pressures placed on them (Van Niekerk and Turpie, 2012).

The statistics generated in the 2011 National Biodiversity Assessment do not paint a pretty picture of estuarine health for South Africa (Driver *et al.*, 2012). Van Niekerk and Turpie (2012), reported a 10% reduction in the number of estuaries in an excellent condition over the course of 2004 to 2011. However, when considering estuarine area itself, the situation becomes more distressing. In 2011, it was estimated by Van Niekerk and Turpie (2012), that 85% of estuarine habitat could be considered to be in a poor to fair state. Although providing a substantial income to local government, estuaries are seldom considered to be a governmental asset due to the underappreciation of its goods and services provided (Van Niekerk and Turpie, 2012). This leaves little investment towards its sustainable management and protection (Lamberth and Turpie, 2003; Van Niekerk and Turpie, 2012). Only around 14% of South Africa's different estuary types are protected (Driver *et al.*, 2012). Despite a reasonably good value of over 60% of the total estuarine area in South Africa being protected, the vast majority of this area is found in the St Lucia estuary. Considering the area protected without the addition of St Lucia leaves only around 10% of the total area of South African estuaries are protected (Driver *et al.*, 2012). Further, even though the St Lucia estuary can be considered reasonably

well protected, it is still considered to be in an ecologically poor state. This is due to the separation of the Umfolozi River from Lake St Lucia as well as the other aspects such as droughts (Driver *et al.*, 2012). Due to its importance, much emphasis has been put on restoring St Lucia back to a good condition.

## **2.3) The physico-chemical components of estuarine health**

### *2.3.1 Role of Temperature in estuaries*

Physico-chemical parameters refer to both the physical and chemical components that make up a water body. Commonly measured physico-chemical parameters include dissolved oxygen, pH, temperature, salinity, chlorophyll-a and various nutrients amongst many others. These parameters play significant roles in the functioning of estuaries and other water bodies.

Temperature refers to the amount of heat the water within an estuarine body, mainly introduced through incoming solar radiation. Temperature within estuaries generally increases throughout the day as more solar radiation is received and decrease at night once the sun sets. Although it mostly follows this general pattern, larger variations in temperature may be caused by tidal actions and the open state of the mouth (Abowei, 2010). During high tides and open mouth condition, warm estuarine water is flushed out the estuary whilst colder ocean water enters (Abowei, 2010). Other sources increasing the temperature within estuaries include effluents entering into the water which may be introduced by industry. Temperature is the single most important abiotic factor as it controls the various biological, chemical and physical processes that occur within the water and surrounding air (Beitinger and Fitzpatrick, 1979; Gholizadeh *et al.*, 2016). As a result, simply determining the temperature of an estuary helps in understanding the state of health of the system as it greatly influences how fish utilise estuaries (Thiel *et al.*, 1995; Abowei, 2010; NOAA, 2012). The most important parameter temperature controls is the amount of oxygen that can be stored within water. An example of how this may affect the concentration is that water at 0 °C can contain up to 14.6 mg of oxygen per litre of water, but at 20 °C, it holds 9.2 mg of oxygen per litre (NOAA, 2012). This is a substantial difference in oxygen levels and affects the size and abundance of organisms that may inhabit the estuary. Temperature is also essential in determining what types of organisms are able to survive in the water as each organism has optimal ranges in which it thrives. A change of more than 1 °C to 2 °C may cause massive thermal stress to animals and plants. Due to its importance in controlling water density, temperature also plays a major role in the mixing distribution of contaminants,

oxygen and nutrients throughout the water column (Trujillo and Thurman, 2011). Temperature may also lead to a decline in the health state of estuaries. As well as limiting both oxygen and nutrient distribution, depending on the type of fish inhabiting the estuary lower temperatures may likely lead to lower rates of growth and metabolism (Abowei, 2010). Nowicki (1994), also found that temperature exponentially increases the rate of denitrification, increasing the availability of nitrogen to estuarine systems. This may lead to potentially fatal algal blooms and subsequent eutrophication. Kurobe *et al.* (2018), found an interesting linkage with global warming and future increased temperatures and its effects on possible biotic life. In their study, it was found that during drought seasons and periods of high temperature in San Francisco estuary, cyanobacterial blooms and the subsequent release of toxins resulted in a significantly high mortality rate in fish embryos. The rate of photosynthesis, metabolic rate and susceptibility of organisms to disease is also influenced by temperature (USEPA, 1997). The optimal temperature within an estuary depends on the species and life stages of organisms inhabiting the estuary, but generally extreme lows and highs lead to decreased health within these systems (Ohrel and Register, 2006).

### *2.3.2 Role of Turbidity and secchi disk depth (SDD) in estuaries*

Turbidity may refer to the clearness of water, with turbid waters more likely to have passing light rays scattered or absorbed. Secchi disk depth is very similar to turbidity as both indicate a waters clarity. A waters clarity or turbidity is determined by sediments from mud, silt, sand and clay, dead plant and animal remains, microorganisms such as bacteria or algae and chemical precipitates (Ohrel and Register, 2006). These greatly affect how much light is able to penetrate and move through the water. Turbidity can therefore be an important parameter when studying the health of estuaries as they affect the depth at which photosynthesis can take place as well as affecting the colour of the water (Gholizadeh *et al.*, 2016). Organisms such as algae and plants are therefore heavily dependent on the water turbidity. By monitoring turbidity, it may also indicate other problems such as excessive shoreline erosion or riverine erosion. Sediments making up turbidity may also clog the gills of fish, smother basal organisms such as oysters (usually killing them) and reduce growth rates as well as resistance to disease amongst estuarine organisms (Ohrel and Register, 2006). Turbidity may also impact on the amount of DO within the estuary. Generally, higher turbidity blocks out sunlight from reaching phytoplankton, increase the temperature of the water through solar absorption and indicate the presence of a large amount of detritus (Ohrel and Register, 2006). All these factors lead to reductions in the amount of stored DO. Turbidity's generally considered healthy are low, with acceptable



drinking water having turbidity's below 1 Nephelometric turbidity unit (NTU) (Fundamentals of environmental measurements, 2016).

### *2.3.3 Role of Salinity, Total dissolved solids (TDS) and Electrical conductivity (EC) in estuaries*

Salinity is one of the most important parameters in any oceanic environment. Whilst the general standard for measuring salinity was in parts per thousand (ppt), it is now considered unitless and measured according to the Practical Salinity Scale. Salinity is sometimes represented by units of PSU (Fundamentals of environmental measurements, 2016). Due to the various important influences, the impacts of salinity on environments has warranted much study over the years (Trujillo and Thurman, 2011). Both temperature and salinity are the main factors controlling the density of water. This leads them to play an essential role in global thermohaline circulation and greatly impacting on the ability of water to mix (Trujillo and Thurman, 2011). Salinity is equally important within estuaries. Here, salinity is often highest at the river mouth (~30 PSU) where ocean water is able to easily flow into the estuary and lowest in the highest reaches where oceanic influence is more limited (~0.5 PSU) (Ohrel and Register, 2006). This may lead to dynamic rises and falls in salinity due to waves and higher tides contributing saline water and precipitation and run off diluting the water. Salinity most importantly directly impacts on the ability of water to dissolve gases and affects what organisms are able to live within the water. One of the most important of these is oxygen. High salinity waters such as ocean water usually hold 20% less oxygen than freshwater under similar conditions (NOAA, 2012). Salinity can be considered as one of the most important parameters in influencing the usage of estuaries by organisms (Marshall and Elliot, 1998). An example of this may be found in phytoplankton, which form the basis of any estuarine food web. Phytoplankton have for a long time been known to be particularly susceptible to the influence of salinity as most possess stenohaline characteristics and suffer osmotic stress with the introduction of salinity (Kirst, 1990; Flaming and Kromkamp, 1994; Bisson and Kirst, 1995). Lionard *et al.* (2005), showed that within Schelde estuary increases or decreases in salinity may lead to reductions in the amounts of phytoplankton present within estuaries. This may even lead to changes in community composition as freshwater phytoplankton get replaced by marine phytoplankton as salinity increases and vice versa (Lionard *et al.*, 2005). Flocculation (the process by which particle aggregate together to form larger objects) is also influenced by salinity (Ohrel and Register, 2006). This may lead to increased turbidity as dissolved particles collide with salt water and begin to precipitate. The salinity also determines how suitable estuarine water would prove for

consumption by humans or animals. Salinity increases or decreases may therefore lead to negative health changes within estuaries.

#### 2.3.4 Role of Chlorophyll-a (Chl-a) in estuaries

Chlorophyll-a are pigments found within photosynthetic organisms, such as algae, that are essential for photosynthesis (Lim and Choi, 2015). These organisms form the base of the food chain and are thus essential to understanding the trophic state that an estuarine environment is currently experiencing. Surface waters with high chl-a content may also indicate the presence of high levels of nutrients such as phosphorus and nitrogen. An excess of nutrients within an estuary may lead to rapid population rises in phytoplankton. An overproduction of these primary producers may lead to negative effects such as eutrophication (Gholizadeh *et al.*, 2016). An overview of the eutrophication process can be seen in Figure 2.3. This can lead to massive fish kills and the loss of estuarine vegetation (Bricker *et al.*, 2008). Determining the chl-a content of a water body is therefore also used as a potential indicator in determining whether an eutrophication event is currently happening or is likely to in future happen (Angela and Nikos, 2010). This may also be used as an indirect indicator of pollution levels within an estuary as often external sources contribute towards this high nutrient content (Bricker *et al.*, 2008). Healthy levels of chl-a can be considered to be estuary specific as they usually differ from estuary to estuary based on climate and nutrient amounts amongst others.

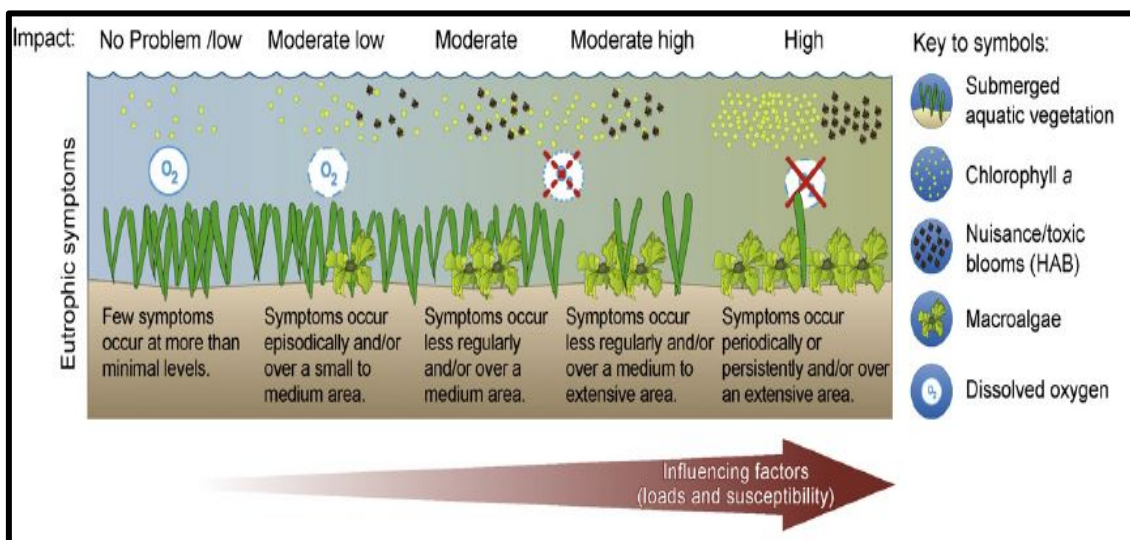


Figure 2.3: Overview of the relationship between the overall eutrophication process, the symptoms and influence factors such as nutrient loads (adapted from Bricker *et al.*, 2008).

### *2.3.5 Role of Dissolved oxygen (DO) in estuaries*

This forms one of the most important physico-chemical parameters within any waterbody due to the fact that all respiring organisms need this to live. Oxygen dissolves through direct diffusion into the water or its production by photosynthetic organisms. The main sources of dissolved oxygen is through photosynthesis from aquatic plants (Abowei, 2010). Further, the actions of both waves and winds may aid in the rate at which oxygen dissolves into the water body. Besides temperature and salinity, the levels of oxygen may change as decomposers use it up in breaking down organic matter. However, if waters are polluted with high biological oxygen demand (BOD) contaminants such as sewage, dissolved oxygen may fall to unhealthy levels (Clark, 1997). This is also a potential indicator that an eutrophication event is currently or will happen (Angela and Nikos, 2010). The prevalence of hypoxic and anoxic conditions may lead to a suppression of respiration and feeding and subsequently cause the death of fish and other organisms. A lack of oxygen may also lead to impaired embryonic development and lowered hatching success (Clark, 1997). This may result in both reproductive and stock-recruitment failures leading to collapses in species richness and abundance and a general unhealthy state within estuaries (Abowei, 2010). UNESCO/WHO (1978), determined that coastal and estuarine waters often require at least 4 mg/l of dissolved oxygen to support a healthy ecosystem. However, for both optimum carrying capacities and optimum estuarine functioning, dissolved oxygen of at least 5 mg/l is preferred.

### *2.3.6 Role of pH in estuaries*

pH is a measure of how basic or acidic the waters within an estuary are (Ohrel and Register, 2006). Factors affecting the pH value within estuaries include minerals dissolved within the water, aerosols and dust, human wastes and photosynthesis and respiration by estuarine inhabitants (Ohrel and Register, 2006). Most aquatic organisms prefer to live in water of pH's between 5 and 9 but many estuarine inhabitants are able to survive within waters where pH ranges from 5.5 to 10 (Moyle, 1993; NOAA, 2012). The typical pH levels within an estuary range from 7 to 7.5 for the more freshwater parts and 8 to 8.6 for more saline parts (Ohrel and Register, 2006). Estuaries with pH values that are lower than 6 are usually characterised by significantly decreased fish egg fertility, hatchability and growth of fry (Matthews, 2012). Despite these severe consequences to aquatic life, Matthews (2012), determined that most fish species fail to differentiate pH's between 5.5 to 10. In general, pH's around 6.5-8 are though to support the most productive estuaries (Ohrel and Register, 2006). Biological processes may

greatly influence the acidity of estuarine water. Photosynthesis may result in waters becoming more acidic as it removes  $\text{CO}_2$  which acts as a buffer against high pH's and makes water more alkaline (Ohrel and Register, 2006). As such, algal blooms are often lethal to aquatic organisms partly due to risen pH levels. Changes in pH may also alter how metals such as copper are able to dissolve within estuarine water. At lower pH's, toxic sediments within the estuary usually resuspend and lead to the poisoning of local organisms.

## **2.4) Estimation of the physico-chemical components of estuarine health**

### *2.4.1 Traditional and Remote sensing based methods of physico-chemical parameter estimation*

If the health of estuarine systems are to be maintained, important physico-chemical parameters such as those mentioned in the previous section need to be monitored and controlled (NOAA, 2012). This monitoring has traditionally been done through on the ground field campaigns involving sampling and lab tests. Over time, these methods have become significantly more advanced. Today, advanced hardware such as water quality sensors are able to instantaneously and accurately obtain measurements of multiple physico-chemical parameters within any body of water. Despite their accuracy, the traditional methods for physico-chemical estimation are not without their drawbacks (Gholizadeh *et al.*, 2016). As the number of water samples taken and parameters tested increase, the costs and effort required to complete such testing often grows considerably. The collecting of water samples may also prove time consuming and tedious, whilst travel to sampling grounds may be difficult or the area inaccessible. The use of traditional in situ methods for the obtaining physico-chemical data may therefore substantially limit studies. This is where remote sensing offers a possible solution.

Due to its synoptic coverage and versatility, remote sensors such as those based on satellites can provide physical and geographical data over large scales and aid in the study of many phenomena. These sensors may therefore serve as powerful tools towards the monitoring of water quality and health of estuarine system. One method of doing this involves the estimation of physico-chemical characteristics from features such as air, water and soils within estuarine bodies for the purpose of water quality assessments (Gholizadeh *et al.*, 2016). The various physico-chemical parameters, how they impact estuarine health and their collection through both field and remote sensing methods are essential to understand if a comprehensive water quality assessment is to be carried out.

#### 2.4.2 Traditional and remote sensing based temperature retrieval

Field based measurements for temperature are usually easy and cheap to perform. A standard thermometer placed within the water is sufficient for the accurate determination of temperature. The thermometer should be placed at least 10 cm beneath the surface of the water and remain there for around 3 - 5 minutes for an accurate reading (Ohrel and Register, 2006). If greater accuracies or speed are required, temperature may also be retrieved through the use of handheld sensors. Lab tests to determine temperature are usually discouraged as due to the time passing between sampling and testing, temperature would change (Ohrel and Register, 2006).

Temperature is usually measured by the thermal infrared bands present on some remote sensors such as bands 10 and 11 for Landsat 8. There have already been a large number of studies that have been able to successfully retrieve both land surface temperatures (LST) and sea surface temperatures (SST) from the Earth's surface (Becker and Li, 1990; Ustin, 2004; Kang *et al.*, 2014; Rajeshwari and Mani, 2014; Brando *et al.*, 2015; Wang *et al.*, 2015). Besides the use of Landsat 8, radar and other passive remote sensors may also be used to determine temperature. Avdan and Jovanoska (2016), devised an equation for temperature estimation using parameters that could be calculated entirely from a Landsat 8 image without the need for other data. The idea behind the development of this method included that current methods require the addition of atmospheric data or complex tools and were both tedious and prone to human errors (Avdan and Jovanoska, 2016). Tested over Ontario and Quebec in Canada, the algorithm achieved acceptable accuracies considering its ease of use with standard deviations ranging between 2.4 °C - 2.7 °C. Khattab and Merkel (2014), similarly made use of the thermal infrared band (band 8) and band 7 on Landsat 5 in order to determine temperature. Accuracies achieved included and  $R^2$  (coefficient of determination) of 0.72 and an SEE (standard error of estimate) of 0.25 when tested over Mosul dam. Khattab and Merkel (2014), also tested the ability of Landsat ETM+ in retrieving temperature and achieved better accuracies of  $R^2 = 0.97$  and  $SEE = 0.119$ . Abdullah (2015), attempted to determine temperature using Landsat 8 without the use of the thermal infrared bands on Dokan lake, Iraq. A model developed for spring achieved a high  $R^2 = 0.86$  but otherwise suffered from poorer accuracy, with other developed algorithms also recording  $R^2 = 0.52$  and  $R^2 = 0.49$  for other seasons.

### *2.4.3 Traditional and remote sensing based Turbidity and secchi disk depth (SDD) retrieval*

Turbidity may be measured in a number of ways. The most basic of these involves inferring turbidity through determining water clarity. The simplest of these involves the use of a secchi disk. This involves the use of a generally black and white chequered weighted disk that is lowered into the water column until the pattern is no longer visible (Fundamentals of environmental measurements, 2016). A reading is taken at this depth and can be used as a measure of water clarity. Another simple, accurate and easy to use method involves the use of a turbidity tube. Sensors may also be used to determine the turbidity content of water and come in many forms (Fundamentals of environmental measurements, 2016). This may come in the form of Nephelometric, backscatter and attenuation sensors. Nephelometric sensors are those sensors which have the light source and photodetector at 90° to each other. This angle is considered the best in determining light scatter for any particle size. However, drawbacks include that it can only be used for low turbidity water (below 40 NTU) and is vulnerable to interference from coloured dissolved material. Backscatter sensors have their light source and photodetectors at a greater than 90° angle to one another. This allows for improved turbidity determination at higher turbidities, especially around 1000 - 4000 NTU. In lower turbidity waters however, they are less accurate and are susceptible to error when dark particles are present. Attenuation sensors measure the light intensity decrease as it travels through sample water in order to determine turbidity. However, these sensors are very vulnerable to interference from the presence of coloured matter within water and are not recommended for surface water sampling.

Turbidity is most commonly measured in nephelometric turbidity units or Jackson turbidity units (JTU). However, both these units (and in fact a great many other units used) are roughly equivalent and therefore interchangeable (Myre and Shaw, 2006). The human eye can detect turbidity's of around 5 NTU and above. Waters that are considered relatively clear may have turbidity up to 25 NTU, muddy waters begin once has reached at least 100 NTU and finally at 2,000 NTU water becomes opaque and little light may travel through (Joyce *et al.*, 1996; Nathanson, 2003). Suspended sediments are the particles responsible for most of the scattering while absorption is mainly controlled by the amount of chlorophyll-a present in the water column (Myint and Walker, 2002).

Remote sensing techniques often involve the use of an appropriately selected single band along with a total suspended matters (TSM) algorithm (Nechad, 2010). However, certain substances

present in the water (such as dark coloured humus) may affect the water colour and therefore reflectance (Feng *et al.*, 2014). It is therefore more efficient to use signal bands or band ratio's to achieve a higher accuracy when determining turbidity. The ratio between green and red and blue and red have both been used previously for Landsat 5 to determine turbidity and TSS and the same algorithm should be applicable to Landsat 8 and Sentinel-2 (Cox *et al.*, 1998; Wang *et al.*, 2006). Lim and Choi (2015), found that suspended sediments levels were related to Landsat 8 band 2 to 5 through regression and have developed band specific algorithms for their calculation. Kapalanga (2015), used Landsat 8 over Olushandja Dam, Namibia in their turbidity estimation. Accuracies of  $R^2 = 0.98$  were found for this study indicating strong estimation ability. Garaba and Zielinski (2015), attempted this over the Wadden Sea using Landsat 8. Accuracies of  $R^2 = 0.73$  were found for this study amongst others. Khattab and Merkel (2014), used Landsat 5 and obtained a  $R^2 = 0.99$  and  $SEE = 0.802$  respectively. Abdullah (2015), attempted to retrieve turbidity over Dokan Lake using Landsat 8. A  $R^2 = 0.99$  and  $R^2 = 0.46$  were obtained for autumn and spring models respectively. Song *et al.* (2011), made use of Landsat 5 and bands 5 and 2 to determine turbidity over Lake Changa, China. Results showed an  $R^2 = 0.88$  and  $SEE = 17.65$ . Finally, Dogliotti *et al.* (2015), achieved good accuracy testing out the 645 nm and 859 nm wavelength bands that are found on many remote sensors over seas and estuaries around the world. With regard to determining SDD's, Hancock (2015), used Landsat 8 to determine SDD in three different American reservoirs: Brookeville, Geist, and Eagle Creek. Using bands 3 and 4, she achieved an accuracy of  $R^2 = 0.58$ . This moderate accuracy was thought to be due to differences in band wavelengths between Landsat 8 and Landsat 7 (for which the original equation was based off of). Through a ratio of the blue and green band, Giardino *et al.* (2001) used Landsat 5 over Lake Iseo, Italy and achieved SDD estimation accuracies of  $R^2 = 0.85$ . Nas *et al.* (2010), retrieved SDD using the blue and red Landsat 5 bands with a  $R^2 = 0.71$ . Alparslan *et al.* (2007), made use of the Landsat 7 remote sensor in their estimation of SDD for Darlik Dam just outside of Istanbul, Turkey. This used bands 1 to 5 and achieved an accuracy of  $R^2 = 0.88$ . Deutsch *et al.* (2014), also made use of the blue and red bands aboard Landsat 7 and 8 in Qaraoun Reservoir, Lebanon. This achieved accuracies of  $R^2 = 0.82$  and  $R^2 = 0.47$  for each sensor respectively. Baban (1993), was an earlier study that made use of Landsat TM and the blue band in order to determine SDD. This was achieved with an accuracy of  $R^2 = 0.83$ .

#### *2.4.4 Traditional and remote sensing based salinity, total dissolved solids (TDS) and electrical conductivity (EC) retrieval*

The collection of salinity traditionally has progressed much over time. Today there are two main popular ways in measuring salinity. Salinity can either be measured through electrical conductivity (EC) or through determining the amount of salt that is dissolved within a solution. This is also known as total dissolved solids (TDS) (Watling, 2007). These results can either be recorded directly as salinity in ppt or as EC/TDS. Electrical conductivity is measured using an electrical conductivity meter which determines how easily electricity passes through a solution (Ohrel and Register, 2006). The more saline the solution, the larger the EC reading becomes. This can be measured either in the lab or during the field campaign. This works based on the amounts of positively and negatively charged ions within the water. Important positively charged ions include sodium, magnesium, calcium and potassium. Although negatively charged ions such as chloride, nitrates and sulphates do not have much of an impact on EC, they play important biological roles (Fundamentals of environmental measurements, 2016). Besides just the measuring of salinity, EC can further it can indicate some of the ionic composition of the water. An example of how this can be important can be seen with cladocerans, who are more sensitive to potassium chloride than sodium chloride (CWT, 2004). Finally, the EC may indicate an external leakage (such as sewage) entering the water.

TDS can be measured in the same way as EC and multiplying by an empirical factor or through gravimetric analysis. Gravimetric analysis involves using an evaporation dish and dissolving all water in order to measure the salt (Fundamentals of environmental measurements, 2016). The term TDS is often more preferred than directly stating the salinity in freshwater situation where salinity values are often very low. TDS, salinity and EC are all highly interlinked and similar. Instead of setting up conductivity standards for water, some governments set up TDS standards (Fundamentals of environmental measurements, 2016). EC and TDS are measured in  $\mu\text{S}/\text{cm}$  and  $\text{mg}/\text{l}$  respectively. EC ranges for fresh, brackish and sea water range from 0 - 1500  $\mu\text{S}/\text{cm}$ , 1500 - 15 000  $\mu\text{S}/\text{cm}$  and above 55 000  $\mu\text{S}/\text{cm}$  respectively. For TDS, ranges for fresh, brackish and sea water range from 0 - 1000  $\text{mg}/\text{l}$ , 1000 - 10 050  $\text{mg}/\text{l}$  and above 36 850  $\text{mg}/\text{l}$  respectively. A refractometer can be used to measure salinity values either in the field or in a lab. Salinity ranges from 0 - 0.5 for freshwater, 0.5 - 30 for brackish water and 30 onwards for sea water (Ohrel and Register, 2006).



Salinity has obvious optical properties within water and has been measured by microwave based sensors since the 1970's and 80's, remaining popular to the current day (Gholizadeh *et al.*, 2016). Aquarius is one such NASA launched microwave radiometer sensor used for this purpose. However, salinity cannot often be measured directly by sensors such as Landsat 8. These sensors therefore rely on the relationship between salinity and temperature (that is measurable with TIRS bands) or coloured dissolved organic matter (CDOM) in order to obtain salinity values (Bai *et al.*, 2013). A recent study by Zhao *et al.* (2017), has also found a relationship between reflectance from bands 1 to 4 and the surface salinity of water. Garaba and Zielinski (2015), used Landsat 8 in an attempt to retrieve water quality parameters such as salinity across the Wadden Sea. They made use of Remote sensing reflectance ( $R_{rs}$ ) in an attempt to reduce atmospheric influences. The study was mildly successful with  $R^2 = 0.84$  and  $R^2 = 0.54$  being recorded for the two algorithms developed. The study did support the fact that water colour may be used as a proxy for measuring salinity. However, it was mentioned that there is a large belief within the scientific community that retrieving salinity by use of ocean colour varies on a case to case basis and is especially challenging in the near-shore environment. Lavery *et al.* (1993), was an earlier study that attempted to retrieve salinity using Landsat TM. This was done across the Harvey Estuary in Western Australia and is one of the rarer attempts at determining salinity in optically complex estuaries. The study achieved accuracies of  $R^2 = 0.75$  and  $R^2 = 0.78$  as well as  $SEE = 1.14$  and  $SEE = 1.75$  for the two equations derived, proving itself successful in estimation. Dewidar and Khedr (2001), also made use of Landsat TM in their salinity estimation in Manzala lagoon. Here, TM bands 2, 3 and 4 were used to derive a salinity algorithm whose accuracy was not tested. Wang and Xu (2008), derived salinity in an estuarine lake based in the Gulf of Mexico also making use of the Landsat TM bands. The models formulated using TM bands 1 to 5 achieved a successful  $R^2 = 0.89$  and RMSE (root mean squared error) of 0.27. Instead of only focusing on measuring the salinity, many studies also focused on or included determining the EC and TDS. Khattab and Merkel (2014), used Landsat 5 to retrieve EC and obtained a coefficient of determination and  $SEE = 0.84$  and  $SEE = 0.007$ . Likewise the same study attempted estimation with Landsat 7 and obtained  $R^2$  and  $SEE$  accuracies of  $R^2 = 0.95$  and  $SEE = 0.033$ . Abdullah (2015), used Landsat 8 in his calculation of EC and achieved accuracies of  $R^2 = 0.49$  and  $R^2 = 0.41$  when calculated in autumn and spring. Khattab and Merkel (2014), used Landsat 5 to retrieve TDS and obtained a  $R^2 = 0.99$  and  $SEE = 0.0004$ . Likewise the same study attempted estimation with Landsat 7 and obtained a  $R^2 = 0.96$  and  $SEE = 0.009$  respectively. Abdelmalik (2018), used ASTER and calculated TDS with accuracies with a  $R^2 = 0.99$  and RMSE of 0.89 in Qaroun Lake, Egypt. Abdullah (2015), used

Landsat 8 in his calculation of TDS and achieved accuracies of  $R^2 = 0.49$  and  $R^2 = 0.41$  when calculated in autumn and spring.

#### 2.4.5 Traditional and remote sensing based Chlorophyll-a (Chl-a) retrieval

Chl-a can be measured in a two broad ways. Classically, this has been done through spectrophotometry (Fundamentals of environmental measurements, 2016). This involves the collection of fairly large water samples, which are then filtered and placed in acetone to extract the chl-a. This solution then undergoes a spectrophotometry-based method such as absorbance or fluorescence which use chlorophyll's known optical properties to determine a final chl-a value. High performance liquid chromatography (HPLC) is another method used and has been shown to provide reliably accurate results (Fundamentals of environmental measurements, 2016). The extraction phase is the same that is followed with spectrophotometry but then uses a fluorometer to determine molecular chlorophyll fluorescence. However, this method is known to be both time consuming and requiring a trained analyst for accurate results. Chl-a can be measured in  $\mu\text{g/l}$  or  $\text{mg/m}^3$ , both of which are essentially the same measurement.

Photosynthetic organisms absorb light from around red and blue wavelengths and reflect in the green wavelength (Gholizadeh *et al.*, 2016). The addition of chlorophyll-b monitoring allows for a broader range of wavelengths to be used, however, it is chlorophyll-a that is usually most favoured. There are many methods of determining the chlorophyll-a content of water bodies. This includes many of which have been developed for Landsat 7 and which would be applicable for use in Landsat 8 and Sentinel-2. Simple methods involve using the ratio between the green and red bands (Allan *et al.*, 2007); The ratio between green and blue as well as between red and infrared (Turner, 2010); and the use of single colour bands (Hadjimitsis and Clayton, 2009). The ASTER remote sensor was used by Nas *et al.* (2007), in their estimation of Chl-a from Beysehir Lake in Turkey. Chl-a was successfully retrieved with an  $R^2 = 0.86$  whilst using bands 1 to 4. Tenjo *et al.* (2015), derived estimation algorithms for use by Landsat 8 using algorithms first developed by Bernstein *et al.* (2005). An excellent accuracy of  $R^2 = 0.97$  was achieved through the use of bands 1 and 3. Cândido *et al.* (2016), performed an extensive study and used various methods in the estimation of Chl-a. The Landsat 8 remote sensor was used for this purpose across São Gabriel do Oeste, Brazil. Generally, high  $R^2$  values above 0.9 were found using all methods with many independent tests done. Two Landsat 8 images were used to test two algorithms each derived from Normalized ratio aquatic vegetation index (NRAVI), ratio aquatic vegetation index (RAVI), Excess green (ExG) and Normalized difference vegetation index

(NDVI). These equations developed generally strong accuracies. Equations based on NRAVI's achieved highs of  $R^2 = 0.99$ ; RAVI achieved highs of  $R^2 = 0.99$ ; ExG of  $R^2 = 0.98$  and NDVI achieved accuracies of  $R^2 = 0.98$ . El-Magd and Ali (2008), made use of Landsat ETM+ to determine chl-a across Lake Manzala. Various band ratios were used, with the most successful being those based on blue and red bands.  $R^2 = 0.75$  and  $R^2 = 0.70$  were achieved through developed algorithms, indicating success. Toming *et al.* (2016), used the more modern Sentinel-2 in their estimation of chl-a over eleven Estonian lakes. Here, bands 4 to 6 achieved  $R^2 = 0.8$  and  $R^2 = 0.83$  when tested across the lakes. Watanabe *et al.* (2015), made use of Landsat 8 in their estimation across the Barra Bonita hydroelectric reservoir, Brazil.  $R^2 = 0.75$  were found using bands 4 and 5. Lower  $R^2$  values were found for many of the other bands and proved inaccurate. Forrer (2012), used Landsat 5 in her chl-a estimation in Bankhead lake, United States. Here, poor accuracies with  $R^2$  values well below 0.61 and SEE's ranging from 1.14 - 3.73 were found for all algorithms developed. Jaelani *et al.* (2016), tested their Landsat 8 models over two oceanic islands in East Java. Very poor accuracies were recorded for their models, with  $R^2 = 0.41$  and  $R^2 = 0.09$  indicating major issues with chl-a estimation. The suspected cause of the low accuracy was thought to be due to on the poor atmospheric correction algorithms used by the USGS. Finally, Lim and Choi (2015), used Landsat 8 as well for their estimation. The Nakdong River in South Korea played host to their tests which achieved success rates of  $R = -0.71$ .

#### *2.4.6 Traditional and remote sensing based Dissolved oxygen (DO) retrieval*

There are three general methods in measuring DO in estuarine waters (Fundamentals of environmental measurements, 2016). Traditionally this was done through a Winkler titration. Inskip (1982), provides many informative aspects regarding this method. However, whilst accurate, this method is prone to human error and is considered the most difficult to perform. There are multiple variants for Winkler titrations. The colorimetric method is another type of method used to measure DO. These are both quick and inexpensive but prone to errors due to redoxing agents present within water (Inskip, 1982). Finally, DO can be measured through the use of a handheld sensor. Today this is the most popular method, allowing readings to be taken in the field or lab both cheaply and easily. These sensors take into account pressure, temperature and salinity, which all affect the amounts of DO (USEPA, 2012). Sensors may either be optical or electrochemical in nature. Optical sensors use the relationship between oxygen and blue light once special dyes have been added. The blue light excites these dyes and interacts with the DO,

indicating how much is present. Dissolved oxygen can be measured in either parts per million (ppm) or mg/l, both of which are essentially the same measurement.

Dissolved oxygen is an important component of water based systems and heavily influences the distribution of all oxygen consuming organisms. Oxygen contents are influenced by many factors. This includes the water temperature, anthropogenic sources, the amount of oxygen taken in by respiring organisms, the amount used in decomposition, the amount brought into the system by plants and photosynthetic organisms and the amount that dissolves into the water from the air (Gholizadeh *et al.*, 2016). Biological oxygen demand is the amount of oxygen that is required by bacteria to decompose organic matter. This may include detritus and organic wastes. Currently there has been no sensor that has been identified as being able to accurately determine the oxygen levels within water bodies. These measurements are usually only confidently accurate with the help of in situ data that is collected and used to model a relationship. Landsat sensors have been the most popular sensors used in trying to model DO. Landsat 5 is one of the more popular sensors in modelling attempts (Miao-fen *et al.*, 2007; He *et al.*, 2008). Theologou *et al.* (2015), and Khalil *et al.* (2016), both attempted to retrieve dissolved oxygen through the use of Landsat 8. These were both performed through the use of a ratio between the blue and red bands (bands 2 and 4 respectively). Theologou *et al.* (2015), tested their algorithms over the Mediterranean sea and a lake near the city of Larissa, Greece. An acceptable and accurate  $R^2 = 0.80$  was obtained for this study. Theologou *et al.* (2015), also made use of Landsat 7 in determining the DO in the same study. Here,  $R^2 = 0.88$  were found. Accuracies of  $R^2 = 0.36$  and  $R^2 = 0.56$  as well as RMSE = 0.39 and RMSE = 0.24 were found for equations developed by Khalil *et al.* (2016), over Bardawil Lagoon, indicating poor accuracy. Abdullah (2015), too made an attempt to retrieve DO over Dokan Lake using Landsat 8. A  $R^2 = 0.73$  provides the method with moderate to good accuracy.

#### 2.4.7 Traditional and remote sensing based pH retrieval

pH can easily be measured in the field or lab using the colorimetric method. Here, reagents are added to the water sample which thereafter react according to the pH and produce a colour change. This can be measured visually or electronically and indicates the pH level within the estuary (Ohrel and Register, 2006; Fundamentals of environmental measurements, 2016). However, it does not have the best accuracy in waters which are coloured. pH meters are a more expensive method than using the colorimetric method but can be used even if the water sample

itself is coloured and are extremely accurate (Ohrel and Register, 2006; Fundamentals of environmental measurements, 2016).

Perivolioti *et al.* (2016), tested the ability of Landsat 7 in pH estimation over Lake Koronia, northern Greece. Through using only the infrared band, they retrieved pH but failed to check for accuracy. Theologou *et al.* (2015), used Landsat 8 and ratios of bands 5 and 6 as well as bands 1 and 4 to accuracies of  $R^2 = 0.86$  and  $R^2 = 0.81$  respectively. Theologou *et al.* (2015), also made use of Landsat 7 and its bands 2 and 7 in to retrieve pH with a  $R^2 = 0.87$ . Khattab and Merkel (2014), used Landsat 5 in their study and obtained a  $R^2 = 0.75$  and  $SEE = 0.087$  respectively. Abdullah (2015), similarly made use of Landsat 8 in his calculation of pH and achieved accuracies of  $R^2 = 0.64$  and  $R^2 = 0.47$  when calculated in autumn and spring.

### CHAPTER THREE: STUDY AREA



*Umdloti Estuary during winter sampling*

### **3.1) Introduction**

This chapter provides a comprehensive review of a multitude of aspects relating to the study site, the Umdloti Estuary. This includes an overview of its general characteristics, source, climate, geology, biology, physico-chemical characteristics and finally its state of health. Images of both the study area itself and its location are provided in Figure 3.1.

### **3.2) Description of the study area**

The eThekweni municipality in KwaZulu-Natal province, South Africa includes around 98 km's of coastline and contains 16 estuaries (Forbes and Demetriades, 2008). These estuaries play significant ecological and economic roles within the province and are amongst the highest value ecosystems found included in the Durban open space system (Forbes and Demetriades, 2008). The Umdloti/Mdloti Estuary forms one of these 16 estuaries and was the area in which this current study was based. According to Begg (1978), the Zulu name, uMdloti, from which the name of the estuary and adjoining river is derived, could be interpreted in three ways. It could mean: the plough; the violent river or the river of the wild tobacco plant. This estuary is one of the larger estuaries found within the municipality and is roughly 140 hectares in size and located around 25 kilometres north of Durban, sandwiched between the small towns of Umdloti and La Mercy (Figure 3.1) (Forbes and Demetriades, 2008). The M4 road bridge runs across the upper reaches of the estuary whilst the lower reaches are bordered by the Umdloti beach and Indian Ocean. The estuary is surrounded by steep hills, packed with indigenous vegetation and access can be obtained through the adjoining beaches. The Umdloti Estuary and surrounding beaches form a popular site for many water based activities. This acts to attract locals and holiday goers who engage in activities such as fishing, swimming and kite surfing.

Common to many South African estuaries, Umdloti itself is a temporarily open-closed estuary with intermittent periods of access to the sea (Forbes and Demetriades, 2008). Although temporarily open-closed, it goes through prolonged periods of closure. The state of the mouth was in closed phase throughout the period of the study. The sand bar that covers the estuarine mouth is sometimes artificially breached throughout the year by upstream sugarcane farmers to prevent flooding of their fields upstream and allow for access over some roads (Forbes and Demetriades, 2008; Pather, 2014). The estuarine mouth sand bar is also occasionally overtopped during high tides, introducing small amounts of seawater into the estuary (Pather, 2014). Closed mouth conditions lead to the estuarine waters being primarily composed of low salinities, which

strongly influence the biological life found within and around the Estuary (Forbes and Demetriades, 2008). Closed mouth conditions may also result the estuary being warmer in general due to the cut off of cooler oceanic water into the estuary. Warmer temperatures may result also in lower amounts of dissolved oxygen as warmer water hold less oxygen. It is rarely breached naturally but was breached in March, 1980 through a combination high equinox tides and rough sea conditions (Pather, 2014). When the Estuary is breached and open to the ocean, it generally brings large changes. If riverine flow is strong enough, it may result in the flushing out of phytoplankton and sediments. This leads to a large reduction in these primary producers (and chlorophyll-a) and turbidity (Forbes and Demetriades, 2008). Salinity is introduced into the estuary during these periods and the water becomes brackish. This tends to increase the amount of fish species diversity with open mouth conditions, due to greater recruitment from previously inaccessible marine species (Forbes and Demetriades, 2008). The Umdloti Estuary becomes essentially empty when the mouth opens as water levels fall (Forbes and Demetriades, 2008).

The source of the estuary is the 90 km Umdloti River. This river rises from around 823 m in the Noodsberg area (Govender, 2009). It flows perennially at a mean annual flow rate of  $2 \text{ m}^3 \cdot \text{s}^{-1}$  (WCW, 2002; Olaniran *et al.*, 2014). Along its course, the river flows through a major concreted dam (Hazelmore) and past the town of Verulam, all located within 20 kilometres upstream of the estuary (Olaniran *et al.*, 2014). The middle courses of this river passes numerous residential and industrial areas (Govender, 2009). Agricultural activities conducted along the length of the Mdloti River include sugarcane, banana and citrus fruit farming and is the location for many cattle pastures (Govender, 2009). There is also a WWTW based upstream of the Umdloti Estuary that has an estimated effluent flow rate of  $400 \text{ m}^3/\text{day}$  into the river (Van Niekerk and Turpie, 2012). The river eventually cuts across the coastal plain and enters into the Indian Ocean, with the point of entry forming the Umdloti Estuary (Govender, 2009).

The estuary experiences a subtropical climate with cool winters and rainy warm summers (Ngetar, 2002). The influence of the warm Agulhas current contributes to the warm to mild conditions experienced by the local climate (Pather, 2014). The average temperatures of summer days are usually hot and range from around  $25^\circ\text{C}$  to  $38^\circ\text{C}$  (Govender, 2009). Winter temperatures are usually moderate, often ranging from around  $9^\circ\text{C}$  -  $19^\circ\text{C}$  (Govender, 2009). Average rainfalls of around 800 mm to 1125 mm are experienced annually (Govender, 2009). Over 80% of all rainfall is received during these summer months (Cooper, 1993). Winter rainfall is considerably lower and usually occurs through the presence of northward moving coastal lows (Pather, 2014). Occasionally the area upriver experiences large amounts of



province-wide flooding. This may eventually lead to the erosion of sediments which find their way into the Umdloti River. The river therefore may receive high sediment loads which may be transported to, and in rarer cases out of, the estuary (Cooper, 1993; Ngetar, 2002).

Geologically, the Umdloti Estuary was identified by Begg (1978), as being composed of an assemblage of tillite, shale and sandstone. The first two metres of deposits within the estuary consists of fine sand, coarse fluvial sand as well as mud and clay lenses (Begg, 1978; Pather, 2014). Sediments in 2007 were found to be composed mainly of coarse and medium sand with the middle to upper reaches being proportionally composed of a greater amount of coarse sediments (Forbes and Demetriades, 2008; Pather, 2014).

Biologically, the type of life found within the estuary has been heavily influenced through the state of the usually closed estuarine mouth. The estuary itself is flanked by the presence of freshwater mangroves that have formed as a result of the low salinities experienced within the estuary (Forbes and Demetriades, 2008). Due to the long periods of mouth closure there is a notable lack of marine species recruitment. The Umdloti Estuary is therefore dominated by freshwater species, particularly by *Gilchristella aestuaria*, the estuarine roundherring (Forbes and Demetriades, 2008). The estuary also boasts a diverse array of fish and bird life. According to Govender (2009), organisms found within the estuary include: 28 different types of fish species; 8 different types of prawn species; 6 different species of crab and over 200 species of bird.

The Umdloti Estuary experiences temperatures typical of a subtropical estuary, where average water temperatures ranged from around 19 °C - 20 °C during winter and 24 °C - 25 °C in spring (Forbes and Demetriades, 2008). Turbidity within the Umdloti Estuary has a long history of being usually low. This is common to closed systems subjected only to wind induced turbulence (Forbes and Demetriades, 2008). As a result, estuarine waters are usually clear. This allows for greater levels of photosynthesis to occur throughout the water column, increasing productivity and indicating no health problems (Forbes and Demetriades, 2008). Turbidity within the Umdloti Estuary has been shown to increase and the waters becoming cloudier during rainfall and runoff events. Salinity, TDS and EC have all historically being recorded to be very low (usually barely considered brackish) within the Umdloti Estuary (Forbes and Demetriades, 2008; Govender, 2009; Olaniran *et al.*, 2014). This is due to prolong periods of mouth closure which cut off the estuary from the ocean and its supply of salty water (Forbes and Demetriades, 2008). In addition, fresh water from upstream further dilutes the estuarine water. Chlorophyll-a

is usually average to high across the Umdloti Estuary, historically ranging from 19 µg/l to 75 µg/l (Perissinotto *et al.*, 2004; Forbes and Demetriades, 2008). The estuary therefore supports a high number of phytoplankton both within the water column and its sediments. However, when high amounts of chl-a are recorded they are usually a result of pollutants such as nitrates entering into the estuary (Forbes and Demetriades, 2008). This usually results in an algal bloom events occurring and crashes in phytoplankton numbers when anoxic conditions begin to persist (Forbes and Demetriades, 2008). The amounts of DO within the Umdloti Estuary has in the past been of issue (Forbes and Demetriades, 2008). The UNESCO/WHO (1978), minimum recommendation of 4 ppm, of DO has often not being met. When DO levels are high (sometimes reaching over 13 ppm), this is usually due to algal bloom which soon destabilise and result in hypoxic/anoxic conditions and fish kills (Forbes and Demetriades, 2008). pH of the water is around 7.6 and has little negative impact on estuarine life (Forbes and Demetriades, 2008).

The health status of the Umdloti Estuary is one that has been considered troubling for a long time. Whitfield and Baliwe (2013), reported that the NBA considered the estuary to be in poor to fair state of health and well-studied. Forbes and Demetriades (2008), compiled an extensive report on the various estuaries found within the eThekweni municipality. All were found to be displaying a varying degree of health, ranging from being considered in good condition to highly degraded. Distressingly, many can be considered to be highly degraded and damaged. Some of this damage was so extensive that they can no longer be considered an estuarine environment. Forbes and Demetriades (2008), reported that Umdloti Estuary could be considered as being in a poor condition and suffering habitat loss. Evidence supporting the poor state included the visibly impoverished macrobenthic communities as shown by the lack of amphipods and isopods (Forbes and Demetriades, 2008). There are many factors which negatively impact on the health of this estuary. It was noted that siltation and sediment loss due to the construction of the Hazelmere Dam, pollution, both subsistence and commercial agriculture (especially sugar cane encroachment), and recreational usage were significant problems with regard to the health of the estuary (Forbes and Demetriades, 2008; Govender, 2009; Whitfield and Baliwe, 2013). Pollutants come in many forms and include an abundance of washed down general rubbish such as plastics. Govender (2009), also found that the health of the middle and lower courses of the Umdloti River were highly impacted upon through human activities such farming. This may negatively affect the amounts of DO and chl-a within the estuary, leading to dramatic drops. Carnie (2014), reported that eutrophication, likely caused through the introduction of agricultural products into the water led to over a thousand fish

deaths in 2014 within the estuary. The WWTW was also considered a potential pollutant, although Forbes and Demetriades (2008), reported that there was a sediment removal program in place to better purify effluents.

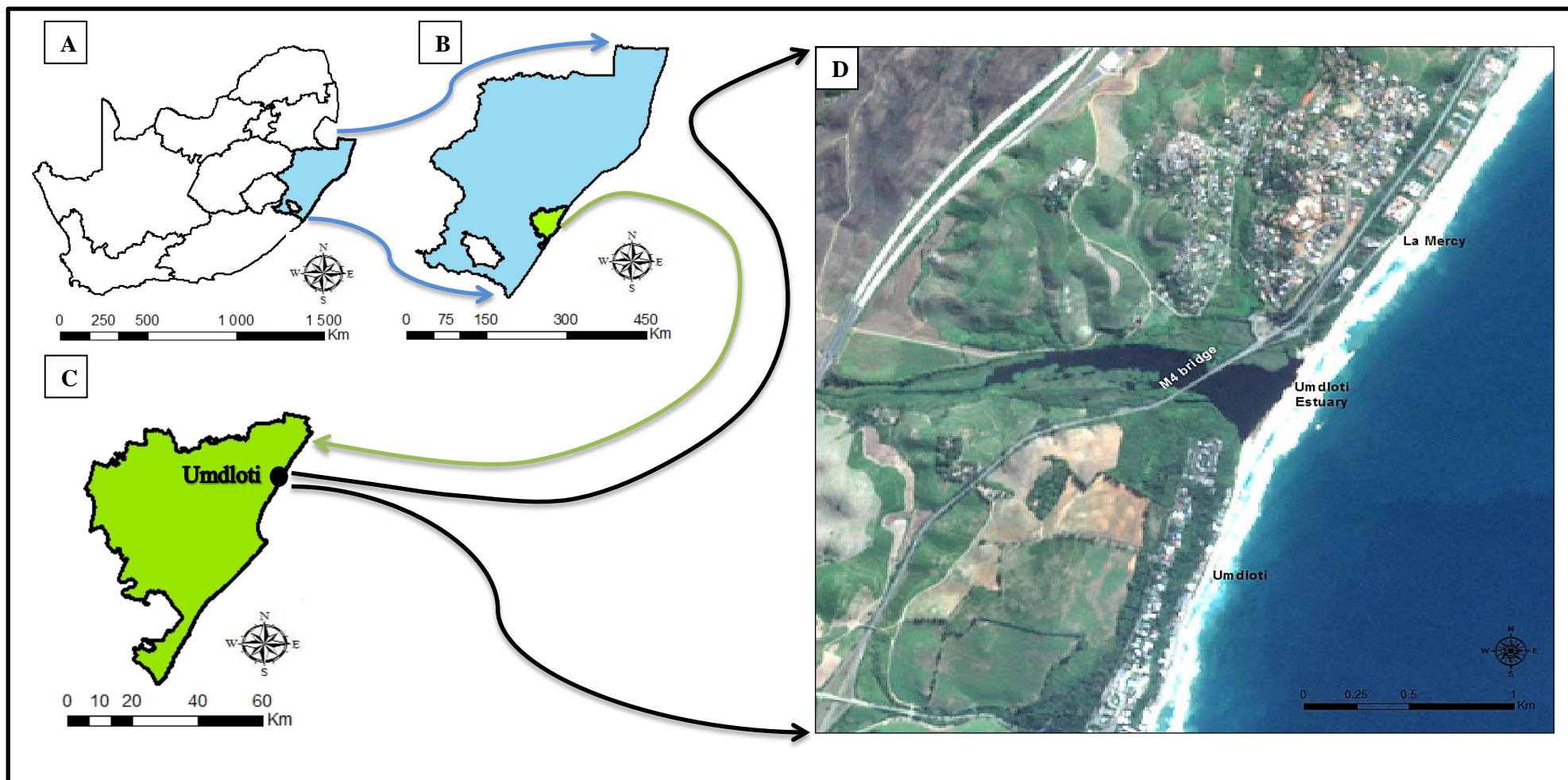


Figure 3.1: The location of Umdlotti with respect to (A) South Africa, (B) the province of Kwazulu-Natal, (C) and the eThekweni municipality. A Sentinel-2 image of the Umdlotti Estuary ( $29^{\circ} 39' 07''$  S;  $31^{\circ} 07' 43''$  E) is also included (D).

## CHAPTER FOUR: METHODOLOGY

### 4.1) Introduction

This chapter and its subsections provides information on the materials and methods employed in this study in order to achieve the stipulated objectives. This includes details on how the in situ collection of physico-chemical parameters is conducted and details of the instruments involved with this. All workings with remote sensing including the acquisition of remote sensing imagery and the estimation of physico-chemical parameters from the remotely sensed images are also discussed. Finally, an overview of the methods used for accuracy assessment are given. All results that are generated following this methodology for this study are presented in the results chapter. The overall methodological process followed over the course of the study is simplified in Figure 4.1.

### 4.2) Methodology

#### *4.2.1 Data collection*

##### 4.2.1.1 Field campaign and laboratory data collection

The field campaign consisted of the collection of Umdloti estuarine water samples as well as the performing of tests to retrieve some physico-chemical parameters conditions in the field. Field campaigns were conducted during the winter (July) and spring (November) periods. For the purpose of sampling, fifteen sampling points that spanned the length and breadth of the estuary were chosen (Figure 4.2). They were all roughly similar distances apart from each other and followed a systematic sampling pattern. This sampling pattern was chosen as it could equally cover the majority of the estuary, without oversampling or under sampling certain areas. This was important as the estuarine parameters are expected to change as one moves away from the mouth. Fifteen samples were done for winter sampling and another fifteen were done for spring sampling. This meant a total of thirty combined samples were therefore collected for Landsat 8 and Sentinel-2 use. A handheld Trimble Juno handheld GPS was used to guide the researcher to the sampling locations and ensured that locations remained accurate. At each sampling point, triplicate samples of estuarine water were taken just below the water surface using 0.5 L plastic bottles. These bottles were uncapped once completely submerged and allowed to fill with water. Once all air pockets were eliminated and the bottle was full, it was again capped whilst

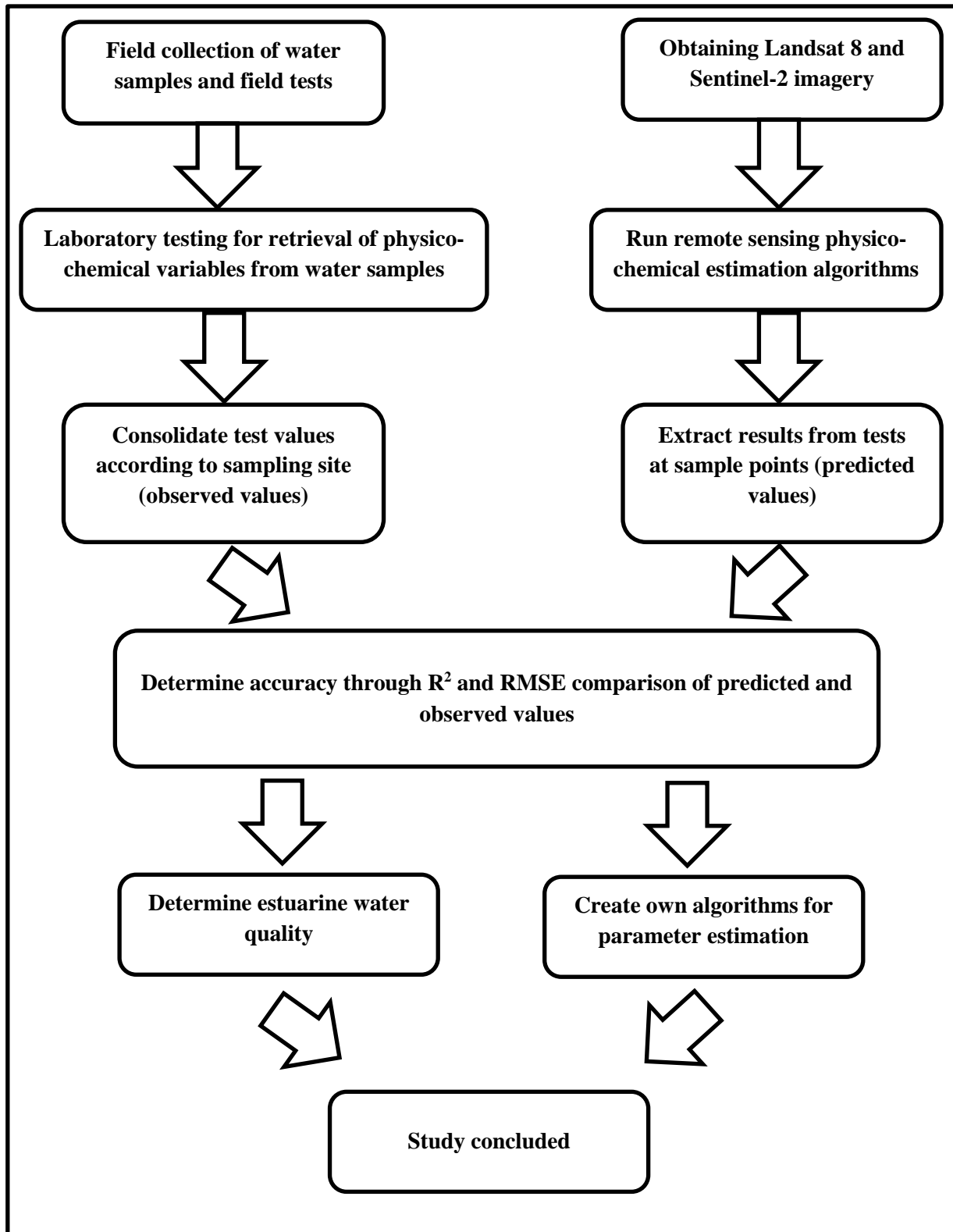


Figure 4.1: Flow diagram displaying basic outline of steps taken to obtain results over course of the study.

underwater. The bottles were then taken out of the water and were immediately stored in a cooler box to keep them cool and away from sunlight. At each sample site, temperature, turbidity and SDD were all measured in situ at the same time as water samples were collected. All sampling took place shortly after the remote sensors passed over the sampling area from 9am to 10am.

At each sampling point, an alcohol-based thermometer was used to measure this temperature. The thermometer was placed below a depth of 10 cm at each sampling point and remained there for around 3 to 5 minutes in order to get an accurate reading as suggested by Ohrel and Register (2006). After this, temperature readings were then recorded and the process was repeated at each sampling point. The method used for the measurement of turbidity was through the use of a turbidity tube. Though simplistic in design, the method has been shown to be both accurate and easy to use (Myre and Shaw, 2006). These tubes also have the advantage of being able to be used onsite (as water turbidity may change with travel or improper storage) and may reveal more information about that turbidity situation within the water than a computer read out may (Myre and Shaw, 2006). The construction of this device is clearly outlined in Myre and Shaw (2006), and involves assembling together a transparent clear plastic pipe, PVC cap, plastic bag, cardboard and the use of a permanent marker. In addition, a wax candle was rubbed over the tube markings and cardboard for waterproofing. In the field, water was slowly added into the tube until the viewing disk could no longer be seen. This depth of water was recorded and Equation 1 was thereafter used to determine the NTU. This equation was shown by Myre and Shaw (2006), to have an  $R^2$  of 0.996. Turbidity values obtained were rounded up to the next whole number.

$$\text{Depth in Centimetres} = 244.13 * (\text{Turbidity in NTU})^{-0.662} \quad (\text{Equation 1})$$

Another simple way of measuring water turbidity involves the use of a secchi disk. This is a usually 20 cm diameter chequered weighted disk attached to a rope that is lowered into the water until it can no longer be seen. The depth at which the disk disappears from sight is referred to as the secchi disk depth. A large secchi disk depth indicates water of low turbidity whilst a low value indicates that the water is highly turbid which may indicate pollution or an excess of suspended particles. This disk was simply lowered into the water at each sampling location until it disappeared from sight, after which its depth was recorded. The disk was then raised until it could be seen again and the depth recorded. The average of these depth recordings was used for the SDD.

Salinity, TDS, EC, chl-a, DO and pH on the other hand were all measured in a laboratory within a short time period of their collection. Samples of estuarine water were collected in field and bought back to a lab for testing of these parameters. A conductivity meter (WTW inoLab Cond Level 1 precision) was used in this retrieval. The conductivity measuring cell was simply placed into each sample and their salinity, TDS and EC obtained. Accuracy reported by the manufacturer for the purpose of estimation is around 99.5% (WTW, 2018). In order to determine the levels of chl-a at the various sampling points, lab tests would have to be performed on the sampled water. Within a couple of hours of their sampling, 250 ml of this water was then vacuum filtered through Whatman glass-fibre filters (GF/F). The filters were folded twice and put into polyethylene test tubes containing 10 ml of 90% acetone, forming a solution. 2000 ul of this solution along with 60 ul of 0.1 N HCL were added to a small glass vial (which had been rinsed with acetone before and after use). A fluorometer (Turner Designs Trilogy Laboratory Fluorometer) was then used on the solution to calculate the chlorophyll-a concentrations. This provided instant chlorophyll-a readings. Equation 2 (Arar and Collins, 1997) was used by the flourometer to calculate the amounts of chlorophyll-a with errors less than 0.05 µg/l.

$$\text{Chl-a } (\mu\text{g/l}) = \text{fluorescence} * (\text{acetone volume (ml)} / \text{water volume (ml)}) \quad (\text{Equation 2})$$

Dissolved oxygen was likewise collected via laboratory analysis. Samples of estuarine water were then immediately bought back to a lab and analysed using an oxygen sensor (WTW Oxi 320/SET). This sensor has an accuracy of within 99.5% (WTW, 2018). pH was measured in the lab from collected water samples, just as was done with many other parameters. These samples were analysed using a Metrohm 827 pH lab probe. This instantly provided the pH value of the water. Accuracy obtained through use of this method is around  $\pm 0.003$  pH (Metrohm, n.d).





Figure 4.2: Google Earth image showing the sampling points (1 – 15) at which water samples were collected and used for physico-chemical parameter estimation (Source: “Umdloti Estuary” 29° 39' 07" S; 31° 07' 43" E. Google Earth. 16 December 2017. 2 February 2018).

#### 4.2.1.2 Remote sensing data acquisition

Due to its synoptic coverage and high spatial resolution, remote sensing satellites can provide physical and geographical data over large scales and aid in the study of many phenomena (Gholizadeh *et al.*, 2016). Remote sensing is therefore perfectly suited to meet the needs of monitoring the health of estuarine systems. In this study, two popular optical remote sensors, Landsat 8 and Sentinel-2, were used to extract water quality parameters within the Umdloti estuary. The Landsat 8 sensor is a multispectral sensor and is run by the United States Geological Survey (USGS). Originally called the Landsat data continuity mission (LDCM), it was launched with the purpose of continuing the unbroken data acquisition started by the launch of the first Landsat in 1972 (Roy *et al.*, 2014). Roy *et al.* (2014), go into detail regarding the various specifics of the sensor. Landsat 8 operates as a pushbroom sensor with a 185 kilometer swath width. It comprises of eleven bands that are recorded by two sensors aboard the satellite. The operational land imager (OLI) consists of nine bands that range from the visible to shortwave infrared. Seven of these bands are consistent with previous Landsat sensors bands whilst an additional two are new. These are the deep blue coastal/aerosol band and the shortwave infrared cirrus band. The thermal infrared sensor (TIRS) is the other sensor aboard Landsat 8. This is mainly used to record thermal energy using the infrared bands 10 and 11. The addition of two thermal bands is also new to Landsat and has created a wide range of opportunities for new thermal applications.

Sentinel-2 on the other hand is run by the European Space Agency (ESA). It was part of the Copernicus program, which aims to launch earth observation satellites to aid in services such as agriculture and forestry monitoring (Drusch *et al.*, 2012). Sentinel-2 was launched as two satellites with the same characteristics (Sentinel-2A in 2015 and Sentinel-2B in 2017) (Bergin, 2017). These two sensors allow for a revisit time of only five days. Both Landsat 8 and Sentinel-2 are similar with regard to many of their characteristics, especially in spectral resolutions. Sentinel-2 is itself a multispectral pushbroom sensor just like Landsat 8 (Drusch *et al.*, 2012). It also images the earth similar to Landsat 8's local time, allowing for historical comparisons. However, unlike Landsat 8, Sentinel-2 records information via its thirteen bands. These bands have similar designations to their Landsat 8 counterparts but thermal infrared bands are not present. These were instead launched with the Sentinel-3 sensor. A comparison of both Landsat 8 and Sentinel-2 can be found in Table 4.1. A visual comparison of these sensors and Landsat 7 ETM+ may be found in Figure 4.3.

Table 4.1: Differences in specifications between Landsat 8 and Sentinel-2 remote sensors (adapted from Roy *et al.*, 2014 and Drusch *et al.*, 2012).

Specification being compared	Landsat 8	Sentinel-2
Spatial resolution range	15 - 100 m	10 - 60m
Radiometric resolution	12 bits per pixel	12 bits per pixel
Temporal resolution	16 days	5 days
Band designation (Band number, central wavelength, spatial resolution)	Band 1, 0.443, 30	Band 1, 0.443, 60
	Band 2, 0.482, 30	Band 2, 0.490, 10
	Band 3, 0.562, 30	Band 3, 0.560, 10
	Band 4, 0.665, 30	Band 4, 0.665, 10
	Band 5, 0.865, 30	Band 5, 0.705, 20
	Band 6, 1.610, 30	Band 6, 0.740, 20
	Band 7, 2.200, 30	Band 7, 0.783, 20
	Band 8, 0.590, 15	Band 8, 0.842, 10
	Band 9, 1.375, 30	Band 8A, 0.865, 20
	Band 10, 10.900, 100	Band 9, 0.945, 60
	Band 11, 12.000, 100	Band 10, 1.375, 60
		Band 11, 1.610, 20
		Band 12, 2.190, 20
Altitude of orbit	705 km	786 km
Launched	2013	2015 (A); 2017 (B)
Owned by	USGS	ESA

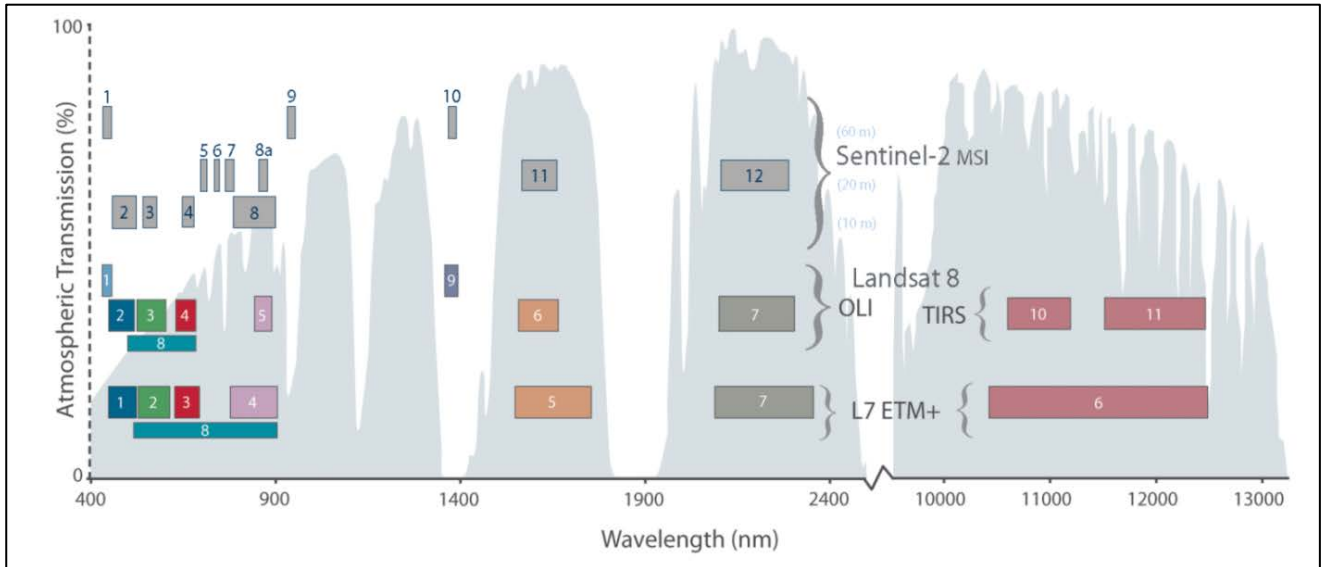


Figure 4.3: Comparison of Landsat 7 ETM+, Landsat 8 and Sentinel-2 band numbers and the wavelengths they cover against a backdrop of atmospheric transmission (NASA, 2015).

The next step towards the estimation of physico-chemical parameters involved the downloading of remote sensing images of the Umdloti Estuary for use in the study. Landsat 8 and Sentinel-2 imagery used in the study was respectively obtained free of charge from the USGS EarthExplorer website (<http://earthexplorer.usgs.gov/>) and the ESA Copernicus Open Access Hub (<https://scihub.copernicus.eu/>) respectively. These images previously could only be accessed from the respective sites but now both Sentinel-2 and Landsat 8 have been made available on the USGS EarthExplorer webpage. Images taken on the dates of July 5<sup>th</sup> 2018 (Landsat 8 winter), July 18<sup>th</sup> 2018 (Sentinel-2 winter) and November 10<sup>th</sup> 2018 (both Landsat 8 and Sentinel-2 spring) were downloaded and used. These dates were primarily chosen to coincide with the pass over of remote sensors and because they were good representatives of both winter and spring conditions. In addition, cloud cover over the study area was negligible. The November 10<sup>th</sup> sampling date also had sensors pass over within a short time period of each other. The same would have been done for the winter sampling date but poor weather conditions restricted this. Full sampling was done on July 5<sup>th</sup> whilst only temperature, turbidity and SDD were sampled on July 18<sup>th</sup>. The images were thereafter ready for analysis for which the GIS software ARC Map 10.4 and remote sensing software ACOLITE was used.

#### 4.2.2 Physico-chemical parameter estimation from remote sensing images

##### 4.2.2.1 Pre-processing and Remote sensing reflectance calculation

Estimation algorithms were those remote sensing algorithms used to retrieve physico-chemical values through remote sensing methods. Not all algorithms required the same levels of pre-processing. In the simplest cases, an algorithm would simply require the conversion of its digital numbers (DN) into top of atmosphere (TOA) reflectance. This was the case when using many algorithms with Landsat 8. Here, bands were converted into top of atmosphere reflectance using an equation supplied from the USGS (Equation 3). This may then further be corrected for sun angle through the use of Equation 4. Sentinel-2 products are downloaded as a Level 1C product, which means they have already been corrected into top of atmosphere reflectance and do not require the steps used by Landsat 8. The quantification value merely need be accounted for in order to make Sentinel-2 images comparable to the TOA reflectance found with Landsat 8. This quantification value can be found in the files that come with the Sentinel-2 image and involves multiplying all bands by 0.0001.

$$R' = M_{\rho} Q_{cal} + A_{\rho} \quad (\text{Equation 3})$$

Where:

$R'$  = Band- specific TOA reflectance, without correction done for the solar angle;  $M_{\rho}$  = Band-specific multiplicative rescaling factor which is retrieved from the metadata (REFLECTANCE\_MULT\_BAND\_x, where x is the band number;  $A_{\rho}$  = Band-specific additive rescaling factor which is retrieved from the metadata (REFLECTANCE\_ADD\_BAND\_x, where x is the band number);  $Q_{cal}$  = Standard unaltered digital number (DN) pixel values.

$$R = \frac{R'}{\cos(\theta_{SZ})} = \frac{R'}{\sin(\theta_{SE})} \quad (\text{Equation 4})$$

Where:

$R$  = Final corrected TOA reflectance;  $\theta_{SE}$  = Local sun elevation angle, provided in the metadata (SUN\_ELEVATION);  $\theta_{SZ}$  = Local solar zenith angle ( $\theta_{SZ} = 90^{\circ} - \theta_{SE}$ ).

More complex algorithms made use of remote sensing reflectance in their estimation of physico-chemical parameters concentrations.  $R_{rs}$  is an inherent component of all optically active features within water bodies (such as algae or seawater itself) and is the reflectance measured after atmospherically correcting both Rayleigh scattering by air molecules and an

aerosol correction (Vanhellemont and Ruddick, 2016). This is usually quite a complex process but may be simplified through the use of remote sensing image processing software. One such software is ACOLITE, developed by the Royal Belgian Institute of Natural Sciences, can be used to automatically extract Rrs. This free of charge, publically available software allows for the development of atmospherically corrected Level 2 Landsat 8 and Sentinel-2 aquatic products based primarily on works by Vanhellemont and Ruddick (2014; 2015; 2016). The calculation of Rrs over the course of this study used the short wave infrared (SWIR) atmospheric correction and per pixel parameter epsilons in order to correct for atmospheric aerosol. These options were selected as the SWIR bands are generally always black across any water type which leads to greater reliability and accuracy in Rrs (Vanhellemont and Ruddick, 2016). Both TOA reflectance and Rrs form the basis of the vast majority of estimation algorithms. Other parameters that were calculated for specific estimation algorithms were discussed in the forthcoming sections.

#### 4.2.2.2 Temperature

Unfortunately, the Sentinel-2 sensors do not possess the thermal infrared bands capable of recording temperature. These bands are present in Sentinel-3 which in turn lacks most of the bands present in Sentinel-2. This could be considered to be a severe limitation on Sentinel-2's ability to retrieve temperature. Despite this Abdullah (2015), did attempt to utilise the coastal blue and red band in an attempt to determine temperature without the use of thermal bands. Temperature could on the other hand be quite simply calculated using Landsat 8 as it contained the Thermal Infrared (TIRS) bands 10 and 11. Khattab and Merkel (2014), used these bands in their calculation of temperature. Temperature was also determined using an adapted sea surface temperature (SST) algorithm developed by Avdan and Jovanoska (2016). This algorithm was used as it was simple to implement and achieved reasonable accuracies (Avdan and Jovanoska, 2016).

The algorithm itself required various sub steps to first be completed before temperature could be retrieved. The first of these steps required the calculation of at-satellite brightness temperatures whilst using Landsat 8. Since Satellite sensors measure the reflectance of the Earth's surfaces as digital numbers, the original imagery was first converted to radiance through algorithms generated by the USGS. Here, the DN of band 10 data were converted to TOA spectral radiance using Equation 5.

$$L_{10\lambda} = M_L Q_{cal} + A_L \quad (\text{Equation 5})$$

Where:

$L_{10\lambda}$  = TOA spectral radiance for band 10;  $M_L$  = Band-specific multiplicative rescaling factor found in the metadata file (RADIANCE\_MULT\_BAND\_x, where x is the band number 10 in this case)  $A_L$  = Band-specific additive rescaling factor found in the metadata file (RADIANCE\_ADD\_BAND\_x, where x is the band number 10 in this case);  $Q_{cal}$  = Original standard pixel values (DN) of band 10

Thereafter the TOA radiance for band 10 was converted from spectral radiance to at-satellite brightness temperature. At-satellite brightness temperature refers to the temperature recorded by the satellite without any corrections being performed. This was done using the Equation 6.

$$BT = \frac{K_2}{\ln\left(1 + \frac{K_1}{L_{10\lambda}}\right)} \quad (\text{Equation 6})$$

Where:

BT = At-satellite brightness temperature for band 10 (Kelvin (K));  $L_{10\lambda}$  = TOA spectral radiance calculated in equation 2 file (RADIANCE\_MULT\_BAND\_x, where x is the band number 10 in this case);  $K_1$  = Band-specific thermal conversion constant found in the metadata file (K1\_CONSTANT\_BAND\_x, where x is the thermal band 10);  $K_2$  = Band-specific thermal conversion constant found in the metadata file (K2\_CONSTANT\_BAND\_x, where x is the thermal band 10).

Next the water emissivities were calculated. The emissivity of objects is mainly determined by its thermo-physical characteristics. For surfaces, the main determinant of these properties are the components that make up that surface (Wang *et al.*, 2015). Normalized Difference Vegetation Index (NDVI) was used to calculate this land surface emissivity as suggested by Zhang *et al.*, (2006). NDVI was calculated using Equation 7.

$$NDVI = \frac{(NIR - VIS)}{(NIR + VIS)} \quad (\text{Equation 7})$$

Where:

NIR = spectral reflectance measurements in the Near Infrared region (Band 5); VIS = spectral reflectance measurements in the visible red region (Band 4).

Thereafter emissivity values were assumed based on the NDVI values that had been calculated in Equation 7. Table 4.2 gives the emissivity values used for the different NDVI's. Water NDVI's over the study area does not go above 0, therefore only the first two rows of Table 4.2 are relevant for the study.

Table 4.2: Surface emissivities calculated from NDVI adapted from Zhang *et al.*, (2006).

NDVI	Surface emissivity ( $\epsilon_i$ )
NDVI < -0.185	0.995
$-0.185 \leq \text{NDVI} < 0.157$	0.970
$0.157 \leq \text{NDVI} \leq 0.727$	$1.0094 + 0.0047 * \ln(\text{NDVI})$
NDVI > 0.727	0.990

The SST for the Landsat 8 images could now be calculated. The emissivity corrected land surface temperature equation was first proposed by Artis and Carnahan (1982). A more modern version adapted for Landsat 8 was used by Avdan and Jovanovska (2016), in their calculation of temperature and used for this study, represented by Equation 8.

$$T_s = \frac{BT}{(1 + (\lambda * \frac{BT}{\rho}) * (\ln(\epsilon)))} - 273.15 \quad (\text{Equation 8})$$

Where:

$T_s$  = land surface temperature in Celsius; BT = At-satellite brightness temperature in Kelvin (calculated in Equation 6);  $\lambda$  = The wavelength of emitted radiance for band 10 (10.895  $\mu\text{m}$ );  $\rho = h * c / \sigma = 1.438 * 10^{-2} \text{ m.K}$ . Here:  $\sigma$  = Boltzmann constant ( $1.38 * 10^{-23} \text{ J/K}$ );  $h$  = Planck's constant ( $6.626 * 10^{-34} \text{ J.s}$ ) and  $c$  = velocity of light ( $2.998 * 10^8 \text{ m/s}$ );  $\epsilon$  = The emissivities determined by Table 4.2.

The value of 273.15 was the constant used in order to convert Kelvin to Celsius for the final LST result. The  $\lambda$  value was suggested by Avdan and Jovanovska (2016), when using band 10 of the Landsat 8 remote sensor.



Table 4.3: Temperature estimation equations adapted for Landsat 8 and Sentinel-2.

Reference	Adapted Equation (Landsat 8)	Adapted Equation (Sentinel-2)	Equation
Avdan and Jovanoska (2016)	$\frac{BT}{(1+(\lambda * \frac{BT}{\rho}) * (\ln(\epsilon)))} - 273.15$	None (Sentinel-2 lacks thermal bands)	Equation 8
Khattab and Merkel (2014)	$25.16 + 19.272 (R_7 / (R_{10} + R_{11})/2))$	None (Sentinel-2 lacks thermal bands)	Equation 9
Abdullah (2015)	$21.765 - 0.001 (R_1 + R_4)$	$21.765 - 0.001 (R_1 + R_4)$	Equation 10

*R*: TOA reflectance for band number; *BT*,  $T_s$ ;  $\lambda$ ,  $\epsilon$ ,  $\rho$  see Equation 8

#### 4.2.4.3 Turbidity and secchi disk depth

Turbidity could be calculated by various methods, many of which were available within the ACOLITE program itself. The method used for this study involved an algorithm developed by Dogliotti *et al.* (2015), that utilised the red band. This band was favoured due to the wider range of turbidity's that can be found in estuaries and to avoid the expected reduced sensitivity of other bands at low turbidity's (Dogliotti *et al.*, 2015). This method of turbidity estimation is calculated via Equation 11. Marine reflectance can be calculated through ACOLITE and is very similar to  $R_{rs}$ . Other turbidity estimation algorithms used are displayed in Table 4.4. All algorithms were chosen based on their accurate  $R^2$  in the retrieval of turbidity in the studies in which they were developed, The Kapalanga (2015), algorithm was selected due to its success estimating turbidity closer to home in an African (Namibian) dam. This relied on a combination reflectance of bands 2 to 5. The Garaba and Zielinski (2015), algorithm was selected due to its simplicity as it was based on a single band (band 4) and was designed to use remote sensing reflectance which has been corrected. Khattab and Merkel (2014), based their algorithm on a ratio of green to red bands in addition to using the near infrared band to estimate turbidity. This was selected as the Khattab and Merkel (2014), study was well grounded scientifically and many of many other algorithms from the study were used to estimate other parameters in this current study. The two Abdullah (2015), equations were chosen for this same reason. Equation 16 was based on a ratio of the reflectance in the coastal blue to red bands in addition to the reflectance in the near infrared band. Equation 17 used a ratio of the blue to red and green to coastal blue reflectance. The Nas *et al.* (2010), made use of the blue, green and red band reflectance and was selected due to its extensive refinement and high accuracy in the Nas *et al.* (2010), study. Song *et al.* (2011), used a ratio of near infrared to blue reflectance and was selected due to its simplicity and effectiveness. The various algorithms used for the estimation

of SDD are recorded in Table 4.5. Hancock (2015), made use of band 3 and 4 reflectance's to estimate SDD. This algorithm was used as it was designed for Landsat and because of its acceptable accuracy across several lakes and reservoirs. Giardino *et al.* (2001), made use of a ratio of blue to green, band reflectance. This algorithm was selected for this current study due to its exceptional accuracy when estimating SDD over lakes. The Nas *et al.* (2010), algorithm used a ratio of blue to red and blue band reflectance, It was selected due to its extensive refinement and high accuracy in the Nas *et al.* (2010), study. The two Alparslan *et al.* (2007), algorithms were based on the reflectance of a combination of bands from blue to near infrared. These algorithms were used to estimate SDD by this current study as they showed good accuracy in the Alparslan *et al.* (2010), study and were the best performing algorithms for that study. The two Deutsch *et al.* (2014), algorithms both made use of a ratio of red (band 4) and blue (band 2) reflectance. These bands were used by this current study as they were simple to use. Finally, Baban (1993), used only the blue band it his algorithm for estimating SDD. This was likewise selected to be used by this current study as it was simple to use, was designed for Landsat and showed good accuracy in determining SDD over clear and no longer clear lakes in the Baban (1993), study.

Table 4.4: Turbidity estimation equations adapted for Landsat 8 and Sentinel-2.

Reference	Adapted Equation (Landsat 8)	Adapted Equation (Sentinel-2)	Equation
Dogliotti <i>et al.</i> (2015)	$A_T^{645} * P_w (645) / (1 - P_w (645) / C^{645})$	$A_T^{645} * P_w (645) / (1 - P_w (645) / C^{645})$	Equation 11
Kapalanga (2015)	$15.31856 - 956.806 (R_2) - 747.376 (R_3) + 1742.455 (R_4) + 165.173 (R_5)$	$15.31856 - 956.806 (R_2) - 747.376 (R_3) + 1742.455 (R_4) + 165.173 (R_{8a})$	Equation 12
Garaba and Zielinski (2015)	$1155.60 (R_{rs4}) - 1.27$	$1155.60 (R_{rs4}) - 1.27$	Equation 13
Khattab and Merkel (2014)	$35.121 - 14.489 ((R_3)/(R_4)) - 0.911 (R_5)$	$35.121 - 14.489 ((R_3)/(R_4)) - 0.911 (R_{8a})$	Equation 14
Nas <i>et al.</i> (2010)	$- 0.221 - 0.463 (R_2) + 0.722 (R_3) + 0.841 (R_4)$	$- 0.221 - 0.463 (R_2) + 0.722 (R_3) + 0.841 (R_4)$	Equation 15
Abdullah (2015)	$- 42.564 + 0.052 ((R_4)+(R_5)) + 13.923 ((R_1)/(R_4))$	$- 42.564 + 0.052 ((R_4)+(R_{8a})) + 13.923 ((R_1)/(R_4))$	Equation 16
Abdullah (2015)	$- 4.223 + 1.412 ((R_2)/(R_4)) + 2.957 ((R_3)/(R_1))$	$- 4.223 + 1.412 ((R_2)/(R_4)) + 2.957 ((R_3)/(R_1))$	Equation 17
Song <i>et al.</i> (2011)	$(R_5)/(R_2)$	$(R_{8a})/(R_2)$	Equation 18

$R$ : TOA reflectance for band number;  $R_{rs}$ : Remote sensing reflectance for band number;  $A_T$  : is a wavelength dependent coefficient ( for red = 228.1);  $C_T$ : is a wavelength dependent coefficient( for red = 0.1641);  $P_w$ : Marine reflectance

Table 4.5: SDD estimation equations adapted for Landsat 8 and Sentinel-2.

Reference	Adapted Equation (Landsat 8)	Adapted Equation (Sentinel-2)	Equation
Hancock (2015)	$- 10.4643 (R_4/ R_3) - 0.0026 (R_4) + 24.9021$	$- 10.4643 (R_4/ R_3) - 0.0026 (R_4) + 24.9021$	Equation 19
Giardino <i>et al.</i> (2001)	$8.01 * (R_2)/ (R_3) - 8.27$	$8.01 * (R_2)/ (R_3) - 8.27$	Equation 20
Nas <i>et al.</i> (2010)	$- 16.89 + 93.84 (R_2/R_4) - 2.162 (R_2)$	$- 16.89 + 93.84 (R_2/R_4) - 2.162 (R_2)$	Equation 21
Alparslan <i>et al.</i> (2007)	$- 10.408 + 0.0542 (R_2) + 0.2703 (R_3) + 0.01 (R_4) - 0.3093 (R_5)$	$- 10.408 + 0.0542 (R_2) + 0.2703 (R_3) + 0.01 (R_4) - 0.3093 (R_{8a})$	Equation 22
Alparslan <i>et al.</i> (2010)	$- 13.438 + 495.487 (R_2) - 347.095 (R_3) - 192.402 (R_4) - 125.433 (R_5)$	$- 13.438 + 495.487 (R_2) - 347.095 (R_3) - 192.402 (R_4) - 125.433 (R_{8a})$	Equation 23
Deutsch <i>et al.</i> (2014)	$-1.3 + 2.7 \ln (R_2/R_4)$	$-1.3 + 2.7 \ln (R_2/R_4)$	Equation 24
Deutsch <i>et al.</i> (2014)	$0.2 + 1.4 \ln (R_2/R_4)$	$0.2 + 1.4 \ln (R_2/R_4)$	Equation 25
Baban (1993)	$5.41 - 0.0748 (R_2)$	$5.41 - 0.0748 (R_2)$	Equation 26

$R$ : TOA reflectance for band number;  $R_{rs}$ : Remote sensing reflectance for band number

#### 4.2.4.4 Salinity, TDS and EC

Studies have shown that sea surface salinity can be derived using multispectral remote sensing in both coastal and estuarine environments (Urquhart *et al.*, 2012; Geiger *et al.*, 2013; Garaba and Zielinski, 2015). Salinity can be measured in several ways, including from inferring the relationship between temperature and salinity. Estimation algorithms used for the purpose of obtaining salinity, TDS and EC are displayed by Tables 4.6, 4.7 and 4.8 respectively.

A large number of salinity estimation algorithms were designed for use in oceans. Garaba and Zielinski (2015), used the remote sensing reflectance of the coastal blue band in an attempt to determine salinity. This algorithm was selected to be used by this current study as it was designed for Landsat 8, was simple to use and proved very effective at estimating coastal salinity in the Garaba and Zielinski (2015), study. The Lavery *et al.* (1993), algorithms made

use of the near infrared (Equation 28) or shortwave infrared (Equation 29) band reflectance to estimate salinity. They were selected for estimating salinity by this current study due to their simplicity of use. Dewidar and Khedr (2001), made use of red band reflectance in combination with a ratio of green and near infrared band reflectance. This algorithm was used to estimate salinity by this current study as it was designed for use by Landsat in estuary like environments. Wang and Xu (2008), made use of a combination of the remote sensing reflectance's of the coastal blue through to the near infrared band. This algorithm was selected for use by this current study to estimate salinity as it was designed for use in an estuarine lake. Zhao *et al.* (2017), likewise made use of the remote sensing reflectance's of the coastal blue through to the red band to determine salinity. It was used by this current study as it was designed for use by Landsat 8 and showed exceptional accuracy in determining oceanic salinity in the Zhao *et al.* (2017), study.

Khatab and Merkel (2014), developed two algorithms for the estimation of TDS. Equation 33 used a ratio of the reflectance of green to red and blue to red. Equation 34 made use of the green and near infrared band reflectance. In addition, both algorithms made use the reflectance captured by the thermal infrared bands aboard Landsat and could therefore not be used for modelling with Sentinel-2 as it lacked these bands. These algorithms were used by this current study as they achieved exception accuracy in estimating TDS in lakes. This was hoped to be translated into success at estimating TDS in an estuary. Abdelmalik (2018), used the reflectance from the near infrared band to determine TDS. This was selected for use by the study as the algorithm showed exceptional accuracy in TDS estimation in the Abdelmalik (2018), study. Abdullah (2015), made use of a simple ratio of the reflectance of the near infrared to coastal blue band to determine TDS. This algorithm was selected for use as it was designed and tested for Landsat 8 freshwater TDS estimation.

Just as was done with TDS, two Khatab and Merkel (2014), algorithms were selected to try estimate EC. Equation 37 used a ratio of the reflectance's of the green to red bands (bands 3 and 4). Equation 38 was more complex and incorporated the reflectance from the thermal and near infrared bands and a ratio of red to green reflectance. Both these algorithms were selected for use as they were designed for Landsat use and were the best performing algorithms in the Khatab and Merkel (2014), study. Abdelmalik (2018), used a ratio of the shortwave infrared to near infrared. This algorithm was selected for use as it also showed exceptional accuracy in estimating EC in the Abdelmalik (2018), study. Finally, two algorithms developed by Abdullah (2015), were selected for use by this current study. Equation 40 made use of a ratio of

shortwave infrared 1 to coastal blue band reflectance. Equation 41 made use of only the shortwave infrared 2 band reflectance. Both these algorithms were selected for use by this current study as they were developed and tested for Landsat 8 EC extraction.

Table 4.6: Salinity estimation equations adapted for Landsat 8 and Sentinel-2.

Reference	Adapted Equation (Landsat 8)	Adapted Equation (Sentinel-2)	Equation
Garaba and Zielinski (2015)	$96.72 (R_{rs1}) + 30.31$	$96.72 (R_{rs1}) + 30.31$	Equation 27
Lavery <i>et al.</i> (1993)	$36.72 - 0.27 (R_5)$	$36.72 - 0.27 (R_{8a})$	Equation 28
Lavery <i>et al.</i> (1993)	$35.55 - 0.92 (R_7)$	$35.55 - 0.92 (R_{12})$	Equation 29
Dewidar and Khedr (2001)	$-18.357 + 222.102 (R_4) + 47.124 (R_3/R_5)$	$-18.357 + 222.102 (R_4) + 47.124 (R_3/R_{8a})$	Equation 30
Wang and Xu (2008)	$4.7648 + 65.242 (R_1) + 122.614 (R_2) - 150.068 (R_3) + 61.054 (R_4) - 91.404 (R_5)$	$4.7648 + 65.242 (R_1) + 122.614 (R_2) - 150.068 (R_3) + 61.054 (R_4) - 91.404 (R_{8a})$	Equation 31
Zhao <i>et al.</i> (2017)	$39.664 - 39.664 (R_{rs1}) + 1067.5 (R_{rs2}) - 189.58 (R_{rs3}) + 1640.8 (R_{rs4}) + 23823 (R_{rs1})^2 - 17844 (R_{rs2})^2 + 1944.7 (R_{rs3})^2 - 94613 (R_{rs4})^2$	$39.664 - 39.664 (R_{rs1}) + 1067.5 (R_{rs2}) - 189.58 (R_{rs3}) + 1640.8 (R_{rs4}) + 23823 (R_{rs1})^2 - 17844 (R_{rs2})^2 + 1944.7 (R_{rs3})^2 - 94613 (R_{rs4})^2$	Equation 32

*R*: TOA reflectance for band number; *R<sub>rs</sub>*: Remote sensing reflectance for band number

Table 4.7: TDS estimation equations adapted for Landsat 8 and Sentinel-2.

Reference	Adapted Equation (Landsat 8)	Adapted Equation (Sentinel-2)	Equation
Khattab and Merkel (2014)	$-0.149 + 0.104 (R_3/R_4) - 0.025 (R_2/R_4) + 0.004 ((R_{10} + R_{11})/2)$	None (Sentinel-2 lacks thermal bands)	Equation 33
Khattab and Merkel (2014)	$-0.920 - 0.002(R_3) + 0.01 ((R_{10} + R_{11})/2) + 0.001(R_5)$	None (Sentinel-2 lacks thermal bands)	Equation 34
Abdelmalik (2018)	$-0.1204 (R_5)^2 + 10.663 (R_5) - 207.21$	$-0.1204 (R_{8a})^2 + 10.663 (R_{8a}) - 207.21$	Equation 35
Abdullah (2015)	$120.750 + 264.752$	$120.750 + 264.752$	Equation 36

$$(R_5/R_1)$$

$$(R_{8a}/R_1)$$

*R*: TOA reflectance for band number; *R<sub>rs</sub>*: Remote sensing reflectance for band number

Table 4.8: EC estimation equations adapted for Landsat 8 and Sentinel-2.

Reference	Adapted Equation (Landsat 8)	Adapted Equation (Sentinel-2)	Equation
Khattab and Merkel (2014)	$0.5185 - 0.3679 / ((R_3)/(R_4))$	$0.5185 - 0.3679 / (R_3/R_4)$	Equation 37
Khattab and Merkel (2014)	$- 0.585 + 0.002(R_5) + 0.008 ((R_{10}+R_{11})/2) + 0.322 ((R_4)/(R_3))$	None (Sentinel-2 lacks thermal bands)	Equation 38
Abdelmalik (2018)	$- 0.1252 ((R_6)/(R_5) * R_7))^2 + 4.1531 ((R_6)/(R_5) * R_7)) + 10.527$	$- 0.1252 ((R_{11})/(R_{8a}) * R_{12}))^2 + 4.1531 ((R_{11})/(R_{8a}) * R_{12})) + 10.527$	Equation 39
Abdullah (2015)	$241.500 + 529.504 ((R_5)/(R_1))$	$241.500 + 529.504 ((R_{8a})/(R_1))$	Equation 40
Abdullah (2015)	$422.034 - 1080.365 (R_6)$	$422.034 - 1080.365 (R_{11})$	Equation 41

*R*: TOA reflectance for band number; *R<sub>rs</sub>*: Remote sensing reflectance for band number

#### 4.2.2.4 Chlorophyll-a

The estimation of chlorophyll-a content through the use of remote sensing methods is one of the most popular objectives when it comes to remotely sensed water quality assessments. These estimation algorithms are often more diverse than those of other water parameters and may include using single bands, rationing or indexes such as NDVI. Therefore a large number of algorithms were tested to determine their efficiency within the Umdloti Estuary. All algorithms used in the study to estimate chl-a were recorded in Table 4.9. Several estimation algorithms were discussed below in order to highlight the different forms these equations may come in. Sometimes other physico-chemical parameters are used to aid in the determination of chl-a, such as the use of water temperature by Bonansea *et al.* (2015), However, these were not tested in this study as it relied on other parameters that we aimed to retrieve.

Nas *et al.* (2007), and Lim and Choi (2015), algorithms made use of a combination of the blue, green, red and near infrared band reflectance's in estimating chl-a. These algorithms was selected for use as it was designed for Landsat usage and previously had performed well in estimating chl-a in freshwater lakes. Tenjo *et al.* (2015), and Ruiz-Verdú *et al.* (2016), both used a ratio of green to coastal blue band remote sensing reflectance to estimate chl-a. This

algorithm was selected for use due to its simplicity and the fact that it was designed to use remote sensing reflectance (which has been atmospherically corrected). One of the more unique methods of its calculation was done by Cândido *et al.* (2016). Cândido *et al.* (2016), used several popular vegetation indices in order to estimate the content of Chl-a. These indices include NDVI ( $\text{NIR} - \text{RED} / \text{NIR} + \text{RED}$ ); Ratio aquatic vegetation index ( $\text{RAVI} = \text{GREEN} / \text{RED}$ ); Normalised Ratio aquatic vegetation index ( $\text{NRAVI} = \text{GREEN} - \text{RED} / \text{GREEN} + \text{RED}$ ) and excess green ( $\text{ExG} = 2 * \text{GREEN} - \text{RED} - \text{BLUE}$ ) which make use of the near-infrared (NIR), Red (RED), Green (GREEN) and Blue (BLUE) bands. These generally had good accuracy in predicting the amounts of Chl-a in the Cândido *et al.* (2016), study and were selected for that reason to be used in this study. El-Magd and Ali (2008), developed two algorithms that were selected for use by this current study as they were simple and easy to use. Both Equation 51 and 52 made use of a ratio of band 2 to band 4 reflectance. The Toming *et al.* (2016), algorithm used a combination of the red, near infrared and shortwave infrared band reflectance's to estimate chl-a. This was used to estimate chl-a by this current study as the algorithm was designed and tested for Sentinel-2 usage and showed good accuracy in the original study. The Watanabe *et al.* (2015), algorithm used a ratio of near infrared to red reflectance to estimate chl-a. this algorithm was selected for use by this current study as it was designed and tested for Landsat 8 and was simplest and most accurate algorithm tested in the Watanabe *et al.* (2015), study. Forrer (2012), used a simple ratio of blue to near infrared band reflectance to estimate chl-a. This was used in this current study as algorithm showed high accuracy and was tested over several freshwater bodies by Forrer (2012). Jaelani *et al.* (2016), used a log ratio of the green to red band reflectance in determining chl-a. The fact that it was designed for Landsat 8 usage and was shown to be reliable by Jaelani *et al.* (2016), supported its use by this current study to estimate chl-a.

Table 4.9: Chl-a estimation equations adapted for Landsat 8 and Sentinel-2.

Reference	Adapted Equation (Landsat 8)	Adapted Equation (Sentinel-2)	Equation
Nas <i>et al.</i> (2007)	$-1.024 + 00086 (R_2) - 0.013 (R_3) - 0.096 (R_4) + 0.367 (R_5)$	$-1.024 + 00086 (R_2) - 0.013 (R_3) - 0.096 (R_4) + 0.367 (R_{8a})$	Equation 42
Tenjo <i>et al.</i> (2015) and Ruiz-Verdú <i>et al.</i> (2016)	$4.46 (R_{rs3}/R_{rs1}) - 0.55$	$4.46 (R_{rs3}/R_{rs1}) - 0.55$	Equation 43
Cândido <i>et al.</i> (2016)	$2.723 - 1.406 (RAVI)$	$2.723 - 1.406 (RAVI)$	Equation 44
Cândido <i>et al.</i> (2016)	$1.318 - 3.036 (NRAVI)$	$1.318 - 3.036 (NRAVI)$	Equation 45
Cândido <i>et al.</i> (2016)	$1.274231 - 0.009154 (ExG)$	$1.274231 - 0.009154 (ExG)$	Equation 46
Cândido <i>et al.</i> (2016)	$39.88 - 32.85 (RAVI)$	$39.88 - 32.85 (RAVI)$	Equation 47
Cândido <i>et al.</i> (2016)	$4.712 - 34.578 (NRAVI)$	$4.712 - 34.578 (NRAVI)$	Equation 48
Cândido <i>et al.</i> (2016)	$0.3855 - 0.1790 (ExG)$	$0.3855 - 0.1790 (ExG)$	Equation 49
Cândido <i>et al.</i> (2016)	$4.079 + 17.218 (NDVI)$	$4.079 + 17.218 (NDVI)$	Equation 50
El-Magd and Ali (2008)	$(R_2) / (R_4)$	$(R_2) / (R_4)$	Equation 51
El-Magd and Ali (2008)	$\text{Log } (R_2 / R_4)$	$\text{Log } (R_2 / R_4)$	Equation 52
Toming <i>et al.</i> (2016)	$(R_5) - ((R_4 + R_6)/2)$	$(R_{8a}) - ((R_4 + R_{11})/2)$	Equation 53
Watanabe <i>et al.</i> (2015)	$(R_{rs5}) / (R_{rs4})$	$(R_{rs8a}) / (R_{rs4})$	Equation 54
Forrer (2012)	$(R_2) / (R_5)$	$(R_2) / (R_{8a})$	Equation 55
Jaelani <i>et al.</i> (2016)	$1.613 ((\log R_{rs2})/(\log R_{rs4})) + 1.0718$	$1.613 (\log R_{rs2})/(\log R_{rs4}) + 1.0718$	Equation 56
Lim and Choi (2015)	$54.658 + 520.451 (R_2) - 1221.89 (R_3) + 611.115 (R_4) - 198.199 (R_5)$	$54.658 + 520.451 (R_2) - 1221.89 (R_3) + 611.115 (R_4) - 198.199 (R_{8a})$	Equation 57

*R*: TOA reflectance for band number; *R<sub>rs</sub>*: Remote sensing reflectance for band number; RAVI: Ratio aquatic vegetation index; NRAVI: Normalised Ratio aquatic vegetation index; ExG: Excess green; NDVI: Normalised difference vegetation index.



#### 4.2.2.6 Dissolved oxygen

DO has traditionally been a difficult to retrieve physico-chemical parameter using remote sensing. As a result, not many studies have managed to develop effective estimation algorithms. This was evidenced in Table 4.10, which included only three algorithms for use in DO estimation. The Theologou *et al.* (2015), and Khalil *et al.* (2016), used a simple ratio of blue to red band reflectance in estimating DO. Theologou *et al.* (2015), used an average of the green and red band reflectance's in their estimation. Abdullah (2015), used a combination of band reflectance's from the coastal blue, blue and near infrared bands. All three algorithms were selected for usage by this study as DO estimation algorithms were difficult to find in literature and all showed success in their respective studies in estimating DO.

Table 4.10: DO estimation equations adapted for Landsat 8 and Sentinel-2.

Reference	Adapted Equation (Landsat 8)	Adapted Equation (Sentinel-2)	Equation
Theologou <i>et al.</i> (2015) ; Khalil <i>et al.</i> (2016)	$(R_2) / (R_4)$	$(R_2) / (R_4)$	Equation 58
Theologou <i>et al.</i> (2015)	$((R_3) + (R_4)) / 2$	$((R_3) + (R_4)) / 2$	Equation 59
Abdullah (2015)	$10.841 - 0.682 ((R_1) / (R_5)) - 0.002 ((R_2) / (R_5) + (B_2))$	$10.841 - 0.682 ((R_1) / (R_{8a})) - 0.002 ((R_2) / (R_{8a}) + (B_2))$	Equation 60

*R*: TOA reflectance for band number; *R<sub>rs</sub>*: Remote sensing reflectance for band number

#### 4.2.2.7 pH

The estimation of water pH using remote sensing methods is often left out in many studies. This is because most studies focus on optically active parameters such as those so far mentioned (Gholizadeh *et al.*, 2016). pH has weak optical characteristics and has a low signal to noise ratio, resulting in it usually being ignored. However this has not stopped attempts at their estimation. Khattab and Merkel (2014), used both Landsat 7 and 5 to determine the pH of water. Since Landsat 7's method made use of bands 61 and 62 (the low and high gain thermal bands) which are not present in Landsat 8, these methodologies were not used. Algorithms used for pH estimation are displayed in Table 4.11.

The Perivolioti *et al.* (2016), algorithm used the remote sensing reflectance of the near infrared band to estimate pH. This was used by this current study as algorithms designed using remote sensing reflectance are usually more accurate. Three Theologou *et al.* (2015), algorithms were used to estimate pH by the current study. These used simple ratios of the near infrared to shortwave infrared 1 band reflectance (Equation 62), coastal blue to red band reflectance's (Equation 63) and a ratio of the blue to shortwave infrared 2 bands (Equation 65). These algorithms were all chosen for their simplicity and because they were the best performing algorithms developed by the Theologou *et al.* (2015), study. Khattab and Merkel (2014), used a simple equation using the shortwave infrared 1 band to estimate pH. This was likewise selected for its simplicity and accuracy in the original study. Finally, the Abdullah (2015), algorithm was slightly more complex and used the shortwave infrared 1 and a ratio of green to red band reflectance's to estimate pH. An overall reason why all algorithms pH estimation algorithms were selected for use by this current study was due to their rarity in literature.

Table 4.11: pH estimation equations adapted for Landsat 8 and Sentinel-2.

Reference	Adapted Equation (Landsat 8)	Adapted Equation (Sentinel-2)	Equation
Perivolioti <i>et al.</i> (2016)	$9.738 - 0.084(R_{rs5})$	$9.738 - 0.084 (R_{rs8a})$	Equation 61
Theologou <i>et al.</i> (2015)	$(R_5) / (R_6)$	$(R_{8a}) / (R_{11})$	Equation 62
Theologou <i>et al.</i> (2015)	$(R_{rs1}) / (R_{rs4})$	$(R_{rs1}) / (R_{rs4})$	Equation 63
Khattab and Merkel (2014)	$9.738 - 0.084 (R_6)$	$9.738 - 0.084 (R_{11})$	Equation 64
Theologou <i>et al.</i> (2015)	$(R_2) / (R_7)$	$(R_2) / (R_{12})$	Equation 65
Abdullah (2015)	$8.790 + 0.141 (R_6) - 0.228 (R_3/R_4)$	$8.790 + 0.141 (R_{11}) - 0.228 (R_3/R_4)$	Equation 66

*R*: TOA reflectance for band number; *R<sub>rs</sub>*: Remote sensing reflectance for band number

#### 4.2.3 Accuracy assessment

Accuracy assessment formed an important component towards checking whether the two remote sensors were able to accurately retrieve physico-chemical parameter concentrations. This first required the in situ collection and testing of water samples. For this, fifteen samples

each were collected during both winter and spring. This cumulatively came up to thirty samples for both seasons. Sampling was done during differing seasons to get a more complete picture of the health state the estuary was in by trying to incorporate seasonal variation and to test the model algorithms under differing seasonal conditions. The comparison of physico-chemical parameters found in these samples with their remotely sensed predicted values allowed for a determination of how accurate remote sensing is at retrieving these parameters.

Accuracy assessment made use of two methods. The regression coefficient of determination ( $R^2$ ) was used to assess the relative fitness of a estimation algorithm in modelling a particular parameter. This was given in Equation 67. Higher  $R^2$  values indicated that the estimation algorithm in question were good predictors for that particular physico-chemical parameter. Root mean squared error (RMSE) was also used as a form of accuracy assessment and was defined as the square root of the residual variance. The equation to calculate RMSE is given in Equation 68. This essentially measured how closely observed values match up with their respective predicted values. Smaller RMSE values indicate a better ability of the model at determining the absolute concentrations of physical-chemical parameters. These two accuracy assessment checks were used on the data retrieved for both sensors winter, spring and combined seasonal sampling. The combined seasonal dataset represented a combination of both winter and spring data in an attempt to determine if the parameter estimation algorithms are able to accurately perform estimation throughout the year. All collected water samples were used in the generation and calibration of new algorithms as well the quality assessment for all models.

$$R^2 = \frac{\sum(x-x')(y-y')}{\sum(x-x')^2(y-y')^2} \quad (\text{Equation 67})$$

Where:

$R^2$  = Coefficient of determination;  $X$  = The x-value observed at a particular sampling point;  $X'$  = The x-value predicted at a particular sampling point;  $Y$  = The y-value predicted at a particular sampling point;  $Y'$  = The y-value predicted at a particular sampling point.

$$RMSE = \sqrt{\frac{\sum_{i=1}^n (Pi - Oi)^2}{n}} \quad (\text{Equation 68})$$

Where:

$RMSE$  = Root mean squared error;  $Pi$  = Predicted value at a particular sampling point;  $Oi$  = Observed value at a particular sampling point;  $n$  = Number of observed and predicted pairs.

#### 4.2.4 Modified algorithms and distribution maps

In an attempt to improve on remote sensing physico-chemical estimation, new estimation algorithms were formulated. New algorithms were modelled using Microsoft Excel and based on the band combinations of the most successful algorithms (in terms of  $R^2$  and RMSE) tested over the course of this study. This modelling involved developing a trend between in situ physico-chemical parameter values and the band combination reflectance values obtained by satellite. Once completed, this allowed for the prediction of these same parameters. These “new” estimation algorithms were thereafter tested for their physico-chemical estimation accuracy. The new equations are represented in Table 4.12. The distribution of each physico-chemical parameter across the estuary was modelled using the new equations in ArcMap 10.4.

Temperature was based off of the Abdullah (2015), algorithm. A combination of bands 1 and 4 were compared with in situ temperature and used to model a 2<sup>nd</sup> degree polynomial equation. Turbidity was based off of the Dogliotti *et al.* (2015), equation. This used the marine reflectance of band 4 to model a 2<sup>nd</sup> degree polynomial to retrieve turbidity. Deutsch *et al.* (2014), (Equation 27) was used as a base to model SDD. For this, bands 2 and 4 were incorporated into a 2<sup>nd</sup> degree polynomial. El-Magd and Ali (2008), was used to model chl-a using a log of combined bands 2 and 4. This was thereafter incorporated into a 4<sup>th</sup> degree polynomial. DO algorithms were based on those developed by Theologou *et al.* (2015). Again bands 2 and 4 were used to formulate a 2<sup>nd</sup> degree polynomial to model DO. The derivation of pH was based off of the work of Khattab and Merkel (2014). The original equation formulated using Landsat 5 and Landsat 7 utilised band 5 which was represented in Landsat 8 by band 6 and Sentinel-2 by band 11. This resulted in a 3<sup>rd</sup> degree polynomial equation for the estimation of pH.

Table 4.12: Newly generated physico-chemical estimation algorithms

Parameter	Adapted Equation	Equation
Temperature	$-17477 (R_{rs1} + R_{rs4})^2 + 1139.7 (R_{rs1} + R_{rs4}) + 6.3866$	Equation 69
Turbidity	$-80.791(P_{w4})^2 + 9.8557 (P_{w4}) + 4.8009$	Equation 70
SDD	$-1.0914 (\ln (R_{rs2}/ R_{rs4}))^2 + 0.5892 (\ln (R_{rs2}/ R_{rs4})) + 1.8502$	Equation 71
Salinity	$35.608 (R_{rs1} + R_{rs2} + R_{rs3} + R_{rs4} + R_{rs5})^2 - 6.8298 (R_{rs1} + R_{rs2} + R_{rs3} + R_{rs4} + R_{rs5}) + 1.1792$	Equation 72
TDS	$31.976 (R_{rs5} / R_{rs1})^3 - 188.19(R_{rs5} / R_{rs1})^2 + 197.58(R_{rs5} / R_{rs1}) + 897.62$	Equation 73
EC	$0.1425 (R_{rs3}/ R_{rs4})^3 - 1.7136 (R_{rs3}/ R_{rs4})^2 + 3.6271 (R_{rs3}/ R_{rs4}) + 0.0967$	Equation 74
Chl-a	$14033 (\log (R_{rs2} / R_{rs4}))^4 - 6251.4 (\log (R_{rs2} / R_{rs4}))^3 + 763.8 (\log (R_{rs2} / R_{rs4}))^2 - 17.395 (\log (R_{rs2} / R_{rs4})) + 0.7519$	Equation 75
DO	$2.7317 (R_{rs2} / R_{rs4})^2 - 8.6415 (R_{rs2} / R_{rs4}) + 9.3987$	Equation 76
pH	$9.738 - 0.084 (R_{11})$	Equation 77

## **CHAPTER FIVE: RESULTS**

### **5.1) Introduction**

This chapter and its subsections serve as a collection for all the results produced throughout the course of this study. This starts with the inclusion of all variables descriptive statistical results that are extracted from in situ water sampling and lab testing. The results of the remote sensing estimation algorithms for each physico-chemical parameter are also given. Included along with this information are maps of the spatial distribution of these parameters throughout the Umdloti Estuary.

### **5.2) Descriptive statistics**

A summary of the descriptive statistics generated for physico-chemical parameters from in situ water sampling and testing is displayed in Table 5.1. This provides an insight on the seasonal conditions the estuary was experiencing. Temperature within the estuary was generally warmish throughout but considerably colder and extending over a greater range in winter. Turbidity and SDD retrieval indicate that water clarity and sunlight penetration was good. Salinity, TDS and EC retrieval indicated that estuarine water was of low salinity. Chl-a retrieved indicates a generally small population of chlorophyll based organisms were present. DO levels indicate moderate to low oxygen contents across the estuary and the retrieved pH indicates that the estuary was slightly alkaline.

Overall, the vast majority of parameters lacked intraseasonal variability and range. Salinity for example did not range by more than 0.1 for winter and 0.3 for spring and have standard deviations below 0.06. Only two parameters (TDS and chl-a) possess standard deviations greater than a whole unit and were the only parameters that showed a relatively larger distributional range. This indicated that most parameters (turbidity, SDD, salinity, TDS and EC) were highly spatially homogenous across the estuary.

A similar lack of variability is found when comparing the parameter interseasonal parameter changes between winter and spring. In general, the majority of parameters differed by relatively small amounts in their range of values between seasons. This is again evidenced best by salinity whose means differed by 0.14 between winter and spring. Exceptions to this included temperature (means of 18.81 °C in winter and 24.70 °C in spring) and to a smaller degree chl-a

(means of 0.61  $\mu\text{g/l}$  in winter and 0.96  $\mu\text{g/l}$  in spring) and dissolved oxygen (means of 2.64 ppm in winter and 3.48 ppm in spring). The low variability and narrow ranges indicate that many physico-chemical parameters remained similarly distributed between seasons.

It should also be noted that many physico-chemical parameters found within the estuary were low in value. This is best evidenced by salinities not larger than 1, turbidity not larger than 5.10 NTU and chl-a not larger than 4.46  $\mu\text{g/l}$ . Estuaries normally have values for these parameters that range much higher than what was found in Umdloti. pH, temperature and SDD could be considered to be displaying a normal, expected range.

Table 5.1: Descriptive statistics from parameters retrieved from in situ sampling.

Parameter	Season	Sample points			
		Minimum	Maximum	Mean	Standard deviation
Temperature ( $^{\circ}\text{C}$ )	Winter	17.50	21.00	18.81	0.79
	Spring	24.60	24.80	24.70	0.10
Turbidity (NTU)	Winter	5.00	5.00	5.00	0.00
	Spring	5.10	5.10	5.10	0.00
Secchi disk depth (m)	Winter	2.33	1.47	1.85	0.23
	Spring	2.33	1.47	1.85	0.23
Salinity	Winter	0.90	1.00	0.99	0.03
	Spring	0.7.0	1.00	0.85	0.06
TDS (mg/l)	Winter	933.00	982.00	955.07	15.09
	Spring	904.00	929.00	921.00	6.14
EC( $\mu\text{S/cm}$ )	Winter	2.13	2.30	2.23	0.04
	Spring	2.13	2.15	2.14	0.01
Chl-a ( $\mu\text{g/l}$ )	Winter	0.13	4.46	0.61	1.10
	Spring	0.38	3.00	0.96	0.65
DO (ppm)	Winter	2.00	3.12	2.64	0.32
	Spring	2.80	4.10	3.48	0.46
pH	Winter	7.34	8.64	7.62	0.33
	Spring	7.06	7.46	7.33	0.12

### 5.3) Statistical analyses

#### 5.3.1 Temperature estimation

##### 5.3.1.1 Using Landsat 8

Landsat 8 temperature estimation is moderately successful. Landsat 8 did a poor job of modelling temperature across the estuary intraseasonally (Table 5.2). This is evidenced by the majority of algorithms attaining  $R^2$  values below 0.182. This indicated almost negligible accuracy. However, this poor ability to model temperature changed once  $R^2$  was calculated for the combined winter and spring dataset (represented in the combined column). Algorithms developed by Khattab and Merkel (2014), (Equation 9) and Abdullah (2015), (Equation 10) and used by this study saw  $R^2$  rise from almost negligible to near perfect accuracies over 0.96. The Avdan and Jovanovska (2016), algorithm (Equation 8) saw a similar large rise in  $R^2$ . These increases indicated that Landsat 8 was effective at more generalised year round modelling. RMSE saw large seasonal changes when using Khattab and Merkel (2014), and Avdan and Jovanovska (2016), algorithms. RMSE for the Abdullah (2015), developed algorithm remained consistent and achieved a stronger average of around 2.996 °C.

Table 5.2: Accuracy of the estimated temperature (°C) using Landsat 8 for Umdloti Estuary.

Equation	Winter		Spring		Combined	
	$R^2$	RMSE	$R^2$	RMSE	$R^2$	RMSE
Equation 8	0.311	1.586	0.182	4.020	0.707	3.056
Equation 9	0.124	7.443	0.131	0.483	0.964	5.274
Equation 10	0.032	3.054	0.094	2.937	0.963	2.996

##### 5.3.1.2 Using Sentinel-2

Only one algorithm, developed by Abdullah (2015), can be considered to be appropriate for temperature calculation using Sentinel-2 remote sensing imagery (Table 5.3). The Avdan and Jovanovska (2016), and Khattab and Merkel (2014), equations required the use of thermal bands. Sentinel-2 does not possess thermal bands and therefore would not be able to model temperature using those two equations. Similar to the results for Landsat 8, low  $R^2$  values can be found for individual winter and spring datasets. When seasonal data is combined, Sentinel-2



displayed a much better ability at modelling overall temperature. RMSE calculated were relatively inconsistent but strong and indicated a generally good ability for determining absolute temperature.

Table 5.3: Accuracy of the estimated temperature (°C) using Sentinel-2 for Umdlotti Estuary.

Equation	Winter		Spring		Combined	
	R <sup>2</sup>	RMSE	R <sup>2</sup>	RMSE	R <sup>2</sup>	RMSE
Equation 10	0.073	1.397	0.281	2.936	0.950	2.299

Overall, temperature estimation algorithms show a moderate to good ability at determining temperature across the estuary. Intraseasonal modelling indicates a poor relative accuracy. The algorithms developed by Khattab and Merkel (2014), and Avdan and Jovanovska (2016), and used by this study are generally inconsistent and restricted to Landsat 8. The Abdullah (2015), algorithm appears to be the better algorithm overall as it can be used with both sensors and has the second highest recorded R<sup>2</sup> (0.963 and 0.950) and best RMSE (2.996 °C and 2.299 °C). Although difficult to compare with only one comparable equation, Sentinel-2 would appear to be the more accurate, albeit less flexible, sensor with lower RMSE but with a slight decrease in ability to model variability.

#### 5.3.1.3 Using newly modified algorithm

The new algorithm (Table 5.4) was based on an Rrs combination of bands 1 and 4 as used by Abdullah (2015). Overall this algorithm was efficient at determining temperature and achieved a high R<sup>2</sup> and low RMSE that showed considerable improvement over those previously used. The algorithm could be considered suitable for temperature estimation during both these seasons but suffers from a poor ability to relatively model temperature intraseasonally.

Table 5.4: Accuracy of the estimated temperature (°C) using newly generated estimation algorithms for Umdlotti Estuary.

Equation	Winter R <sup>2</sup>	Spring R <sup>2</sup>	Combined R <sup>2</sup>	Winter RMSE	Spring RMSE	Combined RMSE
Equation 69	0.03	0.032	0.96	0.827	0.22	0.605

#### 5.3.1.4 Scatterplots of temperature models.

Figure 5.2 illustrates the graphical relationship between the actual measured temperatures and those predicted by the algorithms. A theme common to all scatterplots is the formation of two distinct clusters of points. These clusters are clearly defined by season (winter being a lower temperature value cluster and spring a higher temperature value cluster). This is to be expected due to the seasonal nature of temperature, where temperature would tend to rise and remain much higher in spring than winter. All models achieved high  $R^2$  values which indicates the successful modelling of temperature.

#### 5.3.1.5 Map of estimated temperature

Finally, the estimation algorithm modified by this study are used to map the seasonal distribution of temperature across the Umdloti Estuary (Figure 5.1). This map and future distribution maps are created using only Sentinel-2 imagery. Temperature was generally lower across the estuary in winter (~18.8 to 19.4 °C) than in spring (~24 to 28 °C). In winter the middle of estuary appears to be at a higher temperature than water in other parts. In spring the warmest portions of the estuary are those closest to the sea (eastern border).

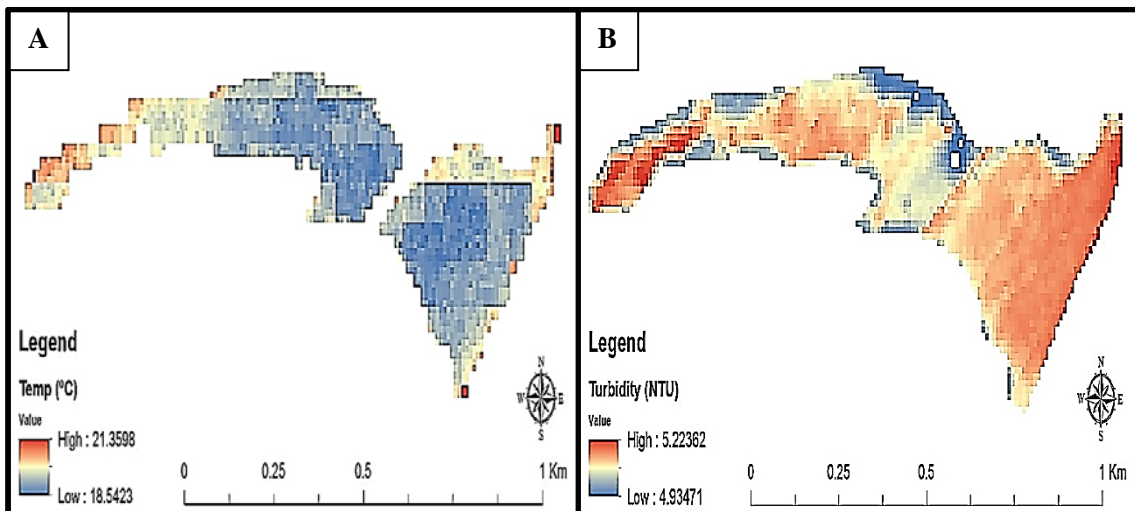


Figure 5.1: Temperature distribution across the Umdloti Estuary for winter (A) and spring (B)

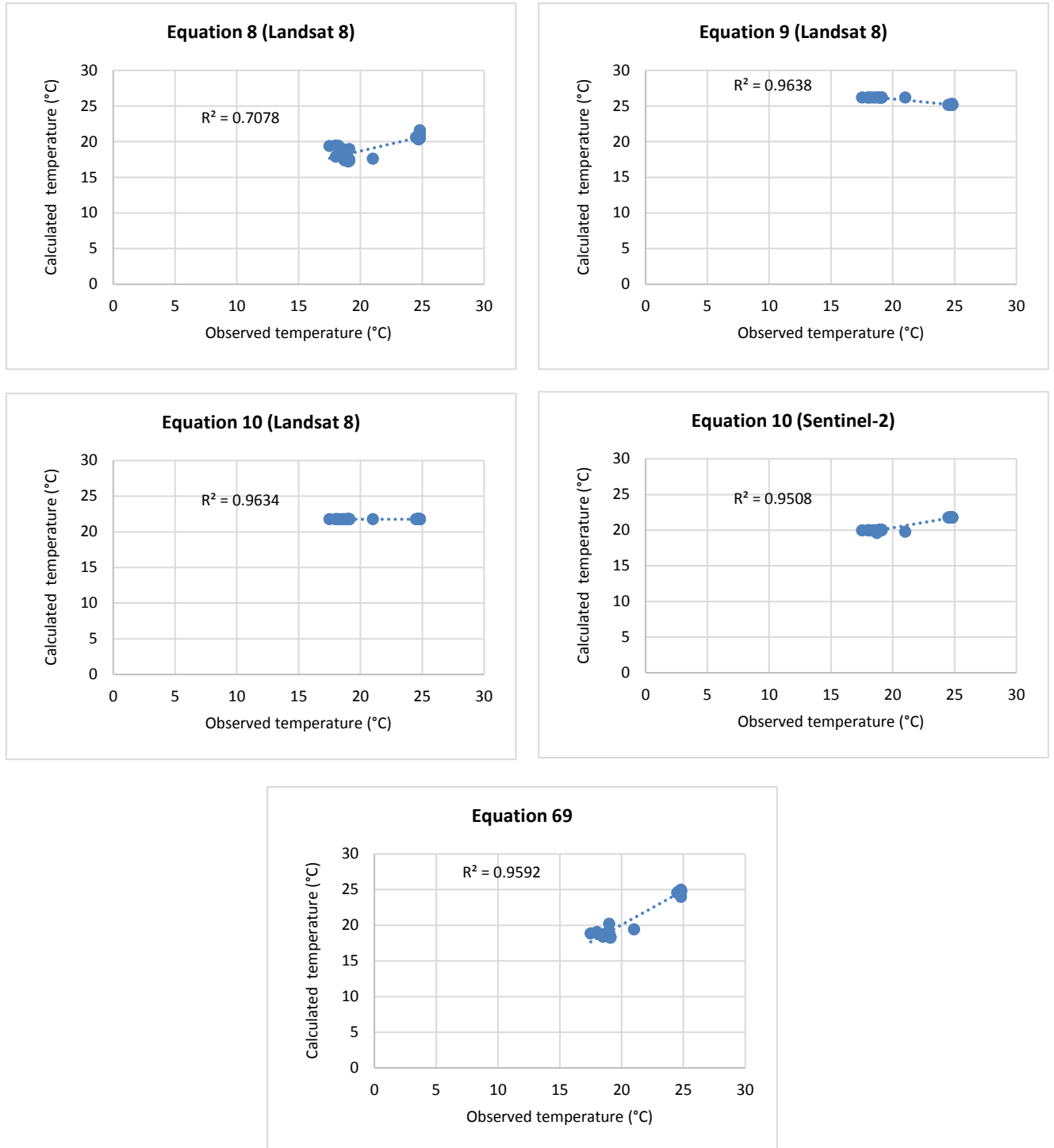


Figure 5.2: Scatterplots of observed vs. calculated values for all temperature estimation algorithms.

### 5.3.2 Turbidity estimation

#### 5.3.2.1 Using Landsat 8

Turbidity estimation results for Landsat 8 were recorded in Table 5.5. Due to the lack of variability in in situ turbidity across the estuary,  $R^2$  values were not able to be recorded for winter or spring seasons. Only once the datasets are combined and compared overall is  $R^2$  able to be retrieved.  $R^2$  values were very high, with six of the eight algorithms recording values above 0.95. The Khattab and Merkel (2014), algorithm (Equation 15) are the only algorithms that failed to register a  $R^2$  above 0.312. RMSE values were also accurately low on average, with half of the algorithms achieving a RMSE below 10 NTU. This indicates a strong ability by Landsat 8 at relatively modelling and absolutely determining turbidity.

Table 5.5: Accuracy of the estimated turbidity (NTU) using Landsat 8 for Umdlotti Estuary.

Equation	Winter		Spring		Combined	
	$R^2$	RMSE	$R^2$	RMSE	$R^2$	RMSE
Equation 11	Not Derived	3.932	Not Derived	2.057	0.989	3.133
Equation 12	Not Derived	8.822	Not Derived	14.631	0.953	12.083
Equation 13	Not Derived	1.003	Not Derived	23.933	0.991	16.938
Equation 14	Not Derived	16.184	Not Derived	15.581	0.312	15.889
Equation 15	Not Derived	5.224	Not Derived	5.292	0.991	5.255
Equation 16	Not Derived	25.510	Not Derived	33.046	0.958	29.517
Equation 17	Not Derived	5.179	Not Derived	5.026	0.719	5.099
Equation 18	Not Derived	4.334	Not Derived	4.072	0.965	4.202

#### 5.3.2.2 Using Sentinel-2

Similar to what is found for Landsat 8, Sentinel-2 (Table 5.6) RMSE is low throughout whilst  $R^2$  values are high. RMSE retrieved during spring were on average substantially higher than retrieved during winter. This indicates the Sentinel-2 based estimation algorithm works better during winter conditions. The Abdullah (2015), algorithm (Equation 17) is the only algorithm to achieve a high and inaccurate RMSE (23.741 NTU).

Table 5.6: Accuracy of the estimated turbidity (NTU) using Sentinel-2 for Umdloti Estuary.

Equation	Winter		Spring		Combined	
	R <sup>2</sup>	RMSE	R <sup>2</sup>	RMSE	R <sup>2</sup>	RMSE
Equation 11	Not Derived	3.744	Not Derived	13.963	0.955	2.755
Equation 12	Not Derived	3.744	Not Derived	13.963	0.995	10.221
Equation 13	Not Derived	3.934	Not Derived	13.996	0.973	10.279
Equation 14	Not Derived	3.980	Not Derived	15.269	0.998	11.156
Equation 15	Not Derived	3.630	Not Derived	5.301	0.999	4.541
Equation 16	Not Derived	4.127	Not Derived	33.319	0.998	23.741
Equation 17	Not Derived	0.943	Not Derived	4.979	0.994	3.582
Equation 18	Not Derived	1.788	Not Derived	3.759	0.728	2.941

### 5.3.2.3 Using newly modified algorithm

The turbidity estimation equation modified by this study is based on Dogliotti *et al.* (2015), and the use of band 4 marine reflectance (Table 5.7). This algorithm displayed almost perfect accuracy in modelling turbidity as shown by a very strong overall R<sup>2</sup> and RMSE. This algorithm is suitable for use both intraseasonally and throughout the year without issue.

Table 5.7: Accuracy of the estimated turbidity (NTU) using newly generated estimation algorithms for Umdloti Estuary.

Equation	Winter R <sup>2</sup>	Spring R <sup>2</sup>	Combined R <sup>2</sup>	Winter RMSE	Spring RMSE	Combined RMSE
Equation 70	Not Derived	Not Derived	0.99	0.006	0.004	0.005

### 5.3.2.4 Scatterplots of turbidity models.

Figures 5.3 to 5.5 illustrate the graphical relationship between the actual measured turbidity and those predicted by the algorithms. Again, all algorithms gathered into two distinct clusters dictated by the winter and spring. The majority of models experienced an almost straight vertical line of best fit from winter to spring. Others (Landsat Equation 14, 15 and 70) clustered around a single spot. R<sup>2</sup> values for the majority of models are good, indicating the successful modelling of turbidity. Equation 14 and 17 are the only algorithms that suffered from poor R<sup>2</sup>.

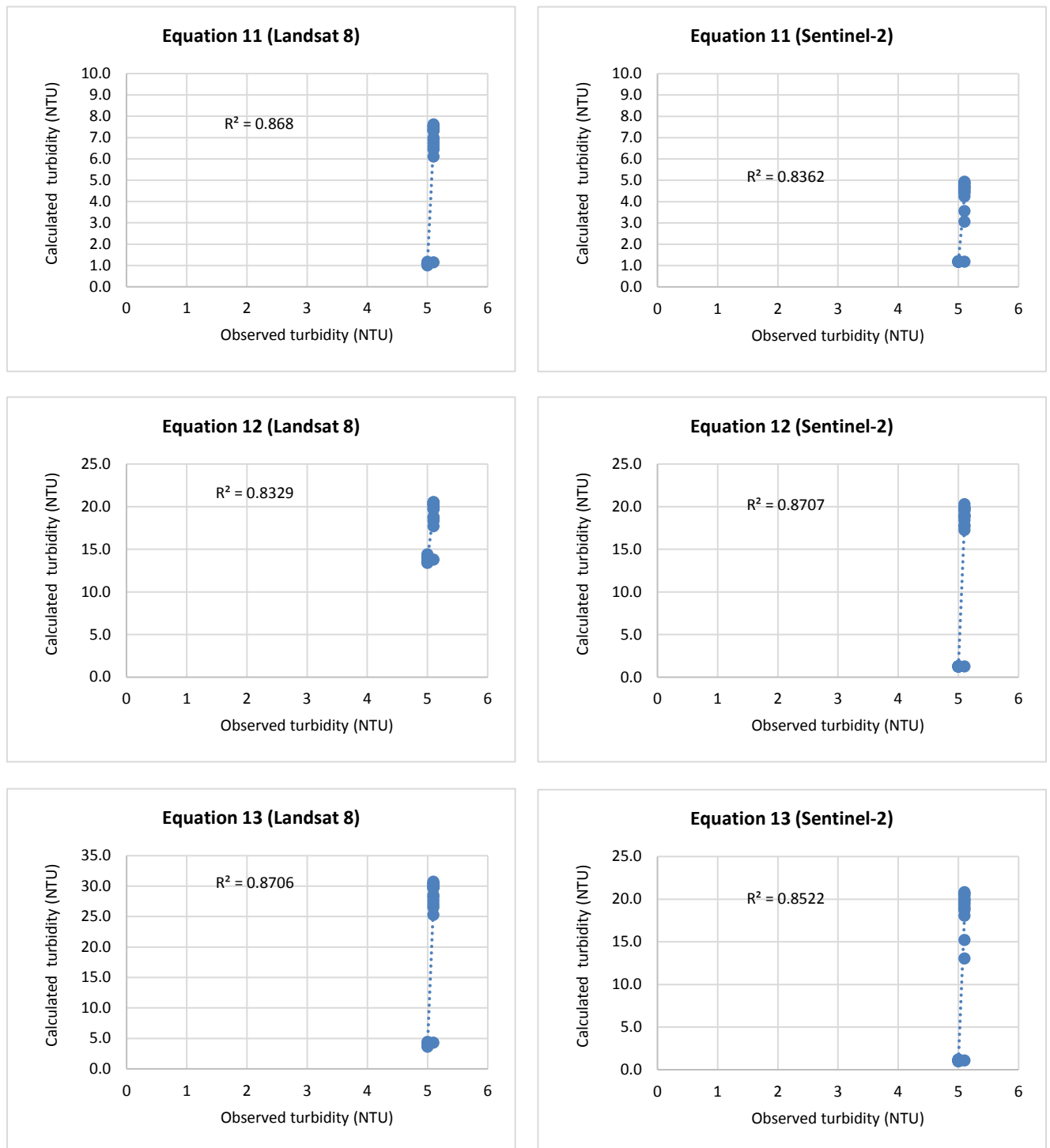


Figure 5.3: Scatterplots of observed vs. calculated values for turbidity estimation algorithms 11 to 13.

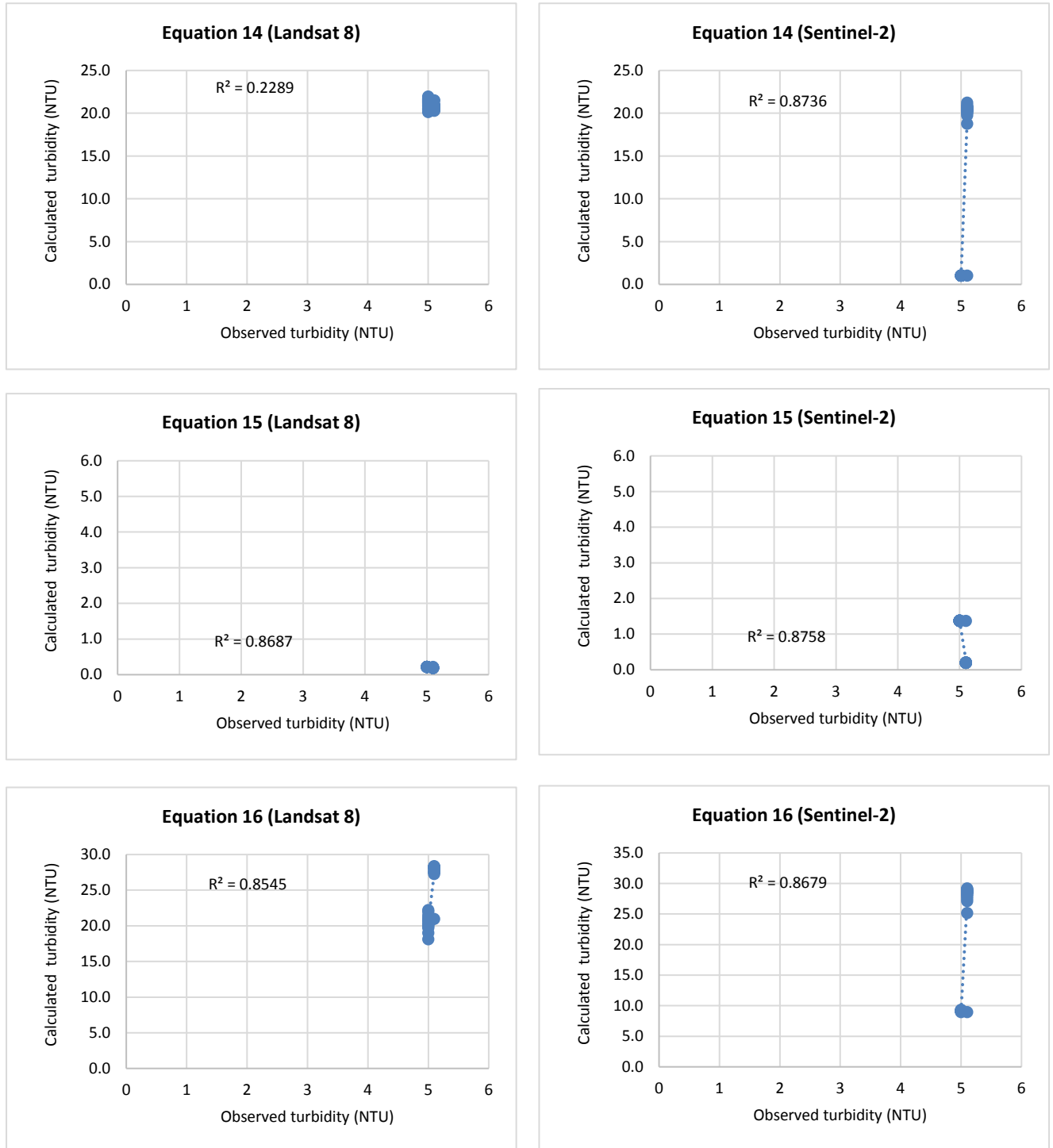


Figure 5.4: Scatterplots of observed vs. calculated values for turbidity estimation algorithms 14 to 16.

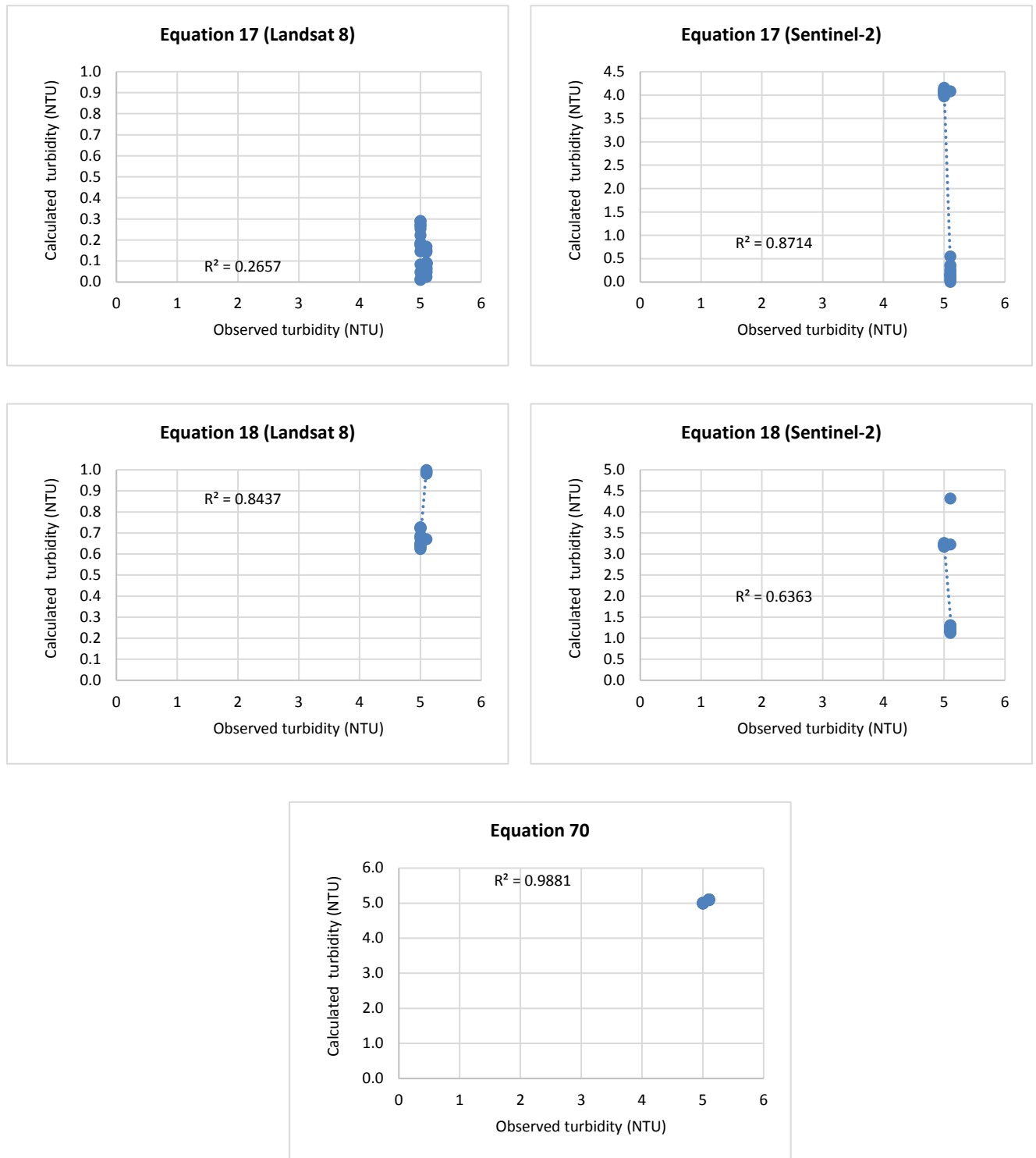


Figure 5.5: Scatterplots of observed vs. calculated values for turbidity estimation algorithms 17, 18 and 70.



### 5.3.2.5 Map of estimated turbidity

The difference in Turbidity between winter and spring seasons is basically negligible. This is evidenced by the small range displayed in both seasons turbidity distribution maps (Figure 5.6). Turbidity in winter is roughly the same throughout the estuary whilst in spring it is slightly higher closest to the ocean and decreasing as one moves towards the estuarine and river banks. However, these differences are unlikely to have a profound impact on the estuary since they are so miniscule.

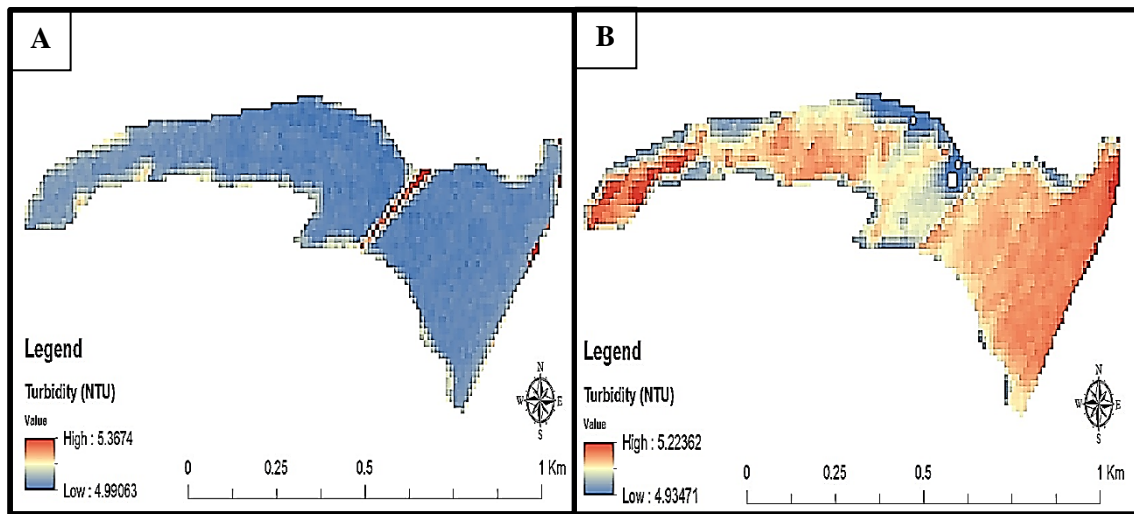


Figure 5.6: Turbidity distribution across the Umdloti Estuary for winter (A) and spring (B)

### 5.3.3 SDD estimation

#### 5.3.3.1 Using Landsat 8

The estimation of SDD using Landsat 8 (Table 5.8) could be considered to be poor. The estimation algorithms suffers from extreme low  $R^2$  values throughout. This is compounded through the obtaining of RMSE values that are often double to many times the depth of the actual estuary. There is no clear algorithm that could be considered accurate and therefore no best algorithm.

Table 5.8: Accuracy of the estimated SDD (m) using Landsat 8 for Umdloti Estuary.

Equation	Winter		Spring		Combined	
	R <sup>2</sup>	RMSE	R <sup>2</sup>	RMSE	R <sup>2</sup>	RMSE
Equation 19	0.045	12.162	0.0188	12.518	0.005	12.341
Equation 20	0.256	3.207	0.230	1.618	0.002	2.540
Equation 21	0.039	131.253	0.143	80.386	0.001	108.833
Equation 22	0.231	12.263	0.085	12.263	0.0657	12.263
Equation 23	0.024	14.695	0.063	19.153	0.0008	17.070
Equation 24	0.038	1.903	0.146	3.012	0.001	2.519
Equation 25	0.038	1.021	0.146	1.590	0.001	1.336
Equation 26	0.127	3.563	0.096	3.561	0.0007	3.562

### 5.3.3.2 Using Sentinel-2

Sentinel-2 SDD estimation (Table 5.9) is similar to that found by Landsat 8 and suffered from a complete lack of accuracy. R<sup>2</sup> values were very low throughout and indicated the algorithms relatively modelled SDD incredibly poorly across the Umdloti Estuary. RMSE values recorded are also larger and inaccurate. Whilst still inaccurate, algorithms are better at retrieving absolute values in winter. Here, many of the RMSE values obtained are below 1 m. However, these are subsequently poorly retrieved in spring, bringing down the overall RMSE.

Table 5.9: Accuracy of the estimated SDD (m) using Sentinel-2 for Umdloti Estuary.

Equation	Winter		Spring		Combined	
	R <sup>2</sup>	RMSE	R <sup>2</sup>	RMSE	R <sup>2</sup>	RMSE
Equation 19	0.000006	0.631	0.124	12.762	0.0008	9.035
Equation 20	0.00006	0.856	0.033	2.269	0.0007	1.715
Equation 21	0.131	0.807	0.035	75.244	0.0007	53.208
Equation 22	0.026	0.526	0.099	12.264	0.0002	8.680
Equation 23	0.270	7.282	0.029	18.760	0.0001	14.230
Equation 24	0.056	2.224	0.037	3.160	0.0001	2.732
Equation 25	0.056	1.384	0.037	1.667	0.0001	1.532
Equation 26	0.056	0.702	0.019	3.562	0.0001	2.567

SSD, as was evidenced by both remote sensors, is very poorly retrieved. Around half of all RMSE's calculated using Sentinel-2 ranged well over 3 m. This is almost double the actual depth of the estuarine floor at some locations. These algorithms can therefore be considered to have poor accuracy. In addition to this, no combined R<sup>2</sup> value was obtained above 0.15. Deutsch

*et al.* (2014), (Equation 25) is the relative best algorithm, albeit with a highly inaccurate RMSE (1.336 m and 1.532 m) and similarly poor  $R^2$  (0.001 and 0.0001). Sentinel-2 was the slightly better sensor in retrieving SDD, although this was done much too poorly to be considered for use.

### 5.3.3.3 Using newly modified algorithm

The newly modified algorithm based on the Deutsch *et al.* (2014), ratio of bands 2 and 4 unfortunately suffers from the same lack of accuracy found using all other algorithms tested (Table 5.10). Whilst RMSE was brought down to just 0.220 m, this still presented a relatively large inability to determine depth. The ability of the algorithm to relatively model SDD is also extremely poor at  $R^2 = 0.02$ .

Table 5.10: Accuracy of the estimated SDD (m) using newly generated estimation algorithms for Umdloti Estuary.

Equation	Winter $R^2$	Spring $R^2$	Combined $R^2$	Winter RMSE	Spring RMSE	Combined RMSE
Equation 71	0.014	0.047	0.02	0.221	0.219	0.220

### 5.3.3.4 Scatterplots of SDD models.

Figures 5.7 to 5.9 illustrate the graphical relationship between the actual measured SDD and those predicted by the algorithms. The majority of SDD estimation equations show distinct winter and spring clusters as seen with previous parameters. However, these clusters are much more visible and far apart than what is found with previous parameters and formed a straight flat line tightly centred along a single y-axis value. As a result, even as the x-axis increased, the y-axis remained the same. This results in  $R^2$  values that are universally poor as the very distinct clusters form a line of best fit that does not pass through a single point on the scatterplot. As a result, SDD estimation could be considered poor. Equations 19, 20, 22, 26 and 72 did not display this clustering when using Landsat (19, 22 and 26) or Sentinel-2 (20 and 72). Their accuracy proved no better as they also tended to form a straight, flat y-asymptote and failed to register any change as x- increased.

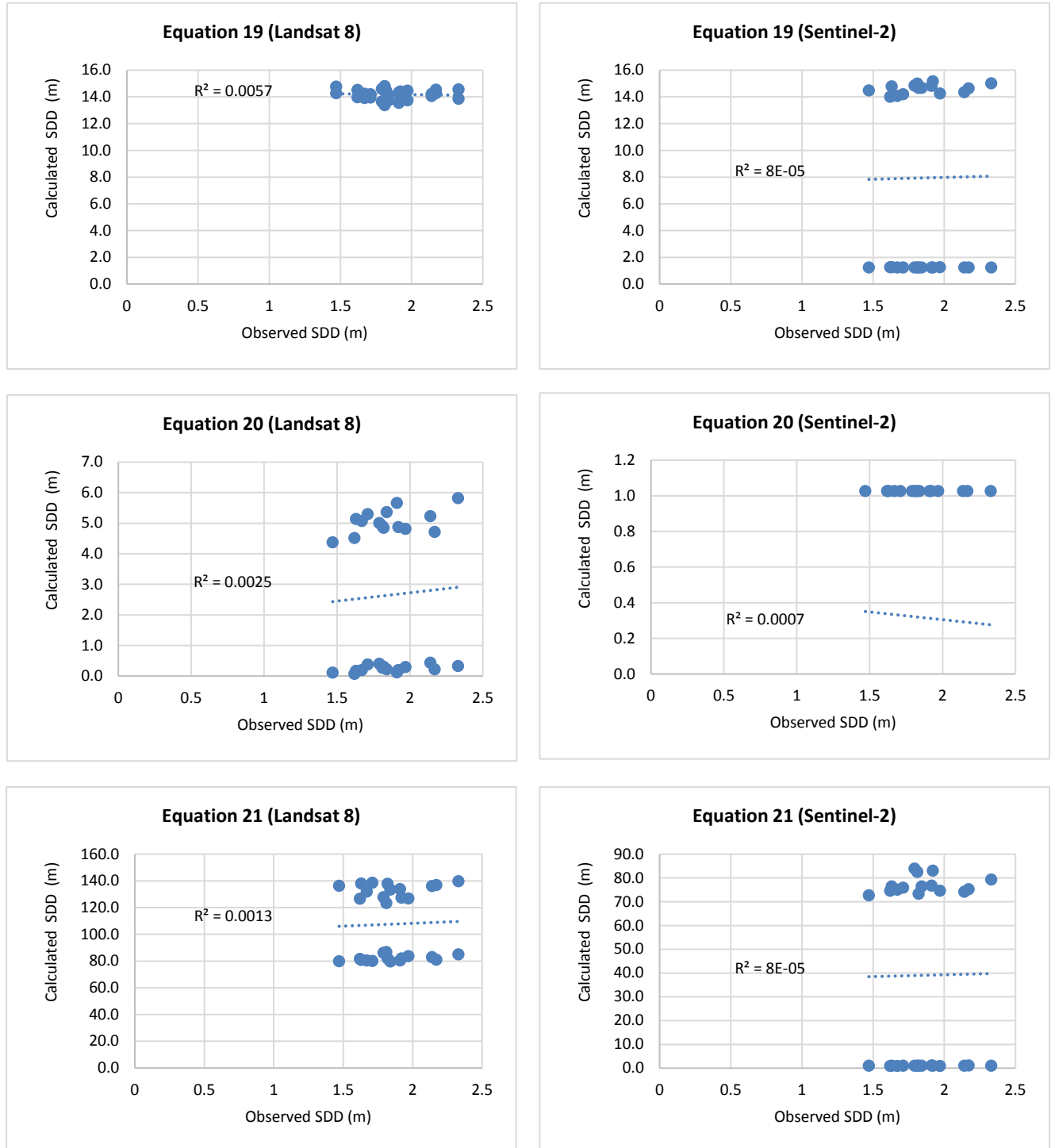


Figure 5.7: Scatterplots of observed vs. calculated values for SDD estimation algorithms 19 to 21.

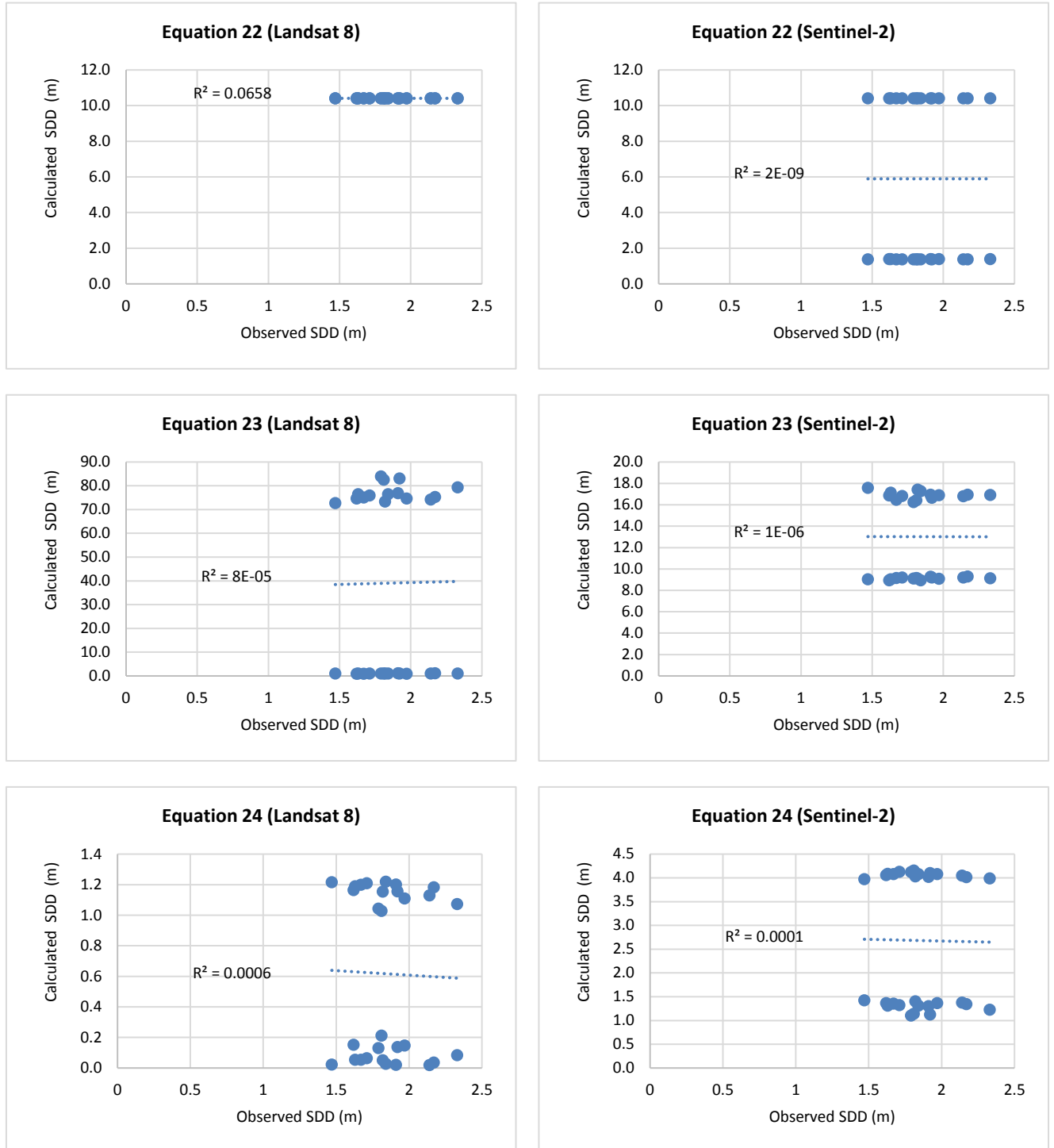


Figure 5.8: Scatterplots of observed vs. calculated values for SDD estimation algorithms 22 to 24.

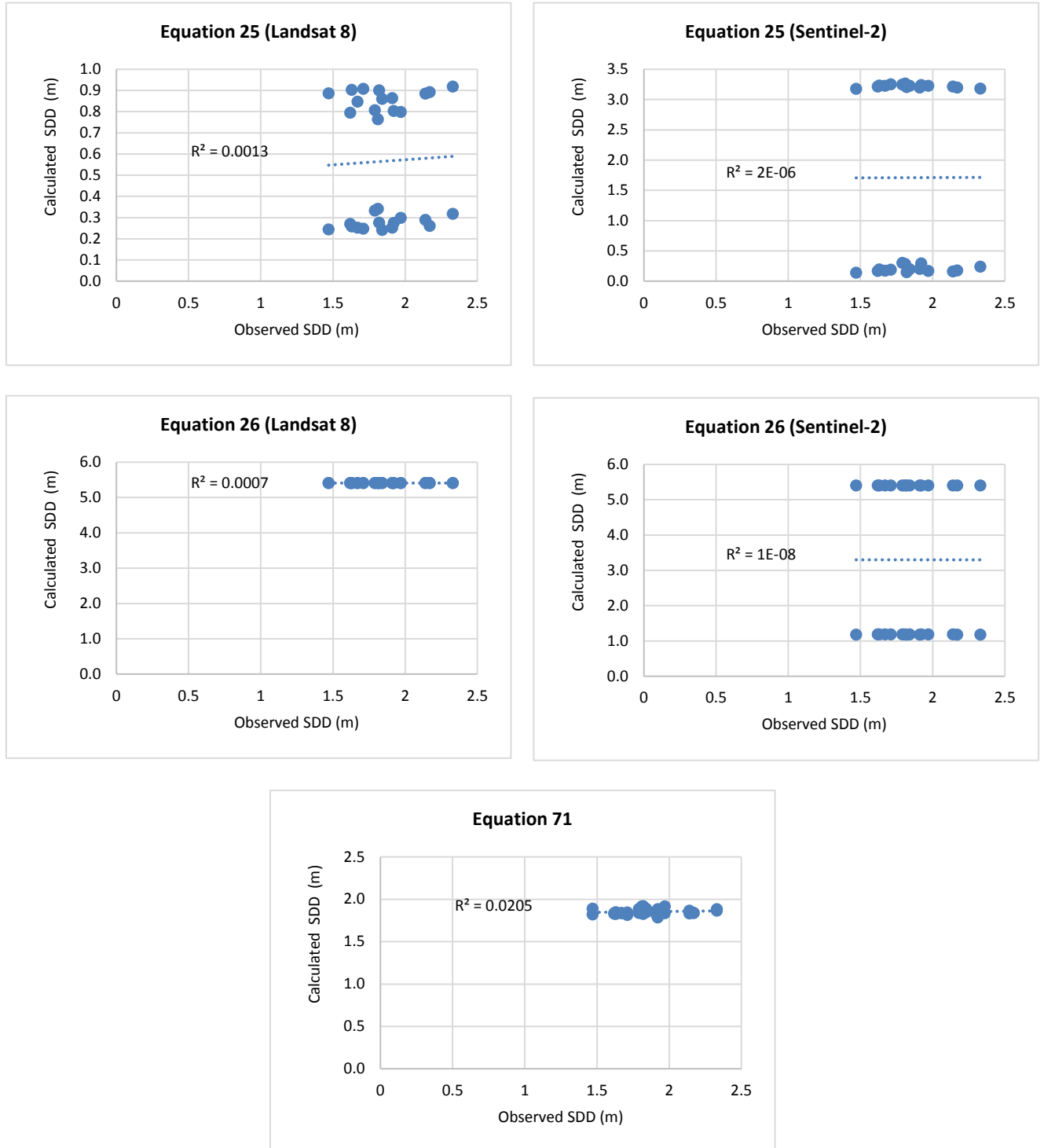


Figure 5.9: Scatterplots of observed vs. calculated values for SDD estimation algorithms 25, 26 and 71.

### 5.3.3.5 Map of estimated SDD

SDD is the most similar in distribution of all the parameters (Figure 5.10). The scales between winter and spring differed by only mere decimal points. The winter distribution of SDD appeared speckled. However, the lack of SDD range predicted means that the speckled appearance does not indicate large differences in SDD. Similarly, spring has a homogenous distribution of SDD throughout with very little variability modelled. Overall, SDD is poorly predicted and mapped across the estuary.

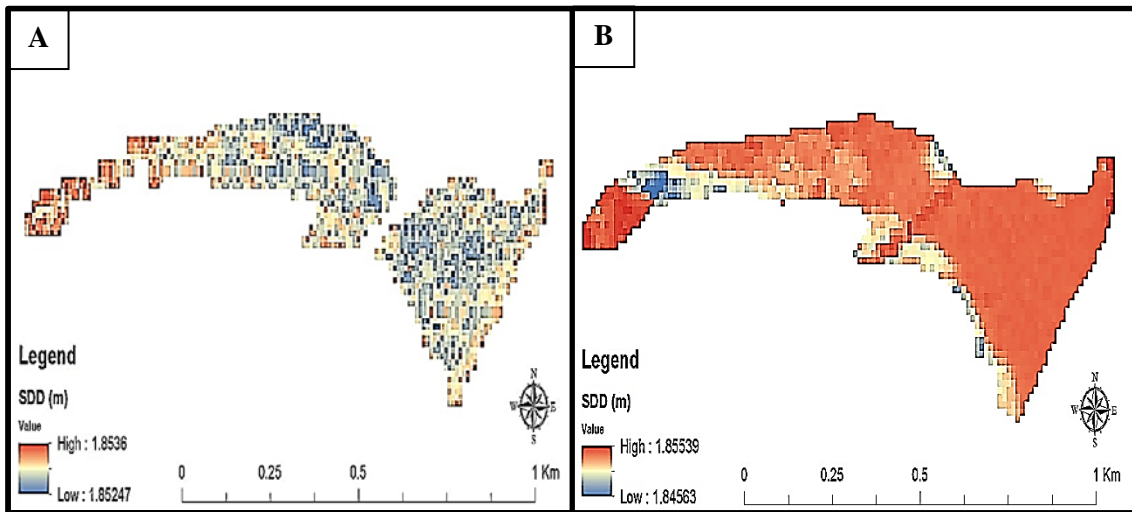


Figure 5.10: SDD distribution across the Umdlotti Estuary for winter (A) and spring (B).

### 5.3.4 Salinity estimation

#### 5.3.4.1 Using Landsat 8

The results of the salinity estimation performed for Landsat 8 are displayed in Table 5.11. Salinity estimation for Landsat 8 overall is very poor. Algorithms showed a poor ability to model variation across the estuary as shown by  $R^2$  values. The exception to this can be found when considering the overall  $R^2$ , with some algorithms receiving acceptable results above  $R^2 = 0.7$ . RMSE is also retrieved very poorly, with most values retrieved ranging into the 30's and above. Considering that this is as saline as the ocean and many times higher than what was observed, accuracy could be considered poor. The algorithm developed by Wang and Xu (2008), (Equation 31) appeared to achieve the only relatively strong RMSE and an accurate  $R^2$ .

Table 5.11: Accuracy of the estimated salinity using Landsat 8 for Umdloti Estuary.

Equation	Winter		Spring		Combined	
	R <sup>2</sup>	RMSE	R <sup>2</sup>	RMSE	R <sup>2</sup>	RMSE
Equation 27	0.119	30.019	0.233	32.111	0.708	30.904
Equation 28	0.107	35.719	0.203	35.859	0.543	46.530
Equation 29	0.002	34.554	0.207	34.657	0.723	41.971
Equation 30	0.119	24.036	0.058	29.820	0.493	28.992
Equation 31	0.089	10.094	0.012	4.189	0.691	5.846
Equation 32	0.001	52.871	0.243	105.305	0.718	76.291

#### 5.3.4.2 Using Sentinel-2

The results for the salinity retrieved using Sentinel-2 (Table 5.12) is similar to those found for Landsat 8. As has been the case with most parameters, winter and spring R<sup>2</sup> values range into very low values whilst when combined, the R<sup>2</sup> shows a significant improvement in modelling relative salinity. RMSE values are exceptionally high and inaccurate throughout, excepting for the algorithm (Equation 31) developed by Wang and Xu (2008), which achieved a relatively low overall RMSE.

Table 5.12: Accuracy of the estimated salinity using Sentinel-2 for Umdloti Estuary.

Equation	Winter		Spring		Combined	
	R <sup>2</sup>	RMSE	R <sup>2</sup>	RMSE	R <sup>2</sup>	RMSE
Equation 27	0.034	30.251	0.048	31.194	0.645	30.726
Equation 28	0.843	72.623	0.044	35.860	0.662	57.271
Equation 29	0.752	60.540	0.190	34.690	0.478	49.338
Equation 30	0.708	36.888	0.112	23.432	0.323	30.901
Equation 31	0.098	4.384	0.059	3.496	0.211	3.964
Equation 32	0.097	53.234	0.185	82.226	0.736	69.263

Overall the accuracy results obtained for retrieving salinity are very poor. Both sensors are capable of using the algorithms to retrieve it but did so poorly. Most RMSE differs by over 30 units and R<sup>2</sup> values calculated are of moderate to low accuracy in both winter and spring. The most accurate of these algorithms was developed by Wang and Xu (2008), with the lowest RMSE by far (5.846 and 3.964) although suffering one of the worst Sentinel-2 R<sup>2</sup> values (0.211). The worst performing algorithm was developed by Zhao *et al.* (2017), which saw an RMSE of 76.291 and 69.263. Both sensors are roughly equally poor at retrieving salinity.



#### 5.3.4.3 Using newly modified algorithm

Salinity retrieved using an algorithm modelled after Wang and Xu (2008), (Table 5.13) achieves reasonable accuracies. Whilst it suffered from low intraseasonal accuracy, a combined  $R^2$  of around 0.7 is better than the majority of algorithms modified by other studies. The RMSE of 0.046 is unsurpassed. The algorithm is therefore considered suitable for salinity modelling and estimation during both seasons.

Table 5.13: Accuracy of the estimated salinity using newly generated estimation algorithms for Umdloti Estuary.

Equation	Winter $R^2$	Spring $R^2$	Combined $R^2$	Winter RMSE	Spring RMSE	Combined RMSE
Equation 72	0.192	0.096	0.70	0.025	0.061	0.046

#### 5.3.4.4 Scatterplots of salinity models.

Figures 5.11 to 5.13 illustrate the graphical relationship between the actual measured salinity and those predicted by the algorithms. The seasonal clustering of points seen in the previous parameters is not expressed as strongly during the sampling of salinity. The distribution of calculated vs. actual salinity points however was not smooth and gradual. These points appear to ‘jump’ from one x-value to another for most algorithms across small x-axis ranges (such as around 30 to 35 and 0.5 to 1 in Equation 27). This ‘jumping’ is undoubtedly caused by the small variability in observed salinity, which ranged from 0.7 to 1. The distribution of these results indicate that the estimation of salinity by the algorithms is fairly successful with only four models (Equation 30 for both Landsat 8 and Sentinel-2 and Equation 29 and 31 for Sentinel-2) achieving results lower than  $R^2 = 0.5$ .

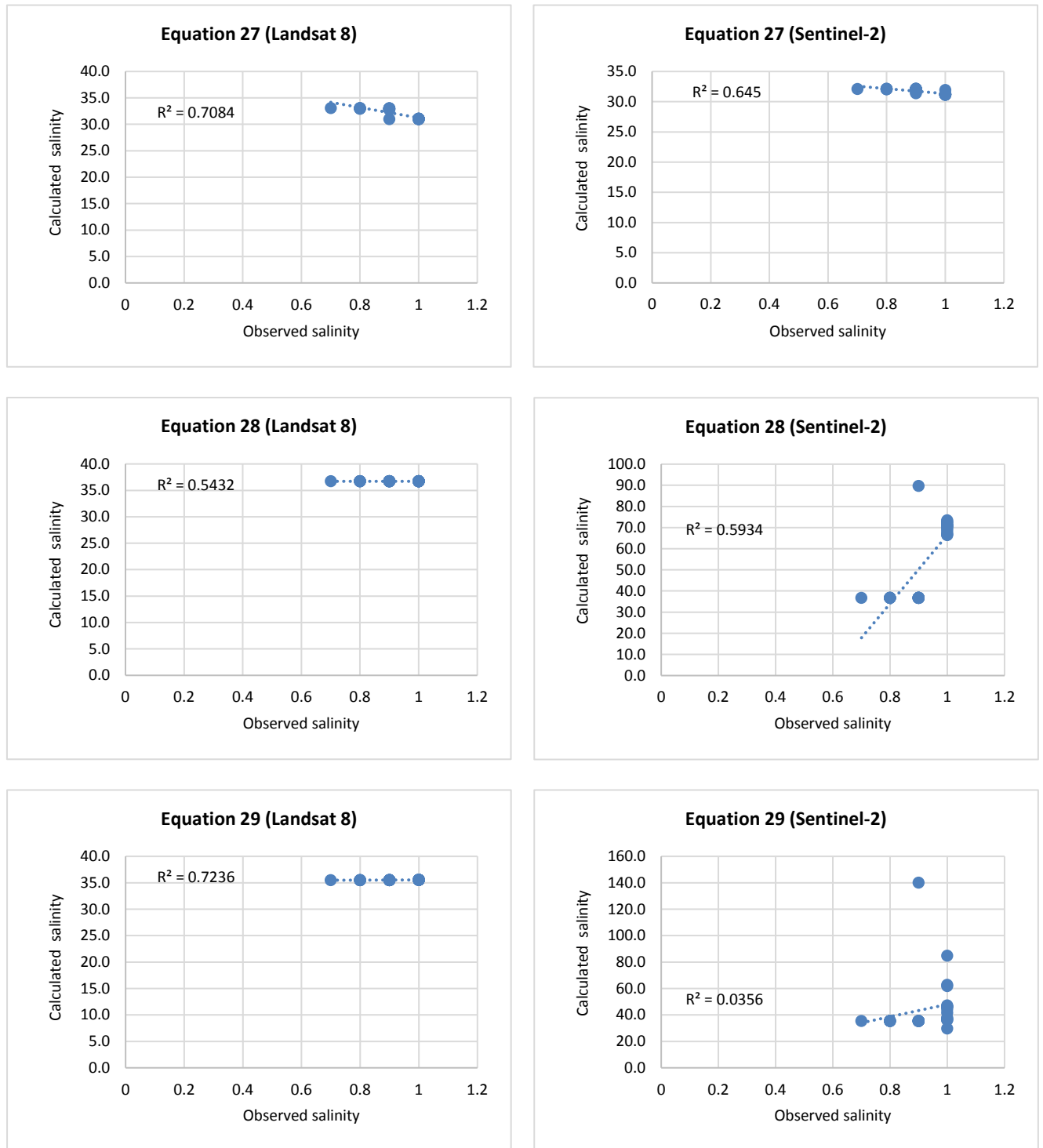


Figure 5.11: Scatterplots of observed vs. calculated values for salinity estimation algorithms 27 to 29.

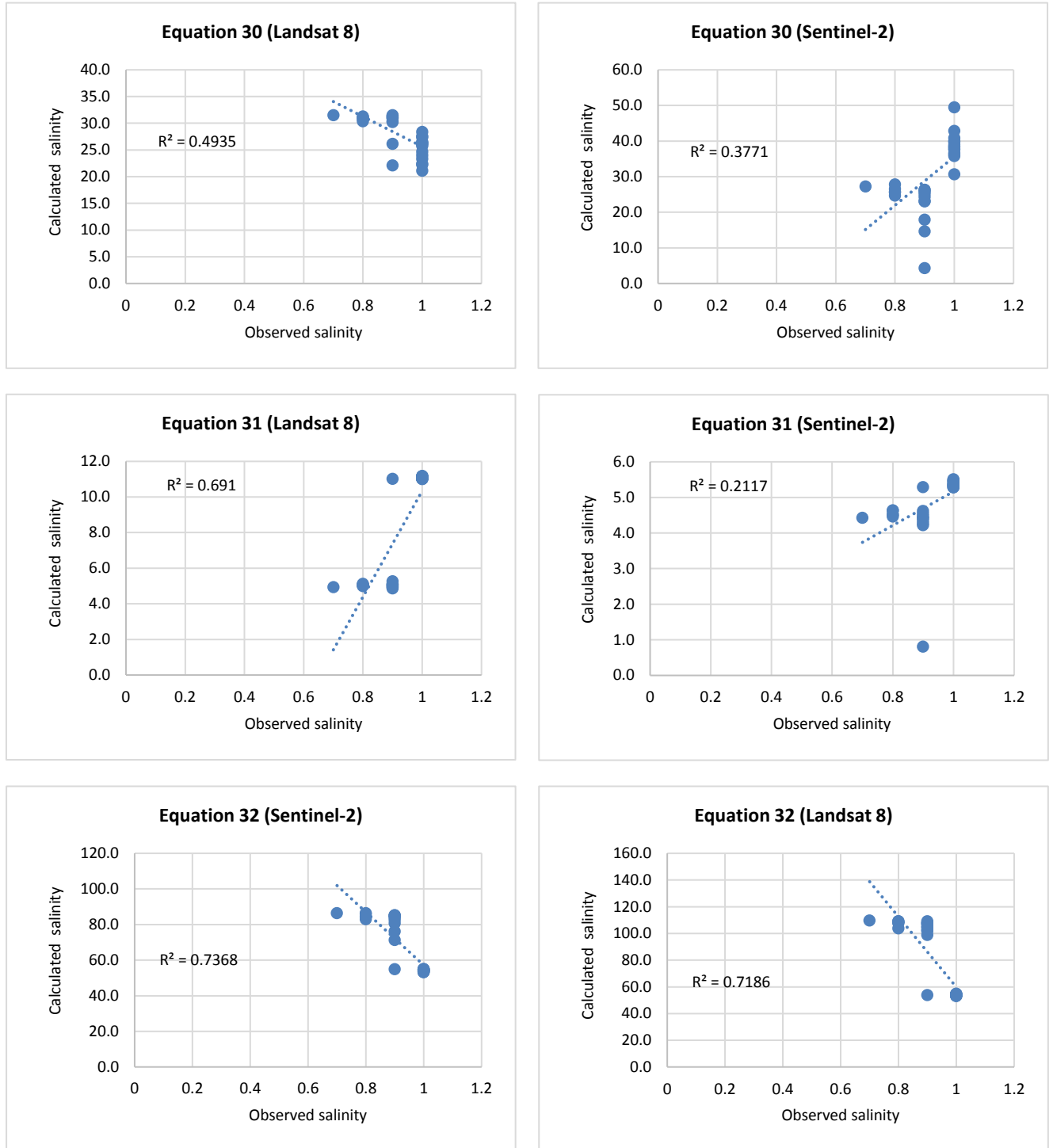


Figure 5.12: Scatterplots of observed vs. calculated values for salinity estimation algorithms 29 to 31.

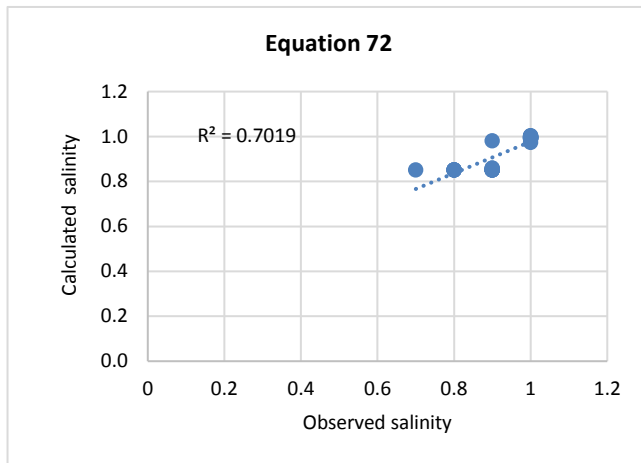


Figure 5.13: Scatterplot of observed vs. calculated values for salinity estimation algorithm 72.

#### 5.3.4.5 Map of estimated salinity

Salinity (Figure 5.14) shared a similar distribution across the estuary in both spring and winter. In winter, salinity was roughly equal throughout, even within the river portions. In spring, salinity was highest closest to the estuarine mouth and generally decreased as one moves away from the mouth.

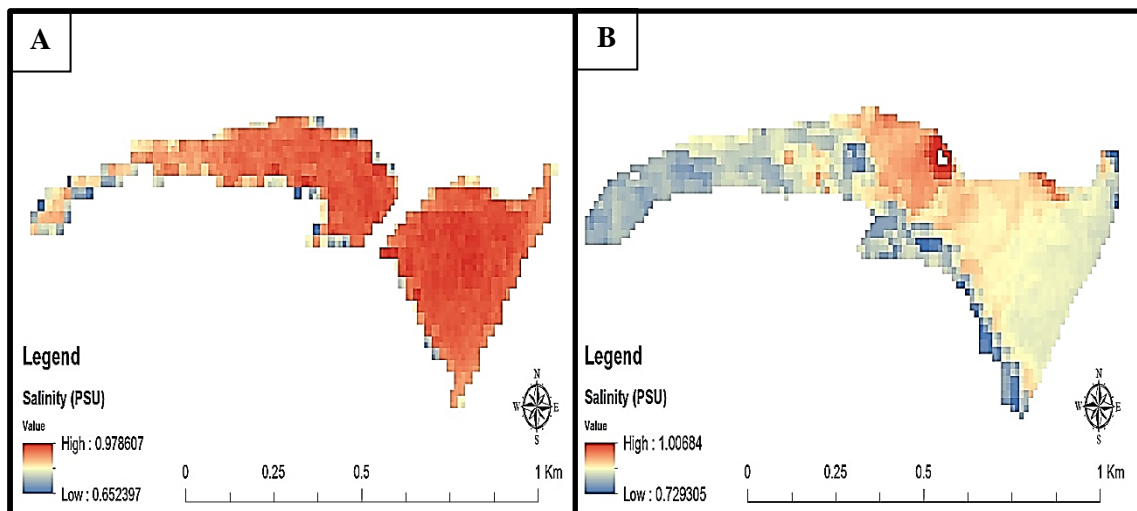


Figure 5.14: Salinity distribution across the Umdloti Estuary for winter (A) and spring (B).

### 5.3.5 TDS estimation

#### 5.3.5.1 Using Landsat 8

Accuracy assessments performed on TDS values retrieved using Landsat 8 are recorded in Table 5.14. Landsat 8 showed some success in TDS estimation. As has been seen with other parameters,  $R^2$  values calculated are low when considering only winter and spring data individually but reached substantially higher accuracies when a combined dataset is used. Interseasonal RMSE is also very similar, indicating a good ability at determining TDS absolute values. Overall Abdulla, (2015) (Equation 36) achieves the best  $R^2$  (0.739) and RMSE (594.268 mg/l) accuracies.

Table 5.14: Accuracy of the estimated TDS (mg/l) using Landsat 8 for Umdloti Estuary.

Equation	Winter		Spring		Combined	
	$R^2$	RMSE	$R^2$	RMSE	$R^2$	RMSE
Equation 33	0.026	955.217	0.002	921.058	0.021	938.293
Equation 34	0.007	956.017	0.108	921.858	0.517	939.093
Equation 35	0.033	1162.316	0.0167	1127.923	0.701	1145.248
Equation 36	0.160	655.199	0.059	526.329	0.739	594.268

#### 5.3.5.2 Using Sentinel-2

Similar to temperature, algorithms developed by Khattab and Merkel (2014), (Equation 33 and Equation 34) utilised the TIRS bands 10 and 11 which are unavailable on Sentinel-2. This meant that results for the Abdulla (2015), (Equation 35) and Abdelmalik (2018), (Equation 36) equations are only calculated for Sentinel-2 (Table 5.15). Sentinel-2 achieves similar results to those achieved by Landsat 8. The most obvious similarity is the low winter and spring and high combined data  $R^2$  values that are again found. RMSE differs greatly between winter and spring for both algorithms and overall values RMSE values were large compared to in situ retrieved parameters.

Table 5.15: Accuracy of the estimated TDS (mg/l) using Sentinel-2 for Umdloti Estuary.

Equation	Winter		Spring		Combined	
	R <sup>2</sup>	RMSE	R <sup>2</sup>	RMSE	R <sup>2</sup>	RMSE
Equation 35	0.037	3116.583	0.002	1127.97	0.686	2343.651
Equation 36	0.206	834.436	0.001	483.838	0.413	682.050

Many of the calculated algorithms RMSE are almost double what the observed values are. Algorithms achieved moderate accuracy in the attempt to model the relationship as detailed by their R<sup>2</sup>. However, despite the large RMSE's and moderate coefficient of determinations, the TDS values still efficiently identify water salinity. This is because a unit increase in TDS is less significant than a unit increase in many other parameters such as salinity due to its much larger scale range. The best algorithm for TDS estimation is developed by Abdullah (2015), due to its relative best RMSE (594.268 mg/l and 682.050 mg/l) and good to moderate R<sup>2</sup> (0.739 and 0.413). Landsat 8 appears to be the better sensor overall to calculate TDS.

#### 5.3.5.3 Using newly modified algorithm

The algorithms modified by this study provide a comfortable balance between R<sup>2</sup> and RMSE. The R<sup>2</sup> value of 0.69 is by no means the most accurate retrieved but provides acceptable accuracy. The RMSE of 11.369 mg/l is superior to those developed by other studies and used for TDS estimation.

Table 5.16: Accuracy of the estimated TDS (mg/l) using newly generated estimation algorithms for Umdloti Estuary.

Equation	Winter R <sup>2</sup>	Spring R <sup>2</sup>	Combined R <sup>2</sup>	Winter RMSE	Spring RMSE	Combined RMSE
Equation 73	0.0158	0.00002	0.69	14.481	6.986	11.369

#### 5.3.5.4 Scatterplots of TDS models.

Figures 5.15 to 5.16 illustrates the graphical relationship between the actual measured TDS and those predicted by the algorithms. The formation of two separate clusters of points due to the season is expressed most by Equation 36 and the Sentinel-2 usage of Equation 35. The rest of the algorithms did not form distinct separate clusters and instead occupied small x and y axis ranges. With the majority of retrieval algorithms achieving  $R^2$  values above 0.6, the estimation of TDS could be considered good.

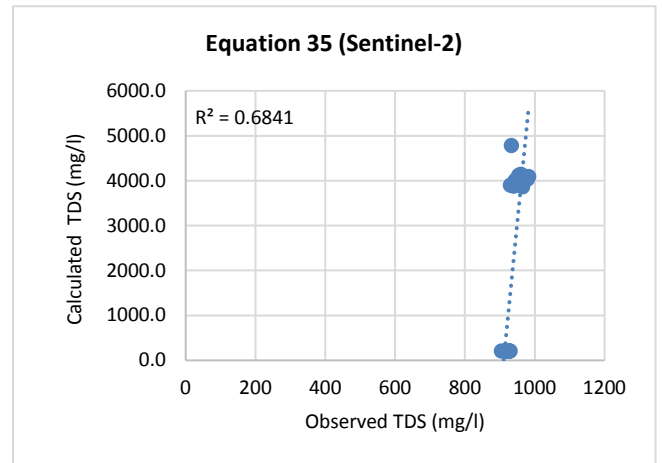
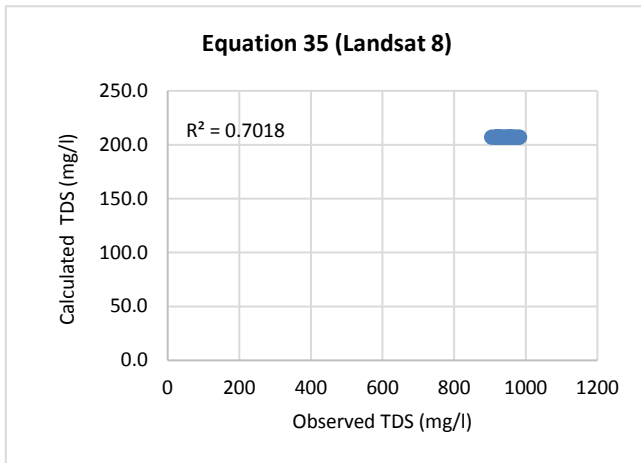
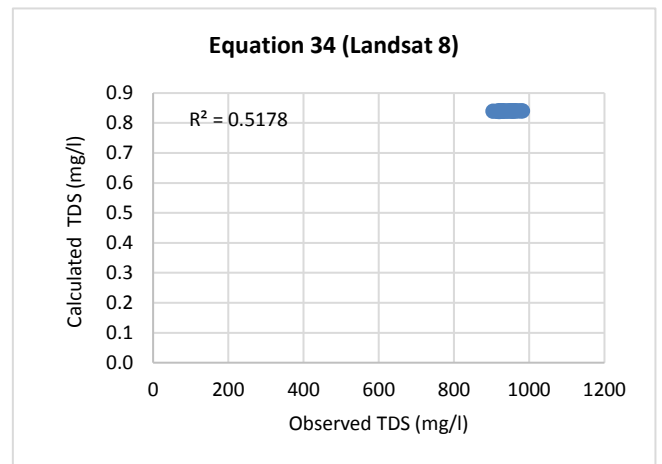
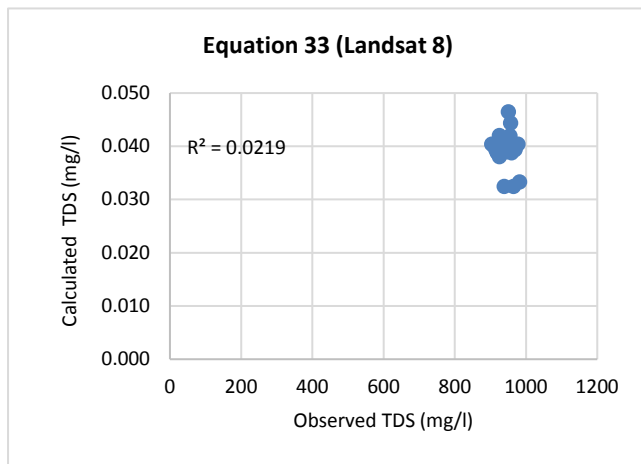


Figure 5.15: Scatterplots of observed vs. calculated values for TDS estimation algorithms 33, 34 and 35.

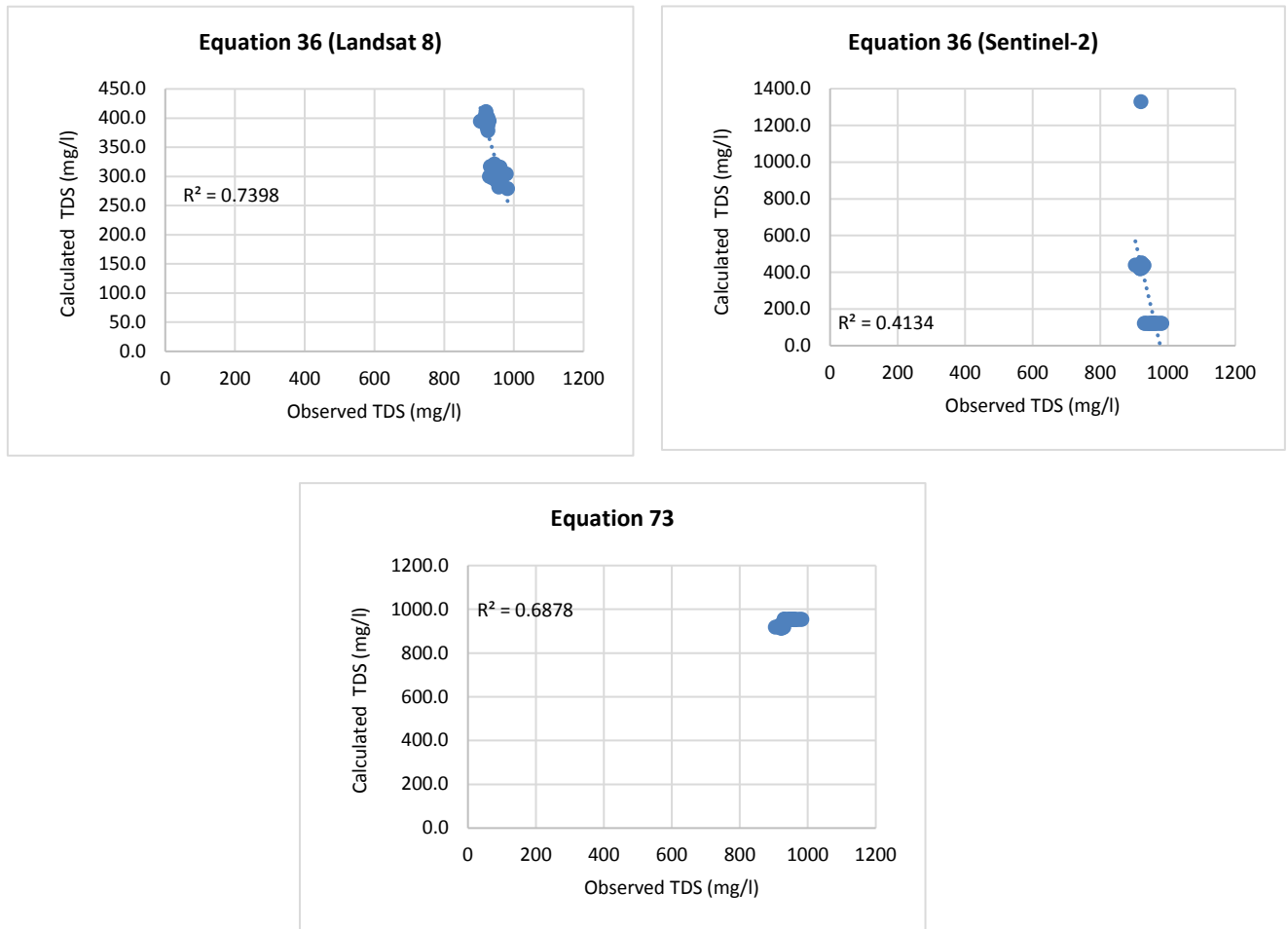


Figure 5.16: Scatterplots of observed vs. calculated values for TDS estimation algorithms 36 and 73.

### 5.3.5.5 Map of estimated TDS

Just as with salinity, the distribution of TDS throughout the estuary is similar in both the winter and spring seasons (Figure 5.17). This is to be expected as both measure the salt content of waters. TDS is distributed relatively uniformly across the estuary. In winter these concentrations spiked near river banks but otherwise was homogenous. TDS is also slightly higher towards the estuarine mouth.



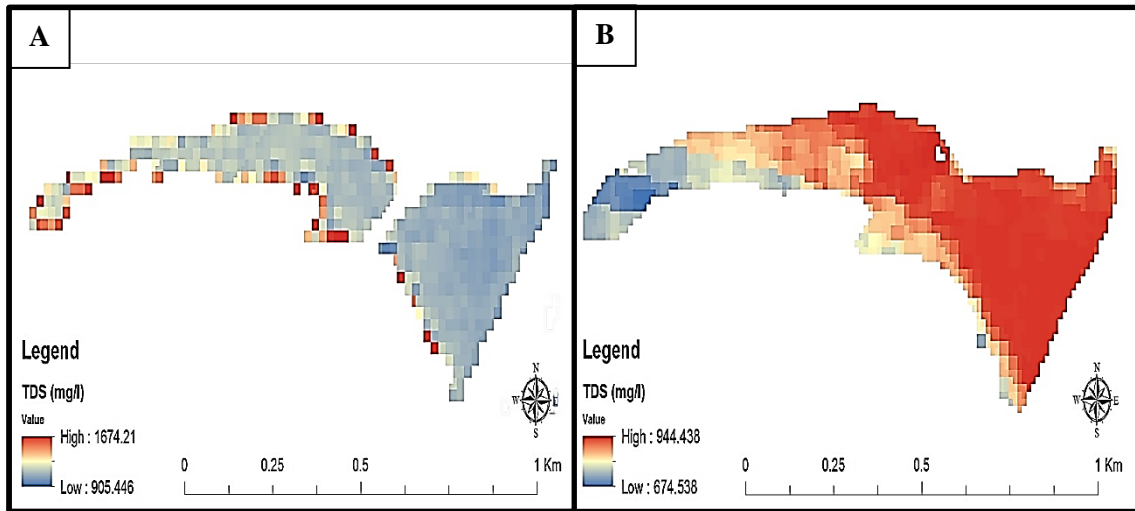


Figure 5.17: TDS distribution across the Umdloti Estuary for winter (A) and spring (B).

### 5.3.6 EC estimation

#### 5.3.6.1 Using Landsat 8

The accuracy of the Landsat 8 estimation algorithms associated with EC were recorded in Tables 5.17.  $R^2$  values for EC estimation using Landsat 8 are low in winter but comparably much higher than they are in spring. Following the pattern found within previous parameters, overall  $R^2$  is much higher for EC estimation and suggests average to good accuracy when it comes to modelling algorithm variability. RMSE ranges from good (those calculated below  $2.5 \mu\text{S/cm}$ ) to astronomically high and inaccurate.

Table 5.17: Accuracy of the estimated EC ( $\mu\text{S/cm}$ ) using Landsat-8 algorithms for Umdloti Estuary.

Equation	Winter		Spring		Combined	
	$R^2$	RMSE	$R^2$	RMSE	$R^2$	RMSE
Equation 37	0.146	2.091	0.140	1.991	0.082	2.042
Equation 38	0.154	2.412	0.001	2.383	0.529	2.398
Equation 39	0.057	8.304	0.030	8.510	0.639	8.408
Equation 40	0.306	598.819	0.027	787.599	0.732	699.606
Equation 41	0.152	413.872	0.037	357.69	0.657	386.802

### 5.3.6.2 Using Sentinel-2

Another equation by Khattab and Merkel (2014), (Equation 38) made use of the Landsat TIRS bands and could unfortunately not be used for accuracy assessment for Sentinel-2. However, Sentinel-2 estimation of EC went off better than it did for Landsat 8 (Table 5.17).  $R^2$  values are much lower during the winter and spring periods but achieve an average to good accuracy when using a combined dataset. RMSE is poorly determined by Abdullah (2015), (Equation 40) but quite accurate when using by Khattab and Merkel (2014), (Equation 37) and Abdelmalik (2018), (Equation 39).

Table 5.18: Accuracy of the estimated EC ( $\mu\text{S/cm}$ ) using Sentinel-2 algorithms for Umdlotti Estuary.

Equation	Winter		Spring		Combined	
	$R^2$	RMSE	$R^2$	RMSE	$R^2$	RMSE
Equation 37	0.010	0.965	0.008	1.983	0.670	1.560
Equation 39	0.0005	1.155	0.031	8.627	0.670	6.154
Equation 40	0.004	0.851	0.00004	1079.687	0.474	763.454
Equation 41	0.001	6.907	0.017	318.580	0.670	225.323

As is the situation with both salinity and TDS, the apparent estimation accuracy for EC can be considered poor. Even the best RMSE values obtained are nearly double the in situ values found with astronomically high inaccurate values obtained for both Abdullah (2015), algorithms (Equation 40 and Equation 41).  $R^2$  values are likewise ranging from good to average/low. However, it should be noted that just as with TDS, the differences between in situ and predicted values are relatively small when considering how EC scales. The Khattab and Merkel (2014), algorithm can be considered the relative best with an accurate RMSE (2.042  $\mu\text{S/cm}$  and 1.560  $\mu\text{S/cm}$ ) but inconsistent  $R^2$  (0.082 and 0.67). The Abdelmalik (2018), algorithm also does a satisfactory job of retrieving EC. Sentinel-2 appears to be the more suitable sensor for determining EC.

### 5.3.6.3 Using newly modified algorithm

The algorithms modified by this study for EC estimation (Table 5.19) is based on a ratio of band 3 and 4 remote sensing reflectance as performed by Khattab and Merkel (2014). The algorithm

achieved a disappointing low  $R^2$  very strong and accurate RMSE. The lack of relative modelling ability shown by the low  $R^2$  values throughout may indicate future issues with EC estimation using this algorithm.

Table 5.19: Accuracy of the estimated EC ( $\mu\text{S/cm}$ ) using newly generated estimation algorithms for Umdloti Estuary.

Equation	Winter $R^2$	Spring $R^2$	Combined $R^2$	Winter RMSE	Spring RMSE	Combined RMSE
Equation 74	0.171	0.010	0.44	0.046	0.031	0.039

#### 5.3.6.4 Scatterplots of EC models.

Figure 5.18 to 5.20 illustrate the graphical relationship between the actual measured EC and those predicted by the algorithms. The majority of algorithms (with the exception of Landsat 8 Equation 37 and Sentinel-2 Equation 39 and 74) show the distinctive seasonal clusters seen in other parameters. Despite this, the algorithms achieved mildly successful  $R^2$  values, indicating some success at estimating EC.

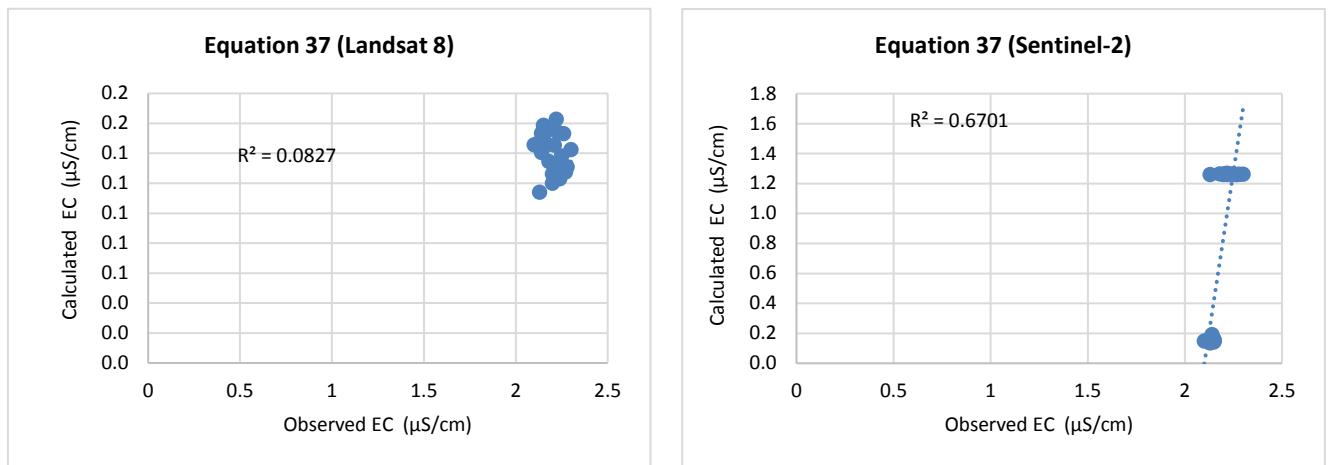


Figure 5.18: Scatterplots of observed vs. calculated values for EC estimation algorithms 37.

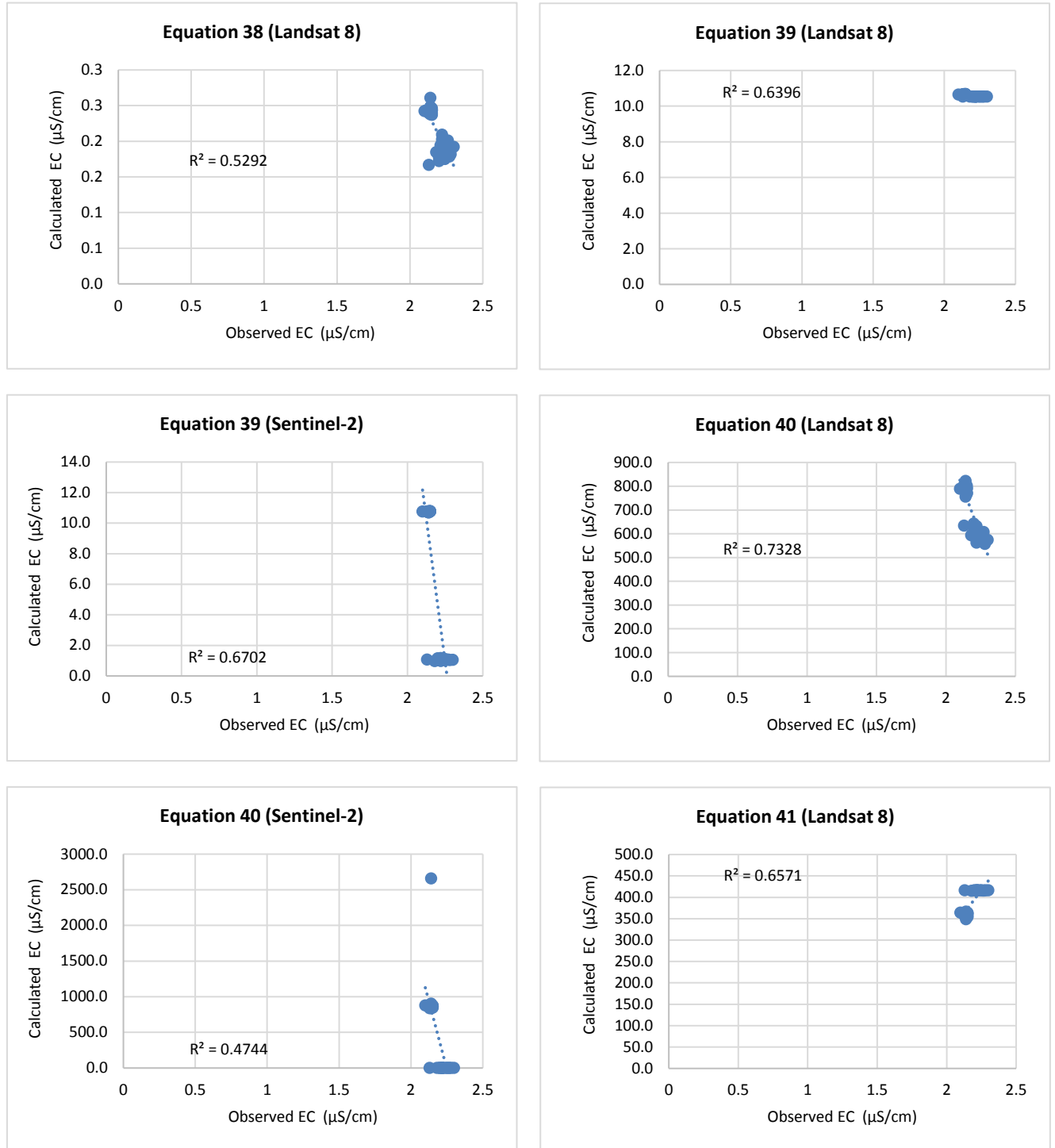


Figure 5.19: Scatterplots of observed vs. calculated values for EC estimation algorithms 38 to 41.

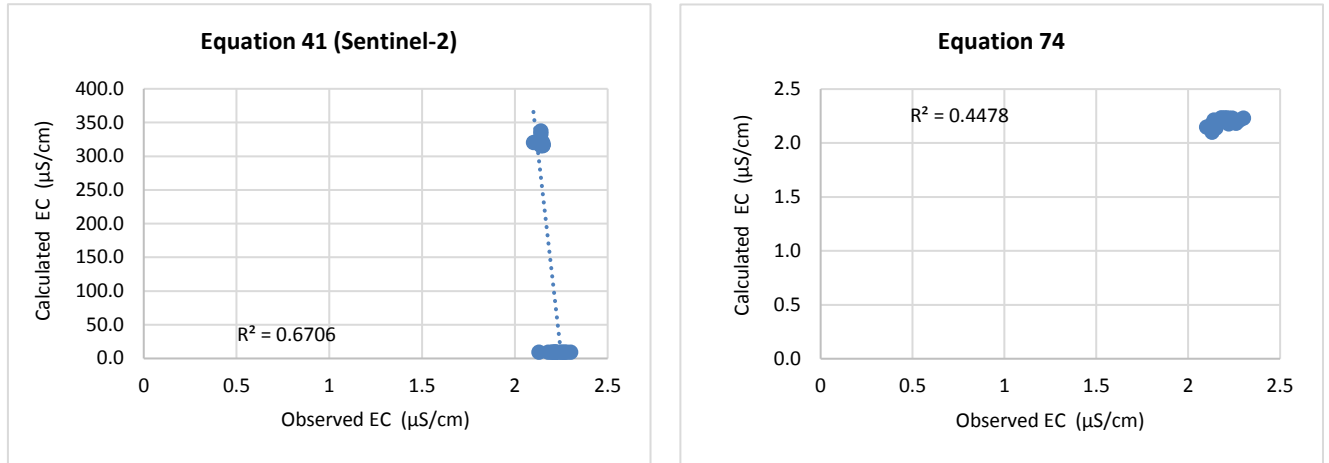


Figure 5.20: Scatterplots of observed vs. calculated values for turbidity estimation algorithms 41 and 74.

### 5.3.6.5 Map of estimated EC

The distribution of EC (Figure 5.21) is substantially speckled in appearance in winter. This indicated a high variability of EC throughout the estuary. These spikes are likely the inability of the estimation algorithms to model a smoother, more likely distribution. The spring distribution of EC displayed a more homogenous appearance. Despite this, there are incidences of EC spikes along river banks. The maps show a moderate ability in modelling the EC.

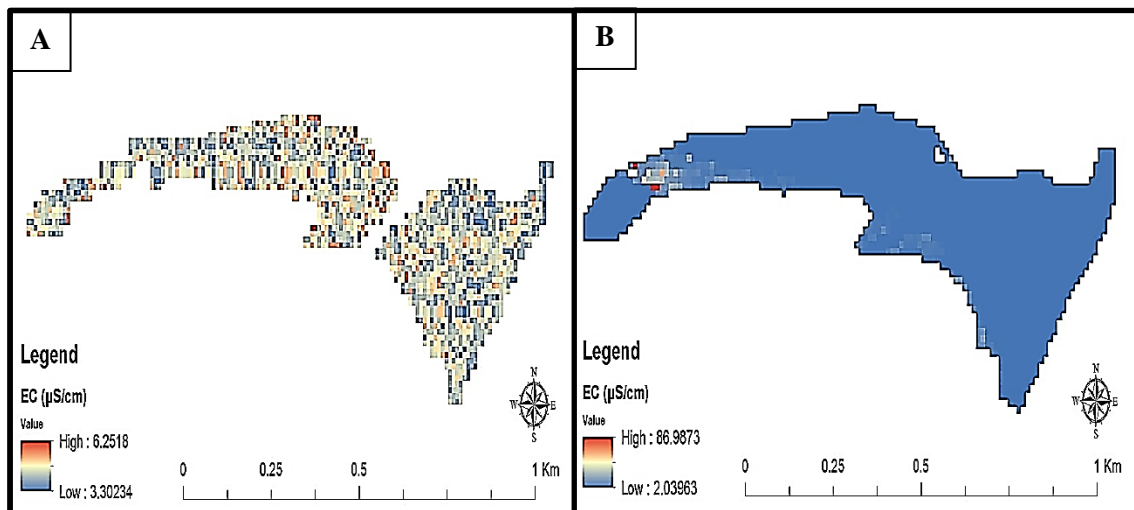


Figure 5.21: EC distribution across the Umdloti Estuary for winter (A) and spring (B).

### 5.3.7 Chl-a estimation

#### 5.3.7.1 Using Landsat 8

Landsat 8 appears to have mixed success in estimating chl-a with the accuracy results recorded over the course of this study recorded in Table 5.20. All Landsat-8 algorithms recorded a very low  $R^2$  throughout all datasets without a single algorithm showing any substantial ability to model chl-a. In contrast to the trend that has been observed with all other parameters, the overall  $R^2$  for most chl-a algorithms is much lower when compared to those calculated for the seasons individually. Positively, the majority of Landsat 8 algorithms achieved low RMSE values (with at least five algorithms below 1  $\mu\text{g/l}$ ). This signified that Landsat 8 was proficient at determining absolute concentrations of chl-a. Despite this generally improved accuracy, some algorithms such as Equation 59, Equation 56 and Equation 57 have very high RMSE's, indicating low accuracy.

Table 5.20: Accuracy of the estimated chl-a ( $\mu\text{g/l}$ ) using Landsat 8 for Umdloti Estuary.

Equation	Winter		Spring		Combined	
	$R^2$	RMSE	$R^2$	RMSE	$R^2$	RMSE
Equation 42	0.0003	50.355	0.415	2.799	0.003	35.661
Equation 43	0.176	2.354	0.065	2.076	0.004	2.220
Equation 44	0.120	3.167	0.158	6.262	0.0004	4.962
Equation 45	0.120	2.389	0.160	3.880	0.0003	3.222
Equation 46	0.120	1.071	0.158	2.735	0.004	2.077
Equation 47	0.085	2.625	0.008	3.889	0.004	3.318
Equation 48	0.006	4.612	0.351	0.696	0.004	3.298
Equation 49	0.120	1.072	0.158	0.714	0.0004	0.911
Equation 50	0.006	83.265	0.355	0.851	0.005	57.880
Equation 51	0.195	1.209	0.436	0.615	0.0008	0.960
Equation 52	0.194	1.161	0.432	0.628	0.023	0.933
Equation 53	0.0007	1.515	0.018	1.134	0.0008	1.339
Equation 54	0.038	1.057	0.005	0.639	0.013	0.873
Equation 55	0.227	1.182	0.022	0.620	0.0003	0.944
Equation 56	0.0002	88.964	0.028	4.132	0.004	62.975
Equation 57	0.006	53.844	0.286	46.640	0.007	50.375

### 5.3.7.2 Using Sentinel-2

The Sentinel-2 chl-a estimation (Table 5.21) displays similar mixed successes to what is found for Landsat 8.  $R^2$  values are generally inaccurately low throughout and found to be even lower when seasonal data is used. Again, RMSE is found to generally be low with a large number of algorithms again achieving RMSE values under or around 1  $\mu\text{g/l}$ . This indicates that whilst Sentinel-2 failed to relatively model chl-a across the estuary, it satisfactorily attempted to estimate the actual values of chl-a.

Table 5.21: Accuracy of the estimated chl-a ( $\mu\text{g/l}$ ) using Sentinel-2 for Umdloti Estuary.

Equation	Winter		Spring		Combined	
	$R^2$	RMSE	$R^2$	RMSE	$R^2$	RMSE
Equation 42	0.006	1.781	0.090	2.966	0.00008	2.446
Equation 43	0.010	2.354	0.021	2.077	0.00001	2.220
Equation 44	0.120	3.167	0.050	5.701	0.012	4.611
Equation 45	0.120	2.389	0.052	3.599	0.0127	3.055
Equation 46	0.120	1.071	0.050	2.813	0.003	2.129
Equation 47	0.085	2.625	0.012	5.933	0.00009	4.588
Equation 48	0.006	4.612	0.225	0.696	0.004	3.298
Equation 49	0.120	1.072	0.050	0.717	0.012	0.912
Equation 50	0.006	83.265	0.224	0.851	0.003	59.880
Equation 51	0.283	1.168	0.080	0.653	0.025	0.946
Equation 52	0.265	1.066	0.088	0.619	0.039	0.872
Equation 53	0.002	1.515	0.009	1.135	0.005	1.338
Equation 54	0.059	1.049	0.016	1.113	0.003	1.082
Equation 55	0.003	1.237	0.0412	0.645	0.004	0.987
Equation 56	0.020	87.627	0.001	5.143	0.004	62.068
Equation 57	0.190	53.058	0.075	47.102	0.0008	50.169

In general, Landsat 8 and Sentinel-2 display mixed but promising success in the estimation of chl-a. The absolute values of chl-a across the estuary were very satisfactorily estimated. This is supported by the fact that five different algorithms obtained overall RMSE's below 1  $\mu\text{g/l}$  for both sensors with a great many other recording values slightly above 1  $\mu\text{g/l}$ . However, both sensors are poor at modelling the variation of chl-a within the estuary. The relative best algorithm is developed by El-Magd and Ali (2008), (Equation 52) with best performing RMSE below 1  $\mu\text{g/l}$  (0.933  $\mu\text{g/l}$  and 0.872  $\mu\text{g/l}$ ) albeit with a very poor  $R^2$  (0.023 and 0.039). Both sensors are very similar in results with Landsat 8 having a slightly better accuracy on average.

### 5.3.7.3 Using newly modified algorithm

The chl-a estimation algorithm modified by this study achieves a moderate to good accuracy (Table 5.22). This algorithm (based on a log ratio of bands 2 and 4) performs far better in Umdloti Estuary than other algorithms used. An  $R^2$  of 0.64, whilst not perfect, was good considering that the vast majority of estimation algorithms tested by this study barely surpassed an  $R^2$  of 0.01. RMSE recorded is also relatively good throughout. This modified algorithm displayed the most consistent results found over the course of the study, which further adds to its reliability.

Table 5.22: Accuracy of the estimated chl-a ( $\mu\text{g/l}$ ) using newly generated estimation algorithms for Umdloti Estuary.

Equation	Winter $R^2$	Spring $R^2$	Combined $R^2$	Winter RMSE	Spring RMSE	Combined RMSE
Equation 75	0.649	0.627	0.64	0.632	0.390	0.525

### 5.3.7.4 Scatterplots of Chl-a models.

Figures 5.22 to 5.27 illustrates the graphical relationship between the actual measured chl-a and that predicted by algorithms. The seasonal clustering of points that has been seen in previous parameters is again found for most chl-a estimation algorithms. The distribution of chl-a points took on one of three patterns. They either form seasonal based clusters, similar to SDD (as seen with Equation 42, 44, 45, 46, 50, 55 and 56), form a horizontal line across the y-axis (as seen with Equations 43 and 54), or form a randomly dispersed pattern (Equation 51 and 52). However, none of these patterns show any modelling promise. As a result, no algorithms show any ability at modelling chl-a. The only exception to this is Equation 75 which provides an  $R^2$  of 0.64 and proved relatively good at modelling chl-a.



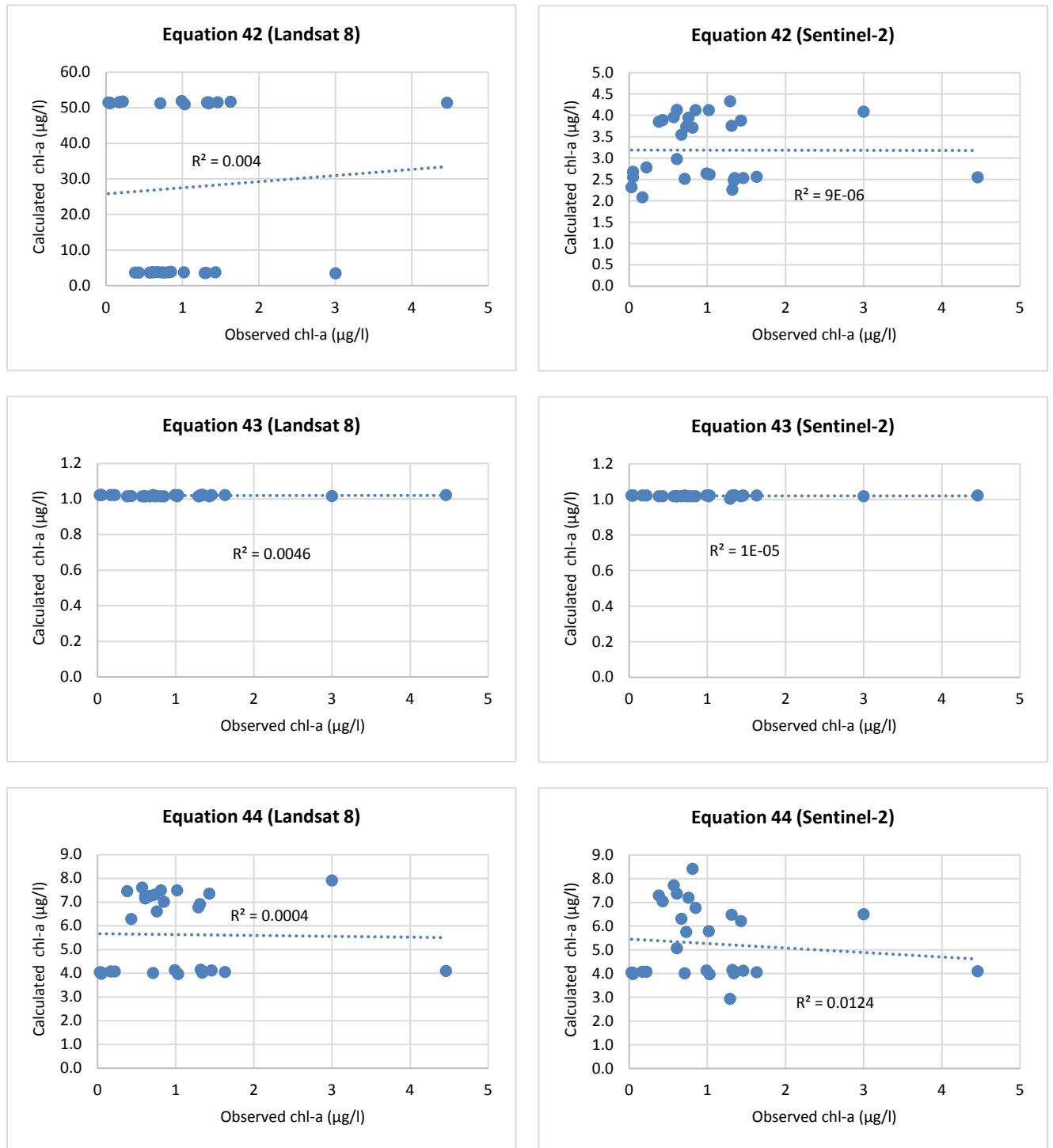


Figure 5.22: Scatterplots of observed vs. calculated values for chl-a estimation algorithms 42 to 44.

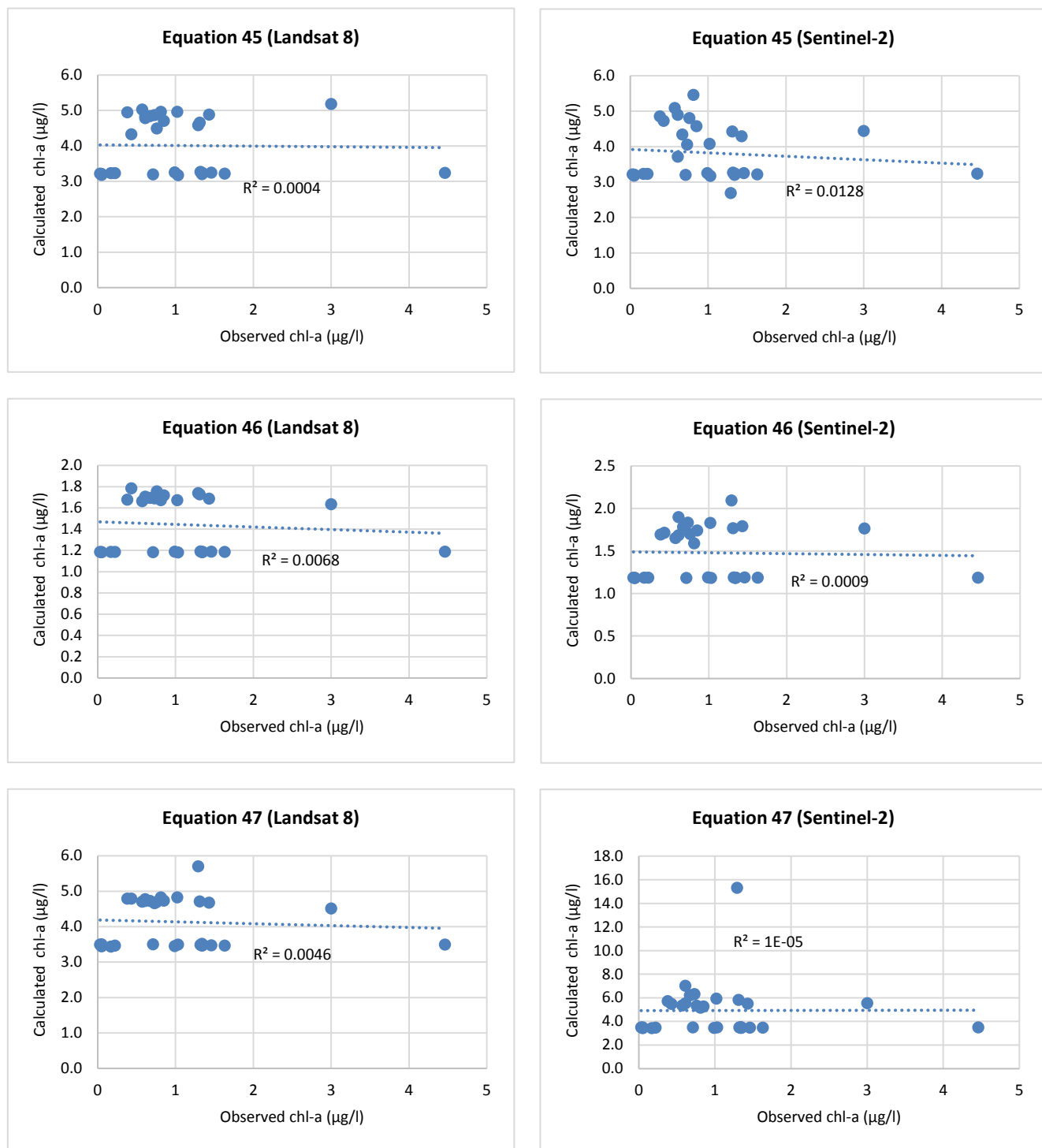


Figure 5.23: Scatterplots of observed vs. calculated values for chl-a estimation algorithms 45 to 47.

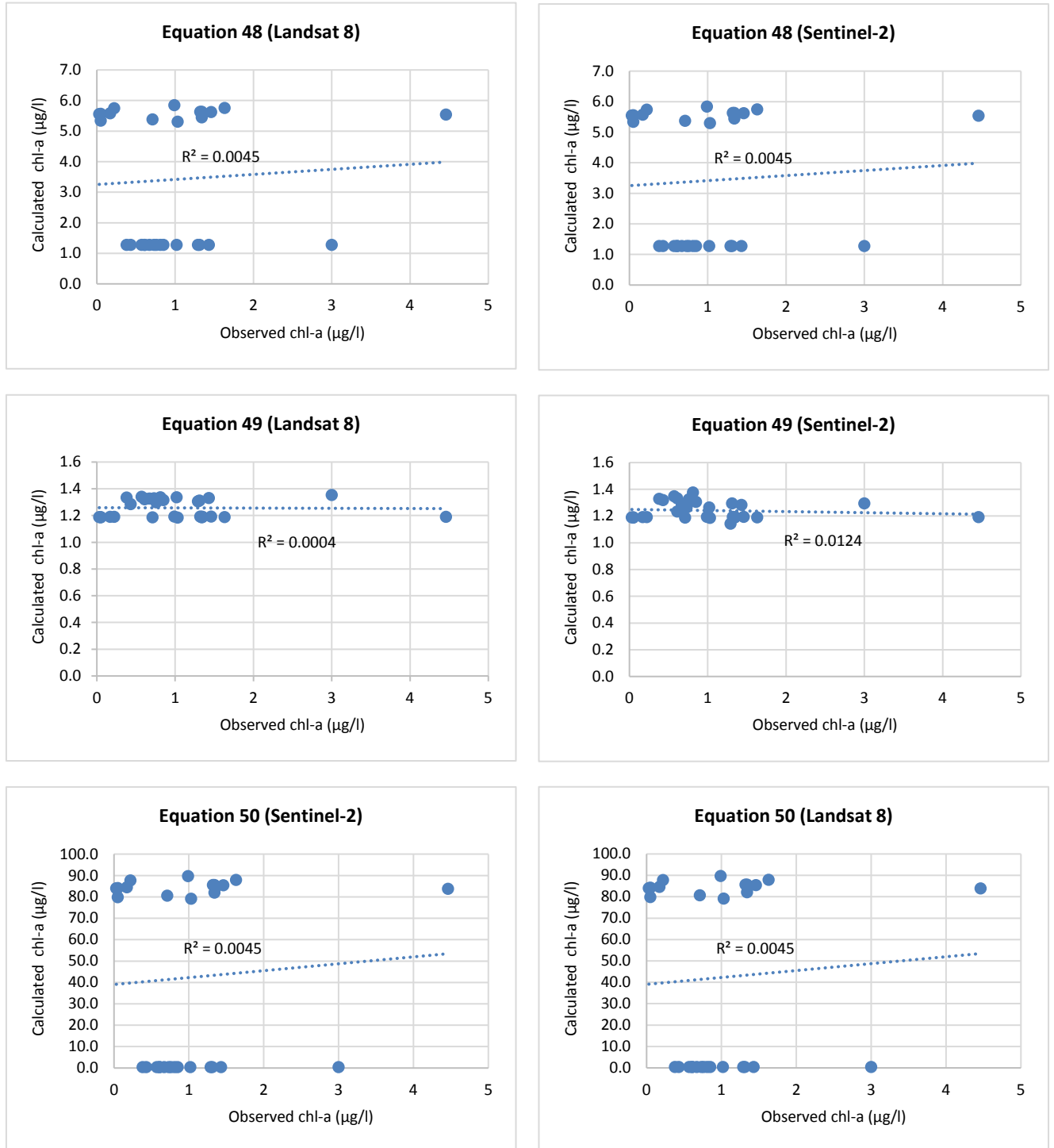


Figure 5.24: Scatterplots of observed vs. calculated values for chl-a estimation algorithms 48 to 50.

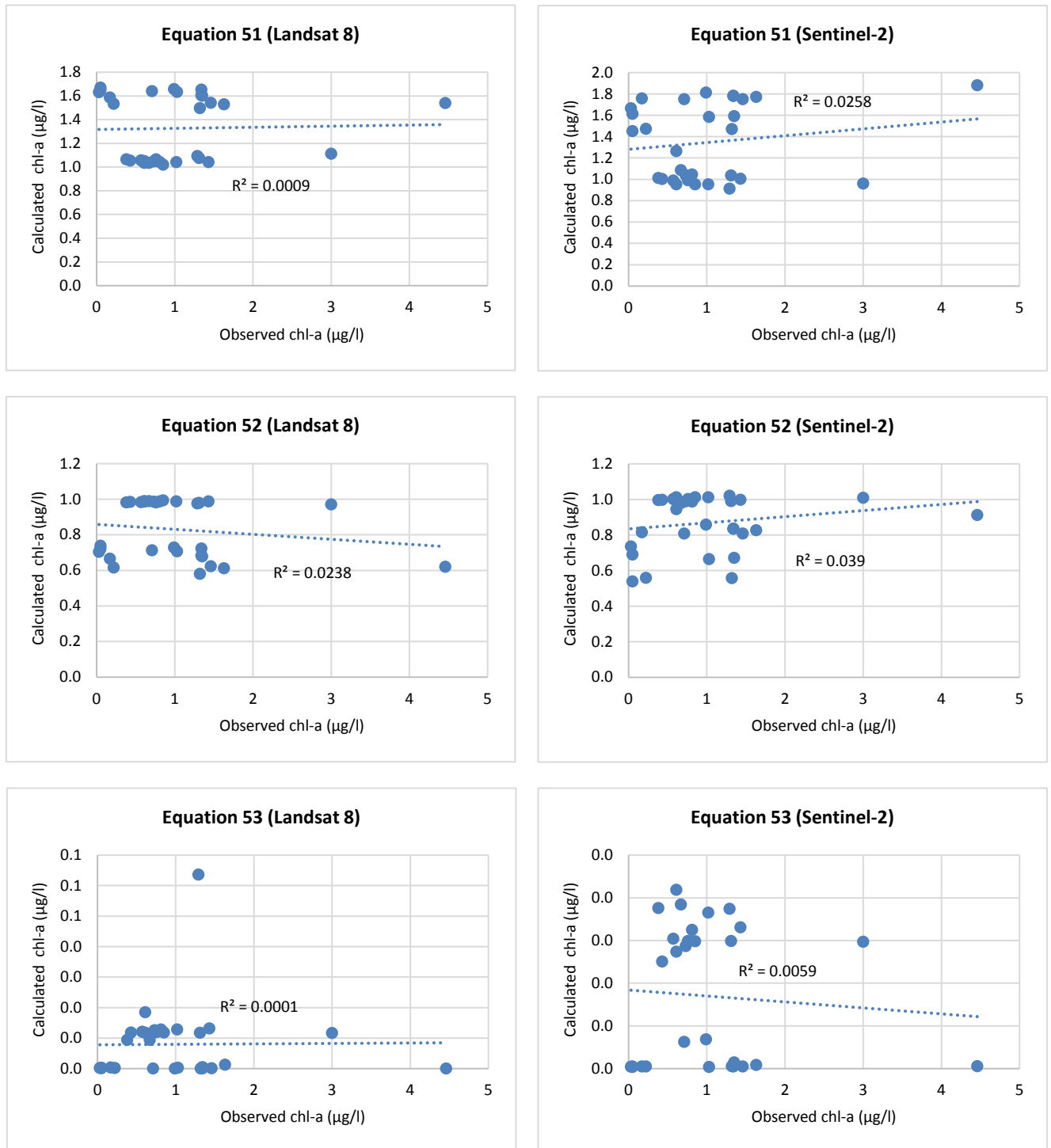


Figure 5.25: Scatterplots of observed vs. calculated values for chl-a estimation algorithms 51 to 53.

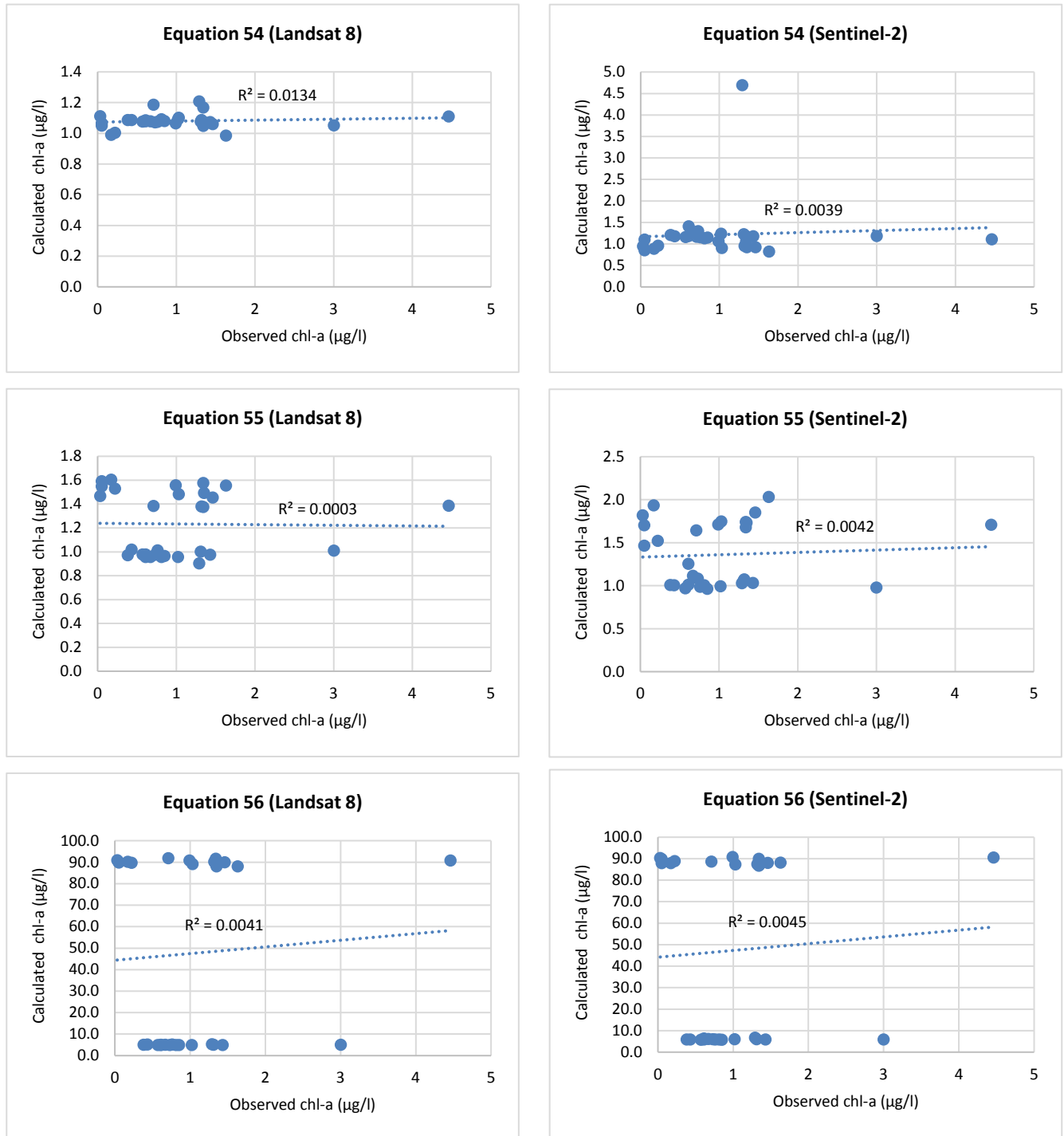


Figure 5.26: Scatterplots of observed vs. calculated values for chl-a estimation algorithms 54 to 56.

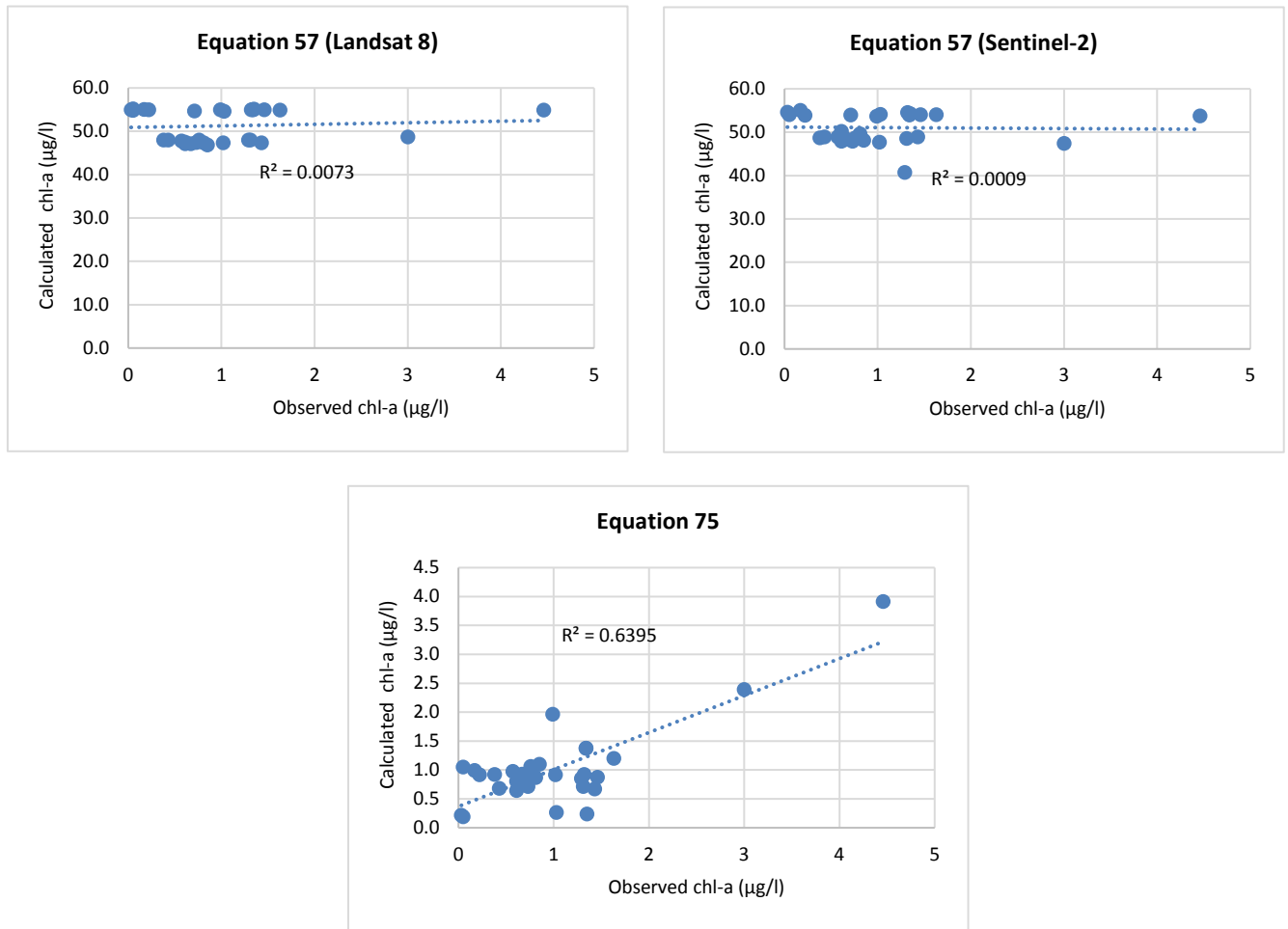


Figure 5.27: Scatterplots of observed vs. calculated values for chl-a estimation algorithms 57 and 75.

#### 5.3.7.5 Map of estimated chl-a

The distribution of chl-a is recorded in Figure 5.28. The winter distribution of chl-a took on a speckled appearance. Recorded chl-a is also generally higher in winter. These are mainly found to feature around ~2.5 to 4 (µg/l). In comparison, the chl-a values in spring are generally lower. There can be found to be some high value spikes in chl-a towards the banks of the estuary as well as towards the western end of the river.

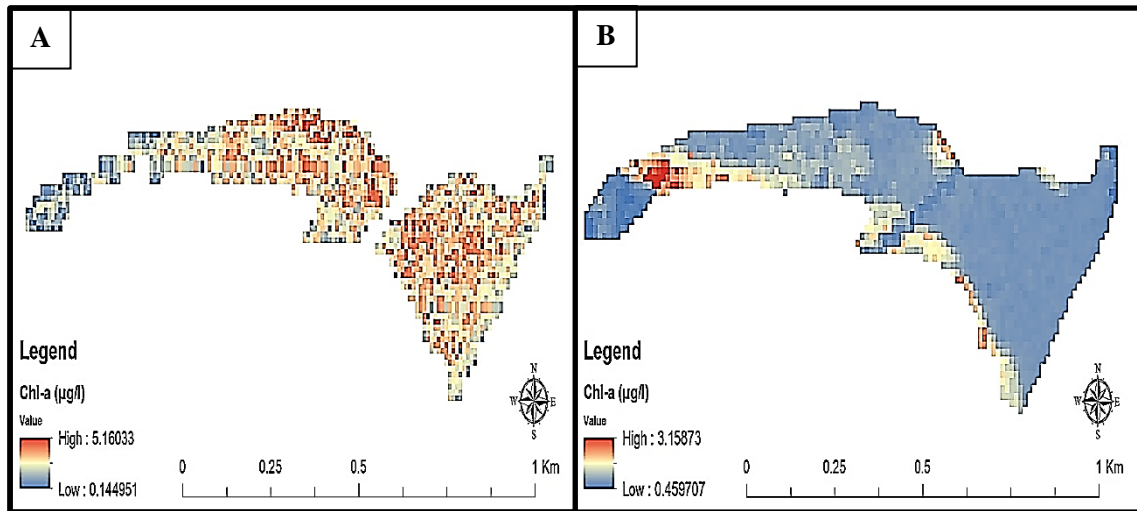


Figure 5.28: Chl-a distribution across the Umdloti Estuary for winter (A) and spring (B).

### 5.3.8 DO estimation

#### 5.3.8.1 Using Landsat 8

The estimation of DO using Landsat 8 images is recorded in Table 5.23. Landsat 8 had relatively poor success in the modelling and absolute estimation of DO.  $R^2$  values are again very low seasonally, but achieve higher (albeit still poor) combined seasonal average accuracies above 0.50 when using an overall dataset. Obtained RMSE is also high, indicating a low accuracy in retrieving absolute values of DO.

Table 5.23: Accuracy of the estimated DO (ppm) using Landsat 8 for Umdloti Estuary.

Equation	Winter		Spring		Combined	
	$R^2$	RMSE	$R^2$	RMSE	$R^2$	RMSE
Equation 58	0.354	1.093	0.065	2.462	0.569	1.905
Equation 59	0.003	2.649	0.00003	3.482	0.542	3.094
Equation 60	0.257	7.195	0.304	6.715	0.545	6.959

#### 5.3.8.2 Using Sentinel-2

A similar situation to what is found with Landsat 8 can be found for Sentinel-2 DO estimation (Table 2.24). The  $R^2$  determined for each algorithm is again negligibly low.  $R^2$  values rose once

a combined seasonal dataset is used to model DO. However, these increases are still not large enough to indicate algorithm reliability. RMSE's obtained are also relatively large for DO. This indicates an overall poor ability of the algorithms to both model and predict DO.

Table 5.24: Accuracy of the estimated DO (ppm) using Sentinel-2 for Umdloti Estuary.

Equation	Winter		Spring		Combined	
	R <sup>2</sup>	RMSE	R <sup>2</sup>	RMSE	R <sup>2</sup>	RMSE
Equation 58	0.024	1.009	0.062	2.518	0.498	1.918
Equation 59	0.050	2.648	0.228	3.491	0.598	3.098
Equation 60	0.002	8.209	0.163	6.826	0.597	7.550

Dissolved oxygen is poorly retrieved by both sensors. Overall, RMSE is high (ranging from 1.90 µg/l to 7.55 µg/l) and R<sup>2</sup> values achieved mostly poor results (none above 60). The best algorithm at estimating DO over the course of this study is developed by Theologou *et al.* (2015), and Khalil *et al.* (2016), (Equation 58). These algorithms achieved an RMSE of 1.905 and 1.918 and R<sup>2</sup> of 0.569 and 0.498. However, even this algorithm have poor accuracy and are not suitable for estimation. Both sensors are very similar with respect to results generated, with Sentinel-2 being slightly more accurate throughout.

#### 5.3.8.3 Using newly modified algorithm

The algorithm modified by this study to estimate DO was shown in Table 5.25. Even though the algorithm is based on a ratio of bands 2 and 4, DO proved difficult to estimate. The R<sup>2</sup> values are relatively better when considering those achieved by the other DO algorithms. However, this is still not large enough to consider the model reliable and good at modelling DO. The RMSE of this new algorithm shows considerable improvement over algorithms and suggests a better ability at determining absolute DO concentrations.

Table 5.25: Accuracy of the estimated DO (ppm) using newly generated estimation algorithms for Umdloti Estuary.

Equation	Winter R <sup>2</sup>	Spring R <sup>2</sup>	Combined R <sup>2</sup>	Winter RMSE	Spring RMSE	Overall RMSE
Equation 76	0.091	0.060	0.58	0.291	0.435	0.370



#### 5.3.8.4 Scatterplots of DO models.

Figures 5.29 to 5.30 illustrate the graphical relationship between the actual measured DO and those predicted by the algorithms. As is found with all previous parameters, there are very distinct seasonal clusters of points for Equations 58 and 59. This is also observed to a smaller degree in Equations 60 and 76. However, these clusters show more variability and were more spread out than is seen for other parameters. As a result, DO is modelled moderately well but never achieves more than an  $R^2$  above 0.6 for any algorithm.

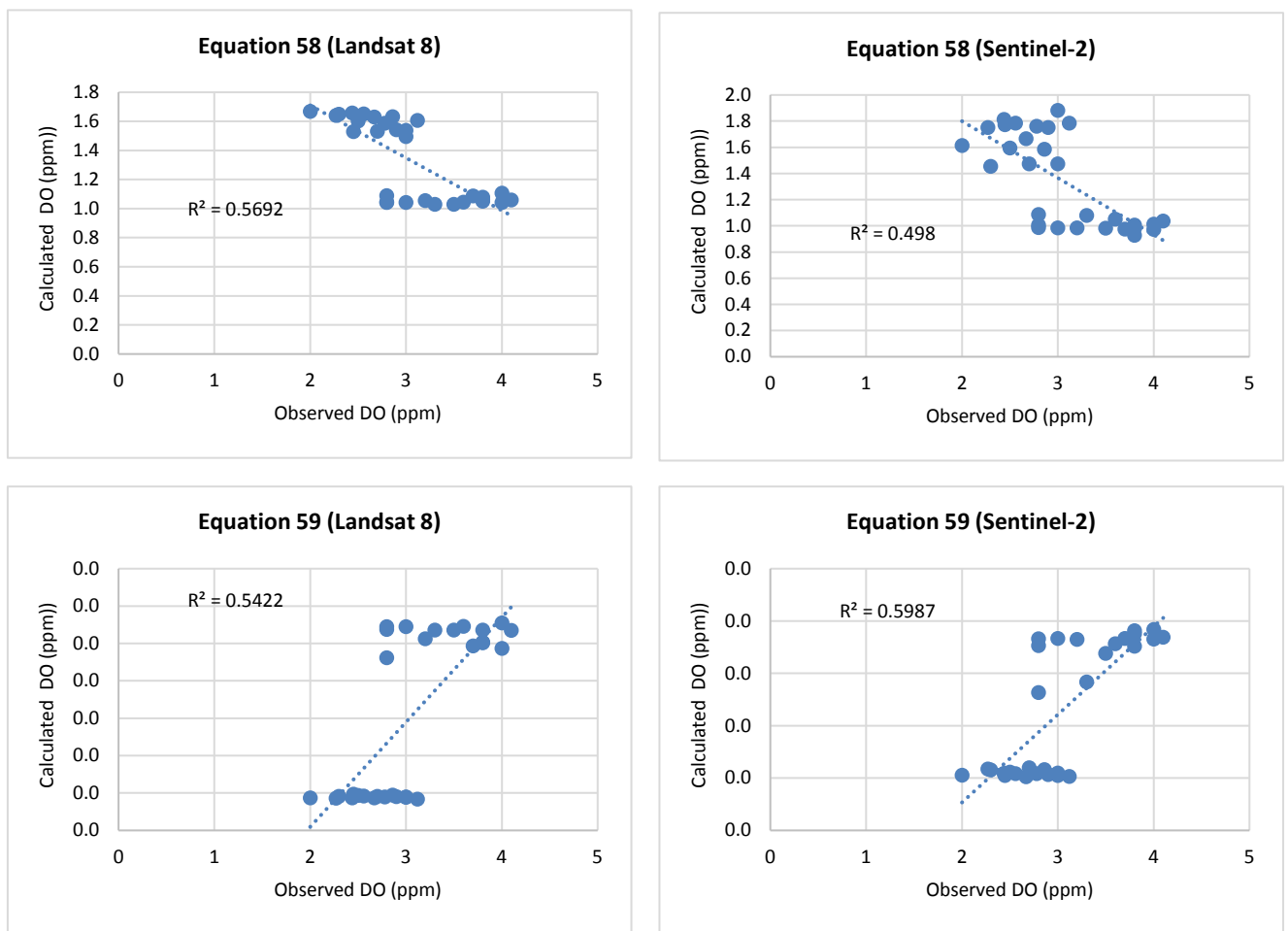


Figure 5.29: Scatterplots of observed vs. calculated values for DO estimation algorithms 58 and 59.

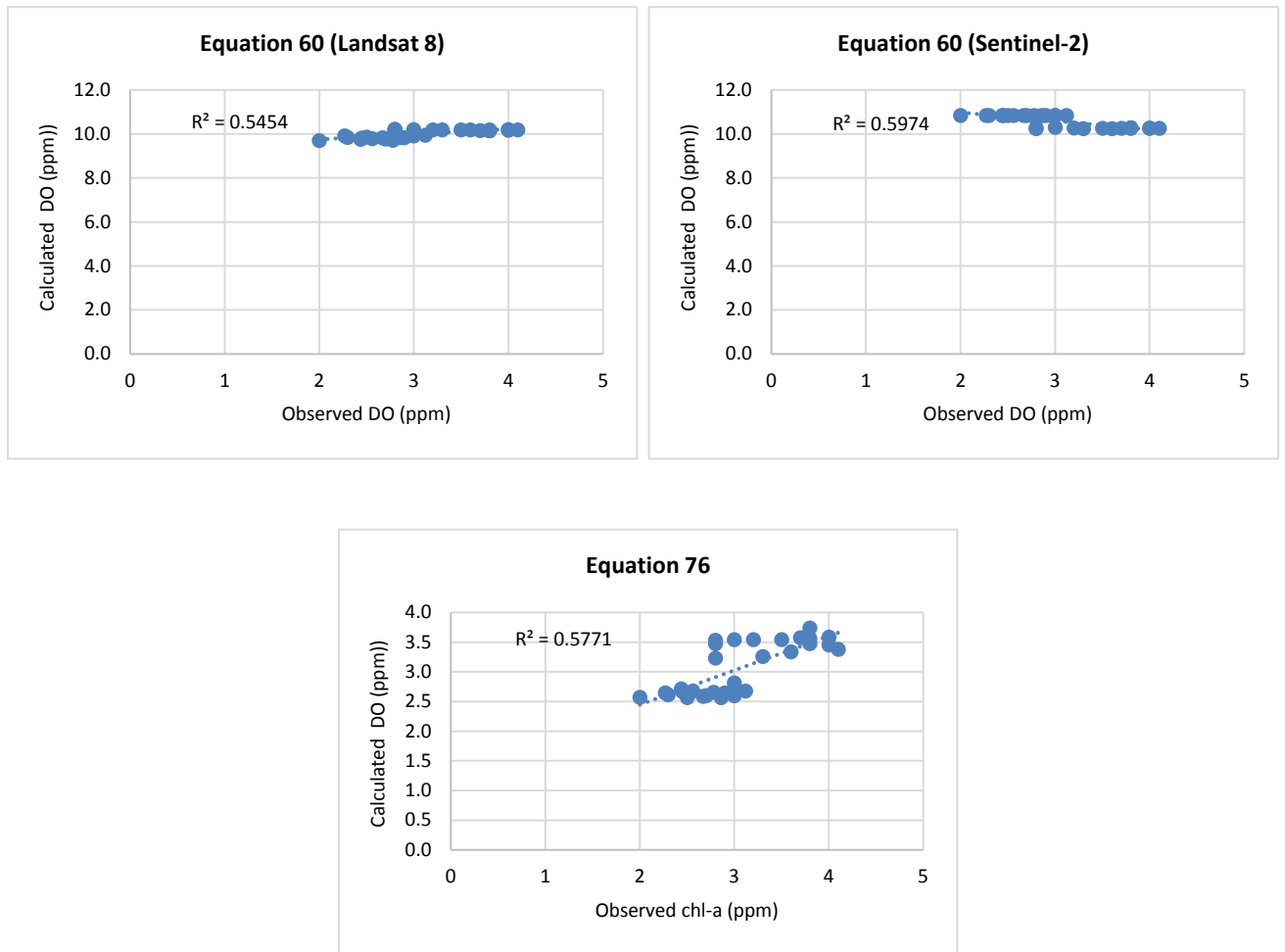


Figure 5.30: Scatterplots of observed vs. calculated values for DO estimation algorithms 60 and 76.

#### 5.3.8.5 Map of estimated DO

The distribution of DO (Figure 5.31) takes on a speckled distribution for winter. Concentrations of DO are generally higher towards the edges of the estuary and lowest towards the mid portions. Spring values are quite different in distribution. The overall DO in spring is much higher and the estuary has a generally constant concentration across its length and breadth.

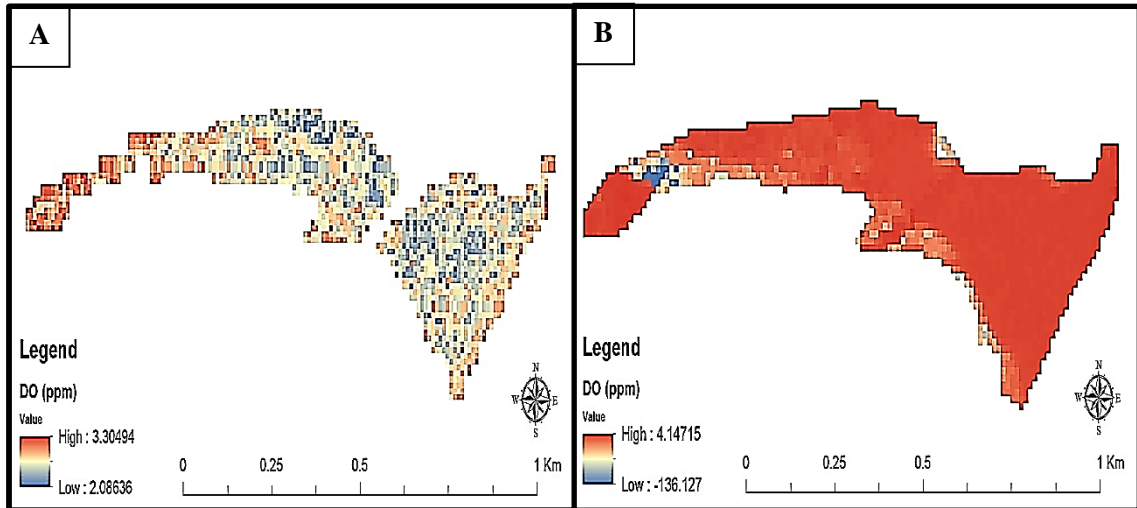


Figure 5.31: DO distribution across the Umdloti Estuary for winter (A) and spring (B).

### 5.3.9 pH estimation

#### 5.3.9.1 Using Landsat 8

The estimation of pH using Landsat 8 is difficult as evidenced by Table 5.26.  $R^2$  values calculated were all below 0.01 for winter and spring and below 0.34 when using the overall combined dataset for estimation. RMSE values are also consistently poor with only one RMSE below 1 (which is still not adequate considering pH ranges from 0 to 14). This indicates a non-existing ability at modelling pH.

Table 5.26: Accuracy of the estimated pH using Landsat 8 for Umdloti Estuary.

Equation	Winter		Spring		Combined	
	$R^2$	RMSE	$R^2$	RMSE	$R^2$	RMSE
Equation 61	0.032	2.145	0.004	2.411	0.273	2.282
Equation 62	0.038	4.287	0.031	5.868	0.283	5.139
Equation 63	0.033	6.036	0.006	6.278	0.341	6.158
Equation 64	0.037	2.145	0.004	2.409	0.260	2.281
Equation 65	0.091	6.082	0.003	5.804	0.059	5.945
Equation 66	0.045	0.906	0.004	1.211	0.278	1.070

### 5.3.9.2 Using Sentinel-2.

Similar to what was observed with the Landsat 8 results, pH is very poorly retrieved by Sentinel-2 (Table 5.27).  $R^2$  values are all below 0.1 for individual winter and spring seasons whilst using an overall seasonal dataset they did not rise above 0.27. RMSE's found are similarly poor in accuracy, with the lowest recorded sitting at 2.022.

Table 5.27: Accuracy of the estimated pH using Sentinel-2 for Umdloti Estuary.

Equation	Winter		Spring		Combined	
	$R^2$	RMSE	$R^2$	RMSE	$R^2$	RMSE
Equation 61	0.031	6.361	0.079	2.412	0.268	4.810
Equation 62	0.001	6.549	0.001	6.063	0.177	6.311
Equation 63	0.030	6.247	0.010	6.297	0.229	6.272
Equation 64	0.015	1.546	0.004	2.406	0.200	2.022
Equation 65	0.033	6.436	0.234	5.394	0.260	5.938
Equation 66	0.032	4.408	0.077	1.235	0.270	3.237

With RMSE's of over 1 for even the best algorithms, pH could be considered to be poorly retrieved.  $R^2$  values obtained during regression are also very poor, with none passing 0.341. The best estimation attempt is developed by Khattab and Merkel (2014), with consistent RMSE's of 2.281 and 2.022 and  $R^2$ 's of 0.260 and 0.200. Overall, Landsat 8 appears to be the better sensor but still produces inaccurate results.

### 5.3.9.3 Using newly modified algorithm

The pH estimation algorithm modified by this study suffer from the same poor accuracy experienced by other algorithms (Table 5.28). The  $R^2$  of 0.29 indicate a complete inability of the algorithm to model pH. However, the RMSE indicates a stronger ability at retrieving absolute values. If the model is able to consistently achieve RMSE values around 0.234 then it may prove relatively useful in determining pH.

Table 5.28: Accuracy of the estimated pH using newly generated estimation algorithms for Umdloti Estuary.

Equation	Winter $R^2$	Spring $R^2$	Combined $R^2$	Winter RMSE	Spring RMSE	Combined RMSE
Equation 77	0.021	0.110	0.29	0.311	0.113	0.234

#### 5.3.9.4 Scatterplots of pH models.

Figures 5.32 to 5.34 illustrates the graphical relationship between the actual measured pH and those predicted by the algorithms. As seen with almost every other parameter, pH forms distinct seasonal clusters that are spaced very far apart (as seen in the Sentinel-2 Equation 61). If not seasonally clustered, the points take on a flat, straight line across the y-axis appearance, with points distributed across many different x-values. These patterns prove difficult to model and as a result, a universally poor  $R^2$  values for all algorithms indicates that pH is not well modelled.

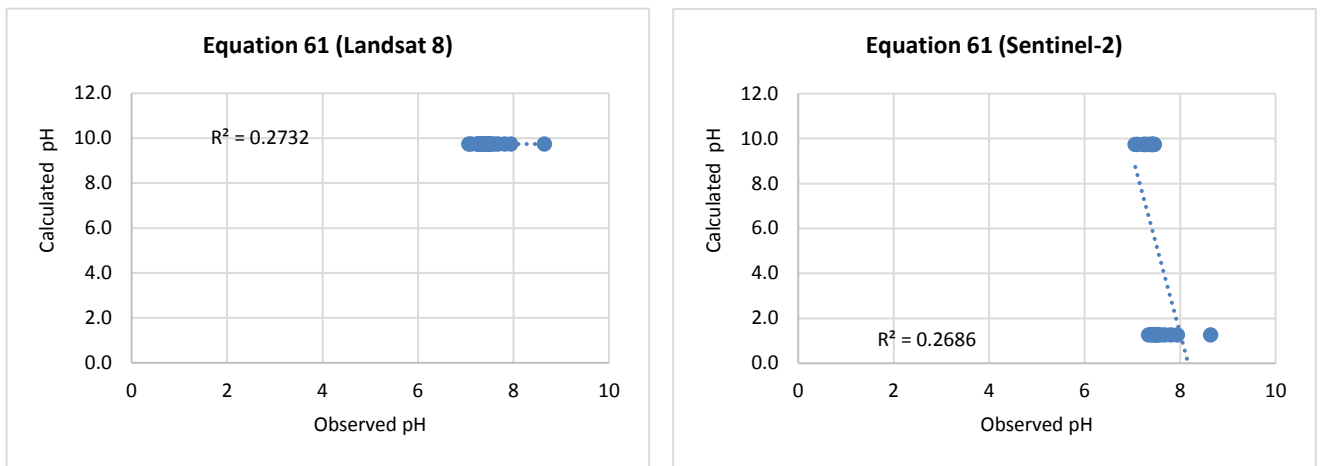


Figure 5.32: Scatterplots of observed vs. calculated values for pH estimation algorithms 61.

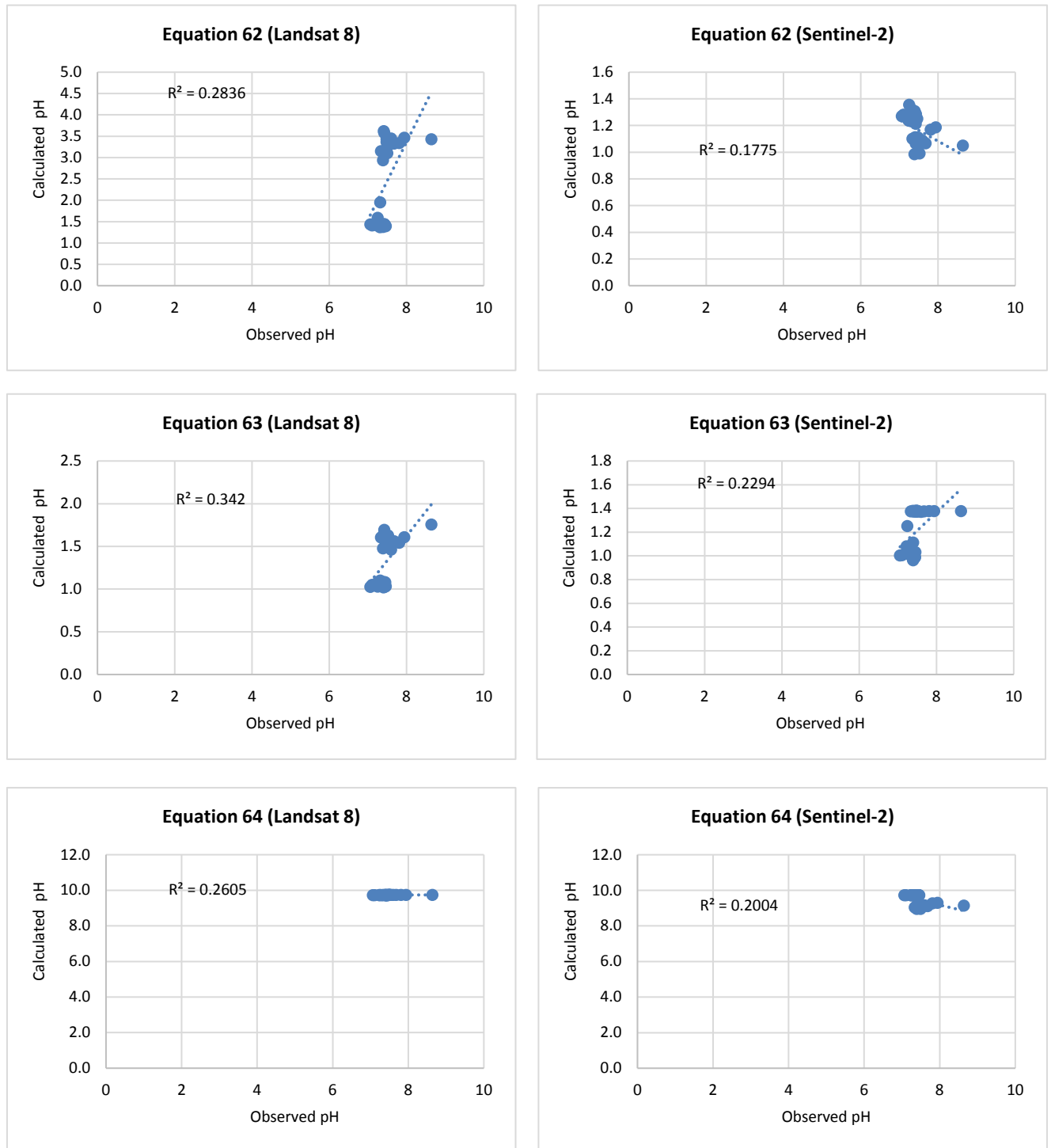


Figure 5.33: Scatterplots of observed vs. calculated values for pH estimation algorithms 62 to 64

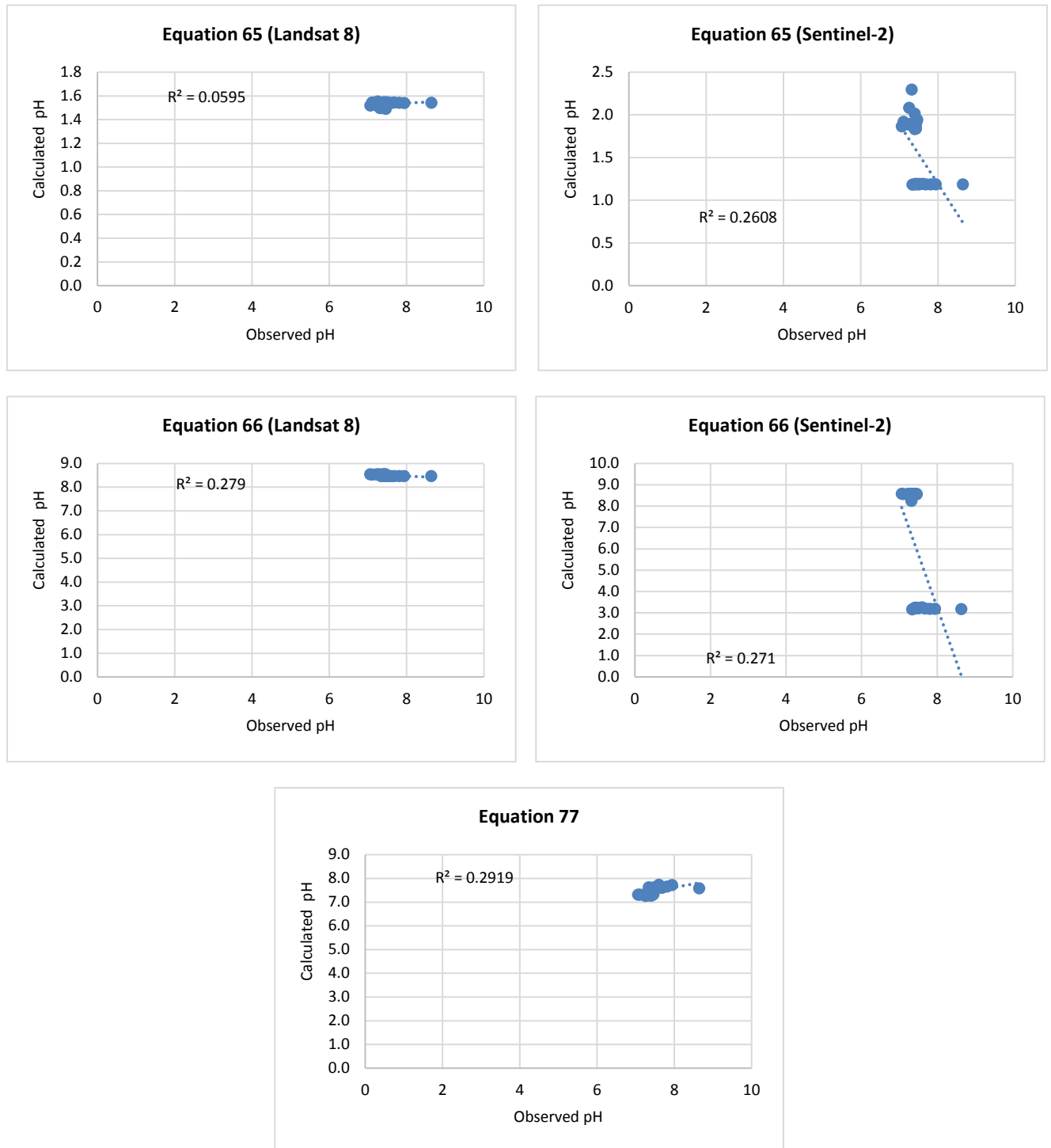


Figure 5.34: Scatterplots of observed vs. calculated values for pH estimation algorithms 65, 66 and 77

### 5.3.9.5 Map of estimated pH

pH differs little between seasons (Figure 5.35). Winter has a pH around 7.6 and is constant throughout the majority of the estuary. Spring on the other hand has a pH of around 7.2 and differs by small amounts across the majority of the estuary. These distribution maps efficiently map the pH found within the estuary.

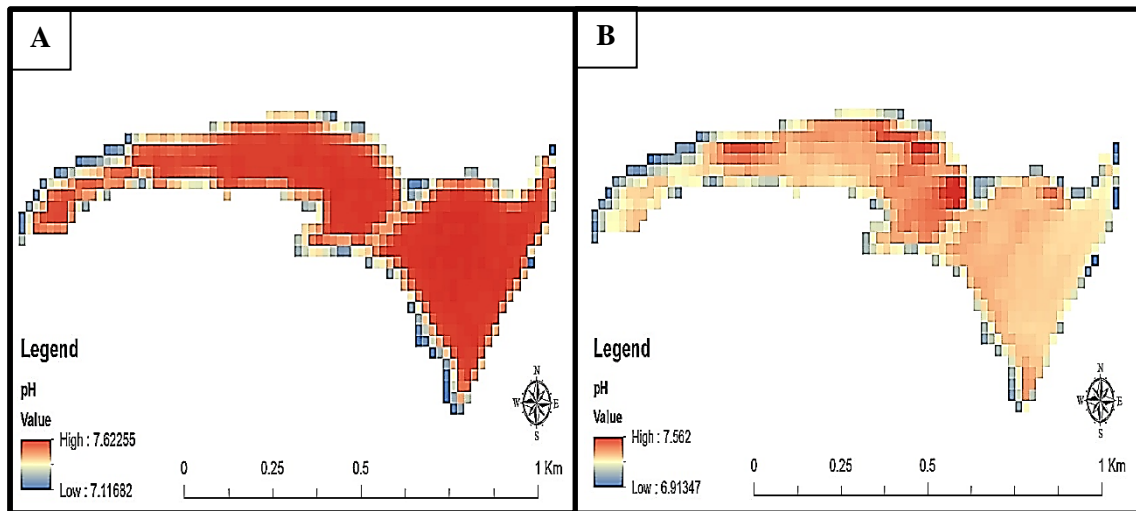


Figure 5.35: pH distribution across the Umdloti Estuary for winter (A) and spring (B).



## CHAPTER SIX: DISCUSSION AND CONCLUSION

### 6.1) Introduction

This final chapter provides a critical discussion of the results in relation to the current body of knowledge of physio-chemical parameter estimation using remote sensing. Following this, the recommendations and limitations found by this study are then given. The study thereafter concludes and gives closing statements.

### 6.2) Discussion

#### 6.2.1 Temperature estimation using remote sensing

The spaceborne Landsat 8 and Sentinel-2 remote sensors that were set the task of estimating water quality physico-chemical parameters from the Umdloti Estuary met with mixed levels of success. These sensors experienced difficulty in modelling certain parameters in the slightly brackish estuarine water whilst others were efficiently and accurately retrieved. This was despite the fact that many of the estimation algorithms were not designed for estuarine use which should have negatively impacted on the ability of the sensors to model parameters.

Temperature over the Umdloti Estuary was estimated with a moderate to good accuracy by this study. With  $R^2$  values above  $R^2 = 0.95$ , the Abdullah (2015), algorithm (Equation 10) displayed an exceptional temperature modelling ability over the Umdloti Estuary. However, the RMSE results were poorer (just below 3 °C) and displayed a weakness in the ability of Landsat 8 and Sentinel-2 in retrieving absolute values. The generally strong  $R^2$  values obtained are similar to those that may be found in literature (Khattab and Merkel, 2013; Syariz *et al.*, 2015). In their own study over Dokan Lake, Abdullah (2015), managed to initially develop algorithms with a similar accurate  $R^2$  (around 0.72 to 0.86) but when applied to actually estimate temperature suffered weaker  $R^2$  accuracies dropping to around  $R^2 = 0.5$ . RMSE values found by this current study are higher than what may be found in literature. Khattab and Merkel (2013), for example found RMSE for their temperature estimation algorithm to reach around 0.4 °C in their study. Despite this, sea surface temperature estimation algorithms with the help of in situ data generally generate accuracies that range between 0.2 to 3.4 °C (Thomas *et al.*, 2002; Syariz *et al.*, 2015). The estimated temperature found by this study was well within in the range without the added help of in situ data. The modified temperature estimation algorithm managed to reduce this RMSE down to 0.6 whilst keeping the accurate  $R^2$ . Since only algorithm coefficients

were changed, this greatly improved accuracy is due to the Abdullah (2015), algorithm being fine-tuned to local estuarine conditions experienced in Umdloti Estuary. The best performing algorithm modified by Abdullah (2015), unconventionally did not rely on the use of the already well established practise of using thermal infrared radiation (3 to 14  $\mu\text{m}$ ) for the estimation of temperature (Gholizadeh *et al.*, 2016). The Abdullah (2015), study based it's algorithm on a correlation of temperature to the coastal blue and red Landsat 8 bands. However, determining the general effectiveness of this combination is hard as there is a lack of literature which has supported or also made use of these bands in temperature estimation. Regardless, the combination of coastal blue and red appeared to work well in both the Abdullah (2015), and this current study and has the added advantage of flexibility as it may be used for both Landsat 8 and Sentinel-2. Future studies attempting temperature estimation in estuaries may want to further verify the efficiency of this algorithm or improve on the use of the Avdan and Jovanovska (2016), algorithm. Although tested as a land surface temperature algorithm, it has the capability to be used for sea surface temperature estimation. This algorithm relies on thermal infrared bands and inbuilt environmental corrections such as for surface emissivity and is therefore more theoretically grounded.

#### 6.2.2 Turbidity estimation using remote sensing

One of the most successful parameters retrieved over the course of the study was that of turbidity. Whilst many of the turbidity estimation algorithms modelled turbidity well, the Dogliotti *et al.* (2015), algorithm (Equation 11) came closest to a performing a perfect estimation. Considering that turbidity levels retrieved from water may easily range into the hundreds and thousands, a low RMSE value of 2.94 NTU and an  $R^2 = 0.97$  could be considered exceptional accuracy. Similar good accuracy for turbidity estimation was found by a multitude of other studies (Al-Fahdawi *et al.*, 2015; Dogliotti *et al.*, 2015; Garaba and Zielinski, 2015; Kapalanga, 2015; Lim and Choi, 2015). The results found by the current study also closely mirrored those found by Dogliotti *et al.* (2015). Whilst testing their algorithm in a multiple estuaries and across a wide range of turbidity conditions, Dogliotti *et al.* (2015), achieved the same accuracy as found by the current study ( $R^2 = 0.97$ ). In their study Dogliotti *et al.* (2015), also found that turbidity retrieved was between 12% and 22% of the observed in situ value. In comparison, the majority of this current study's RMSE ranged between 55% to 61% of the observed in situ values. Whilst this was less accurate than that found by in the Dogliotti *et al.* (2015), study, these values did not represent large changes in turbidity and still correctly identified the estuary as experiencing low turbidity. The use of a modified Dogliotti *et al.*

(2015), algorithm by this current study resulted in a near perfect estimation with  $R^2 = 0.99$  and RMSE achieving an accurate value of 0.005 NTU. Again, since there was no change in the bands used, this improved accuracy could be put down to the fine-tuning of band coefficients to conditions experienced by Umdloti Estuary. Possible future complications impacting on the accuracy of this current study's turbidity estimation algorithm may arise due to several factors. One factor involves the complete lack of intraseasonal variation found during in situ sampling. Due to this, a respective  $R^2$  was unable to be calculated for seasonal data. This would leave some doubt as to the reliability of turbidity estimation during these seasons as only a combined seasonal dataset could be used. Further, in situ turbidity found during both seasons ranged between only 5 to 5.1 NTU. Remote sensing estimation of turbidity would likely differ in ability under differing turbidity conditions (Gholizadeh *et al.*, 2016). Future studies attempting to estimate turbidity should ensure that turbidity estimation algorithms are tested over different ranges of turbidity.

### 6.2.3 SDD estimation using remote sensing

Whilst turbidity was one of the best estimated parameters, SDD was the worst estimated. Despite being the relative best algorithm, Deutsch *et al.* (2014), (Equation 25) only managed to achieve an inaccurate average  $R^2$  below  $R^2 = 0.001$  and RMSE of 1.434 m (almost double the depth of the estuary in certain parts). Whilst usually not as poor as was found in this current study, poor accuracy associated with SDD retrieval may be found in literature (Wang *et al.*, 2006; Deutsch *et al.*, 2014; Hancock, 2015). This inaccuracy would be unexpected considering that both turbidity and SDD are linked to water clarity and therefore should achieve roughly similar accuracies. A possible reason given by Giardino *et al.* (2001), suggested that chl-a, dissolved organics and inorganic suspended sediments as well as the bottom effects from the shallow parts of the estuary may greatly interfere with a remote sensors ability to determine SDD. In their study, Deutsch *et al.* (2014), achieved a much stronger accuracy with an  $R^2 = 0.87$ . However, other algorithms they had developed to estimate SDD suffered from low  $R^2$  values ranging between 0.38 to 0.47. Deutsch *et al.* (2014), noted SDD algorithms are not always accurate if used by remote sensors other than those they were developed for. Even using a modified algorithm, an  $R^2 = 0.02$  and RMSE of 0.220 m does little to establish a suitable relationship between reflectance and in situ SDD. A recommendation suggested by Hancock (2015), was that in order to accurately retrieve SDD, algorithms would have to be validated and modified for use in the water bodies they would be needed in. Future studies may want to develop algorithms from scratch for SDD retrieval in the Umdloti Estuary.

#### 6.2.4 Salinity, TDS and EC estimation using remote sensing

Salinity was initially poorly estimated but this changed once a modified algorithm was used. The initial poor accuracy was evidenced best in this current study by the relative strongest Wang and Xu (2008), algorithm (Equation 31) achieving an average  $R^2 = 0.41$  and an RMSE of 4.8. This poor accuracy is generally rare as the majority of studies find better estimated salinity (Lavery *et al.*, 1993; Wang and Xu, 2008; Zhao *et al.*, 2017). Wang and Xu (2008), for example estimated salinity with an  $R^2 = 0.89$  and RMSE of 0.49. Possible reasons for this poor accuracy include that nearly all salinity estimation algorithms were designed for use over oceanic environments. Salinity, TDS and EC are all measures that are used to relate the amount of salt present within water. Whilst TDS and EC are popular for use in estuaries and freshwater, salinity algorithms are generally not. The Lavery *et al.* (1993), study is an exception to this as they successfully estimated salinity in an estuary with an  $R^2$  above  $R^2 = 0.7$ . They cautioned that the success in their salinity retrieval may not necessarily make their algorithm suitable for use in other estuaries due to the unique constituents that make up estuarine water. The unique water composition of the Umdloti Estuary may therefore impact on salinity retrieval. The use of a modified Wang and Xu (2008), algorithm by this study saw a greatly improved accuracy with an  $R^2 = 0.70$  and RMSE of 0.046 being obtained. The use of this new algorithm therefore suggests a strong potential for future salinity estimation in Umdloti Estuary. However, future testing of this algorithm is advised to determine if this accuracy would be consistent.

TDS and EC were two variables that along with salinity were used to measure the salt content of the Umdloti Estuary. The estimation of both TDS and EC using Landsat 8 and Sentinel-2 could be considered to have been moderately successful. This was despite the fact that both parameters achieved a poor to moderate  $R^2$  and their RMSE was almost double the actual in situ values. The Abdulla (2015), algorithm (Equation 36) for example was used by this current study to determine TDS and achieved an average  $R^2 = 0.57$  and RMSE of 638 mg/l. EC was determined using the Khattab and Merkel (2014), algorithm (Equation 37) and achieved average accuracies of  $R^2 = 0.38$  and a RMSE of 1.8  $\mu\text{S/cm}$ . One of the reasons why both TDS and EC could have been considered to have been reasonably well estimated was because of their strong and accurate RMSE. Within estuarine water both TDS and EC are commonly able to scale into units numbering tens of thousands. These parameters can therefore scale very high and often do so rapidly. The fact that their recorded RMSE was so relatively low leaves them with a strong absolute accuracy. This is supported by the fact that both TDS and EC correctly record the estuary as having a more freshwater composition than just brackish water. Still, this accuracy is

generally poorer than those found in literature. This is especially true for the  $R^2$ . Al-Fahdawi *et al.* (2015), and Khattab and Merkel (2014), found TDS and EC estimation accuracies above  $R^2 = 0.84$ . Once algorithms were modified and used by this current study, accuracy improved. The modified Abdulla (2015), algorithm further improved on TDS accuracy achieving an  $R^2 = 0.69$  and RMSE of 11.369 mg/l. The modified Khattab and Merkel (2014), algorithm also achieved improved EC accuracies of  $R^2 = 0.44$  and an RMSE of 0.039  $\mu\text{S/cm}$ . The algorithms modified by this study therefore made good inroads in improving these parameters  $R^2$  (excepting EC) and increasing RMSE accuracy, leading to greatly increased reliability that are comparable with other studies (Khattab and Merkel, 2013; Abdullah, 2015; Al-Fahdawi *et al.*, 2015; Mushtaq and Nee Lala, 2017). Therefore TDS could be considered to have been successfully estimated. Caution should continue to be attached to the use of the modified EC algorithm due to its poor relative modelling ability.

#### 6.2.5 Chl-a estimation using remote sensing

Chlorophyll-a was a particularly interesting parameter over the course of this study. El-Magd and Ali (2008), (Equation 52) was the relative best estimation algorithm and achieved an average  $R^2 = 0.02$  and RMSE of 0.9  $\mu\text{g/l}$ . Chl-a contained some of the lowest  $R^2$  values recorded over the course of the study. This lack of ability to record variability within estuaries has been found in other studies such as those by Harding *et al.* (2005); Koponen (2006); Werdell *et al.* (2009), and Wang *et al.* (2011). As a result, all used algorithms completely failed to efficiently model the distribution using remote sensing imagery. A possible reason for this was that in situ sampling showed that chl-a was highly heterogeneous in distribution across the estuary, with random spikes of highs and lows. This made it difficult to compare in situ and remote sensing data as Koponen (2006), proposed that remote sensors greatly average pixel values, resulting in the masking of these spikes. El-Magd and Ali (2008), explained that the low accuracy in chl-a retrieval could be reduced due to the presence and interference by inorganic suspended sediments and dissolved organic matter to reflectance. Despite this, chl-a algorithms generally were good at obtaining absolute values as shown by their low RMSE. The majority of algorithms therefore suitably and accurately identified the estuary as possessing low levels of chl-a even if  $R^2$  was negligibly low. El-Magd and Ali (2008), in their own study achieved a combination of both negligible strong accuracies, with  $R^2$  ranging from  $R^2 = 0.02$  to  $R^2 = 0.75$ . The algorithm modified by this study for chl-a estimation was by far the most consistent on a seasonal basis and provided reasonably good and reliable accuracy ( $R^2 = 0.64$  and RMSE of 0.525  $\mu\text{g/l}$ ). In these ways it may be considered one of the best successes of this study. Due to

the averaging of pixel values, future studies should take note that spatial resolution (in addition to spectral resolution) should be considered a particularly important component when attempting chl-a estimation (Koponen, 2006). Sentinel-2 with its superior spatial resolution performed better in mapping these spikes.

#### 6.2.6 DO estimation using remote sensing

DO could be considered to have been poorly retrieved. The relative best algorithm by Theologou *et al.* (2015), and Khalil *et al.* (2016), (Equation 58), could only achieve an average  $R^2 = 0.53$  and RMSE of around 1.91  $\mu\text{g/l}$ . This poor accuracy for DO retrieval is not uncommon in literature (Abdulla, 2015; Khalil *et al.*, 2016; Mushtaq and Nee Lala, 2017). Theologou *et al.*, (2015) and Khalil *et al.* (2016), found higher accuracies for their studies with  $R^2$  retrieved usually above  $R^2 = 0.75$ . However, Khalil *et al.* (2016), also obtained DO estimation accuracy similar to this study for one of their algorithms using bands 2 and 4. Modified algorithms did little to improve this accuracy and achieved a  $R^2 = 0.58$  and RMSE of 0.370  $\mu\text{g/l}$ .

#### 6.2.7 pH estimation using remote sensing

Similarly to what was found when estimating DO, pH could also be considered to have been one of the most poorly estimated parameters. The relative best algorithm by Khattab and Merkel (2014), (Equation 64), recorded an average  $R^2 = 0.23$  and RMSE of around 2.15. This poor accuracy has been found in other studies (Abdulla, 2015; Mushtaq and Nee Lala, 2017). Khattab and Merkel (2014), found better accuracies in their own study with  $R^2$  values reaching above  $R^2 = 0.75$ . The use of modified algorithms did little to improve this accuracy (except with respect to RMSE) resulting in a  $R^2 = 0.29$  and RMSE of 0.234.

#### 6.2.8 Reasons for the success and failure of remote sensing estimation

There are some general reasons why some parameters were better estimated. Amongst the most successfully estimated parameters found over the course of this study are those of turbidity, temperature and chl-a. A possible reason for the high accuracy could be attributed to these parameters popularity. Turbidity, temperature and chl-a are easily among some of the most popular water-based parameters studied and retrieved through remote sensing (Abdullah, 2015; Gholizadeh *et al.*, 2016). This popularity is partly due the large role of these parameters with regard to environmental health. Temperature for example controls many essential water borne

processes and as such is considered important to record whenever water samples are taken (Abdullah, 2015). However, a better explanation of their popularity is due to the fact that remote sensing physico-chemical estimation relies heavily on the optical properties of an entity and all three parameters are considered highly optically reactive (Gholizadeh *et al.*, 2016). This strong optical reactivity, long term study and continuous refinement have resulted in the development of many accurate and reliable algorithms. Chl-a for example has also been accurately retrieved for years through use of broadband sensors such as Landsat (Dekker and Peters, 1993).

Despite the successes, the remote sensors also performed poorly in the estimation of some water quality parameters. Examples of poorly estimated variables found by this current study include SDD, pH and initially salinity estimation. Their retrieval all resulted in a weak to negligible relationship being established between the Landsat 8 and Sentinel-2 reflectance and actual in situ values. The lack of accurate estimation success could be put down to a several factors. An estuary is a dynamic and complex water body, receiving constant influxes such as salty water from the oceans or sedimentation from rivers (Le *et al.*, 2013). This leads estuaries containing water that is often more optically complex than other water bodies (El Magd and Ali, 2008). This optical complexity is due to a mix of optically reactive water constituents such as coloured dissolved organic matter, sediments and detritus particles (Le *et al.*, 2013). This makes estimation difficult as all estuaries have their own unique and dynamic optical complexity. Algorithms that were formulated for use in either marine or fresh water environments usually experience lower retrieval accuracies when used in estuaries. One such example found by this current study was salinity retrieval using the Zhao *et al.* (2017), algorithm. During the Zhao *et al.* (2017), salinity estimation, it was noted that on the same images in which estuarine salinity was poorly retrieved, marine pixels neighbouring the Umdloti Estuary had salinities that were more in line with what would normally be expected of salinities in the ocean. Ultimately, to ensure a greater reliability when using parameter estimation algorithms for estuaries, these algorithms should be refined and tested over time and different conditions (Lavery *et al.*, 1993; Abdulla, 2015; Mushtaq and Nee Lala, 2017).

Some parameters were also just not as popular in remote sensing literature. These parameters, such as pH and DO, had far fewer studies being based on their estimation. The main reasons for the literature absence could be explained by their weaker optical properties and low signal to noise ratio (Gholizadeh *et al.*, 2016). This often increased the difficulty in attempting to model these parameters (as also found by this current study). Despite this, these parameters play

essential roles in maintaining water body environmental health and this has not stopped scientists attempting to develop algorithms for their estimation.

For every single parameter besides chl-a, the  $R^2$  calculated intraseasonally for the winter and spring seasons were found to be substantially lower than those calculated for a combined dataset for both seasons. This may be caused by a number of issues. One of the main possible causes is that the majority of estimation algorithms failed to register any substantial variability in modelling across the estuary. The vast majority of algorithms were unable to transform the small differences in band reflectance into meaningful values and therefore estimated parameters did not differ across the estuary in value except in the lowest of decimal points. This gave seasonal data very small variability tightly centred around the parameter mean. In addition, values retrieved in situ displayed a greater variability, albeit still small. When  $R^2$  was calculated, the lack of variability made the assessment very susceptible to any variability and registered this as a low  $R^2$ . A combined seasonal dataset greatly expanded on the variability and allowed greater  $R^2$  values to be calculated. This phenomenon can be seen in other studies (Syariz *et al.*, 2015; Ligi *et al.*, 2017).

A possible cause for this lack of variability is the fact that the estuarine area is much smaller than most other water bodies used in physico-chemical parameter estimation studies. The Umdloti Estuary is around 1.4 km<sup>2</sup> in size with all sample sites located within this area (Forbes and Demetriades, 2008). In comparison, literature reviewed over the course of this study all made use of substantially larger waterbodies. These water bodies often ranged tens of kilometres in length and width with sampling points distributed kilometres apart throughout. Sampling points in this study sometimes differed by less than 100 m. The small size of the Umdloti Estuary would therefore likely geographically limit the amount of parameter variability that might be found across it (in accordance with Tobler's first law) (Tobler, 1970). In addition, the estuary has been closed off from the ocean over the course of the study, keeping many parameters homogenous in distribution. Therefore, even seemingly small changes in parameter values (such as small seasonal changes or random chance) may greatly affect the  $R^2$  equation as it would be very sensitive to these changes.

Another possible reason is that low  $R^2$  is not uncommon in seasonal comparisons and when using algorithms modified for different sites (Kowalczyk *et al.*, 2010; Ligi *et al.*, 2017). Differences in conditions such as the amount of CDOM, sun glint and haze all contribute to these differences (Ligi *et al.*, 2017). Ligi *et al.* (2017), tested 58 algorithms meant to retrieve



chl-a, CDOM and total suspended matter in the Baltic Sea over spring and summer. The results for their chl-a estimation as well as the other parameters were similar to the distributions and results found by this study. They concluded that while there were some algorithms that could be used seasonally, many others had low accuracy and were unsuitable for use. Algorithms specifically modified for those sites and seasons could therefore be considered the most accurate and best used. Difficulties associated with empirical estimation algorithms such as those used in this study include that they often need to be specifically tailored to local waters, seasonal conditions and remote sensors (Metsamaa *et al.*, 2006; Ligi *et al.*, 2017). This was impossible to do over Umdloti Estuary as no studies have been previously been performed to remotely retrieve physico-chemical parameters.

Two (temperature and turbidity) out of the nine parameters could be considered to have been successfully retrieved by Landsat 8 and Sentinel-2 with their best estimation algorithms achieving  $R^2$  values above 0.95 using a combined seasonal dataset. The rest of the parameters met with a mixed moderate ( $R^2$  above 0.5) and/or outright poor ( $R^2$  below 0.5) accuracy. Chl-a, TDS and EC algorithms displayed good absolute accuracy but suffered from a poor ability to relatively model their distributions. Absolute accuracy (indicated by RMSE) was generally better estimated by the remote sensors. With the exception of salinity, DO and pH, the remote sensors estimated absolute values of physico-chemical parameters satisfactorily. This accuracy improved once existing algorithms were modified. Once modified, most of the parameters achieved satisfactory average accuracies above  $R^2 = 0.58$  and strong RMSE values. The modified algorithms of chl-a, TDS and salinity improved accuracy enough to be considered reliable. EC and DO estimation algorithms proved good at determining absolute values but otherwise suffered from a poor ability to relatively model EC. Despite the stronger accuracies, algorithms modified by this current study are otherwise untested and caution should be attached to their use. SDD and pH were poorly estimated and were the only parameters which could not be successfully obtained from the Umdloti Estuary using Landsat 8 and Sentinel-2.

#### 6.2.9 Comparison of performance between Landsat 8 and Sentinel-2

One of the main questions to be answered by the study was which sensor was better suited towards retrieving water based parameters? Through the observation of both  $R^2$  and RMSE, it can be seen that Landsat 8 and Sentinel-2 estimations were mostly similar, differing by usually small amounts for the majority of algorithms. In the end it is more a matter of preference. This seems to be supported by an absence in the comparison of these two sensors in literature. Not a

single study was found that competitively compared the two sensors ability in water quality estimation. Sentinel-2 has far superior spatial and temporal resolutions (Drusch *et al.*, 2012; Roy *et al.*, 2014). The spatial resolutions of 10 m and 20 m for most bands allow areas to be imaged in greater detail. The ability of Sentinel-2 to image an area at least three times before the next Landsat 8 sensor is able to image that same area allow for the greater monitoring of change within areas. However, Landsat 8 has been around for a longer period of time, has used similar bands to previous Landsat's and has always been free and easily accessible. As a result, there have had many more studies that have made use of either Landsat 8 or previous Landsat sensor for water parameter estimation. While many of the imaging bands remain roughly the same between the two sensors, some differ in the wavelength range covered and therefore using an algorithm modified for Landsat may be prone to accuracies when used for Sentinel-2 estimation. This problem proved to not have been a major issue over the course of the study as many Sentinel-2 algorithms generated similar accuracies to those produced and used for Landsat 8. Exceptions can be found for salinity, TDS and EC estimations where large differences existed. However, these were already very inaccurately retrieved. Landsat 8 also possessed TIRS bands, which Sentinel-2 did not. This significantly limits the ability of Sentinel-2 in measuring temperature. Despite this, studies excluding temperature will find Sentinel-2 the better sensor to use once more studies have accurately adapted algorithms for use by the sensor. A better plan still would be to use both sensors in the estimation of water based parameters as both are sufficiently suited for the job. Many other sensors, such as those that are hyperspectral or possess superior spatial resolutions may be more suited for such estimations. Despite this, the high cost of acquiring images from these sensors is likely to leave both Sentinel-2 and Landsat 8 as the most accessible remote sensors for environmental management.

#### *6.2.10 Assessment of estuarine health*

Estuaries have generated much scientific interest as a result of their high productivity, provision of ecosystem services and their status as unique habitats (Meng and Liu, 2010). These areas also show extreme vulnerability and are increasingly threatened. Rapid risk identification and estuary protection is therefore of paramount importance. As a result, indicators of estuarine health have begun to form essential components in evaluating the health of estuarine systems (Carrasco *et al.*, 2007). Water quality studies make use of these indicators to assess health. These studies are defined by Usali and Ismail (2010), as the process of determining the various chemical, physical and biological characteristics of waterbodies as well as identifying potential contamination sources that degrade the quality of water.

The samples collected and analysed by this current study provided an insight into the water quality present within the estuary. This may provide clues as to the health state of the Umdloti Estuary. The Umdloti Estuary and Mdloti River have been popular areas of study and this allows direct comparisons to be made between current conditions and those experienced in the past. However, what comprises a healthy estuary is sometimes ambiguous as estuaries are highly dynamic in conditions that may be present. Forbes and Demetriades (2008), define a healthy estuary as one where. These includes that all important physical processes maintaining estuarine habitats are functioning, that biological diversity expected from such a trophic state is present and where anthropogenic activities are not resulting in the degradation or changes in habitats and loss of goods and services.

Seasonally, the physico-chemical water quality did not differ much between winter and spring in Umdloti Estuary. The only obvious but expected increase was the seasonal change in water temperature. Average water temperatures ranged from around 19 °C - 20 °C during winter and 24 °C - 25 °C in spring. This is roughly an average increase of 5 °C but could easily be explained by the increased intensity of solar radiation experienced during the spring season (Abdulla, 2011). The greater range of temperature in winter may also be explained by the sun rising later in the morning than it does in spring. Similar temperatures from spring/summer time were found by other studies (Forbes and Demetriades, 2008; Deale, 2010; Olaniran *et al.*, 2014). Temperature falls within the normally expected levels required for an estuary to be considered productive and are not biologically significant or impacting negatively on the estuary (Ohrel and Register, 2006; Forbes and Demetriades, 2008).

Turbidity and SDD distributions were very similar during both winter and spring seasons. Turbidity saw a slight increase in spring whilst SDD remained the same. This indicated that water clarity was very high over the course of the study. High water clarity in the form of low turbidity and larger SDD values are expected to be found in normally closed systems which end up only being subject to wind induced turbulence (Forbes and Demetriades, 2008). Other studies conducted within the Umdloti Estuary found similar low turbidity's (Forbes and Demetriades, 2008; Olaniran *et al.*, 2014). Olaniran *et al.* (2014), did once find higher turbidity values over the seasons of spring and summer which they attributed to the increased rainfall and runoff that would be experienced during those seasons. There were no significant precipitation around this current study's sampling dates. Umdloti did experience some rainfall weeks before the spring sampling day (November 10<sup>th</sup>) but this was relatively insignificant and likely did not

impact on clarity. The turbidity and SDD readings suggests the estuary is composed of clear water where light is able to penetrate through to the bottom reaches. This would allow greater levels of photosynthesis to occur throughout the water column, increasing productivity and indicating no health problems (Forbes and Demetriades, 2008).

Salinity, TDS and EC all remained relatively the same between seasons. These levels were generally low, staying around 0.93, 940 mg/l and 1.80  $\mu\text{S}/\text{cm}$  for each parameter respectively. The water within estuaries is usually characteristically brackish as water from the sea and rivers interact and mix. However, the mouth of the Umdloti Estuary has been well known to undergo prolonged phases of staying closed, limiting saltwater intrusion (Forbes and Demetriades, 2008). During the study, the state of the estuarine mouth has been closed for some time and experienced limited saline influences. Salinities, TDS and EC concentrations recorded are so low that water across the estuary can be considered approaching or slightly brackish (Ohrel and Register, 2006). This is especially true for TDS and EC whose values are well below the brackish threshold (1500 and 1000 respectively). These low values for all three parameters are commonly reported in studies focusing on the Umdloti Estuary (Forbes and Demetriades, 2008; Govender, 2009; Olaniran *et al.*, 2014). Forbes and Demetriades (2008), suggest that this could be a limiting factor to possible marine fish and benthic fauna as they would be unable to survive within the estuary.

Just as with temperature, chl-a saw a mean increase during the spring season (0.61  $\mu\text{g}/\text{l}$  in winter vs. 0.9646  $\mu\text{g}/\text{l}$  in spring). However, these increases were usually quite small and each sample site differed by usually less than a single unit. Generally, chl-a concentrations were quite low within the estuary. This is in contrast to what has been found in some of the previous studies conducted within Umdloti Estuary where chl-a values were found to be much higher (Perissinotto *et al.*, 2004; Forbes and Demetriades, 2008). Perissinotto *et al.* (2004), previously estimated that chl-a levels should average at around 19  $\mu\text{g}/\text{l}$  across the estuary. Forbes and Demetriades (2008), found concentrations averaging around 70 to 75  $\mu\text{g}/\text{l}$  in their 2008 study. However, both these studies occurred within the Umdloti Estuary during a period of high nutrient loadings caused by anthropogenic activities such as the introduction of wastewater effluent (Forbes and Demetriades, 2008). The high values of chl-a found in these studies could therefore be attributed to algal blooms that would have followed. The low chl-a values obtained during the study could indicate a reduction of nutrients from these anthropogenic sources into the estuary. In general, subtropical estuaries such as Umdloti characteristically support large amounts of phytoplankton (Perissinotto *et al.*, 2002; Forbes and Demetriades, 2008). However,

these may not always be present within the water column. Perissinotto *et al.* (2002), found similar low chl-values to this study within Mpenjati during its closed phase. They hypothesised that during the stagnant and calm conditions experienced during a closed phase, the majority of the phytoplankton simply sunk down in estuarine bed, vastly depopulating the water column (Perissinotto *et al.*, 2002). This was supported by samples taken from the estuarine bed, which showed some of the highest recorded chl-a values in literature. Nozais *et al.* (2001), in their own study within Umdloti Estuary likewise found extremely high levels of chl-a within sediments (also of the highest reported in literature) whilst in the water column chl-a levels were very low (similar to those found in this study). Adams *et al.* (1999), also reported this phenomenon as common in Great Brak Estuary and obtained values similar to this study. Gama *et al.* (2005), suggests that phytoplankton numbers are ultimately linked to both the rate of flow and sedimentation. Low turbidity found in Umdloti may suggest low sedimentation inputs. Chl-a concentrations within the water body itself was also very low. Chl-a serves as an important indicator of the trophic state of a water body due to its strong linkages with nutrient concentration and algal production (Gholizadeh *et al.*, 2016). Although the low concentrations should negatively impact on the trophic state of the estuary, this reading is ambiguous as subtropical estuaries often display this phenomenon but have some of the highest levels of chl-a within their sediments. However, Umdloti Estuary has been known to go through devastating eutrophic events caused by the introduction of nutrients and subsequent growth in algae. Carnie (2014), reported that a eutrophic event caused by the introduction of agricultural products into the water led to over a thousand fish deaths in 2014 within the estuary. Chl-a values for Umdloti could therefore be considered normal but should be monitored.

DO levels within the estuary were slightly higher in the spring months than they were during winter (2.63 ppm in winter vs. 3.48 ppm in spring). However, just as was the case with chl-a, this increase was not a large one and may just be due to chance. UNESCO/WHO (1978), determined that in order to be healthy and fulfil its function estuaries need at least 4 ppm, with 5 ppm being ideal. The estimations of DO from the estuary fall short of that which may lead to problems being experienced. A study done by Forbes and Demetriades (2008), found low DO contents within the Umdloti Estuary over summer 2008. However, during winter 2007, the same study recorded DO concentrations well above 6 ppm. Forbes and Demetriades (2008), reasoned that the large increases and then crashes in DO were due to the algal blooms that occurred during that year. This was not likely occurring during this study due to the low amounts of chl-a recorded. No other studies that measured DO within the Umdloti Estuary were found. An alternative explanation is that the low number of phytoplankton and chl-a would likely lead to

low outputs of oxygen and is a possible reason for the lower values found. A similar limiting factor was the low concentrations of DO found within the estuary (Forbes and Demetriades, 2008). These are below the standard set by UNESCO/WHO (1978), and could indicate the presence of hypoxic conditions. If the situation further deteriorates, it is possible these may lead to anoxia and future fish kills

pH was again very similar in distribution during both winter and spring. Although slightly higher in winter (7.615) than spring (7.326), this would not impact on the functioning of the estuary. When compared to literature, the pH are within the normally expected levels required for the Umdloti Estuary to be considered productive and are not biologically significant or impacting negatively on the estuary (Ohrel and Register, 2006; Forbes and Demetriades, 2008; Govender, 2009; Olaniran *et al.*, 2014).

Although not directly measured, there were other types of pollution affecting the estuary. Some could be directly observed, such as the presence of general plastic and paper waste (seen in Figure 6.1). There were many plastics and papers found within the estuary and it was also the site for a small dumping spot. Naidoo *et al.* (2015), determined that although not as large a problem within Umdloti Estuary as it is in other eThekwinini based estuaries, there were significant levels of plastic within the estuary. These plastics pose a particular threat to filter feeding organisms and may reduce chl-a levels within sediment as it blocks out sunlight (Naidoo *et al.*, 2015). It was also observed by this current study that some locals used the estuary to wash clothes (with chemicals) and as an ablution facility. The lack of testing done during these studies is not able to tell whether these activities are having a significant impact on the estuary. However, Umdloti Estuary has had a disturbing eutrophication history due to contaminants and high nutrient loadings in the past (Forbes and Demetriades, 2008; Olaniran *et al.*, 2014).

The sampling of physico-chemical parameters revealed that the Umdloti Estuary is currently experiencing a poor state of health. Comparisons with other studies that attempted to determine the Umdloti Estuary health supports this theory. Forbes and Demetriades (2008), found very similar conditions to those found by this study and assessed Umdloti as being in a poor state of health. Olaniran *et al.* (2012), found that many of the physico-chemical parameters measured in the Umdloti River were not in compliance with standards set by the WHO. Since this river solely flows directly into Umdloti Estuary, it supports the idea that the Umdloti Estuary can be considered to be in a poor condition. Whitfield and Baliwe (2013), concluded that the estuary is

in a fair state but faces massive pressures. Overall, this indicates that a cause for concern for the health of the Umdloti Estuary.



Figure 6.1: Image taken during winter sampling showing large amounts of plastic pollution present.

#### *6.2.11 Limitations and Recommendations*

Possibly the biggest limitation faced by this study was the fact that only thirty samples were able to be used to both test and generate algorithms. This meant that only two days of sampling for each remote sensor was able to be conducted. These two days of sampling were used to generalise the conditions experienced by winter and spring. Therefore, the full seasonal variability of physico-chemical parameters may not have been fully captured and left the seasonal samples that were collected highly susceptible to the impacts of any undiscovered confounding factors that may have been present on these days. This was evident when looking at scatterplots of the data. Most of the data formed distinct winter and spring seasonal clusters that were often centred around values that were very different from each other. This occurred despite the fact that for the vast majority of physico-chemical parameters, the in situ variability remained small. This indicated that season had a strong impact on the estimation algorithms ability to estimate physico-chemical conditions. Studies like Abdulla (2011), in fact develop their estimation algorithms with season in mind. In future, more sampling should be conducted

to ensure that the whole range of variability is collected and avoid the clustering of data according to season.

As mentioned earlier in the discussion, another limitation was the small size of the estuary. The Umdloti Estuary was by far the smallest estuary when compared to other remote sensing studies found in all literature reviewed by this study. This limited the amount of physico-chemical variability that would be found in situ and therefore limited the range of values the estimation algorithms could be tested across. The small size of the estuary also restricted the amount of sampling that could be done. Finally, the small size of the Umdloti Estuary meant that remote sensors would be expected to suffer accuracy issues. This is due to the impacts from edge pixels and the fact that any confounding factors will have a greater impact if present within a smaller area. In future, estimation algorithms should be tested across larger estuaries and a larger amount of physico-chemical variability to refine them.

Whilst full sampling was done on July 5<sup>th</sup> and November 10<sup>th</sup>, only temperature, turbidity and SDD were sampled on July 18<sup>th</sup>. This was due to unforeseen circumstances and meant that within the thirteen days between the 5<sup>th</sup> and 18<sup>th</sup> of July, some of the physico-chemical parameters may have differed. SDD is linked to turbidity and since turbidity remained the same on the 18<sup>th</sup>, SDD would have likewise remained the same. Salinity, TDS and EC are also almost guaranteed to have remained the same as the estuary had not been breached and no significant rainfalls occurred in the nearly two week timeframe. pH is also likely to have remained unchanged or at least very similar. This is supported by sampling that occurred in spring, where pH values recorded were very similar. Only chl-a and DO may have possibly changed over that period. However, no significant events that may affect these numbers (such as large rainfalls, breaching of the estuarine mouth or algal blooms) were observed. In future, full sampling would be recommended to better prepare the models for physico-chemical estimation.

Although the use of remote sensing methods provides many advantages in the monitoring of estuarine systems and the assessment of water quality parameters, it is not without its own limitations. Some parameters over the course of this study were not at all reliably retrieved, SDD and pH being the most obvious. Many important physico-chemical components such as pH, various nitrogen based compounds and dissolved phosphorus are not usually measured in remote sensing water studies as they have weak optical properties (Gholizadeh *et al.*, 2016). Estuarine waters themselves are quite complex and impact on the sensors ability to retrieve parameters. For some physico-chemical parameters the accuracy that is obtained will therefore



always be of questionable quality (Gholizadeh *et al.*, 2016). Water complexity may also affect optically reactive parameters. Kutser (2009), found that remote sensing was rendered useless in the measuring of the densest areas of phytoplankton blooms in the Baltic Sea due to atmospheric and processing errors. A cause of this may be the limitation in the amounts of bands and bandwidths found within Landsat 8 and Sentinel-2 (Kutser, 2009). The use of sensors with higher spectral resolutions (such as hyperspectral sensors) may provide the accuracy needed for these parameters estimation. However, the cost to acquire the images may in fact be as expensive as collecting the data in the field and present some of the greatest obstacles to determining the health of the system (Gholizadeh *et al.*, 2016). Remote sensing is also usually only able to measure the conditions present on the very top of the water and is not able to determine what conditions are like with depth (Gholizadeh *et al.*, 2016). These factors should be considered for future sampling.

As with all remote sensing studies, the atmospheric conditions heavily influence the quality of the results that were achieved. Conditions such as cloud cover and haze will always limit the ability of sensors to receive accurate, instant results if they are present. However, remote sensing software such as the ACOLITE program developed by the royal Belgium institute of technology are increasing in ability in accounting for the effects of atmosphere. Remote sensing reflectance refers to the actual reflectance of light when interacting with the water after eliminating atmospheric effects. Its calculation is therefore an important step in achieving accurate results, but this is both complex and tedious. The ACOLITE program is able to instantly and easily calculate this parameter (amongst others) for both the Sentinel-2 and Landsat 8 remote sensors. This leads to significantly more accurate results, as seen with many of the algorithms modified from this study. A recommendation is that software programmes such as these are improved upon and used in more studies to evaluate their usefulness.

There has been a general push towards estimation algorithms that make use of band ratioing (El Magd and Ali, 2008). This is due to several advantages that ratioing offers such as the reduced influence of atmospheric illumination (Han and Jordan 2005; Jensen 2005; El Magd and Ali, 2008). Gin *et al.* (2002), for example proposed the use of a ratio of bands for the estimation of chl-a which worked very well in this current study. Over the course of this study five out of the nine most successful algorithms for each parameter made use of this ratioing. Future studies may concentrate more on the use of band ratioing in the development of future estimation algorithms.

Finally, there is considerable evidence both from this study and past studies that the Umdloti Estuary is in a poor state of health (Forbes and Demetriades, 2008; Olaniran *et al.*, 2014). The estuary should continue to be monitored and legislations and actions taken to reduce the impacts of these entities on the health of the Umdloti Estuary. The estuary is known to be susceptible to eutrophication due to chemical loads. The construction of the Hazelmere Dam and a WWTW upstream have contributed significantly toward this poor health and resulted in a highly modified estuary (Forbes and Demetriades, 2008). The correction of these issues should therefore be a priority.

### **6.3) Conclusion**

Sentinel-2 and Landsat 8 showed good promise in the estimation of physico-chemical parameters but are unlikely to ever successfully estimate every physico-chemical parameter. Despite this, these sensors will have a continued important role to play in the assessment and management of estuarine health. Their accessibility, cost, advanced specifications and program continuity will undoubtedly see to these sensors continued popularity. This study provided strong evidence for their success. The estimation algorithms for parameters such as SDD and pH require greater development, refinement and testing if they are to be useful in an estuarine environment. As it stands, turbidity and temperature may be relatively easily and accurately retrieved from the Umdloti Estuary. Salinity, TDS, EC and chl-a were at times poorly modelled but their respective RMSE indicated that their absolute values could still be accurately retrieved. In future the algorithms tested and modified by this study will aid in the estimation of parameters not only from the Umdloti Estuary but in similar estuaries as well. The continued use of water quality estimation algorithms in retrieving these parameters will lead to decreased costs, time spent in the field and allows for estimation in difficult to reach areas. This may lead to the more efficient monitoring of estuarine systems. The state of the Umdloti Estuary as found by this study can be considered to be poor. Low levels of salinity, chl-a and DO suggest a low productivity environment that would limit intrusion by marine organisms (even if the mouth opened) and is at risk of hypoxia. However, values of turbidity and SDD retrieved suggested that water clarity is not an issue within the estuary. Suggestions proposed by this study include the continued use and refinement of algorithms (especially within estuarine environments) to achieve greater accuracy and greater efforts put in to limit the impacts of human pollution within the estuary. In conclusion, this study strongly shows off the ability of both these popular sensors in forming an important component of any estuarine health assessment and pushes for these sensors to begin to play greater roles in providing geographical information.

## REFERENCES

- Abdelmalik, K.W., 2018. Role of statistical remote sensing for inland water quality parameters prediction. *The Egyptian Journal of Remote Sensing and Space Science*, 21 (2), pp.193-200.
- Abdullah, H.S., 2015. Water quality assessment for Dokan Lake using Landsat 8 OLI satellite images (Masters Thesis, University of Sulaimani).
- Able, K.W., Neuman, M.J. and Wennhage, H., 2005. Ecology of juvenile and adult stages of flatfishes: distribution and dynamics of habitat associations. In: Flatfishes: biology and exploitation. Blackwell Science Ltd, Hoboken, New Jersey, pp.164-184.
- Abowei, J.F.N., 2010. Salinity, dissolved oxygen, pH and surface water temperature conditions in Nkoro River, Niger Delta, Nigeria. *Advance Journal of Food Science and Technology*, 2(1), pp.36-40.
- Adams, J.B., Bate, G.C. and O'Callaghan, M., 1999. Primary producers. In: Allanson, B. R., Baird, D. (Eds.), *Estuaries of South Africa*, Cambridge University Press, Cambridge, England.
- Al-Fahdawi, A.A., Rabee, A.M. and Al-Hirmizy, S.M., 2015. Water quality monitoring of Al-Habbaniyah Lake using remote sensing and in situ measurements. *Environmental monitoring and assessment*, 187(6), pp.1-11.
- Allan, M.G., Hicks, B.J. and Brabyn, L., 2007. *Remote sensing of water quality in the Rotorua lakes*. CBER Contract Report No. 51. The University of Waikato, Hamilton.
- Alongi, D.M., 1998. Coastal ecosystem processes. CRC Press, Boca Raton, US, p.419.
- Alparslan, E., Aydoğan, C., Tufekci, V. and Tüfekci, H., 2007. Water quality assessment at Ömerli Dam using remote sensing techniques. *Environmental monitoring and assessment*, 135(1), pp.391-398.
- Angela, D. and Nikos, T., 2010. Physico-chemical characterization of the shallow mixing zone of two estuaries, Lesvos Island, NE Aegean, Greece. *Transitional Waters Bulletin*, 2(4), pp.17-25.

Arar, E.J. and G.B. Collins. 1997. *In vitro determination of chlorophyll a and pheophytin a in marine and freshwater algae by fluorescence*. Method 445.0. National Exposure Research Laboratory, USEPA, Cincinnati, US.

Arkema, K.K., Guannel, G., Verutes, G., Wood, S.A., Guerry, A., Ruckelshaus, M., Kareiva, P., Lacayo, M. and Silver, J.M., 2013. Coastal habitats shield people and property from sea-level rise and storms. *Nature Climate Change*, 3(10), pp.913-918.

Artis, D.A. and Carnahan, W.H., 1982. Survey of emissivity variability in thermography of urban areas. *Remote Sensing of Environment*, 12(4), pp.313-329.

Baban, S.M., 1993. Detecting water quality parameters in the Norfolk Broads, UK, using Landsat imagery. *International Journal of Remote Sensing*, 14(7), pp.1247-1267.

Bai, Y., Pan, D., Cai, W.J., He, X., Wang, D., Tao, B. and Zhu, Q., 2013. Remote sensing of salinity from satellite-derived CDOM in the Changjiang River dominated East China Sea. *Journal of Geophysical Research: Oceans*, 118(1), pp.227-243.

Baran, E., and Hambrey, J., 1999. Mangrove conservation and coastal management in southeast Asia: What impacts on fishery resources?. *Marine Pollution Bulletin*, 37, pp.431-440.

Barbier, E.B., 2014. Valuing the storm protection service of estuarine and coastal ecosystems. *Ecosystem Services*, 11, pp.32-38.

Barbier, E.B., Hacker, S.D., Kennedy, C., Koch, E.W., Stier, A.C. and Silliman, B.R., 2011. The value of estuarine and coastal ecosystem services. *Ecological monographs*, 81(2), pp.169-193.

Barbier, E.B., Koch, E.W., Silliman, B.R., Hacker, S.D., Wolanski, E., Primavera, J., Granek, E.F., Polasky, S., Aswani, S., Cramer, L.A. and Stoms, D.M., 2008. Coastal ecosystem-based management with nonlinear ecological functions and values. *Science*, 319(5861), pp.321-323.

Beck, M.W., Heck Jr, K.L., Able, K.W., Childers, D.L., Eggleston, D.B., Gillanders, B.M., Halpern, B., Hays, C.G., Hoshino, K., Minello, T.J. and Orth, R.J., 2001. The identification, conservation, and management of estuarine and marine nurseries for fish and invertebrates: a better understanding of the habitats that serve as nurseries for marine species and the factors that create site-specific variability in nursery quality will improve conservation and management of these areas. *Bioscience*, 51(8), pp.633-641.

Becker, F. and Li, Z.L., 1990. Towards a local split window method over land surfaces. *Remote Sensing*, 11(3), pp.369-393.

Begg, G., 1978. *The Estuaries of Natal*. Natal Town and Regional Planning Report 41, pp. 214-215.

Beitinger, T.L. and Fitzpatrick, L.C., 1979. Physiological and ecological correlates of preferred temperature in fish. *American Zoologist*, 19(1), pp.319-329.

Bergin, C. 2017. Sentinel-2B rides Vega to join Copernicus fleet.  
<https://www.nasaspaceflight.com/2017/03/sentinel-2b-vega-ride-join-copernicus-fleet/>  
 (accessed: 13/03/2017).

Bernstein, L.S., Adler-Golden, S.M., Sundberg, R.L., Levine, R.Y., Perkins, T.C., Berk, A., Ratkowski, A.J., Felde, G. and Hoke, M.L., 2005, July. A new method for atmospheric correction and aerosol optical property estimation for VIS-SWIR multi-and hyperspectral imaging sensors: QUAC (QUick atmospheric correction). In: *2005 IEEE International Geoscience and Remote Sensing Symposium (IGARSS)*, Seoul, South Korea, pp.3549-3552.

Bianchi, T.S., 2007. Biogeochemistry of Estuaries. Oxford University Press, Oxford.

Bisson, M.A. and Kirst, G.O., 1995. Osmotic acclimation and turgor pressure regulation in algae. *Naturwissenschaften*, 82(10), pp.461-471.

Bonansea, M., Rodriguez, M.C., Pinotti, L. and Ferrero, S., 2015. Using multi-temporal Landsat imagery and linear mixed models for assessing water quality parameters in Río Tercero reservoir (Argentina). *Remote Sensing of Environment*, 158, pp.28-41.

Brando, V.E., Braga, F., Zaggia, L., Giardino, C., Bresciani, M., Matta, E., Bellafigliore, D., Ferrarin, C., Maicu, F., Benetazzo, A. and Bonaldo, D., 2015. High-resolution satellite turbidity and sea surface temperature observations of river plume interactions during a significant flood event. *Ocean Science*, 11(6), pp.909-920.

Breaux, A., Farber, S. and Day, J., 1995. Using natural coastal wetlands systems for wastewater treatment: an economic benefit analysis. *Journal of environmental management*, 44(3), pp.285-291.

Breen, C.M. and McKenzie, M., 2001. *Managing estuaries in South Africa: an introduction*. Institute of Natural Resources, Pietermaritzburg, South Africa, pp.66.

Bricker, S.B., Clement, S.G., Pirhall, D.E., Orlando, S.P. and Farrow, D.R.G. 1999. *National estuarine eutrophication assessment: A summary of conditions, historical trends, and future outlook*. National Oceanic and Atmospheric Administration, Silver Spring, Maryland.

Bricker, S.B., Longstaff, B., Dennison, W., Jones, A., Boicourt, K., Wicks, C. and Woerner, J., 2008. Effects of nutrient enrichment in the nation's estuaries: a decade of change. *Harmful Algae*, 8(1), pp.21-32.

Butchart, S., Dieme-Amting, E., Gitay, H., Raaymakers, S. and Taylor, D., 2005. *Ecosystems and human well-being: Wetland and water synthesis*. World Resources Institute, Washington, DC.

Cândido, A.K.A.A., Paranhos Filho, A.C., Haupenthal, M.R., da Silva, N.M., de Sousa Correa, J. and Ribeiro, M.L., 2016. Water quality and chlorophyll measurement through vegetation indices generated from orbital and suborbital images. *Water, Air, & Soil Pollution*, 227(7), p.224.

Cabral, H.N., Vasconcelos, R., Vinagre, C., França, S., Fonseca, V., Maia, A., Reis-Santos, P., Lopes, M., Ruano, M., Campos, J. and Freitas, V., 2007. Relative importance of estuarine flatfish nurseries along the Portuguese coast. *Journal of Sea Research*, 57(2), pp.209-217.

Campbell, C.R., 2010. Blue carbon–British Columbia: The case for the conservation and enhancement of estuarine processes and sediments in BC. Sierra Club of BC, Victoria, BC.

Carnie, T. 2014. Wave of fish deaths in eThekweni. <https://www.iol.co.za/news/wave-of-fish-deaths-in-ethekweni-1719250> (accessed: 6/11/2017).

Carrasco, N.K., Perissinotto, R. and Miranda, N.A., 2007. Effects of silt loading on the feeding and mortality of the mysid *Mesopodopsis africana* in the St. Lucia Estuary, South Africa. *Journal of Experimental Marine Biology and Ecology*, 352(1), pp.152-164.

Cilliers, G.J. and Adams, J.B., 2016. Development and implementation of a monitoring programme for South African estuaries. *Water SA*, 42(2), pp.279-290.

Clark, J.R., 1997. Coastal zone management handbook. *Oceanographic Literature Review*, 5(44), pp.527.

Clarkson, B.R., Ausseil, A.G.E. and Gerbeaux, P., 2013. Wetland ecosystem services. Ecosystem services in New Zealand: conditions and trends. Manaaki Whenua Press, Lincoln, pp.192-202.

Clean Water Team (CWT). 2004. *Electrical conductivity/salinity Fact Sheet, FS-3.1.3.0 (EC)*. In: The Clean Water Team Guidance Compendium for Watershed Monitoring and Assessment, Version 2.0. California State Water Resources Control Board (SWRCB), Sacramento, CA.

Cooper, J.A.G., 1993. Sedimentation in a river dominated estuary. *Sedimentology*, 40(5), pp.979-1017.

Cooper, J. A. G., 2001. Geomorphological variability among microtidal estuaries from the wave-dominated South African coast. *Geomorphology*, 40, pp.99-122.

Cooper, J. A. G., Jayiya, T., Van Niekerk, L., De Wit, M., Leaner, J. and Moshe, D., 2003. *An assessment of the economic values of different uses of estuaries in South Africa*. CSIR, Stellenbosch, South Africa.

Costanza, R., d'Arge, R., De Groot, R., Farber, S., Grasso, M., Hannon, B., Limburg, K., Naeem, S., O'Neill, R.V., Paruelo, J. and Raskin, R.G., 1998. The value of the world's ecosystem services and natural capital. *Ecological economics*, 25(1), pp.3-16.

Cox J., R.M., Forsythe, R.D., Vaughan, G.E. and Olmsted, L.L., 1998. Assessing water quality in Catawba River reservoirs using Landsat thematic mapper satellite data. *Lake and Reservoir Management*, 14(4), pp.405-416.

Crooks, S., Herr, D., Tamelander, J., Laffoley, D. and Vandever, J., 2011. *Mitigating climate change through restoration and management of coastal wetlands and near-shore marine ecosystems: challenges and opportunities*. Environment Department Paper 121, World Bank, Washington, DC.

Crossland, C.J., Baird, D., Ducrotoy, J.P., Lindeboom, H., Buddemeier, R.W., Dennison, W.C., Maxwell, B.A., Smith, S.V. and Swaney, D.P., 2005. The coastal zone-a domain of global interactions. In: *Coastal Fluxes in the Anthropocene*, Springer, Berlin, Germany, pp.1-37.

Day, J.H., 1980. What is an estuary. *South African Journal of Science*, 76(5), pp.198-198.

de Sousa, R.C., Pereira, L.C., da Costa, R.M. and Jiménez, J.A., 2014. Tourism carrying capacity on estuarine beaches in the Brazilian Amazon region. *Journal of Coastal Research*, 70, pp.545-550.

Deale, M., 2010. Recovery Dynamics of Zooplankton Following a Mouth-breaching Event in the Temporarily-open Mdloti Estuary (Masters thesis, University of KwaZulu-Natal).

Dekker, A.G. and Peters, S.W.M., 1993. The use of the Thematic Mapper for the analysis of eutrophic lakes: a case study in the Netherlands. *International Journal of Remote Sensing*, 14(5), pp.799-821.

Deutsch, E., Alameddine, I. and El-Fadel, M., 2014. Developing Landsat Based Algorithms to Augment in Situ Monitoring of Freshwater Lakes and Reservoirs. *11th International Conference on Hydroinformatics*, New York City, USA.

Dewidar, K. and Khedr, A., 2001. Water quality assessment with simultaneous Landsat-5 TM at Manzala Lagoon, Egypt. *Hydrobiologia*, 457(1), pp.49-58.



Dogliotti, A.I., Ruddick, K.G., Nechad, B., Doxaran, D. and Knaeps, E., 2015. A single algorithm to retrieve turbidity from remotely-sensed data in all coastal and estuarine waters. *Remote Sensing of Environment*, 156, pp.157-168.

Donnelley, J.P. and Bertness, M.D., 2001. Rapid shoreward encroachment of salt marsh cordgrass in response to accelerated sea-level rise. *Proceedings of the National Academy of Sciences*, 98(25), pp.14218-14223.

Driver, A., Sink, K.J., Nel, J.N., Holness, S., Van Niekerk, L., Daniels, F., Jonas, Z., Majiedt, P.A., Harris, L. and Maze, K., 2012. *National Biodiversity Assessment 2011: An assessment of South Africa's biodiversity and ecosystems*. Synthesis Report. South African National Biodiversity Institute and Department of Environmental Affairs, Pretoria, South Africa.

Drusch, M., Del Bello, U., Carlier, S., Colin, O., Fernandez, V., Gascon, F., Hoersch, B., Isola, C., Laberinti, P., Martimort, P. and Meygret, A., 2012. Sentinel-2: ESA's optical high-resolution mission for GMES operational services. *Remote sensing of Environment*, 120, pp.25-36.

Dumbauld, B.R., Hosack, G.R. and Bosley, K.M., 2015. Association of juvenile salmon and estuarine fish with intertidal seagrass and oyster aquaculture habitats in a northeast Pacific estuary. *Transactions of the American Fisheries Society*, 144(6), pp.1091-1110.

Elliott, M., Mander, L., Mazik, K., Simenstad, C., Valesini, F., Whitfield, A. and Wolanski, E., 2016. Ecoengineering with ecohydrology: successes and failures in estuarine restoration. *Estuarine, Coastal and Shelf Science*, 176, pp.12-35.

Feely, R.A., Alin, S.R., Newton, J., Sabine, C.L., Warner, M., Devol, A., Krembs, C. and Maloy, C., 2010. The combined effects of ocean acidification, mixing, and respiration on pH and carbonate saturation in an urbanized estuary. *Estuarine, Coastal and Shelf Science*, 88(4), pp.442-449.

Fundamentals of environmental measures (FEM). 2016. Water quality. <http://www.fondriest.com/environmental-measurements/parameters/water-quality> (accessed: 1/11/2017).

Feng, L., Hu, C., Chen, X. and Song, Q., 2014. Influence of the Three Gorges Dam on total suspended matters in the Yangtze Estuary and its adjacent coastal waters: Observations from MODIS. *Remote Sensing of Environment*, 140, pp.779-788.

Forbes, A.T. and Demetriades, N.T., 2008. *Estuaries of Durban, KwaZulu-Natal, South Africa*. Report for the Environmental Management Department, eThekweni Municipality, Durban, South Africa.

Fichot, C.G., Downing, B.D., Bergamaschi, B.A., Windham-Myers, L., Marvin-DiPasquale, M., Thompson, D.R. and Gierach, M.M., 2015. High-resolution remote sensing of water quality in the San Francisco Bay–Delta estuary. *Environmental science & technology*, 50(2), pp.573-583.

Filla, G.D.F. and Monteiro-Filho, E.L.D.A., 2009. Monitoring tourism schooners observing estuarine dolphins (*Sotalia guianensis*) in the Estuarine Complex of Cananéia, south-east Brazil. *Aquatic Conservation: Marine and Freshwater Ecosystems*, 19(7), pp.772-778.

Fisher, B. and Turner, R.K., 2008. Ecosystem services: classification for valuation. *Biological conservation*, 141(5), pp.1167-1169.

Flameling, I.A. and Kromkamp, J., 1994. Responses of respiration and photosynthesis of *Scenedesmus protuberans* Fritsch to gradual and steep salinity increases. *Journal of Plankton Research*, 16(12), pp.1781-1791.

Forrer, D.C., 2012. Applications of Landsat-5 TM imagery in assessing and mapping water quality in Bankhead Reservoir of the Black Warrior River (Doctoral dissertation, University of Alabama).

Gama, P.T., Adams, J.B., Schael, D.M. and Skinner, T., 2005. Phytoplankton chlorophyll a concentration and community structure of two temporarily open/closed estuaries. *Water Research Commission Report*, 1255(1), p. 5

Garaba, S.P. and Zielinski, O., 2015. An assessment of water quality monitoring tools in an estuarine system. *Remote Sensing Applications: Society and Environment*, 2, pp.1-10.

Garrod, B. and Wilson, J.C., 2004. Nature on the edge? Marine ecotourism in peripheral coastal areas. *Journal of sustainable tourism*, 12(2), pp.95-120.

Gedan, K.B., Kirwan, M.L., Wolanski, E., Barbier, E.B. and Silliman, B.R., 2011. The present and future role of coastal wetland vegetation in protecting shorelines: answering recent challenges to the paradigm. *Climatic Change*, 106(1), pp.7-29.

Geiger, E.F., Grossi, M.D., Trembanis, A.C., Kohut, J.T. and Oliver, M.J., 2013. Satellite-derived coastal ocean and estuarine salinity in the Mid-Atlantic. *Continental Shelf Research*, 63, pp.S235-S242.

Glibert, P.M. and Terlizzi, D.E., 1999. Cooccurrence of elevated urea levels and dinoflagellate blooms in temperate estuarine aquaculture ponds. *Applied and Environmental Microbiology*, 65(12), pp.5594-5596.

Gholizadeh, M.H., Melesse, A.M. and Reddi, L., 2016. A Comprehensive Review on Water Quality Parameters Estimation Using Remote Sensing Techniques. *Sensors*, 16(8), p.1298.

Giardino, C., Pepe, M., Brivio, P.A., Ghezzi, P. and Zilioli, E., 2001. Detecting chlorophyll, Secchi disk depth and surface temperature in a sub-alpine lake using Landsat imagery. *Science of the Total Environment*, 268(1), pp.19-29.

Gin, K.Y.H., Koh, S.T., Lin, I.I. and Chan, E.S., 2002. Application of spectral signatures and colour ratios to estimate chlorophyll in Singapore's coastal waters. *Estuarine, Coastal and Shelf Science*, 55(5), pp.719-728.

Good, J.W., Weber, J.W., Charland, J.W., Olson, J. V. and Chapin, K. V. 1998. *National Coastal Zone Management Effectiveness Study: Protecting Estuaries and Coastal Wetlands*. Final Report to the NOAA Office of Ocean and Coastal Resources Management. Oregon Sea Grant Special Report PI-98-001. National Oceanic and Atmospheric Administration, Corvallis, OR.

Govender, S., 2009. An investigation of the natural and human induced impacts on the Umdloti catchment. (Master's Thesis, University of KwaZulu-Natal).

Gruska, P., 1999. The River Odra Estuary as a Gateway for Alien Species Immigration to the Baltic Sea Basin. *Acta Hydrochim hydrobiol*, 27(5), pp.374-382.

Hadjimitsis, D.G. and Clayton, C., 2009. Assessment of temporal variations of water quality in inland water bodies using atmospheric corrected satellite remotely sensed image data. *Environmental monitoring and assessment*, 159(1), pp.281-292.

Han, L. and Jordan, K.J., 2005. Estimating and mapping chlorophyll-a concentration in Pensacola Bay, Florida using Landsat ETM+ data. *International Journal of Remote Sensing*, 26(23), pp.5245-5254.

Hancock, M.J., 2015. Predicting Water Quality by Relating Secchi Disk Transparency Depths to Landsat 8 (Masters Thesis, Indiana University).

Hanekom, D., 1992. Growth, production and consumption of the thalassinid prawn *Upogebia africana* (Ortmann) in the Swartkops estuary. *African Zoology*, 27(3), pp.130-139.

Harding, L.W., Magnuson, A. and Mallonee, M.E., 2005. SeaWiFS estimations of chlorophyll in Chesapeake Bay and the mid-Atlantic bight. *Estuarine, Coastal and Shelf Science*, 62(1), pp.75-94.

Harris, P., Muelbert, J., Muniz, P., Yin, K., Ahmed, K., Folorunsho, R., Caso, M., Vale, C.C., Machiwa, J., Ferreira, B. and Bernal, P., 2016. Estuaries and Deltas. [https://www.researchgate.net/profile/Peter\\_Harris14/publication/291958524\\_Chapter\\_44\\_Estuaries\\_and\\_Deltas/links/56a79e9f08aeded22e36ef52/Chapter-44-Estuaries-and-Deltas.pdf](https://www.researchgate.net/profile/Peter_Harris14/publication/291958524_Chapter_44_Estuaries_and_Deltas/links/56a79e9f08aeded22e36ef52/Chapter-44-Estuaries-and-Deltas.pdf) (accessed: 30/01/2018).

He, W., Chen, S., Liu, X. and Chen, J., 2008. Water quality monitoring in a slightly-polluted inland water body through remote sensing—case study of the Guanting Reservoir in Beijing, China. *Frontiers of Environmental Science & Engineering in China*, 2(2), pp.163-171.

Hellweger, F.L., Schlosser, P., Lall, U., Weissel, J.K., 2004. Use of satellite imagery for water quality studies in New York Harbor. *Estuarine, Coastal and Shelf Science*, 61, pp.437-448.

Heydorn A.E.F. and Bickerton I. B., 1982. *Report no. 9. Uilkraals (CSW 17)*. In: Estuaries of the Cape. Part 2. Synopsis of available information on individual systems, Heydorn A.E.F. and Grindley, J.R. (Eds.). CSIR Research Reports. CSIR, Stellenbosch.

Inskip, P.D., 1982. *Habitat suitability index models: northern pike*. United States Department of the Interior, Fish and Wildlife Service, FWS/OBS-82/10.17, 40. Fort Collins, CO.

IWRMPJVN, 2010. *Integrated Water Resources Management Plan for Namibia*. Ministry of Agriculture, Water and Forest, Windhoek, Namibia.

Jaelani, L.M., Limehuwey, R., Kurniadin, N., Pamungkas, A., Koenhardono, E.S. and Sulisetyono, A., 2016. Estimation of Total Suspended Sediment and Chlorophyll-A Concentration from Landsat 8-Oli: The Effect of Atmosphere and Estimation Algorithm. *IPTEK The Journal for Technology and Science*, 27(1), pp.16-23.

Jensen, J.R., 2005. *Introductory Digital Image Processing, A Remote Sensing Perspective*. Prentice Hall, Upper Saddle River, New Jersey.

Jordan, S.J. and Peterson, M.S., 2012. *Contributions of estuarine habitats to major fisheries. Estuaries: Classification, Ecology, and Human Impacts*. Nova Science, Hauppauge, New York.

Joyce, T.M., McGuigan, K.G., Elmore-Meegan, M. and Conroy, R.M., 1996. Inactivation of fecal bacteria in drinking water by solar heating. *Applied and Environmental Microbiology*, 62(2), pp.399-402.

Kang, K.M., Kim, S.H., Kim, D.J., Cho, Y.K. and Lee, S.H., 2014, July. Comparison of coastal sea surface temperature derived from ship-, air-, and space-borne thermal infrared systems. In: *2014 IEEE International Geoscience and Remote Sensing Symposium (IGARSS)*, Quebec City, Canada, pp.4419-4422.

Kapalanga, T.S., 2015. *Assessment and development of remote sensing based algorithms for water quality monitoring in Olushandja Dam, north-central Namibia*. (Masters Thesis, University of Zimbabwe).

Kennish, M.J., 2002. Environmental threats and environmental future of estuaries. *Environmental conservation*, 29(1), pp.78-107.

- Khalil, M.T., Saad, A.E.H.A., Ahmed, M.H., El Kafrawy, S.B. and Emam, W.W., 2016. Integrated Field Study, Remote Sensing and GIS Approach for Assessing and Monitoring Some Chemical Water Quality Parameters in Bardawil Lagoon, Egypt. *International Journal of Innovative Research in Science, Engineering and Technology*, 5(8), pp.14656-14669.
- Khattab, M.F. and Merkel, B.J., 2014. Application of Landsat 5 and Landsat 7 images data for water quality mapping in Mosul Dam Lake, Northern Iraq. *Arabian Journal of Geosciences*, 7(9), pp.3557-3573.
- Kirst, G.O., 1990. Salinity tolerance of eukaryotic marine algae. *Annual review of plant biology*, 41(1), pp.21-53.
- Klemas, V., 2011. Remote sensing of wetlands: case studies comparing practical techniques. *Journal of Coastal Research*, 27(3), pp.418-427.
- Koponen, S., 2006. Remote sensing of water quality for Finnish lakes and coastal areas. (Doctoral dissertation, Helsinki University of Technology).
- Kowalczyk, P., Darecki, M., Zablocka, M. and Gorecka, I., 2010. Validation of empirical and semi-analytical remote sensing algorithms for estimating absorption by Coloured Dissolved Organic Matter in the Baltic Sea from SeaWiFS and MODIS imagery. *Oceanologia*, 52(2), pp.171-196.
- Kurobe, T., Lehman, P.W., Haque, M.E., Sedda, T., Lesmeister, S. and Teh, S., 2018. Evaluation of water quality during successive severe drought years within Microcystis blooms using fish embryo toxicity tests for the San Francisco Estuary, California. *Science of The Total Environment*, 610, pp.1029-1037.
- Kutser, T., 2009. Passive optical remote sensing of cyanobacteria and other intense phytoplankton blooms in coastal and inland waters. *International Journal of Remote Sensing*, 30(17), pp.4401-4425.
- Lamberth, S.J. and Turpie, J.K., 2003. The role of estuaries in South African fisheries: economic importance and management implications. *African Journal of Marine Science*, 25(1), pp.131-157.

- Lavery, P., Pattiaratchi, C., Wyllie, A. and Hick, P., 1993. Water quality monitoring in estuarine waters using the Landsat Thematic Mapper. *Remote sensing of environment*, 46(3), pp.268-280.
- Le, C., Hu, C., Cannizzaro, J., English, D., Muller-Karger, F. and Lee, Z., 2013. Evaluation of chlorophyll-a remote sensing algorithms for an optically complex estuary. *Remote Sensing of Environment*, 129, pp.75-89.
- Li, M., Chen, Z., Finlayson, B., Wei, T., Chen, J., Wu, X., Xu, H., Webber, M., Barnett, J. and Wang, M., 2014. Water diversion and sea-level rise: potential threats to freshwater supplies in the Changjiang River estuary. *Estuarine, Coastal and Shelf Science*, 156, pp.52-60.
- Ligi, M., Kutser, T., Kallio, K., Attila, J., Koponen, S., Paavel, B., Soomets, T. and Reinart, A., 2017. Testing the performance of empirical remote sensing algorithms in the Baltic Sea waters with modelled and in situ reflectance data. *Oceanologia*, 59(1), pp.57-68.
- Lim, J. and Choi, M., 2015. Assessment of water quality based on Landsat 8 operational land imager associated with human activities in Korea. *Environmental monitoring and assessment*, 187(6), p.384.
- Lionard, M., Muylaert, K., Van Gansbeke, D. and Vyverman, W., 2005. Influence of changes in salinity and light intensity on growth of phytoplankton communities from the Schelde river and estuary (Belgium/The Netherlands). *Hydrobiologia*, 540(1), pp.105-115.
- Mann, B.Q., James, N.C. and Beckley, L.E., 2002. An assessment of the recreational fishery in the St Lucia estuarine system, KwaZulu-Natal, South Africa. *South African Journal of Marine Science*, 24(1), pp.263-279.
- Marshall, S. and Elliott, M., 1998. Environmental influences on the fish assemblage of the Humber estuary, UK. *Estuarine, Coastal and Shelf Science*, 46(2), pp.175-184.
- Matthews, W.J., 2012. Patterns in freshwater fish ecology. Springer Science & Business Media, Berlin, Germany.

McLusky, D.S. and Elliott, M., 2004. The estuarine ecosystem: ecology, threats and management. Oxford university press, Oxford, England.

Medwet. 2017. The RAMSAR convention. <http://medwet.org/aboutwetlands/ramsarconvention/> (accessed: 20/02/2017)

Meng, W. and Liu, L., 2010. On approaches of estuarine ecosystems health studies. *Estuarine, Coastal and Shelf Science*, 86(3), pp.313-316.

Metrohm. N.d. 827 pH mobile / 827 pH lab manual. <https://www.metrohm.com/en-za/products-overview/%7B5AC2AA1D-80F9-4FEC-99D8-4A0186408A43%7D> (accessed: 09/02/2018).

Metsamaa, L., Kutser, T. and Strombeck, N., 2006. Recognising cyanobacterial blooms based on their optical signature: a modelling study. *Boreal Environment Research*, 11(6), pp.493-506.

Miao-fen, H., Xu-feng, X., Xiao-Ping, Q.I., Wu-Yi, Y.U. and Yi-min, Z., 2007, July. Identification mode of chemical oxygen demand in water based on remotely sensing technique and its application. In: *2007 IEEE International Geoscience and Remote Sensing Symposium (IGARSS)*, Barcelon, Spain, pp.1738-1741.

Mitsch, W.J., and J.G. Gosselink. 2007. Wetlands. John Wiley & Sons, Inc, Hoboken, New Jersey.

Moore, J.W., Gordon, J., Carr-Harris, C., Gottesfeld, A.S., Wilson, S.M. and Russell, J.H., 2016. Assessing estuaries as stopover habitats for juvenile Pacific salmon. *Marine Ecology Progress Series*, 559, pp.201-215.

Moore, M.V., Pace, M.L., Mather, J.R., Murdoch, P.S., Howarth, R.W., Folt, C.L., Chen, C.Y., Hemond, H.F., Flebbe, P.A. and Driscoll, C.T., 1997. Potential effects of climate change on freshwater ecosystems of the New England/Mid-Atlantic Region. *Hydrological processes*, 11(8), pp.925-947.

Morgan, P.A., Burdick, D.M. and Short, F.T., 2009. The functions and values of fringing salt marshes in northern New England, USA. *Estuaries and Coasts*, 32(3), pp.483-495.



- Morris, J.T., Sundareshwar, P.V., Nietch, C.T., Kjerfve, B. and Cahoon, D.R., 2002. Responses of coastal wetlands to rising sea level. *Ecology*, 83(10), pp.2869-2877.
- Movik, S., Mehta, L. and van Koppen, B., 2016. Emergence, interpretations and translations of IWRM [Integrated Water Resources Management] in South Africa. *Water Alternatives*, 9(3), pp.456-472.
- Moyle, P.B., 1995. Fish: an enthusiast's guide. University of California Press, Berkley.
- Muller, C., 2017. Evaluating the importance of mangroves as fish nurseries in selected warm temperate South African estuaries (Masters thesis, Nelson Mandela Metropolitan University).
- Murray, T.S., Magoro, M.L., Whitfield, A.K. and Cowley, P.D., 2015. Movement behaviour of alien largemouth bass *Micropterus salmoides* in the estuarine headwater region of the Kowie River, South Africa. *African Zoology*, 50(4), pp.263-271.
- Mushtaq, F. and Nee Lala, M.G., 2017. Remote estimation of water quality parameters of Himalayan lake (Kashmir) using Landsat 8 OLI imagery. *Geocarto international*, 32(3), pp.274-285.
- Myint, S.W. and Walker, N.D., 2002. Quantification of surface suspended sediments along a river dominated coast with NOAA AVHRR and SeaWiFS measurements: Louisiana, USA. *International Journal of Remote Sensing*, 23(16), pp.3229-3249.
- Myre, E. and Shaw, R., 2006. The turbidity tube: simple and accurate measurement of turbidity in the field. Michigan Technological University, Houghton, US.
- Naidoo, T., Glassom, D. and Smit, A.J., 2015. Plastic pollution in five urban estuaries of KwaZulu-Natal, South Africa. *Marine pollution bulletin*, 101(1), pp.473-480.
- Nas, B., Ekercin, S., Karabörk, H., Berktaş, A. and Mulla, D.J., 2010. An application of Landsat-5TM image data for water quality mapping in Lake Beyşehir, Turkey. *Water, Air, & Soil Pollution*, 212(1), pp.183-197.

NASA. 2015. Sentinel-2A Launches—Our Compliments & Our Complements. <https://landsat.gsfc.nasa.gov/sentinel-2a-launches-our-compliments-our-complements/> (accessed: 14/02/2018).

Nathanson, J., A. 2003. Basic Environmental Technology: Water Supply, Waste Management, and Pollution Control. Prentice Hall, Upper Saddle River, New Jersey.

Nechad, B., Ruddick, K.G. and Park, Y., 2010. Calibration and validation of a generic multisensor algorithm for mapping of total suspended matter in turbid waters. *Remote Sensing of Environment*, 114(4), pp.854-866.

Nel, J.L., Driver, A., Strydom, W.F., Maherry, A., Petersen, C., Hill, L., Roux, D.J., Nienaber, S., Van Deventer, H., Swartz, E. and Smith-Adao, L.B., 2011. *Atlas of Freshwater Ecosystem Priority Areas in South Africa: Maps to support sustainable development of water resources*. Water Research Commission Report No. TT, 500(11), Water Research Commission, Pretoria, South Africa.

Ngetar, N.S., 2002. Post-dam Sediment Dynamics Below the Inanda Dam at the Mgeni Estuary, KwaZulu Natal (South Africa) (Masters thesis, University of Natal, Durban).

NOAA. 2008. Estuaries. [https://oceanservice.noaa.gov/education/tutorial\\_estuaries/welcome.html](https://oceanservice.noaa.gov/education/tutorial_estuaries/welcome.html) (accessed: 22/02/2017).

NOAA. 2012. Monitoring estuaries. [http://oceanservice.noaa.gov/education/kits/estuaries/media/supp\\_estuar10a\\_temp.html](http://oceanservice.noaa.gov/education/kits/estuaries/media/supp_estuar10a_temp.html) (accessed: 22/02/2017).

NOAA. 2017. What is an estuary?. <https://oceanservice.noaa.gov/facts/estuary.html> (accessed: 31/09/2017).

Nowicki, B.L., 1994. The effect of temperature, oxygen, salinity, and nutrient enrichment on estuarine denitrification rates measured with a modified nitrogen gas flux technique. *Estuarine, Coastal and Shelf Science*, 38(2), pp.137-156.

Nozais, C., Perissinotto, R. and Mundree, S., 2001. Annual cycle of microalgal biomass in a South African temporarily-open estuary: nutrient versus light limitation. *Marine Ecology Progress Series*, 223, pp.39-48.

Ochiewo, J., Shaghude, Y.W., Mburu, J.W., Uku, J., Nyandwi, N., Onganda, H., Magori, C., Sanga, I., Arthurton, R.S., Okemwa, G.M. and Fulanda, B., 2002. *Assessment of socio-economic impacts of prawn trawling on the artisanal fisheries of Malindi and Ungwana Bay*. In: Current status of trawl fishery of Malindi-Ungwana Bay-Final report. Kenya Marine and Fisheries Research Institute, Mombasa, Kenya.

Ohrel, R.L. and Register, K.M., 2006. *Volunteer estuary monitoring: a methods manual*. Ocean Conservancy and US EPA, Washington, DC.

Okey, T.A., Alidina, H.M., Lo, V., Montenegro, A. and Jessen, S., 2012. *Climate change impacts and vulnerabilities in Canada's Pacific marine ecosystems*. CPAWS BC and WWF-Canada, Vancouver, BC.

Olaniran, A.O., Naicker, K. and Pillay, B., 2014. Assessment of physico-chemical qualities and heavy metal concentrations of Umgeni and Umdloti Rivers in Durban, South Africa. *Environmental monitoring and assessment*, 186(4), pp.2629-2639.

Paavola, M., Olenin, S. and Leppäkoski, E., 2005. Are invasive species most successful in habitats of low native species richness across European brackish water seas?. *Estuarine, Coastal and Shelf Science*, 64(4), pp.738-750.

Pather, K., 2014. Spatio-temporal Variations of the Sedimentology and Geochemistry of Six Estuaries Within the EThekweni Municipality, KwaZulu-Natal, South Africa (Masters Thesis, University of KwaZulu-Natal).

Perissinotto, R., Blair, A., Connell, A., Demetriades, N.T., Forbes, A.T., Harrison, T.D., Iyer, K., Joubert, M., Kibirige, I., Mundree, S. and Simpson, H., 2004. *Contributions to information requirements for the implementation of resource directed measures for estuaries*. In: Volume 2: responses of the biological communities to flow variation and mouth state in two Kwazulu-Natal temporarily open/closed estuaries. Water Research Commission Report 1247/2, Pretoria, South Africa.

- Perissinotto, R., Nozais, C. and Kibirige, I., 2002. Spatio-temporal dynamics of phytoplankton and microphytobenthos in a South African temporarily-open estuary. *Estuarine, Coastal and Shelf Science*, 55(1), pp.47-58.
- Perivolioti, T.M., Mouratidis, A., Doxani, G. and Bobori, D., 2016, August. Monitoring the Water Quality of Lake Koronia Using Long Time-Series of Multispectral Satellite Images. *Living Planet Symposium*, 740, p.249.
- Pinto, R., Brouwer, R., Patrício, J., Abreu, P., Marta-Pedroso, C., Baeta, A., Franco, J.N., Domingos, T. and Marques, J.C., 2016. Valuing the non-market benefits of estuarine ecosystem services in a river basin context: Testing sensitivity to scope and scale. *Estuarine, Coastal and Shelf Science*, 169, pp.95-105.
- Rajeshwari, A. and Mani, N.D., 2014. Estimation of land surface temperature of Dindigul district using Landsat 8 data. *International Journal of Research in Engineering and Technology*, 3(5), pp.122-126.
- Riou, P., Le Pape, O. and Rogers, S.I., 2001. Relative contributions of different sole and plaice nurseries to the adult population in the Eastern Channel: application of a combined method using generalized linear models and a geographic information system. *Aquatic living resources*, 14(2), pp.125-135.
- Robb, C.K., 2014. Assessing the impact of human activities on British Columbia's estuaries. *PloS one*, 9(6), pp.99578.
- Ross, D.A., 1995. Introduction to Oceanography. Harper Collins College Publishers, New York, USA.
- Roy, D.P., Wulder, M.A., Loveland, T.R., Woodcock, C.E., Allen, R.G., Anderson, M.C., Helder, D., Irons, J.R., Johnson, D.M., Kennedy, R. and Scambos, T.A., 2014. Landsat-8: Science and product vision for terrestrial global change research. *Remote sensing of Environment*, 145, pp.154-172.

Ruiz-Verdú, A., Jiménez, J.C., Lazzaro, X., Tenjo, C., Delegido, J., Pereira, M., Sobrino, J.A. and Moreno, J., 2016, July. Comparison of MODIS and Landsat-8 estimations of chlorophyll-a and water temperature over Lake Titicaca. In: *2016 IEEE International Geoscience and Remote Sensing Symposium (IGARSS)*, Beijing, China, pp. 7643-7646.

Savenije, H.H., 2006. Salinity and tides in alluvial estuaries. Elsevier. Amsterdam, The Netherlands.

Scavia, D., Field, J.C., Boesch, D.F., Buddemeier, R.W., Burkett, V., Cayan, D.R., Fogarty, M., Harwell, M.A., Howarth, R.W., Mason, C. and Reed, D.J., 2002. Climate change impacts on US coastal and marine ecosystems. *Estuaries*, 25(2), pp.149-164.

Sentinel-2. 2017. Earth Resources Observation and Science (EROS) Center. <https://eros.usgs.gov/Sentinel-2> (accessed: 29/03/2017).

Shepard, C.C., Crain, C.M. and Beck, M.W., 2012. The protective role of coastal marshes: a systematic review and meta-analysis. *PloS one*, 6(11), pp.27374.

Sheridan, P., and C. Hays. 2003. Are mangroves nursery habitat for transient fishes and decapods? *Wetlands*, 23, pp.449-458.

Somvanshi, S., Kunwar, P., Singh, N.B., Shukla, S.P., Pathak, V., 2012. Integrated remote sensing and GIS approach for water quality analysis of Gomti river, Uttar Pradesh. *International Journal of Environmental Sciences*, 3(1), pp.62-74.

Song, K., Wang, Z., Blackwell, J., Zhang, B., Li, F., Zhang, Y. and Jiang, G., 2011. Water quality monitoring using Landsat Themate Mapper data with empirical algorithms in Chagan Lake, China. *Journal of Applied Remote Sensing*, 5(1), pp.053506-053506.

Syariz, M.A., Jaelani, L.M., Subehi, L., Pamungkas, A., Koenhardono, E.S. and Sulisetyono, A., 2015. Estimation of sea surface temperature over poteran island water of indonesia with Landsat 8 tirs image: A preliminary algorithm. *The International Archives of the Photogrammetry, Remote Sensing and Spatial Information Sciences*, XL-2/W4, pp.87-90.

Taylor, G.C., Weyl, O.L., Cowley, P.D. and Allen, M.S., 2015. Dispersal and population-level mortality of *Micropterus salmoides* associated with catch and release tournament angling in a South African reservoir. *Fisheries Research*, 162, pp.37-42.

Tenjo, C., Ruiz-Verdú, A., Delegido, J., Peña, R. and Moreno, J., 2015. Determinación de componentes ópticamente activos en aguas continentales a partir de imágenes Landsat 8. *UD y la GEOMÁTICA*, 9, pp.37-46.

Theologou, I., Patelaki, M. and Karantzalos, K., 2015. Can single empirical algorithms accurately predict inland shallow water quality status from high resolution, multi-sensor, multi-temporal satellite data?. *The International Archives of Photogrammetry, Remote Sensing and Spatial Information Sciences*, 40(7), p.1511.

Thiel, R., Sepulveda, A., Kafemann, R. and Nellen, W., 1995. Environmental factors as forces structuring the fish community of the Elbe Estuary. *Journal of Fish Biology*, 46(1), pp.47-69.

Thomas, A., Byrne, D. and Weatherbee, R., 2002. Coastal sea surface temperature variability from Landsat infrared data. *Remote Sensing of Environment*, 81(2-3), pp.262-272.

Titus, J.G., Hudgens, D.E., Trescott, D.L., Craghan, M., Nuckols, W.H., Hershner, C.H., Kassakian, J.M., Linn, C.J., Merritt, P.G., McCue, T.M. and O'Connell, J.F., 2009. State and local governments plan for development of most land vulnerable to rising sea level along the US Atlantic coast. *Environmental Research Letters*, 4(4), p.044008.

Tobler, W.R., 1970. A computer movie simulating urban growth in the Detroit region. *Economic geography*, 46, pp.234-240.

Toming, K., Kutser, T., Laas, A., Sepp, M., Paavel, B. and Nõges, T., 2016. First experiences in mapping lake water quality parameters with Sentinel-2 MSI imagery. *Remote Sensing*, 8(8), p.640.

Tong, C., Wang, W.Q., Huang, J.F., Gauci, V., Zhang, L.H. and Zeng, C.S., 2012. Invasive alien plants increase CH<sub>4</sub> emissions from a subtropical tidal estuarine wetland. *Biogeochemistry*, 111(1), pp.677-693.

Trujillo, A. P. and Thurman H. V. 2011. Essentials of oceanography. Prentice Hall Recommended Reading Walker, New Jersey, USA.

Turner, D. 2010. *Remote Sensing of Chlorophyll a Concentrations to Support the Deschutes Basin Lake and Reservoirs TMDLs*. Report to EPA for 104b3 2009 grant, component 4. Oregon Department of Environmental Quality, Portland, OR.

Turpie, J.K. and Clark, B.M., 2007. *The health status, conservation importance, and economic value of temperate South African estuaries and development of a regional conservation plan*. Draft report. Anchor Environmental Consultants, Cape Town, South Africa.

Turpie, J.K., Adams, J.B., Joubert, A., Harrison, T.D., Colloty, B.M., Maree, R.C., Whitfield, A.K., Wooldridge, T.H., Lamberth, S.J., Taljaard, S. and Van Niekerk, L., 2002. Assessment of the conservation priority status of South African estuaries for use in management and water allocation. *Water SA*, 28(2), pp.191-206.

U.S Commission on Ocean Policy. 2004. *An Ocean Blueprint for the 21st Century*, Washington, DC.

UNESCO/WHO, 1978. *Water quality survey*. Studies and reports in hydrology, 23. United Nation Educational Scientific and Cultural Organization and World Health Organization, Paris, France.

Urquhart, E.A., Zaitchik, B.F., Hoffman, M.J., Guikema, S.D. and Geiger, E.F., 2012. Remotely sensed estimates of surface salinity in the Chesapeake Bay: A statistical approach. *Remote Sensing of Environment*, 123, pp.522-531.

Usali, N. and Ismail, M.H., 2010. Use of remote sensing and GIS in monitoring water quality. *Journal of sustainable development*, 3(3), p.228.

USEPA (United States Environmental Protection Agency). 1997. *Volunteer Stream Monitoring: A Methods Manual*. USEPA Office of Water, Washington, DC

USEPA (United States Environmental Protection Agency). 2012. Dissolved Oxygen and Biochemical Oxygen Demand. Water Monitoring and Assessment.

<http://water.epa.gov/type/rsl/monitoring/vms52.cfm> (accessed: 19/01/2018).

Ustin, S., 2004. Manual of remote sensing: Remote sensing for natural resource management and environmental monitoring. John Wiley & Sons, Hoboken, New Jersey.

van Niekerk, L. 2007. *Hydrodynamics*. In: Whitfield, A., Bates, G. (Eds.), A review of information on temporarily open/closed estuaries in the warm and cool temperate biogeographic regions of South Africa, with particular emphasis on the influence of river flow on these systems. WRC Report 1581/1/07. Water Research Commission, Pretoria, South Africa.

Van Niekerk, L. and Turpie, J. K. 2012. *National Biodiversity Assessment 2011: Technical Report. Volume 3: Estuary Component*. CSIR Report CSIR/NRE/ECOS/ER/2011/0045/B. CSIR, Stellenbosch, South Africa.

Vanhellemont, Q. and Ruddick, K., 2014. Turbid wakes associated with offshore wind turbines observed with Landsat 8. *Remote Sensing of Environment*, 145, pp.105-115.

Vanhellemont, Q. and Ruddick, K., 2015. Advantages of high quality SWIR bands for ocean colour processing: Examples from Landsat-8. *Remote Sensing of Environment*, 161, pp.89-106.

Vanhellemont, Q. and Ruddick, K., 2016, May. ACOLITE for Sentinel-2: Aquatic Applications of MSI imagery. In: *2016 ESA Living Planet Symposium*, Prague, Czech Republic.

Wagner, E., Dumbauld, B.R., Hacker, S.D., Trimble, A.C., Wisehart, L.M. and Ruesink, J.L., 2012. Density-dependent effects of an introduced oyster, *Crassostrea gigas*, on a native intertidal seagrass, *Zostera marina*. *Marine Ecology Progress Series*, 468, pp.149-160.

Wang, F., Han, L., Kung, H.T. and Van Arsdale, R.B., 2006. Applications of Landsat-5 TM imagery in assessing and mapping water quality in Reelfoot Lake, Tennessee. *International Journal of Remote Sensing*, 27(23), pp.5269-5283.



- Wang, F. and Xu, Y.J., 2008. Development and application of a remote sensing-based salinity prediction model for a large estuarine lake in the US Gulf of Mexico coast. *Journal of hydrology*, 360(1), pp.184-194.
- Wang, M., Shi, W. and Tang, J., 2011. Water property monitoring and assessment for China's inland Lake Taihu from MODIS-Aqua measurements. *Remote Sensing of Environment*, 115(3), pp.841-854.
- Wang, F., Qin, Z., Song, C., Tu, L., Karnieli, A. and Zhao, S., 2015. An improved mono-window algorithm for land surface temperature estimation from Landsat 8 thermal infrared sensor data. *Remote sensing*, 7(4), pp.4268-4289.
- Watanabe, F.S.Y., Alcântara, E., Rodrigues, T.W.P., Imai, N.N., Barbosa, C.C.F. and Rotta, L.H.D.S., 2015. Estimation of chlorophyll-a concentration and the trophic state of the Barra Bonita hydroelectric reservoir using OLI/Landsat-8 images. *International journal of environmental research and public health*, 12(9), pp.10391-10417.
- Water Research Commission (WRC). 2002. *State of Rivers Report: uMgeni River and neighbouring rivers and streams*. WRC Report No.200(02). Water Research Commission, Pretoria, South Africa.
- Watling, K. 2007. *Measuring salinity*. Department of Natural Resources and Water, Queensland, Australia.
- Waycott, M., Duarte, C.M., Carruthers, T.J., Orth, R.J., Dennison, W.C., Olyarnik, S., Calladine, A., Fourqurean, J.W., Heck, K.L., Hughes, A.R. and Kendrick, G.A., 2009. Accelerating loss of seagrasses across the globe threatens coastal ecosystems. *Proceedings of the National Academy of Sciences*, 106(30), pp.12377-12381.
- Werdell, P.J., Bailey, S.W., Franz, B.A., Harding, L.W., Feldman, G.C. and McClain, C.R., 2009. Regional and seasonal variability of chlorophyll-a in Chesapeake Bay as observed by SeaWiFS and MODIS-Aqua. *Remote Sensing of Environment*, 113(6), pp.1319-1330.
- Whitfield, A.K., 1992. A characterization of southern African estuarine systems. *Southern African Journal of Aquatic Science*, 18(1), pp.89-103.

Whitfield, A.K. and Baliwe, N.G., 2013. *A century of science in South African estuaries: Bibliography and review of research trends*. SANCOR Occasional Report No.7. South African Institute for Aquatic Biodiversity, Grahamstown, South Africa.

WHO/UNICEF, 2010. *Progress on Sanitation and Drinking-water: 2010 Update*. World Health Organization and UNICEF, Geneva, Switzerland.

Wooldridge, T., 2007. *C.A.P.E. Estuaries Guideline 3: Collection of bait organisms in estuaries*. C.A.P.E Estuaries Program No.1. Cape Town, South Africa.

WTW. 2018. Operating manuals. <https://www.wtw.com/en/service/downloads/operating-manuals.html> (accessed: 08/02/2018).

Zedler, J.B. and Kercher, S., 2005. Wetland resources: status, trends, ecosystem services, and restorability. *Annual Review of Environment and Resources*, 30, pp.39-74.

Zhang, Y., Yu, T., Gu, X., Zhang, Y.X., Chen, L., Yu, S.S., Zhang, W.J. and Li, X.W., 2006. Land surface temperature retrieval from CBERS-02 IRMSS thermal infrared data and its applications in quantitative analysis of urban heat island effect. *JOURNAL OF REMOTE SENSING-BEIJING*, 10(5), p.789

Zhao, J., Temimi, M. and Ghedira, H., 2017. Remotely sensed sea surface salinity in the hypersaline Arabian Gulf: Application to landsat 8 OLI data. *Estuarine, Coastal and Shelf Science*, 187, pp.168-177.

Zibrowius, H., 1991. Ongoing modification of the Mediterranean marine fauna and flora by the establishment of exotic species. *Mésogée*, 51, pp.83-107.